Porcine peritoneum: A multifunctional xenograft for a diverse range of clinical indications

Thesis submitted to the National University of Ireland Galway for the degree of

Doctor of Philosophy (PhD) in Biomedical Engineering

By

Héctor Capella-Monsonís

November 2020

Regenerative, Modular & Developmental Engineering Laboratory (REMODEL)
Science Foundation Ireland (SFI) Centre for Research in Medical Devices (CÚRAM)
National University of Ireland Galway (NUI Galway)

Research supervisor: Dimitrios I. Zeugolis

Table of contents

Acknowledgements

Firstly, I would like to thank my supervisor Dimitrios I. Zeugolis for this opportunity and his support, guidance and patience during this project. Also, I would like to thank Peter Gingras and Justin Baker, from Viscus Biologics, for their collaboration and help throughout the project.

I would like also to thank all the people from Regenerative, Modular & Developmental Engineering Laboratory (REMODEL) and Science Foundation Ireland (SFI) Centre for Research in Medical Devices (CÚRAM). Specifically, I would like to thank Dr Oliver Carroll and Kyriakos Spanoudes. Also, I would like to mention the support and help received by Dr Stephen Kearns (Galway Hospital) during the project.

This project would not have been possible without the support from the funding agencies: Science Foundation Ireland / European Regional Development Fund (Grant Agreement Number: 13/RC/2073) and the Science Foundation Ireland, Career Development Award (Grant Agreement Number: 15/CDA/3629).

In a more personal tone, I would like to thank all the friends I made during my stay in Galway, who became my second family. Specially, I would like to thank Alex, Eugenia, Joao, Enrico, Andrea, Steff, Kyriakos, Nacho, Meletis, Brian, James, Marc, Sergio, Merari, Eleni, Georgina, Paco, Rosella, Elena, Vaibhav, Dimitris, Ana Lucia and Salome.

I would like also to thank my friends from Spain (El Guateque) and my brothers, Alvaro and Manuel. They have always been there when I needed them.

Finally, my biggest and most sincere thanks is for my parents, whose support has been indispensable during all these years. For my father Alvaro, who taught me to stand up in front of adversity, to look forward and to enjoy life surrounded by those who really matter. For my mother Emi, who always believed in me, showed me her love, pushed me to be happy and, even though she is not here anymore, I can feel she still does. Love you mum. Love you dad. This thesis is for you both.

List of figures

CD31 area quantification (**B**) showed no differences between groups in the absence of hADSC and in the presence of hADSC, a significantly higher area of CD31 in comparison to sham was observed in all groups and only the BM side of the XenoMEM™ showed significantly higher CD31 expression than the hADSC injection. Cell counting from DAPI stained sections (**C**) sections did not reveal any differences in cell density in the wounds between the groups in the absence or presence of hADSC. Data presented as average ± standard deviation (n=6). ** indicates a significantly ($p < 0.05$) higher value than sham group, # indicates a significantly ($p < 0.05$) lower value than ADSC group, ## indicates a significantly ($p < 0.01$) higher value than ADSC group. 189

List of tables

List of abbreviations

Alpha-Minimal Essential Medium (α-MEM)

Atomic force microscopy (AFM)

Basement membrane (BM)

Collagen / oxidized regenerated cellulose – Promogran™ (CORC-PG)

Counting of colony forming units (CFU)

Conditioned media (CM)

Connective tissue (CT)

4′,6-diamidino-2-phenylindole (DAPI)

Dermal fibroblasts, adult (DF)

Differential scanning calorimetry (DSC)

Dioctyl adipate (DOA)

Dulbecco's Modified Eagle Medium (DMEM)

1-Ethyl-3-(3-dimethylaminopropyl) carbodiimide hydrochloride (EDC)

Ethylenediaminetetraacetic acid (EDTA)

Ethylene oxide (ETO)

Extracellular matrix (ECM)

Fast Fourier transform (FFT)

Fibroblast growth factor (FGF)

Foetal bovine serum (FBS)

Glutaraldehyde (GTA)

Glycosaminoglycan (GAG)

Haematoxylin/eosin (H&E)

Hexamethylene diisocyanate (HMDI)

Human adipose derived stem cells (hADSCs)

Human umbilical vein endothelial cells (HUVECs)

Human tenocytes (TCs)

Hyaluronic acid (HA)

Interleukin (IL)

ITS+1 (insulin, transferrin, sodium selenite, linoleic-bovine serum albumin)

Lysogenic broth (LB)

Lipopolysaccharides (LPS)

Masson’s Trichrome (Masson’s TC)

Matrix metalloproteinase (MMP)

Mesenchymal stem cells (MSCs)

Normal goat serum (NGS)

Optical density (OD)

Ovine forestomach - Endoform™ (OF-EF)

Papillae (PL)

Paraformaldehyde (PFA)

Penicillin / streptomycin (P/S)

Peracetic acid (PAA)

Phorbol 12-myristate 13-acetate (PMA)

Phosphate buffered saline (PBS)

Porcine mesothelium-MesoBiomatrix® (PM-MB)

Porcine mesothelium - Puracol® Ultra ECM / XenoMEM™ (PM-PC)

Porcine urinary bladder - MatriStem® (PUB-MS)

Radioimmunoprecipitation assay (RIPA)

Scanning electron microscopy (SEM)

Serosa (SR)

Small intestinal submucosa (SIS)

Sodium dodecyl sulphate-polyacrylamide gel electrophoresis (SDS-PAGE)

Sterility assurance level (SAL)

Supercritical carbon dioxide ($ScCO_2$)

Tissue culture plastic (TCP)

Tissue necrosis factor α (TNF- α)

Transforming growth factor β (TGF-β)

Vascular endothelial growth factor (VEGF)

Abstract

Decellularised xenografts are an inherent component of regenerative medicine. Their preserved structure, mechanical integrity and biofunctional composition have well established them in reparative medicine for a diverse range of clinical indications. Nonetheless, the scattered results observed with tissue grafts in clinics makes patent that the ideal tissue graft does not exist yet. This motivates the investigation of alternative sources of xenografts. Herein, we investigated the potential of an under-investigated tissue graft source, porcine peritoneum / mesothelium, as biomaterial for tendon tissue engineering, as wound healing material and as stem-cell delivery vehicle.

In order to assess the potential of decellularised porcine peritoneum (XenoMEM™) as a material for tendon tissue engineering, we correlated its properties to a commercially available collagen matrix (TenoGlide®). XenoMEM™ presented lower cross-linking ratio ($p < 0.05$), higher mechanical properties ($p < 0.01$), lower coefficient of friction ($p < 0.01$) and higher ($p < 0.05$) cytocompatibility with human tenocytes than TenoGlide®. In addition, XenoMEM™ exhibited lower ($p < 0.05$) immune response than TenoGlide® with macrophages. Collectively, these data support the use of XenoMEM™ in tendon tissue engineering.

To assess porcine peritoneum as wound healing biomaterial, we compared the biochemical and biological properties of the only two commercially available porcine mesothelium grafts (Meso Biomatrix® and XenoMEM™ / Puracol® Ultra ECM) to traditionally used wound healing grafts (Endoform™, ovine forestomach and MatriStem®, porcine urinary bladder) and biomaterials (Promogran™, collagen / oxidised regenerated cellulose). The Endoform™ and the Puracol® Ultra ECM showed the highest ($p < 0.05$) soluble collagen and elastin content. The MatriStem® had the highest ($p < 0.05$) FGFb content, whilst the Meso Biomatrix® had the highest ($p < 0.05$) TGF-β1 and VEGF content. All materials showed tissue-specific structure and composition. The Endoform™ and the Meso Biomatrix® had some nuclei residual matter. All tissue grafts showed similar ($p > 0.05$) response to enzymatic degradation, whereas the Promogran™ was not completely degraded by MMP-8 and was completely degraded by elastase. The Promogran™ showed the highest ($p < 0.05$) permeability to bacterial infiltration. The Promogran™ showed by far the lowest dermal fibroblast and THP-1 attachment and growth. All tested materials showed significantly lower ($p < 0.05$) TNFα expression than the LPS group. The MatriStem® and the Puracol® Ultra ECM promoted the highest ($p < 0.05$) number of micro-vessel formation, whilst the

Promogran™ the lowest ($p < 0.05$). Jointly, these data confer that porcine mesothelium has the potential to be used as a wound healing material.

Finally, we assessed the potential of porcine peritoneum (XenoMEM™) and other two commercially available extracellular matrix-based biomaterials [a collagen / glycosaminoglycan scaffold (Integra™ Matrix Wound Dressing) a porcine urinary bladder (MatriStem™)] as human adipose derived stem cell delivery vehicles. Both tissue grafts induced significantly ($p < 0.01$) higher human adipose derived stem cell proliferation *in vitro* over the collagen scaffold, especially when the cells were seeded on the basement membrane side. Human adipose derived stem cell phenotype and trilineage differentiation potential was preserved in all biomaterials. In a splinted wound healing nude mouse model, in comparison to sham, biomaterials alone and cells alone groups, all biomaterials seeded with human adipose derived stem cells showed a moderate improvement of wound closure; a significantly ($p < 0.05$) lower wound gap and scar index; and a significantly ($p < 0.05$) higher proportion of mature collagen deposition and angiogenesis (the highest, $p < 0.01$, was observed for the cell loaded at the basement membrane XenoMEM™ group). All cell-loaded biomaterial groups retained more cells at the implantation side than the direct injection group, even though they were loaded with half of the cells. Therefore, these results further advocate the use of extracellular matrix-based biomaterials (in particular porcine peritoneum) as human adipose derived stem cell delivery vehicles.

Altogether, this study supports further preclinical and clinical investigation on porcine peritoneum as biomaterial for the fields assessed, whilst the positive results observed encourage further analysis in other scenarios of regenerative medicine.

Keywords

Tissue grafts, Xenograft, Biomaterials, Porcine peritoneum, Tendon tissue engineering, Wound healing, Stem cell delivery

Chapter 1

Introduction

Part of this chapter has been submitted for publication:

Capella-Monsonís, H. & Zeugolis, D. I. (2020). *Decellularised xenografts in regenerative medicine: From processing to clinical application.* **Xenotransplantation**, Submitted.

1.1. Project rationale and objectives

Although decellularised xenografts represent a valuable alternative and are extensively used in several regenerative medicine applications, they still face limitations and scattered results. Therefore, further efforts in the understanding and development of xenografts, researching alternative sources and their investigation in alternative regenerative medicine applications is required. Decellularised porcine peritoneum is a readily available biomaterial source (i.e. waste from meat industry, similarity between human and pig tissues) which gathers few studies and has been only applied in soft tissue engineering. Therefore, we ventured to investigate its potential in three different applications:

Phase 1 – Decellularised porcine peritoneum as tendon barrier biomaterial

Adhesions in tendon still represent a burden that has not response in orthopaedic surgery, where mechanical barriers are a potential option in pre-clinical models but have not reached the clinics. We hypothesised that decellularised porcine peritoneum, due to its preserved characteristics and integration of a basement membrane, will promote the formation of an epithelium which prevents adhesion formation. Objectives:

- To characterise the biochemical (e.g. composition, free amines), biophysical (e.g. structure, coefficient of friction) and biological (e.g. enzymatic degradation) properties of porcine peritoneum and compare them to a commercially available collagen scaffold employed as a tendon barrier in clinics.
- To assess the *in vitro* response of porcine peritoneum to various cell types (e.g. human dermal fibroblasts, human tenocytes, macrophages) and compare it to a commercially available collagen scaffold.

To assess the formation of a functional epithelium *in vitro* on both sides of the porcine peritoneum and collagen matrix.

Phase 2 – Decellularised porcine peritoneum matrix as a biomaterial for wound healing applications

Porcine mesothelium preserves ECM structure and biofunctional molecules such basement membrane markers and growth factors, which pose potential advantages for wound healing applications but has not been tested to this end. Therefore, we hypothesised that the properties of decellularised porcine peritoneum would result suitable for wound healing applications. Objectives:

- Assess the biochemical and biological properties of the only two commercially available decellularised porcine peritoneum products and compare them to those observed in established wound healing products.
- Assess the response *in vitro* of relevant cells types for wound healing (adult dermal fibroblast and macrophages) to decellularised porcine peritoneum and compare them to established wound healing products.
- Assess the angiogenic potential of decellularised porcine peritoneum *in vitro* and *ex vivo* and compare them to established wound healing products.

Phase 3 – Decellularised porcine peritoneum as stem cell delivery system

Stem cell-based therapies, although having proven their potential in clinics, still face major drawbacks such as poor cell localisation, where biomaterials, and particularly tissue grafts, pose an attractive and emerging option for this end. Therefore, we hypothesised that decellularised porcine peritoneum is a suitable biomaterial for adipose derived stem cells (ADSC) delivery system. Objectives:

- Assess the effect on ADSC response and phenotype by decellularised porcine peritoneum. Compare these effects to those observed in a decellularised porcine urinary bladder and a collagen scaffold.
- Assess the potential of porcine peritoneum as stem cell delivery biomaterial in a splinted full thickness wound model in athymic mice and compare it with that observed in a decellularised porcine urinary bladder and a collagen scaffold.

1.2. Background

As result of injuries and diseases, 4.5 million reconstructive surgeries are performed every year in the United States alone with billions associated healthcare expenditure [1]. Chronic wounds, for example, cost US$37 billion to the United States healthcare system every year [2]. Advances in cell-based tissue engineering and regenerative medicine aspire to provide therapeutic treatments for injuries and diseases and to reduce the cost of their treatments. Indeed, numerous studies have shown the potential of cell-based therapies to treat different diseases, including cancer, neurodegenerative disorders, endocrine system related disorders, cardiovascular diseases and to induce regeneration of soft and hard tissues [3-7]. Despite the tremendous progress shown in cell-based therapies, several risks and limitations still need to be addressed [8, 9], including the loss of most cells after delivery [10, 11], poor cell engraftment at the site of interest [12], the need of large amounts of cells and efficient systems to culture them [13], the inefficacy

to bridge large gaps of tissue and the lack of mechanical stability [14]. All these limitations can be potentially addressed by the appropriate selection of a clinical indication specific biomaterial.

An ideal biomaterial for tissue engineering applications should guarantee cytocompatibility, maintain appropriate / desired cellular functions and phenotype for the specific application, induce tissue growth and provide mechanical support until it is absorbed and replaced by natural extracellular matrix (ECM). Synthetic biomaterials can be tailored to obtain desired topographical, mechanical, chemical and morphological properties [15, 16], however, they do not support cell attachment and bioactivity due to the lack of functional domains / cell recognition sites and often induce foreign body response and acute inflammation [16-18]. On the other hand, natural biomaterials present biological compatibility and functionality due to their cell recognition motifs that promote cell adhesion, proliferation and differentiation and advances in chemistry through provision of elegant crosslinking systems offer control over mechanical stability and biodegradation [19, 20]. However, natural biomaterials are of inconsistent composition and high variability as a function of source or batch [21-24]. Independently on whether the biomaterial is natural or synthetic in origin and despite the significant strides in engineering, currently available scaffold fabrication technologies poorly imitate the *in vivo* architecture, mechanical properties and compositional complexity of native tissues. Considering that decellularised grafts closely imitate the biophysical, biochemical and biological milieu of the tissue to be replaced, they can overcome all the aforementioned limitations of natural and synthetic scaffolds and ultimately provide functional reparative therapies, as long as issues associated with immune rejection and availability, in the case of allografts, are addressed.

Undeniably, tissue grafts are an inherent part of tissue engineering and regenerative medicine with numerous products being clinically available for a diverse range of clinical indications (**Table 1.1**). Herein, we discuss advancements and limitations in xenograft development and how processing steps (e.g. decellularisation, crosslinking, sterilisation) affect their properties and differentiate success from failure in their clinical applications.

1.3. Processing of tissue grafts

Each processing step in the developmental cycle of a tissue graft can influence its mechanical, chemical and biological features, determining the success or failure of the implant [25-27]. It is therefore an active field of development, as evidenced by numerous registered processing protocols (e.g. Tutoplast® (RTI Biologics) [28], BioCleanse® (RTI

Surgical) [29], dCELL® Process (Tissue Regenix) [30], Tecnoss® (Tecnoss®) [25]) that is also well-regulated (i.e. FDA provides guidance on medical devices containing materials from animal sources [31], any product related on xenotransplantation in humans [32], and specific documentation for registering newly developed materials of animal origin [33]). The general steps necessary to manufacture a tissue graft and the associated quality control checkpoints are sequentially summarised in **Figure 1.1**. In this section, we provide an overview of these processing steps.

1.3.1. Donor and tissue selection

Porcine and bovine tissues are primarily used in biomedical field, although studies have been carried out using also equine [34, 35], ovine [36], caprine [37], kangaroo [38], buffalo [39] and ostrich [40]. The properties of the graft depend not only on the species, but also on the breed, age [41] and tissue section [42, 43] from where the graft is collected. Among all animal sources, the pig is preferred due to its abundant availability, similar size to human tissues, relative low cost of breeding and extended knowledge of its physiology [44-48]. Bovine tissues, although have shown similarities to human tissues [48, 49], in general, their size in adult animals is not appropriate for use in humans and breeding associated expenditure significantly increases the value of goods, creating reimbursement issues.

Advancements in molecular biology and genetic edition has allowed for the development of genetically modified animals as source of organs or tissues. Most of these studies are carried out in domestic pigs to prevent the immune rejection of the grafts [50], where site-specific nucleases are employed to prevent the presence of the Gal epitope in the donor cells by inactivating the α-1,3-galactosyltransferase enzyme [50, 51]. Several studies have demonstrated safety and efficacy in preclinical models for skin [52, 53], liver [54], cornea [55] and kidney [56] between genetically modified pigs and non-human primates (in combination with immunosuppressive drugs) and clinical trials are expected in the coming years.

The age of the animal can also influence the characteristics and properties of the tissue graft. For example, the level of crosslinks is age-dependent [57] and influences, among others, the thermal stability and mechanical properties. In addition, the age influences cell-binding sites [58, 59], impacting on cellular behaviour and phenotype *in vitro* and *in vivo* [60, 61]. For instance, in pig pancreas islets xenotransplantation for the treatment of diabetes, islets from adult pigs present higher resistance to *in vivo* degradation and higher neovascularisation potential due to the presence of a mature ECM [41]. Small intestinal

submucosa (SIS) has also been shown to present different mechanical, structural and biological characteristics, as well as M2 macrophage immune response and remodelling potential as a function of the stage of maturity of the pigs [62, 63].

Screening of the donor is also necessary before harvesting a graft. Although screening of human patients is relatively easy due to availability of medical records [64], this safety net is not necessarily available in animal-derived grafts that harbour high risks of infection of multiple pathogens [65, 66], but not so much of viral contaminants [67]. The FDA has stablished guidelines on infectious diseases in xenotransplantation to prevent and control interspecies disease transmission with full instructions and precautions that should be carried out during animal breeding and tissue harvesting [68].

1.3.2. Decellularisation, crosslinking, sterilisation and preservation

Once the xenograft donor and tissue source have been chosen, its processing follows a sequential order that includes decellularisation, crosslinking (optional), sterilisation and preservation, using a variety of techniques and agents (**Table 1.2**). Decellularisation of tissue grafts should have minimal effect on the integrity, microstructure, composition and biological activity of the ECM, whilst removing all cellular material and reducing antigens that could trigger immune response [69]. Cellular remnants contain domains that are recognised as foreign matter and trigger immune response [70, 71] and, although ECM components are highly preserved among species [72-76], decellularised ECM components can also elicit immune response [77] that can induce macrophage polarisation to M1 or M2 phenotypes [70]. Classically, the presence of cells [78] and/or cellular material [71] promotes M1 inflammatory response [79, 80], whereas effectively decellularised scaffolds are related to M2 phenotype [80-82]. However, recent studies suggest that decellularised scaffolds promote a combined M1/M2 macrophage phenotype, involving adaptative immunity [83, 84] and triggering remodelling. A typical decellularisation process involves the lysis of cellular matter with physical means or chemical agents, followed by separation of cellular matter from the ECM with enzymes and finally removal of cell matter and debris with detergents [85].

Table 1.1. List of commercially available xenografts for clinical applications, their processing steps and the clinical scenarios where they are applied. n.d.: not disclosed.

Product	Manufacturer	Species	Tissue	Decellularisation	Crosslinking	Sterilisation	Clinical target(s)
4BONE™ XBM	MIS Implants Technologies Ltd.	Bovine	Bone	High temperature	No	Gamma	Bone, dentistry
Artegraft®	Artegraft®	Bovine	Carotid artery	Chemical	Dialdehyde starch	Propylene oxide in ethyl alcohol	Cardiovascular
Avalus™	Medtronic	Bovine	Pericardium	No	GTA and AOA™	Liquid chemical sterilisation	Chemical
Bio-Oss®	Geistlich	Bovine	Bone	High temperature	No	Gamma	Bone, dentistry
Biogide®	Geistlich	Porcine	Dermis	n.d.	No	Gamma	Bone, dentistry
CardioCel®	Admedus	Bovine	Pericardium	ADAPT®	GTA	ADAPT®	Cardiovascular
Carpentier-Edwards Perimount	Edwards Lifesciences	Bovine	Pericardium	XenoLogix™ ThermaFix™	GTA	GTA	Cardiovascular
Collamend™	Davol Inc.	Porcine	Dermis	Chemical (salts, acids, detergents and hydrogen peroxide)	EDC	ETO	Hernia
Conexa®	Tornier®	Porcine	Dermis	Chemical (salts and detergents) and enzymatic (Gal epitope)	No	n.d.	Tendon
CorMatrix	CorMatrix Cardiovascular	Porcine	SIS	n.d.	No	ETO	Cardiovascular
Creos™ Xeno Protect	Nobel Biocare	Porcine	n.d.	n.d.	No	n.d.	Bone, dentistry
CuffPatch™	Organogenesis	Porcine	SIS	n.d.	EDC	Gamma	Tendon
Endobon®	Zimmer Biomet	Bovine	Bone	High temperature	No	n.d.	Bone, dentistry

Product	Manufacturer	Species	Tissue	Decellularisation	Crosslinking	Sterilisation	Clinical target(s)
Endoform™	Hollister Woundcare®	Ovine	Forestomach	Chemical (osmotic gradient and detergents)	No	ETO	Wound healing
EZ Derm	Mölnlycke Health Care Limited	Porcine	Dermis	n.d.	Aldehyde	Aldehyde	Wound healing
Gen-Os	OsteoBiol® Tecnoss®	Equine	Bone	High temperature	No	Gamma	Bone, dentistry
Kerecis Omega3 Wound	Kerecis Ltd	Fish (Cod)	Dermis	Physical	No	n.d.	Wound healing
MatriStem™ / Gentrix™	ACell®	Porcine	Bladder	Chemical (PAA, ethanol and dH_2O)	No	E-beam	Wound healing
Matrix Patch®	Autotissue	Equine	Pericardium	Chemical (DOA)	No	Chemical	Cardiovascular
Medeor®	DSM	Porcine	Dermis	OPTRIX™	No	ETO	Hernia, tendon, skin
Meso BioMatrix®	DSM	Porcine	Peritoneum	OPTRIX™	No	ETO	Soft tissue
Miromesh®	Miromatrix® Medical Inc	Porcine	Liver	Perfusion. Chemical (detergents) and enzymatic	No	E-beam	Hernia
mp3® / Gen-Os	OsteoBiol® Tecnoss®	Porcine	Bone	High temperature	No	Gamma	Bone, dentistry
OASIS®	Cook® Biotech	Porcine	SIS	Chemical (PAA)	No	ETO	Wound healing
PeriGuard®	Baxter Healthcare Corporation	Bovine	Pericardium	Chemical (Basic, ethanol and propylene oxide)	GTA	Ethanol and propylene oxide	Hernia, cardiac surgery

Product	Manufacturer	Species	Tissue	Decellularisation	Crosslinking	Sterilisation	Clinical target(s)
Permacol™ / Zimmer™ / EnduraGen / Pelvicol®	Tissue Science Laboratories Covidien	Porcine	Dermis	Enzymatic	HMDI	Gamma	Hernia, wound healing, tendon, soft tissue
Primatrix™	TEI Biosciences	Bovine	Foetal dermis	n.d.	No	ETO	Wound healing
ProCol®	LeMaitre® Vascular	Bovine	Mesenteric vein	Chemical	GTA	Gamma	Cardiovascular
Protexa®	Tecnoss	Porcine	Dermis	Enzymatic, chemical and physical at low temperature	No	Gamma	Hernia, soft tissue
Restore™	Depuy Synthes	Porcine	SIS	n.d.	No	E-beam	Tendon
SJM Pericardial Patch	St. Jude Medical Inc.	Bovine	Pericardium	No	GTA	n.d.	Cardiovascular
Strattice™	LifeCell™ Corporation	Porcine	Dermis	Chemical (detergents) and enzymatic (Gal epitope))	No	E-beam	Hernia, soft tissue
Surgimend®	Integra LifeSciences	Bovine	Foetal dermis	Chemical	No	ETO	Hernia
Surgisis® / Biodesign® / AxoGuard®	Cook® Medical	Porcine	SIS	Chemical (PAA and hypotonic rinses)	No	ETO	Hernia, nerve
SynerGraft® 100	CryoLife	Bovine	Ureter	Hypotonic and enzymatic (nucleases)	No	n.d.	Cardiovascular
Tarsys®	IOP Inc	Porcine	SIS	n.d.	No	ETO	Soft tissue
TissueMend ™	Stryker® / TEI Biosciences	Bovine	Fetal dermis	Chemical	No	ETO	Tendon

Product	Manufacturer	Species	Tissue	Decellularisation	Crosslinking	Sterilisation	Clinical target(s)
Toronto SPV® Valve	St. Jude Medical Inc.	Porcine	Heart valve	No	GTA	GTA	Cardiovascular
Tutobone®	Tutogen Medical	Bovine	Bone	Chemical (Hypotonic, solvents, H_2O_2)	No	Gamma	Bone
Tutopatch® / Tutomesh®	RTI Biologics®	Bovine	Pericardium	Tutoplast®	No	Gamma	Hernia, wound healing, soft tissue
UNITE™ Biomatrix / OrthADAPT™	Synovis	Equine	Pericardium	n.d.	UltiFix Process	Ethylene dichloride	Wound healing, Tendon
Veritas	Baxter Healthcare Corporation	Bovine	Pericardium	Chemical (Acid)	No	E-beam	Hernia, soft tissue
XCM Biologic®	Ethicon	Porcine	Dermis	OPTRIX™	No	ETO	Hernia, tendon, wound healing
XenMatrix	Davol Inc.	Porcine	Dermis	AquaPure™	No	E-beam	Hernia
Xenoderm	MBP	Porcine	Dermis	n.d.	HMDI	Gamma	Skin, wound healing

Figure 1.1. Sequential processing of any tissue xenograft from any source (exemplified with pig cardiac tissue), along with quality control check points.

Crosslinking is a process which ends with an interconnection between molecules. Although it occurs *in vivo* as a posttranslational modification of proteins via enzymatic and non-enzymatic mechanisms, the native crosslinking of tissue grafts may be insufficient and previous decellularisation process may compromise ECM's mechanical properties and stability upon implantation. Therefore, exogenous crosslinking can be used to increase mechanical properties and the reabsorption time *in vivo* [86]. However, crosslinking decreases the number of available recognition cues for cell attachment and degradation products can elicit cytotoxicity [87, 88] and calcification [89], particularly those elicited by chemical agents [90, 91]. This has motivated research into natural agents [92-95], bearing always in mind that the ideal crosslinker should be economical, effective and with minimal side effects.

Sterilisation aims to reach a sterility assurance level (SAL), referring to the likelihood of bioburden present after the sterilisation; where a recommended level for devices in contact with blood is SAL 10^{-6} [96]. The use of xenografts carries the risk of pathogen transmission between species, which makes necessary the application of effective sterilisation methods at the final stages of their processing. The ideal sterilisation technique must be safe, easy to use and effective. Steam, chemicals and high temperatures should be employed with caution as they have the potential to disrupt and denature the ECM structure, making them unsuitable for the sterilisation of tissue grafts. Gamma or E-beam ionizing radiation, ethylene oxide (ETO) or peracetic acid (PAA) are in general preferred for tissue graft sterilisation, as ISO standards for medical devices are already established [97]. Nonetheless, they also can compromise the properties of tissue grafts [98-100]. Therefore, other methods such as supercritical carbon dioxide ($ScCO_2$) are being explored as alternatives, with promising results to-date [101-103].

The effects that the preservation and the duration of storage have on a tissue graft are commonly overlooked and not specified in the protocols, however they can affect the structure and therefore the properties of a decellularised graft [104]. The most extended techniques for the preservation of acellular tissue grafts are freeze drying and cryopreservation. Freeze drying results in stable materials that can be further sterilised with physical irradiation methods or ETO. However, during the process crystal nucleation occurs, which may damage the ECM structure, thus, parameters such as temperature and cooling speed should be closely monitored and appropriately optimised [104, 105]. Lyoprotectants that protect the tissue from the crystals growth can be used, although they may also affect the ECM structure and its biomechanical properties [106]. Cryopreservation is a cooling process in wet state in the presence of cryoprotectants.

Table 1.2. Summary of decellularisation, crosslinking, sterilisation and preservation methods and agents employed for the processing of tissue grafts.

Method / agent	Mode of action	Examples of tissues	Drawbacks
Decellularisation			
Application methods			
Immersion / mechanical agitation	Incubation at determined conditions of time and agitation Thin tissues need short times at high agitation, thick tissues require long periods at middle agitation	SIS, urinary bladder, tendon, dermis [113, 114], pericardium [115], amniotic membrane [116], urinary bladder [117]	Most employed method High amount of reactive is needed
Perfusion	Distribution of decellularising agents through tissue's vasculature Constant or gradual pressure Indicated for whole, highly vascularised organs	Heart [118, 119], lung, trachea [120], liver [121, 122], kidney [122, 123], SIS [124], skeletal muscle [125] and skin [126]	The optimal protocol is still elusive Shear forces are likely to damage the basement membrane of tissue's vasculature Not efficient in dense ECM tissues
Physical methods			
Freezing / thawing	Crystals formed during the decrease of temperature break down cell's cytosol and membrane	Tendon [127], cartilage [128], skin [129], lung [130], artery [131], intervertebral disc [132], spleen [133], nerve [134], SIS [135], cornea [136]	Can damage tissue graft ECM and structure, affecting its mechanical properties

Method / agent	Mode of action	Examples of tissues	Drawbacks
Sonication	Ultrasounds facilitate the penetration of decellularising agents and destroy cell's membranes and nuclei	Larynx [137], trachea [138], myocardium [139]	It affects tissue's ECM and structure Attention must be paid to pH, temperature and conductivity
Supercritical carbon dioxide	High-transport and inert gas that promotes cell removal without interacting the ECM	Aorta [140], adipose tissue [141], tendon [142]	It affects GAG and growth factor content
Chemical agents			
Alkaline (sodium hydroxide, ammonia, calcium oxide) and acid agents (deoxycholic acid, peracetic acid, acetic acid)	Solubilisation of cytosol and disruption of nucleic acids	Pericardium [115], cornea [143], kidney [144], bladder [145], amniotic membrane [116], artery [146], urinary bladder [117], tendon-bone interface [147], tendon [148], liver [149]	It affects the integrity of ECM components
Detergents	Solubilisation of cell membranes and breakage of interactions between DNA, protein and lipids		
Non-ionic (TritonX100)	Attack the interaction of lipids with other lipids and proteins	Aorta [150], aortic valve [151], liver [152], umbilical vein [153] or annulus fibrosus [154]	Lower capacity than other methods to remove cellular material
Ionic (SDS, TritonX200)	Include cationic or anionic group Effective at solubilising membrane proteins	Liver [152], annulus fibrosus [154], nerve [155]	Denaturing agents that negatively affect ECM content

Method / agent	Mode of action	Examples of tissues	Drawbacks
Zwitterionic (CHAPS, SB10)	Detergents that combine properties of both ionic and non-ionic detergents	Cardiac vessels [156], heart [157], lung [158]	Negative effect in ECM
Hypotonic and hypertonic solutions (NaCl 1.5 M, Na Cl 3 M)	It lyses cells through osmotic pressure It cannot remove cell remnants	SIS [159], cornea [160], aortic valve [151], cartilage [161]	Ineffective on their own to remove cell debris
Alcohols and solvents (Isopropanol, ethanol, tributyl phosphate)	Cell lysis by dehydration, precipitation of remaining DNA and solubilisation of lipids	Adipose tissue [162], cornea [163], temporomandibular joint disc [164], tendon [148], cartilage [161]	It affects mechanical properties and ECM structure
Chelators (EDTA, EGTA)	Isolate calcium and magnesium ions, necessary for fibronectin and collagen cell binding	Liver [165], trachea [166]	Not effective on their own
Enzymatic agents			
Proteases	Cleaving of specific substrate and recognition motifs of proteins		
Trypsin	Cleaves cell adhesion proteins on the carboxyl side of the aminoacids arginine and lysine	Kidney [144], skin [26], aortic valve [151], annulus fibrosus [154]	Prolonged exposures result in ECM damage
Dispases	Cleave collagen type IV and fibronectin Employed to remove epithelium layers	Cornea [136, 167], skin [168]	It disrupts ECM components of the basement membrane
Collagenase	Cleave specific sites of different collagen types	Aortic valves [169]	It causes severe damage to on ECM

Method / agent	Mode of action	Examples of tissues	Drawbacks
Nucleases	Hydrolyse the bonds of ribonucleic and deoxyribonucleic acid chains; endonucleases cleave the interior bonds and exonucleases target the terminal ones	Cornea [167], muscle [170]	Ineffective on their own Concerns as immune response trigger
α-galactosidase	Cleaves GAGs present in the ECM (reduction of Gal-epitope)	Pericardium [171, 172], anterior cruciate ligament [173]	Reduction of GAGs It affects mechanical properties
Lipase	Hydrolysis of lipids present in the tissue	Amniotic membrane [174]	Ineffective on its own Requires the use of solvents
Crosslinking			
Physical crosslinking			
UV radiation	Free radicals produced by irradiation for bonds from aromatic amino acid residuals	Bovine pericardium [175]	Physical crosslinkers are not effective in tissue grafts and are rarely employed
Dehydrothermal	Removal of bound water and formation of ester and amide bonds intramolecularly	Skin [176]	

Method / agent	Mode of action	Examples of tissues	Drawbacks
Chemical agents			
Glutaraldehyde (GTA)	Reacts with primary amines generating intra and intermolecular bonds, reaction between an amino group and an aldehyde group from lysine or hydroxylysine or through reaction between two contiguous aldehydes	Oesophagus [177], liver [178], amniotic membrane [179], pericardium [90], aorta [180, 181], aortic valve [180]	Cytotoxic effects, acute immune reaction upon implantation and calcification Detoxification with glycine is advised
1-Ethyl-3-(3-dimethylaminopropyl) carbodiimide hydrochloride (EDC)	Activation of carboxylic groups from aspartic and glutamic acid residues followed by a reaction with primary amines from lysine, forming an amide bond	SIS [182], pericardium [183, 184], skin [185], heart valves [186],	Lower crosslinking efficiency than GTA Inflammation effects and calcification, but at a lower extent than GTA
Epoxy compounds (HDMI, polyglydicyl ether)	Epoxy compounds form bonds between amino, carboxyl and hydroxyl groups	Skin [187, 188], aorta [189], pericardium [92]	Lower efficiency than GTA and EDC Related to cytotoxicity and inflammation

Method / agent	Mode of action	Examples of tissues	Drawbacks
Natural agents			
Genipin	Polyphenols carbonyl functional groups react with primary free amines or through the formation of a nitrogen-irinoid and a further aromatic monomer	Pericardium [95], trachea [190], cartilage [191], annulus fibrosus [192], liver [178].	Lower efficiency than chemical agents High cost
Other polyphenols (Procyanidins, epigallocatechin gallate)		Cartilage [191], arteries [193], heart valves [194]	Early stage of research Low crosslinking efficiency
Sterilisation			
Physical sterilisation			
Gamma irradiation	Ionising radiation (gamma and electron beam) damages the nucleic acids of the pathogens directly or indirectly through radiolysis of water and production of hydroxyl radicals	Tendon [195], cartilage [100], lungs [196]	High doses negatively affect ECM structure and mechanical properties
Electron-beam		Tendon [197, 198], ligament [199], bone [200]	Low penetration capacity in dense ECM tissues It affects ECM structure and mechanical properties

Method / agent	Mode of action	Examples of tissues	Drawbacks
Supercritical carbon dioxide ($ScCO_2$)	High penetration and transport capacity, while inert, serves as a mean to wash off pathogens without interacting with ECM	Meniscus [101], tendon [201], heart [102], lungs [103]	Low efficacy on its own, but great potential in combination with other chemical agents Early stage of research It affects ECM structure
Chemical sterilisation			
Ethylene oxide (ETO)	Microbicidal, fungicidal and antiviral activity based on the alkylation of nucleic acids and enzymes	Bladder [202], cartilage [100], liver [149], skin [203]	Lower penetrability than physical agents Requires complex equipment
Peracetic acid (PAA)	Powerful oxidising agent which is bactericidal and fungicidal at low dilutions	Cartilage [100], liver [149], urethra [204], nerve [205], tendon [206], trachea [207], SIS [208]	Cytotoxic without appropriate rinsing It affects cell viability It partially crosslinks ECM
Gas plasma	Charged gas which contains the same proportions of anions and cations, interacting with the metabolites of microorganisms by oxidation / reduction processes	Bone [209, 210], cornea [112]	Early stage of research It affects ECM structure

Method / agent	Mode of action	Examples of tissues	Drawbacks
Preservation			
Freeze drying	Sublimation process that results in dry and stable grafts	Arteries [104], heart valves [106], nerve [105]	Formed nucleation crystals affect ECM structure and mechanical properties Lyoprotectants can be used, but compromise cytocompatibility
Cryopreservation	Cooling process in wet state in the presence of a cryoprotectants solution	Tendon [211], aorta [107], heart valves [108]	Long preservation times negatively affect ECM structure and mechanical properties Cryoprotectants can elicit cytotoxicity

Cryopreservation has been shown to preserve the functionality of tissue grafts [107, 108], but cryoprotectants may induce a cytotoxic side effect [109].

In the processing of a tissue graft, once each step has been finalised, the assessment of its efficacy and effects on the material have to be assessed. Efficacy of decellularisation is generally assessed through histology and DNA quantification, where 50 DNA ng / mg dry tissue is considered a safe threshold [110]. The degree of crosslinking can be calculated by quantifying the free amines or denaturation temperature [111]. Counting of colony forming units (CFU) / ml after sterilisation can be employed to calculate the reduction on the number of viable microorganisms [112]. Also, effects of the processing steps on the ECM structure and the mechanical properties of the grafts must be analysed, followed by classic *in vitro* and *in vivo* compatibility assays and specific assays for the specific future application of the tissue graft.

1.3. Xenografts in clinical indications

Many xenografts are commercially available for various clinical indications. **Table 1.3** summarises *in vitro*, *in vivo* and clinical data that have been obtained to-date with commercially available xenografts. In this section, we discuss advances and shortfalls of xenografts per clinical indication.

1.3.1. Soft tissue

Porcine dermis is extensively used in hernia and abdominal wall repair [212]. Although crosslinking provides desirable properties for hernia repair (e.g. longer durability, more stable mechanical properties in early stages of healing), crosslinked xenografts are associated with scattered results, complications (e.g. mechanical failure, disintegration, infection) and gather the highest number FDA reports [213]. Therefore, crosslinked xenografts in hernia repair require further improvement of the crosslinking techniques, implementing de-toxification steps or alternative crosslinking approaches. This can be substantiated considering that non-crosslinked porcine dermal matrices have shown better integration and mechanical properties after implantation [213] and acceptable results in clinics [214-217], which match the lower immune response observed *in vitro* [218] and *in vivo* [219]. Similar results have also been obtained in cases of infections, where non-crosslinked dermis [220] has shown superior outcomes to crosslinked porcine dermal xenografts [221, 222]. It is worth noting that although the use of xenografts is generally accepted as safe in contaminated fields, this is still a matter of debate in the field [223]. Porcine SIS is also considered as a suitable and safe material for hernia repair in clinics

[224, 225], matching the performance of synthetic meshes [226]. However, it has not shown suitability when employed as abdominal wall reinforcement in challenging scenarios, offering poor mechanical resilience ending in the discomfort of the patient and complications [227]. This could be related to its lower mechanical properties and resistance to enzymatic degradation, when compared to other tissue sources like dermis or crosslinked xenografts [228].

Xenografts are also extensively used in wound treatment and skin replacement [229-232]. Crosslinked porcine dermis resulted in opposing conclusions in late 1980s / early 1990s as partial thickness wound dressing [233, 234]. Later studies, however, have shown the beneficial effects of porcine dermis as skin substitute in the treatment of burns and surgical wounds [235, 236]. More recently, foetal bovine dermis has shown positive results as wound healing material in diabetic ulcers [237-239], promoting faster healing than other products such as allogeneic grafts [240]. This can be attributed to the lower crosslinking content that results in faster remodelling [62, 63], as *in vitro* [241] and *in vivo* [242] studies support. Porcine SIS [243] and urinary bladder [244] are also customarily employed in wound healing, where they have shown improved and accelerated healing of ulcerous wounds [245-247] and have showed similar or superior performance to biomaterials [248, 249] and allografts [250] and at a substantial lower cost [251]. Also, ovine forestomach [252], equine pericardium [253] and even fish skin [254] have shown promising results in small clinical trials, but further investigation is required to demonstrate safety and efficacy.

In breast reconstruction, acellular dermal matrices are used extensively [255-258] with, in general, low rates of complications [259-262], although some adverse effects (e.g. infection, necrosis) have been reported [263-265]. Similarly to skin replacement, positive outcomes have also been observed in breast reconstruction using foetal bovine dermis [266-268]. Other products such as bovine pericardium [269, 270], porcine peritoneum [271] and porcine SIS [272-274] have also been tested in small clinical trials with acceptable outcomes in breast reconstruction.

Despite all these positive patient outcomes, all studies agree that randomised clinical trials with larger number of patients are needed to further support the use of xenografts in soft tissue repair.

1.3.2. Tendon, bone and dentistry

Commercially available xenografts in tendon regeneration are used as augmentation systems. Tendon augmentation with porcine SIS has been related to failure in clinical

trials [275-277], with no improvement in healing and mechanical properties, which was associated to the inefficient decellularisation and the consequent immune reaction, as reported in *in vivo* studies [278, 279]. Crosslinked xenografts, such as equine pericardium, did not yield positive outcomes in clinical trials [35, 280], which can be attributed to crosslinking-induced immune reactions. Porcine dermis xenografts (e.g. Conexa® [281, 282]) on the other hand have shown positive results in tendon augmentation [283-285], possibly attributed to efficient decellularisation and/or crosslinking protocols and selecting a tissue with appropriate composition and mechanical resilience. In any case, overall, no definitive tendon augmentation device seems to be available. Although xenografts play a crucial role in irreparable defects augmentation, in moderate to large injuries, they have not achieved a satisfactory outcome.

Bone xenografts provide an optimal microenvironment for cell adhesion, proliferation and infiltration *in vitro* and *de novo* bone generation *in vivo*. This osteoinductive effect is related to the preserved micro- and macro- structure of the decellularised bone together with the partial preservation of ECM components [286]. Despite their high availability, low cost and good mechanical and osteoinductive properties, only a few bone xenografts are available, which have shown limited positive clinical results [287, 288], and as a result, they are rarely employed in orthopaedics [289]. Nonetheless, advances in materials sciences and tissue engineering have resulted in the development of composite materials combining xenogeneic mineral matrix, synthetic and/or natural polymers, which have been tested positively in clinical trials [290-292].

In dentistry, xenografts are used as bone-filling materials, with data to-date showing superiority in clinical outcomes even over autologous treatments [293]. These materials are normally deproteinised with high temperature processing, maintaining the mineral component and microstructure of the bone [294]. Bovine, porcine and equine in origin grafts have shown positive results *in vitro* [295], in preclinical models [296] and in clinical setting [297-299]. Porcine non-crosslinked dermis has also been used successfully as augmentation / contention system in clinical trials [300, 301], largely attributed to its integration with the surrounding soft tissue, which prevents the second operation that synthetic materials require for removal [302].

1.3.3. Cardiovascular

In cardiac graft replacement or patching, decellularised porcine SIS is one of the most employed material [303], but only few clinical studies can be considered in a class III relevance, and the reported class IV correspond to case series or small trials [304, 305].

In addition, high heterogenicity in responses has been observed, together with considerable complications, such as inflammatory response [306] and/or graft failures [307, 308]. These complications were often related to high pressure conditions, which could be indicative of the low performance due to insufficient mechanical properties of the source of tissue, as observed *in vitro* [303]. Therefore, crosslinked materials with enhanced mechanical properties, like bovine pericardium, that include processing steps preventing crosslinker-related complications (e.g. calcification [309]) have been developed, which have shown positive short-term results in paediatric cardiovascular applications [309-311], but long-term assessment is required.

Table 1.3. Indicative in vitro, in vivo and clinical studies of commercially available xenografts.

Xenograft product	*In vitro* studies	*In vivo* studies	Clinical studies	Main findings
Artegraft®	-	-	[317, 318]	*Clinical data:* As haemodialysis access or lower extremity bypass, initial positive results regarding primary and secondary patency values until 5 years, comparable to synthetic ePTFE
Avalus™	-	-	[322]	*Clinical data*: Safety for aortic valve replacement in 686 patients reported in a prospective non-randomised multi-centre study, although bleeding rates increased in the long-term follow-up
Bio-Oss®	[295]	-	[298, 299]	*In vitro*: Promoted secretion of VEGF by periodontal ligament cells, but in a lower extent than other xenogeneic bone grafts from porcine and equine origin *Clinical data*: Increased osteogenesis and width of the alveolar process alone or in combination with autogenous tissue, with a high (96 %) survival of dental implants
CardioCel®	[329, 330]	[309, 331, 332]	[309-311]	*In vitro*: Closest mechanical properties to young aortic valves leaflets in a comparative study including other crosslinked materials High cytocompatibility and capability to promote the adhesion and proliferation of mesenchymal stem cells (MSCs) *In vivo:* Effective delivery of MSCs in a mice infarcted model, promoting regeneration and integration of the tissue

				A lamb aortic valve replacement and pericardial patch showed integration, remodelling and absence of calcification after 7 months. Contrary, a vascular patch in pigs showed severe calcification after 1 year *Clinical data*: Short-term small studies have shown good performance and integration of the material in repaired aortic valves of paediatric patients. Contrary, 2 years follow-up study of 101 infant patients with congenital heart diseases showed some cases of aorta thickening, although no calcification
Carpenter-Edwards Perimount	-	-	[321]	*Clinical data:* Low incidence of valve-related complications and deterioration in a retrospective study on 2,659 patients (70.7 ± 10.4 years) after 20 years follow-up
Collamend ™	[218, 228, 333]	[219, 334-336]	-	*In vitro:* Presented higher mechanical properties and resistance to enzymatic degradation than other tissue sources and non-crosslinked matrices Elicited an inflammatory response as per cytokine production by macrophages *in vitro* *In vivo*: Subcutaneous models showed poor cell invasion, remodelling and neovascularisation, higher inflammation and immune response that non-crosslinked matrices. Longer times of resorption than other non-crosslinked matrices (up to 24 weeks in rats). Hernia models in rats have shown complications, seroma and inflammatory events. Similar data were obtained in a rabbit model, although with positive results in mechanical properties. A mature hernia pig model showed positive results in tissue mechanical properties after integration, although with evidence of adhesions

Conexa®	[337]	[281, 282]	[280, 284]	*In vitro*: High cytocompatibility with tenocytes, allowing the highest adhesion, proliferation and promoting the expression of tenocyte markers compared to crosslinked materials *In vivo*: A subcutaneous model in vervet monkeys showed the absence of inflammatory immune reaction thanks to the cleaving of the Gal epitope (α-galactosidase processing). In a rotator cuff augmentation model in vervet monkeys, promoted remodelling in 6 months and prevented immune reaction *Clinical data*: Promoted pain relief and recovery of the motion and strength in rotator cuff massive tears in two studies of 1 and 26 patients
CorMatrix	[338-340]	[340-344]	[304-308]	*In vitro*: Suboptimal hemodynamic properties were observed in a left heart simulator. Antimicrobial activity up to 6 days was granted after antibiotic impregnation. Demonstrated good cytocompatibility with MSCs *In vivo*: Positive results in terms of remodelling and functionality as cardiac patch in rat models. In larger models (pig, dog, sheep) as myocardium and vascular graft has shown good remodelling, prevention of calcification and low immunogenicity. As valve replacement in pigs showed suboptimal mechanical and functional features *Clinical data:* High heterogeneity in responses has been observed and considerable complications like inflammation response, patch failures or incomplete resorption. These complications were more related to high pressure conditions. Positive results have recently been reported only in small trials. Discouraging results include: 32 % recurrence in leaflet augmentation, regurgitation and inflammatory response of paediatric repaired valves after

				midterm follow-up. Histological data after paediatric heart surgery reported associated fibrosis, foreign-body reaction, necrosis and chronic inflammation
CuffPatch™	[345, 346]	[347, 348]	-	*In vitro*: Similar mechanical properties to crosslinked fresh equine pericardium. Lower mechanical properties than crosslinked dermal grafts *In vivo*: Abdominal wall models in rats showed adverse immune response and M1 polarisation of macrophages
Endoform™	[229, 232]	[232, 349]	[252]	*In vitro*: Retained soluble compounds able to modulate proteases (MMPs and elastase) action and to promote angiogenesis. *In vivo*: Rotator cuff augmentation model in rats showed higher histological levels of repaired tendons than sham, but not mechanical nor functional improvement. Full thickness wound model in pigs revealed a better and faster remodelling than sham *Clinical data:* Case series of 19 participants reported a 50 % closure of chronic wounds after 12 weeks, concluding with the potential of the material for the treatment of chronic wounds
EZ Derm	-	-	[233-236, 350]	*Clinical data:* Clinical data from the late 1980s and early 1990s yielded scattered results as full-thickness wound dressing. More recent studies of partial-thickness and paediatric burns reported a firm adherence which provided beneficial conditions to the healing process, like reduced infections and evaporation, at a reduced cost
Kerecis Omega 3 Wound	[351]	[352]	[254, 353]	*In vitro*: Higher porosity, cell ingrowth and anti-bacterial properties due to the presence of omega-3 than a commercially available decellularised dermis allograft *In vivo:* Shown to be safe and effective in a dura mater regeneration pilot study in sheep

				Clinical data: Double-blinded and randomised trial showed equal efficacy than decellularised porcine SIS, with no adverse immune reactions to both xenografts, agreeing with recent findings in challenging ulcer wounds small studies
MatriStem ™	-	-	[244, 250, 251, 354-358]	*Clinical data:* Demonstrated healing enhancement in small case series of chronic wounds and deep partial thickness burns. Healing potential and remodelling its further enhanced when employed as micronized matrix. Similar performance (< 20% closure rate) to a fibroblastic cultured autograft at a considerably lower cost in the treatment of foot ulcers. Slightly better performance than allogeneic skin substitutes but at a substantial lower cost revealed by a multicentre study of 13,000 cases of diabetic foot ulcers. Small series in the reconstruction of finger, vagina and urethra have shown promising results
Meso Biomatrix®	-	-	[271, 359]	*Clinical data*: Scattered results as single-stage implant-based breast reconstruction material regarding safety for this purpose (integration, inflammation, patient comfort)
Medeor®	[360]	-	-	*In vitro*: Presence of soluble factors able to promote cell proliferation and invasion in a higher extent than other commercially available xenografts (dermis) and allografts (dermis)
Miromesh®	-	[361]	-	*In vivo*: Better integration and cell infiltration than a dermis xenograft in a hernia model in rats
OASIS®	[230, 232, 241, 362]	[232]	[243, 245, 246, 248, 249, 251, 363]	*In vitro:* Retained soluble compounds and growth factors able to promote cell proliferation and angiogenesis. Higher inflammatory (M1/M2 score) response by THP-1 than bovine dermis, human dermis and a collagen scaffold *In vivo:* Full-thickness wound model in pigs revealed a better and faster remodelling than sham.

				Clinical data: Promoted better remodelling, lower inflammation and faster healing of ulcers compared to other standards (i.e. wet dressings) combined with negative pressure and showed no complications. Data confirmed with histopathological studies. Similar or improved performance than hydrogel products (i.e. hyaluronic acid or becaplermin) in means of patient comfort and rate of healing. Slightly better performance than allogeneic skin substitutes but at a substantial lower cost revealed by a multicentre study of 13,000 cases of diabetic foot ulcers
OrthADAPT™ / UNITE™ Biomatrix	[337, 345]	-	[35, 253, 280, 364]	*In vitro*: At different crosslinking treatments, no relation between crosslinking degree and mechanical properties. Supported tenocytes adhesion, but at lower extent than other non-crosslinked materials. It did not promote the expression of tendon markers in tenocytes *Clinical data:* Promoted the healing of 75.7 % in recurrent diabetic foot ulcers of 34 patients after 12 weeks of treatment, confirming the positive results observed in a previous study in 23 patients. In tendon repair, an adverse acute reaction of one patient with an augmented Achilles tendon repair has been reported, similar to another case series of 6 patients suffering irreparable tears in rotator cuff
Osteobiol® / Gen-Os	[295]	[296]	[297]	*In vitro*: Promoteed VEGF production of periodontal ligament cells and angiogenesis in endothelial cells in a higher extent than a bovine bone xenograft *In vivo*: Lower inflammatory reaction in rats muscle implantation than an alloplastic material. *Clinical data: S*mall study with 15 patients showed a reduction of the hard tissue resorption improving the outcomes after tooth extraction

Periguard®	[228, 329, 333, 338]	-	-	*In vitro:* Suboptimal hemodynamic properties were observed in a left heart simulator. Closest mechanical properties to young aortic valves leaflets in a comparative study including other crosslinked materials. Presents higher mechanical properties and resistance to enzymatic degradation than other tissue sources (SIS) and non-crosslinked matrices
Permacol™	[218, 228, 333, 337, 345, 346, 360, 365-368]	[219, 334, 335, 348, 366, 367, 369-375]	[221, 222, 283, 376-382]	*In vitro:* Presented higher mechanical properties and resistance to enzymatic degradation than other tissue sources and non-crosslinked matrices. Supported the adhesion and invasion of MSCs, fibroblast, tenocytes, etc., but at a lower extent than other non-crosslinked matrices, cytotoxic events related to crosslinking. Elicited an inflammatory response as per cytokine production by macrophages *in vitro* *In vivo*: Subcutaneous models showed poor cell invasion, remodelling and neovascularisation, higher inflammation and immune response that non-crosslinked matrices. Longer times of resorption than other non-crosslinked matrices (up to 24 weeks in rats). Hernia models in rodents and rabbits showed optimal mechanical properties performance, although poor resorption and fibrotic tissue formation. Similar data were obtained in tendon and vascular patch models. Skin regeneration models in rats revealed a very modest performance due to poor resorption and epithelisation *Clinical data*: Scattered results observed in pelvic wall repair (i.e. positive patient satisfaction and graft performance compared to synthetic substitutes after 1 year follow up versus relation to complications and recurrence) and in hernia repair of contaminated fields (i.e. positive outcomes and no recurrence versus 50-88 % recurrence and 37 % rate of infection). Treatment

				of massive tears in rotator cuff showed improvement in pain relief and shoulder functionality in small studies (5 and 10 patients). Breast reconstruction small case series showed an acceptable outcome in skin-sparing mastectomy regarding patient satisfaction scores and absence of complications. In eyelid repair, it was related to a higher rate of complications than other xenografts and materials provoked by its stiffness and low resorption
Primatrix™	[241]	[242]	[237-240]	*In vitro*: Lower M1/M2 macrophage polarisation score than other crosslinked and non-crosslinked xenografts *In vivo*: Low immune and inflammatory response in a mice subcutaneous model. Material was remodelled by day 14 *Clinical data*: Several studies have shown a faster healing than standard of care and other materials such as SIS or urinary bladder in diabetic ulcers, showing no complications and a complete integration. Similar results than those offered by allogeneic skin replacements have also been reported
ProCol®	-	-	[312, 313]	*Clinical data:* Failure of the graft as vessel replacement was reported in all implantations of a small study (6 patients) due to aneurism and thrombosis, where other trial of 32 patients also showed insufficient values of primary patency in critical limb ischemia repairs
Protexa®	-	[383]	[265]	*In vivo:* Positive immune response and integration, although authors considered it performed at a lower level than a porcine SIS material *Clinical data:* Showed good cosmetic results in a 48 patients comparative trial with the titanium mesh TiLOOP®, but with higher rate of complications

Restore™	[337, 346, 368]	[278, 279, 347, 348, 373]	[275-277, 280]	*In vitro*: Elastic modulus comprised between human rotator cuff values, but lower strength and strain. Lower mechanical properties than dermal derived grafts in both tensile tests and suture pull-out test. Lower cytocompatibility with tenocytes than non-crosslinked dermal grafts. *In vivo:* Related to a M2 polarization and remodelling in an abdominal wall model in mice, although other studies in rabbits and mice also report an inflammatory reaction to the material due to ineffective decellularisation, which can be decreased with the use of autologous cells. In tendon repair models (e.g. rotator cuff in rabbits and lambs), showed an initial inflammatory response and a later complete resorption, but without recovery of mechanical properties *Clinical trials*: Negative results were obtained in clinical trials; the material did not improve the healing and mechanical functionality of massive nor moderate rotator cuff tears, with a high rate of complications like inflammation and immune reaction
SJM Pericardial Patch	[329, 338]	-	[320]	*In vitro*: Closest hemodynamic characteristics to normal aortic valves in a comparative study. *Clinical* data: Low rate of early mortality and complications and positive haemodynamic performances such as effective orifice area index in a multicentre study of 1,024 patients of 72.5 ± 9.0 years
Strattice™	[218, 228, 360, 384, 385]	[334, 383, 384, 386-388]	[214-217, 220, 259-264]	*In vitro*: High rate of structure preservation and similar resistance to enzymatic degradation than native tissue, although lower resistance than other dermal crosslinked xenografts. Presence of soluble factors able to promote cell proliferation in a higher extent than other commercially crosslinked xenografts (dermis) and allografts (dermis). Lower activation and production of

				inflammatory cytokines by mononuclear cells elicited than crosslinked dermal xenografts. Resistance to bacterial penetration due to compact structure *In vivo*: Lower inflammatory response and faster degradation and remodelling than crosslinked dermal xenografts in subcutaneous models in rodents and pigs. In hernia models in rats, it has shown a positive performance regarding integration, low inflammatory response and the mechanical properties of the hernia repair, which was confirmed in an abdominal wall repair in monkeys *Clinical data*: Positive outcomes for hernia repair demonstrated at a short / mid-term, showing elevated (>70%) success repair in high risk population and similar rates of recovery and recurrence than those observed in synthetic partially absorbable meshes. Scattered results were observed in breast reconstruction, where several studies point its safety and efficiency with a low rate of complications, and others report a high incidence of complications (i.e. infection, necrosis) and unsuitability for one-stage implant-based breast reconstruction
Surgimend ™	-	-	[266-268]	*Clinical data:* Low rate of complications, high patient satisfaction and high objective satisfaction as tissue-expander breast reconstructions in studies of 28 and 65 patient, and as material for implant-based reconstruction following skin-sparing mastectomy in 118 patients
Surgisis®	[218, 228, 366]	[219, 335, 366, 371]	[224-227, 274, 389-392]	*In vitro*: Lower resistance to enzymatic degradation than dermal xenografts and crosslinked grafts. Supported the invasion and growth of MSCs for stem cell delivery and elicits a lower activation and production of inflammatory cytokines by mononuclear cells than crosslinked xenografts

				In vivo: Lower mechanical performance in rat and rabbit hernia models than crosslinked grafts at early stages, but a better resorption and mechanical stability of the repair at later stages motivated by the remodelling of the tissue. This remodelling was enhanced when delivering autologous MSCs *Clinical data:* Suitability and safety was demonstrated for several hernia repairs (i.e. inguinal, hiatal) in several clinical trials, showing no complications nor immune rejection up to 5 years follow-up. Contrary, its unsuitability as abdominal wall reinforcement in challenging population was reported when placed in preperitoneal sub-lay. A small trial showed positive and promising results in means of integration and aesthetics in nasal reconstruction. Few clinical trials have shown potential as nerve conduit in cubital tunnel syndrome and lingual nerve repair, where no complications and significant improvement in pain and functionality were reported, similarly to a collagen type I stablished product
SynerGraft®	-	-	[314, 316]	*Clinical data:* High rate of complications reported as blood vessel replacement, including thrombosis and aneurism dilatation, related to immune reactions provoked by an inefficient decellularisation after histopathological study
Tarsys®	-	-	[272, 273]	*Clinical data:* Significant improvement of functionality in lower eyelid retraction surgery, with no recurrence surgery, low rate of complications, no infections and satisfactory cosmetic results
TissueMend™	[340, 346, 393]	[340, 348]	-	*In vitro*: Higher mechanical properties (suture pull-out) than SIS xenografts, but lower than other crosslinked dermal grafts. No improvement in the mechanical properties observed on augmented

				tendons with this material in an *ex vivo* mechanical analysis. High cytocompatibility with MSCs for stem cell delivery purposes *In vivo:* Encapsulation of the tissue was observed in an abdominal wall repair in rats, although without an inflammatory reaction elicited by other crosslinked xenografts compared. It has been effectively used as a MSCs delivery system in an infarcted heart model in mice, improving remodelling and angiogenesis
TutoBone®	-	-	[288]	*Clinical data:* A 10-year retrospective study including 556 patients reported inferior results to autografts in terms of cervical fusion, but similar to other alternative options and at a lower cost
Tutomesh®	-	[388, 394]	[270]	*In vivo*: Lower collagen deposition and mechanical properties in a rabbit ventral hernia repair than a dermal xenograft. In a rat Achilles tendon repair, it showed capability to integrate and the absence of host response, but with no functional nor mechanical assessment. *Clinical data:* Breast reconstruction in 24 patients supported the safety of the material and technical efficiency, although postoperative seroma formation was reported as risk
Veritas	[228, 384]	[384]	[269]	*In vitro*: Studies on biochemical and biophysical properties have shown low ECM structure preservation, low thermal stability and low resistance to enzymatic degradation *In vivo*: Moderate inflammation in a full thickness abdominal defect in monkeys (higher than a dermal xenograft but lower to crosslinked xenografts), but a fast resorption *Clinical data:* Retrospective multicentre study on 54 patients showed low rate of complications, at a similar or lower level than those observed in allogeneic dermal matrix products

XCM Biologic® Tissue Matrix	-	[383]	[280]	*In vivo:* In a ventral hernia rabbit model, similar results in integration when compared to other two non-crosslinked dermal xenografts, although it did not show the optimal performance regarding collagen deposition and mechanical properties *Clinical data:* Higher pain relief and functionality recovery in rotator cuff massive tears than those treated with porcine SIS or equine pericardium in a study including 22 patients
XenMatrix ™	[228, 384]	[384]	-	*In vitro*: Lower preservation of ECM structure and resistance to collagenase degradation than other dermal xenografts and native tissue, and higher enzymatic degradability than crosslinked xenografts *In vivo*: Severe inflammatory response by the host in an abdominal wall defect in monkeys

Vascular replacement xenografts (e.g. crosslinked bovine vein, bovine ureter) have mainly resulted in failure [312-314]. These poor outcomes were related to inappropriate processing, which resulted in insufficient mechanical properties to support the pressure of the circulatory system [315] and low antigen removal [316]. Having said that, recent reports on bovine artery crosslinked with starch dialdehyde (as opposed to GTA) have shown positive results as haemodialysis access [317] or as lower extremity bypass [318]. However, their implantation is not a generalised procedure, as their performance has not improved synthetic grafting. Further efforts in the processing technology and recellularisation of the grafts are needed to improve the current outcomes [319].

In the field of valve replacement, the use of the stented valves is a common procedure, which utilises metal / polymeric stents and processed animal tissue (e.g. bovine or porcine cardiac tissue processed with glutaraldehyde and anti-calcification solvent). Stented valves were established in clinical practice due to their effective performance in adult patients and low rate of complications [320, 321] and reduced long-term calcification [322]. Stentless analogue valves have been also designed to obtain hemodynamic patterns closer to physiological levels and are clinically available [323], demonstrating similar clinical success to stented ones in a long-term basis and less complications in the early stages after implantation [324, 325]. However, no reliable valve replacement graft is available for paediatric patients with congenital heart diseases [326], where decellularisation and recellularisation is the main option to overcome the limitations that tissue grafts present in valve repair [327, 328].

1.4. Conclusions and future perspectives

The low availability of autologous and allogeneic tissues, coupled with advances in decellularisation, crosslinking, sterilisation and preservation, have made numerous, primarily, porcine and bovine xenografts commercially and clinically available for a diverse range of tissue engineering and regenerative medicine applications. In general, non-crosslinked grafts (in particular, grafts from young animals) demonstrate better resorption for tissues that do not require mechanical resilience. Crosslinking, although significantly improves mechanical properties, is often associated with immune response and calcification, imposing the need for development and assessment of new methods. Although preclinical and clinical studies have demonstrated, in most cases, safety and efficacy, the field urgently requires randomised double-blinded clinical trials to safely conclude on the potential of a specific xenograft for a specific clinical indication. Considering the, unmatched by human-made devices, physicochemical and biological

similarity of xenografts to human tissues, we believe that xenografts will continue gaining pace in modern regenerative medicine.

1.6. References

[1] J.M. Grasman, M.J. Zayas, R.L. Page, G.D. Pins, Biomimetic scaffolds for regeneration of volumetric muscle loss in skeletal muscle injuries, Acta Biomater 25 (2015) 2-15.

[2] G.C. Gurtner, M.A. Chapman, Regenerative medicine: Charting a new course in wound healing, Adv Wound Care 5(7) (2016) 314-328.

[3] S.U. Kim, H.J. Lee, Y.B. Kim, Neural stem cell-based treatment for neurodegenerative diseases, Neuropathology 33(5) (2013) 491-504.

[4] P.P. Lui, Stem cell technology for tendon regeneration: current status, challenges, and future research directions, Stem Cells Cloning 8 (2015) 163-74.

[5] A.R. Shrivats, M.C. McDermott, J.O. Hollinger, Bone tissue engineering: State of the union, Drug Discov Today 19(6) (2014) 781-786.

[6] B.O. Diekman, F. Guilak, Stem cell-based therapies for osteoarthritis: Challenges and opportunities, Curr Opin Rheumatol 25(1) (2013) 119-126.

[7] N. Ojeh, I. Pastar, M. Tomic-Canic, O. Stojadinovic, Stem cells in skin regeneration, wound healing, and their clinical applications, Int J Mol Sci 16(10) (2015) 25476-25501.

[8] A. Bajek, N. Gurtowska, J. Olkowska, L. Kazmierski, M. Maj, T. Drewa, Adipose-derived stem cells as a tool in cell-based therapies, Arch Immunol Ther Exp (Warsz) 64(6) (2016) 443-454.

[9] J.A. Heslop, T.G. Hammond, I. Santeramo, A. Tort Piella, I. Hopp, J. Zhou, R. Baty, E.I. Graziano, B. Proto Marco, A. Caron, P. Skold, P.W. Andrews, M.A. Baxter, D.C. Hay, J. Hamdam, M.E. Sharpe, S. Patel, D.R. Jones, J. Reinhardt, E.H. Danen, U. Ben-David, G. Stacey, P. Bjorquist, J. Piner, J. Mills, C. Rowe, G. Pellegrini, S. Sethu, D.J. Antoine, M.J. Cross, P. Murray, D.P. Williams, N.R. Kitteringham, C.E. Goldring, B.K. Park, Concise review: workshop review: understanding and assessing the risks of stem cell-based therapies, Stem Cells Transl Med 4(4) (2015) 389-400.

[10] C. Qi, X. Yan, C. Huang, A. Melerzanov, Y. Du, Biomaterials as carrier, barrier and reactor for cell-based regenerative medicine, Protein & Cell 6(9) (2015) 638-653.

[11] S. Lee, E. Choi, M.-J. Cha, K.-C. Hwang, Cell adhesion and long-term survival of transplanted mesenchymal stem cells: a prerequisite for cell therapy, Oxid Med Cell Longev 2015 (2015) 632902.

[12] M. Mimeault, R. Hauke, S.K. Batra, Stem cells: A revolution in therapeutics—recent advances in stem cell biology and their therapeutic applications in regenerative medicine and cancer therapies, Clin Pharmacol Ther 82(3) (2007) 252-264.

[13] M.A. Lilly, M.F. Davis, J.E. Fabie, E.B. Terhune, G.I. Gallicano, Current stem cell based therapies in diabetes, Am J Stem Cells 5(3) (2016) 87-98.

[14] R. Cancedda, B. Dozin, P. Giannoni, R. Quarto, Tissue engineering and cell therapy of cartilage and bone, Matrix Biol 22(1) (2003) 81-91.

[15] K.P. Fuller, D. Gaspar, L.M. Delgado, A. Pandit, D.I. Zeugolis, Influence of porosity and pore shape on structural, mechanical and biological properties of poly ϵ-caprolactone electro-spun fibrous scaffolds, Nanomedicine 11(9) (2016) 1031-1040.

[16] A.A. Chaudhari, K. Vig, D.R. Baganizi, R. Sahu, S. Dixit, V. Dennis, S.R. Singh, S.R. Pillai, Future prospects for scaffolding methods and biomaterials in skin tissue engineering: A review, Int J Mol Sci 17(12) (2016) 1974.

[17] F.M. Chen, X. Liu, Advancing biomaterials of human origin for tissue engineering, Prog Polym Sci 53 (2016) 86-168.

[18] K. Sadtler, M.T. Wolf, S. Ganguly, C.A. Moad, L. Chung, S. Majumdar, F. Housseau, D.M. Pardoll, J.H. Elisseeff, Divergent immune responses to synthetic and biological scaffolds, Biomaterials (2018).

[19] A. Sorushanova, L.M. Delgado, Z. Wu, N. Shologu, A. Kshirsagar, R. Raghunath, A.M. Mullen, Y. Bayon, A. Pandit, M. Raghunath, D.I. Zeugolis, The Collagen Suprafamily: From Biosynthesis to Advanced Biomaterial Development, Adv Mater 31(1) (2019) e1801651.

[20] W.L. Stoppel, C.E. Ghezzi, S.L. McNamara, L.D.B. III, D.L. Kaplan, Clinical applications of naturally derived biopolymer-based scaffolds for regenerative medicine, Ann Biomed Eng 43(3) (2015) 657-680.

[21] N. Shanmugasundaram, T. Ravikumar, M. Babu, Comparative physico-chemical and in vitro properties of fibrillated collagen scaffolds from different sources, J Biomater Appl 18(4) (2004) 247-64.

[22] D.J. Cannon, P.F. Davison, Aging, and crosslinking in mammalian collagen, Exp Aging Res 3(2) (1977) 87-105.

[23] T.L. Willett, R.S. Labow, I.G. Aldous, N.C. Avery, J.M. Lee, Changes in collagen with aging maintain molecular stability after overload: evidence from an in vitro tendon model, J Biomech Eng 132(3) (2010) 031002-031002-8.

[24] S. Browne, D.I. Zeugolis, A. Pandit, Collagen: finding a solution for the source, Tissue Eng Part A 19(13-14) (2013) 1491-4.

[25] S. Ghanaati, M. Barbeck, P. Booms, J. Lorenz, C.J. Kirkpatrick, R.A. Sader, Potential lack of "standardized" processing techniques for production of allogeneic and xenogeneic bone blocks for application in humans, Acta Biomater 10(8) (2014) 3557-3562.

[26] J.E. Reing, B.N. Brown, K.A. Daly, J.M. Freund, T.W. Gilbert, S.X. Hsiong, A. Huber, K.E. Kullas, S. Tottey, M.T. Wolf, S.F. Badylak, The effects of processing methods upon mechanical and biologic properties of porcine dermal extracellular matrix scaffolds, Biomaterials 31(33) (2010) 8626-8633.

[27] T.J. Keane, S.F. Badylak, The host response to allogeneic and xenogeneic biological scaffold materials, J Tissue Eng Regen Med 9(5) (2015) 504-511.

[28] C. Schoepf, The Tutoplast® Process: a review of efficacy, Zimmer Dental 17 (2008) 40-50.

[29] H.B. Colaço, B.R. Lord, D.L. Back, A.J. Davies, A.A. Amis, A. Ajuied, Biomechanical properties of bovine tendon xenografts treated with a modern processing method, J Biomech 53 (2017) 144-147.

[30] C. Williams, E. Ingham, J. Dixon-Hardy, J. Egan, A popperian analysis of translation in biological science, ISPIM Innovation Symposium, The International Society for Professional Innovation Management (ISPIM), 2013, p. 1.

[31] Medical devices containing materials derived from animal sources (Except for in vitro diagnostic devices), in: FDA (Ed.) 2019.

[32] Source animal, product, preclinical, and clinical issues concerning the use of xenotransplantation products in humans, in: FDA (Ed.) 2016.

[33] FDA Animal products database data entry form, in: FDA (Ed.) 1998.

[34] G. Mulder, D.K. Lee, A retrospective clinical review of extracellular matrices for tissue reconstruction: equine pericardium as a biological covering to assist with wound closure, Wounds 21(9) (2009) 254-61.

[35] W.T. DeCarbo, B.M. Feldner, C.F. Hyer, Inflammatory reaction to implanted equine pericardium xenograft, J Foot Ankle Surg 49(2) (2010) 155-8.

[36] S. Lun, S.M. Irvine, K.D. Johnson, N.J. Fisher, E.W. Floden, L. Negron, S.G. Dempsey, R.J. McLaughlin, M. Vasudevamurthy, B.R. Ward, B.C.H. May, A functional extracellular matrix biomaterial derived from ovine forestomach, Biomaterials 31(16) (2010) 4517-4529.

[37] S.K. Gupta, A.K. Dinda, P.D. Potdar, N.C. Mishra, Fabrication and characterization of scaffold from cadaver goat-lung tissue for skin tissue engineering applications, Mater Sci Eng C Mater Biol Appl 33(7) (2013) 4032-8.

[38] W.M. Neethling, S. Cooper, J.J. Van Den Heever, J. Hough, A.J. Hodge, Evaluation of kangaroo pericardium as an alternative substitute for reconstructive cardiac surgery, J Cardiovasc Surg (Torino) 43(3) (2002) 301-6.

[39] V. Kumar, N. Kumar, A.K. Gangwar, A.C. Saxena, Using acellular aortic matrix to repair umbilical hernias of calves, Aust Vet J 91(6) (2013) 251-253.

[40] M.M. Maestro, J. Turnay, N. Olmo, P. Fernández, D. Suárez, J.M.G. Páez, S. Urillo, M.A. Lizarbe, E. Jorge-Herrero, Biochemical and mechanical behavior of ostrich pericardium as a new biomaterial, Acta Biomater 2(2) (2006) 213-219.

[41] H.T. Zhu, L. Yu, Y. Lyu, B. Wang, Optimal pig donor selection in islet xenotransplantation: current status and future perspectives, J Zhejiang Univ Sci B 15(8) (2014) 681-91.

[42] N.J. Turner, D. Pezzone, S.F. Badylak, Regional variations in the histology of porcine skin, Tissue Eng Part C Methods 21(4) (2015) 373-84.

[43] M.S. Sacks, C.J.C. Chuong, R. More, Collagen fiber architecture of bovine pericardium, ASAIO J 40(3) (1994) M632-M637.

[44] D.K.C. Cooper, Y. Ye, L.L. Rolf, N. Zuhdi, The pig as potential organ donor for man, in: D.K.C. Cooper, E. Kemp, K. Reemtsma, D.J.G. White (Eds.), Xenotransplantation, Springer Berlin Heidelberg, Berlin, Heidelberg, 1991, pp. 481-500.

[45] S. Debeer, J.B. Le Luduec, D. Kaiserlian, P. Laurent, J.F. Nicolas, B. Dubois, J. Kanitakis, Comparative histology and immunohistochemistry of porcine versus human skin, Eur J Dermatol 23(4) (2013) 456-66.

[46] P.P. Lelovas, N.G. Kostomitsopoulos, T.T. Xanthos, A comparative anatomic and physiologic overview of the porcine heart, J Am Assoc Lab Anim Sci 53(5) (2014) 432-8.

[47] M. Omar, A. Dratzidis, M. Klintschar, S. Kwisda, C. Krettek, M. Ettinger, Are porcine flexor digitorum profundus tendons suitable graft substitutes for human hamstring tendons in biomechanical in vitro-studies?, Arch Orthop Trauma Surg 136(5) (2016) 681-686.

[48] C. Domnick, B. Wieskötter, M.J. Raschke, M. Schulze, D. Kronenberg, M. Wefelmeier, M.F. Langer, M. Herbort, Evaluation of biomechanical properties: are porcine flexor tendons and bovine extensor tendons eligible surrogates for human tendons in in vitro studies?, Arch Orthop Trauma Surg 136(10) (2016) 1465-1471.

[49] B.L. Proffen, M. McElfresh, B.C. Fleming, M.M. Murray, A comparative anatomical study of the human knee and six animal species, Knee 19(4) (2012) 493-9.

[50] M. Hryhorowicz, J. Zeyland, R. Słomski, D. Lipiński, Genetically modified pigs as organ donors for xenotransplantation, Mol Biotechnol 59(9-10) (2017) 435-444.

[51] M. Wijkstrom, H. Iwase, W. Paris, H. Hara, M. Ezzelarab, D.K.C. Cooper, Renal xenotransplantation: experimental progress and clinical prospects, Kidney Int 91(4) (2017) 790-796.

[52] D.A. Leonard, C. Mallard, A. Albritton, R. Torabi, M. Mastroianni, D.H. Sachs, J.M. Kurtz, C.L. Cetrulo, Jr., Skin grafts from genetically modified α-1,3-galactosyltransferase knockout miniature swine: A functional equivalent to allografts, Burns 43(8) (2017) 1717-1724.

[53] A.A.L. Barone, M. Mastroianni, E.A. Farkash, C. Mallard, A. Albritton, R. Torabi, D.A. Leonard, J.M. Kurtz, D.H. Sachs, C.L. Cetrulo Jr, Genetically modified porcine split-thickness skin grafts as an alternative to allograft for provision of temporary wound coverage: preliminary characterization, Burns 41(3) (2015) 565-574.

[54] Z. Zhang, X. Li, H. Zhang, X. Zhang, H. Chen, D. Pan, H. Ji, L. Zhou, J. Ling, J. Zhou, S. Yue, D. Wang, Z. Yang, K. Tao, K. Dou, Cytokine profiles in Tibetan macaques following α-1,3-galactosyltransferase-knockout pig liver xenotransplantation, Xenotransplantation 24(5) (2017) e12321.

[55] X. Dong, H. Hara, Y. Wang, L. Wang, Y. Zhang, D.K.C. Cooper, Y. Dai, Z. Pan, Initial study of α1,3-galactosyltransferase gene-knockout/CD46 pig full-thickness corneal xenografts in rhesus monkeys, Xenotransplantation 24(1) (2017) e12282.

[56] H. Iwase, H. Hara, M. Ezzelarab, T. Li, Z. Zhang, B. Gao, H. Liu, C. Long, Y. Wang, A. Cassano, E. Klein, C. Phelps, D. Ayares, A. Humar, M. Wijkstrom, D.K.C. Cooper, Immunological and physiological observations in baboons with life-supporting genetically engineered pig kidney grafts, Xenotransplantation 24(2) (2017) 10.1111/xen.12293.

[57] T. Moriguchi, D. Fujimoto, Age-related changes in the content of the collagen crosslink, pyridinoline, J Biochem 84(4) (1978) 933-5.

[58] K. Lynch, M. Pei, Age associated communication between cells and matrix: a potential impact on stem cell-based tissue regeneration strategies, Organogenesis 10(3) (2014) 289-298.

[59] A. Kurtz, S.-J. Oh, Age related changes of the extracellular matrix and stem cell maintenance, Prev Med 54, Supplement (2012) S50-S56.

[60] L.M. Godin, B.J. Sandri, D.E. Wagner, C.M. Meyer, A.P. Price, I. Akinnola, D.J. Weiss, A. Panoskaltsis-Mortari, Decreased laminin expression by human lung epithelial

cells and fibroblasts cultured in acellular lung scaffolds from aged mice, PLoS One 11(3) (2016) e0150966.

[61] J. Labat-Robert, Cell–matrix interactions in aging: role of receptors and matricryptins, Ageing Research Reviews 3(2) (2004) 233-247.

[62] S. Tottey, S.A. Johnson, P.M. Crapo, J.E. Reing, L. Zhang, H. Jiang, C.J. Medberry, B. Reines, S.F. Badylak, The effect of source animal age upon extracellular matrix scaffold properties, Biomaterials 32(1) (2011) 128-136.

[63] B.M. Sicari, S.A. Johnson, B.F. Siu, P.M. Crapo, K.A. Daly, H. Jiang, C.J. Medberry, S. Tottey, N.J. Turner, S.F. Badylak, The effect of source animal age upon the in vivo remodeling characteristics of an extracellular matrix scaffold, Biomaterials 33(22) (2012) 5524-5533.

[64] S. Vaishnav, C. Thomas Vangsness Jr, New techniques in allograft tissue processing, Clin Sports Med 28(1) (2009) 127-141.

[65] J.A. Fishman, L. Scobie, Y. Takeuchi, Xenotransplantation-associated infectious risk: a WHO consultation, Xenotransplantation 19(2) (2012) 72-81.

[66] S.-A. Busby, C. Crossan, J. Godwin, B. Petersen, C. Galli, E. Cozzi, Y. Takeuchi, L. Scobie, Suggestions for the diagnosis and elimination of hepatitis E virus in pigs used for xenotransplantation, Xenotransplantation 20(3) (2013) 188-192.

[67] J.A. Fishman, C. Patience, Xenotransplantation: Infectious risk revisited, Am J Transplant 4(9) (2004) 1383-1390.

[68] PHS guideline on infectious disease issues on xenotransplantation, in: FDA (Ed.) 2001.

[69] M.B. Ezzelarab, B. Ekser, A. Azimzadeh, C.C. Lin, Y. Zhao, R. Rodriguez, G.J. Echeverri, H. Iwase, C. Long, H. Hara, D. Ayares, R.N. Pierson, A.W. Thomson, D.K.C. Cooper, Systemic inflammation in xenograft recipients precedes activation of coagulation, Xenotransplantation 22(1) (2015) 32-47.

[70] B.N. Brown, J.E. Valentin, A.M. Stewart-Akers, G.P. McCabe, S.F. Badylak, Macrophage phenotype and remodeling outcomes in response to biologic scaffolds with and without a cellular component, Biomaterials 30(8) (2009) 1482-1491.

[71] T.J. Keane, R. Londono, N.J. Turner, S.F. Badylak, Consequences of ineffective decellularization of biologic scaffolds on the host response, Biomaterials 33(6) (2012) 1771-1781.

[72] R.V. Iozzo, Perlecan: A gem of a proteoglycan, Matrix Biol 14(3) (1994) 203-208.

[73] C.D. Constantinou, S.A. Jimenez, Structure of cDNAs encoding the triple-helical domain of murine α2 (VI) collagen chain and comparison to human and chick

homologues. Use of polymerase chain reaction and partially degenerate oligonucleotides for generation of novel cDNA clones, Matrix 11(1) (1991) 1-9.

[74] K. Takahara, G.G. Hoffman, D.S. Greenspan, Complete structural organization of the human α1(V) collagen gene (COL5A1): Divergence from the conserved organization of other characterized fibrillar collagen genes, Genomics 29(3) (1995) 588-597.

[75] M. Okumura, R.J. Matthews, B. Robb, G.W. Litman, P. Bork, M.L. Thomas, Comparison of CD45 extracellular domain sequences from divergent vertebrate species suggests the conservation of three fibronectin type III domains, The Journal of Immunology 157(4) (1996) 1569-1575.

[76] C. Liu, S.D. Dib-Hajj, S.G. Waxman, Fibroblast growth factor homologous factor 1B binds to the C terminus of the tetrodotoxin-resistant sodium channel rNav1.9a (NaN), J Biol Chem 276(22) (2001) 18925-33.

[77] M.T. Kasimir, E. Rieder, G. Seebacher, A. Nigisch, B. Dekan, E. Wolner, G. Weigel, P. Simon, Decellularization does not eliminate thrombogenicity and inflammatory stimulation in tissue-engineered porcine heart valves, J Heart Valve Dis 15(2) (2006) 278-86; discussion 286.

[78] M. Sandor, H. Xu, J. Connor, J. Lombardi, J.R. Harper, R.P. Silverman, D.J. McQuillan, Host response to implanted porcine-derived biologic materials in a primate model of abdominal wall repair, Tissue Eng Part A 14(12) (2008) 2021-31.

[79] F.O. Martinez, Macrophage activation and polarization, Front Biosci 13(13) (2008) 453.

[80] S.F. Badylak, T.W. Gilbert, Immune response to biologic scaffold materials, Semin Immunol 20(2) (2008) 109-116.

[81] M.J. Cronce, R.A. Faulknor, I. Pomerantseva, X.H. Liu, S.M. Goldman, E.C. Ekwueme, O. Mwizerwa, C.M. Neville, C.A. Sundback, In vivo response to decellularized mesothelium scaffolds, J Biomed Mater Res B Appl Biomater 106(2) (2018) 716-725.

[82] A.J. Allman, T.B. McPherson, S.F. Badylak, L.C. Merrill, B. Kallakury, C. Sheehan, R.H. Raeder, D.W. Metzger, Xenogeneic extracellular matrix grafts elicit a Th2-restricted immune response, Transplantation 71(11) (2001) 1631-1640.

[83] M.T. Wolf, S. Ganguly, T.L. Wang, C.W. Anderson, K. Sadtler, R. Narain, C. Cherry, A.J. Parrillo, B.V. Park, G. Wang, F. Pan, S. Sukumar, D.M. Pardoll, J.H. Elisseeff, A biologic scaffold-associated type 2 immune microenvironment inhibits tumor formation and synergizes with checkpoint immunotherapy, Sci Transl Med 11(477) (2019).

[84] K. Sadtler, S.D. Sommerfeld, M.T. Wolf, X. Wang, S. Majumdar, L. Chung, D.S. Kelkar, A. Pandey, J.H. Elisseeff, Proteomic composition and immunomodulatory properties of urinary bladder matrix scaffolds in homeostasis and injury, Semin Immunol 29 (2017) 14-23.

[85] T.W. Gilbert, T.L. Sellaro, S.F. Badylak, Decellularization of tissues and organs, Biomaterials 27(19) (2006) 3675-3683.

[86] B. Ma, X. Wang, C. Wu, J. Chang, Crosslinking strategies for preparation of extracellular matrix-derived cardiovascular scaffolds, Regen Biomater 1(1) (2014) 81-9.

[87] D.I. Zeugolis, G.R. Paul, G. Attenburrow, Cross-linking of extruded collagen fibers--a biomimetic three-dimensional scaffold for tissue engineering applications, J Biomed Mater Res A 89(4) (2009) 895-908.

[88] L.M. Delgado, K. Fuller, D.I. Zeugolis, (*) Collagen Cross-Linking: Biophysical, Biochemical, and Biological Response Analysis, Tissue Eng Part A 23(19-20) (2017) 1064-1077.

[89] P. Sinha, D. Zurakowski, T.K. Kumar, D. He, C. Rossi, R.A. Jonas, Effects of glutaraldehyde concentration, pretreatment time, and type of tissue (porcine versus bovine) on postimplantation calcification, J Thorac Cardiovasc Surg 143(1) (2012) 224-7.

[90] J.K. McDade, E.P. Brennan-Pierce, M.B. Ariganello, R.S. Labow, J. Michael Lee, Interactions of U937 macrophage-like cells with decellularized pericardial matrix materials: Influence of crosslinking treatment, Acta Biomater 9(7) (2013) 7191-7199.

[91] I. Sallent, H. Capella-Monsonis, D.I. Zeugolis, Production and Characterization of Chemically Cross-Linked Collagen Scaffolds, Methods in molecular biology (Clifton, N.J.) 1944 (2019) 23-38.

[92] H.W. Sung, R.N. Huang, L.L. Huang, C.C. Tsai, C.T. Chiu, Feasibility study of a natural crosslinking reagent for biological tissue fixation, J Biomed Mater Res 42(4) (1998) 560-567.

[93] H.-W. Sung, R.-N. Huang, L.L.H. Huang, C.-C. Tsai, In vitro evaluation of cytotoxicity of a naturally occurring cross-linking reagent for biological tissue fixation, J Biomater Sci Polym Ed 10(1) (1999) 63-78.

[94] Y. Chang, C.-C. Tsai, H.-C. Liang, H.-W. Sung, In vivo evaluation of cellular and acellular bovine pericardia fixed with a naturally occurring crosslinking agent (genipin), Biomaterials 23(12) (2002) 2447-2457.

[95] H.G. Lim, S.H. Kim, S.Y. Choi, Y.J. Kim, Anticalcification effects of decellularization, solvent, and detoxification treatment for genipin and glutaraldehyde fixation of bovine pericardium, Eur J Cardiothorac Surg 41(2) (2012) 383-90.

[96] A. Dziedzic-Goclawska, A. Kaminski, I. Uhrynowska-Tyszkiewicz, W. Stachowicz, Irradiation as a safety procedure in tissue banking, Cell Tissue Bank 6(3) (2005) 201-19.

[97] J.J. Song, H.C. Ott, Organ engineering based on decellularized matrix scaffolds, Trends Mol Med 17(8) (2011) 424-432.

[98] L.M. Delgado, A. Pandit, D.I. Zeugolis, Influence of sterilisation methods on collagen-based devices stability and properties, Expert Rev Med Devices 11(3) (2014) 305-314.

[99] H. Nguyen, D.A. Morgan, M.R. Forwood, Sterilization of allograft bone: effects of gamma irradiation on allograft biology and biomechanics, Cell Tissue Bank 8(2) (2007) 93-105.

[100] A.M. Matuska, P.S. McFetridge, The effect of terminal sterilization on structural and biophysical properties of a decellularized collagen-based scaffold; implications for stem cell adhesion, J Biomed Mater Res B Appl Biomater 103(2) (2015) 397-406.

[101] D. Bui, V. Lovric, R. Oliver, N. Bertollo, D. Broe, W.R. Walsh, Meniscal allograft sterilisation: effect on biomechanical and histological properties, Cell Tissue Bank 16(3) (2015) 467-75.

[102] R.S. Hennessy, S. Jana, B.J. Tefft, M.R. Helder, M.D. Young, R.R. Hennessy, N.J. Stoyles, A. Lerman, Supercritical carbon dioxide-based sterilization of decellularized heart valves, JACC Basic Transl Sci 2(1) (2017) 71-84.

[103] J.L. Balestrini, A. Liu, A.L. Gard, J. Huie, K.M. Blatt, J. Schwan, L. Zhao, T.J. Broekelmann, R.P. Mecham, E.C. Wilcox, L.E. Niklason, Sterilization of Lung Matrices by Supercritical Carbon Dioxide, Tissue Eng Part C Methods 22(3) (2016) 260-9.

[104] W.S. Sheridan, G.P. Duffy, B.P. Murphy, Optimum parameters for freeze-drying decellularized arterial scaffolds, Tissue Eng Part C Methods 19(12) (2013) 981-90.

[105] R. Sridharan, R.B. Reilly, C.T. Buckley, Decellularized grafts with axially aligned channels for peripheral nerve regeneration, J Mech Behav Biomed Mater 41 (2015) 124-35.

[106] S. Wang, T. Goecke, C. Meixner, A. Haverich, A. Hilfiker, W.F. Wolkers, Freeze-dried heart valve scaffolds, Tissue Eng Part C Methods 18(7) (2012) 517-25.

[107] M. Gallo, A. Bonetti, H. Poser, F. Naso, T. Bottio, R. Bianco, A. Paolin, P. Franci, R. Busetto, A.C. Frigo, E. Buratto, M. Spina, M. Marchini, F. Ortolani, L. Iop, G. Gerosa, Decellularized aortic conduits: could their cryopreservation affect post-implantation

outcomes? A morpho-functional study on porcine homografts, Heart Vessels 31(11) (2016) 1862-1873.

[108] M. Seifert, A. Bayrak, M. Stolk, N. Souidi, M. Schneider, U.A. Stock, K.G.M. Brockbank, Xeno-immunogenicity of ice-free cryopreserved porcine leaflets, J Surg Res 193(2) (2015) 933-941.

[109] W.B. Martin, R. Sicard, S.M. Namin, T. Ganey, Methods of cryoprotectant preservation: Allogeneic cellular bone grafts and potential effects, Biomed Res Int 2019 (2019) 5025398.

[110] T.W. Gilbert, J.M. Freund, S.F. Badylak, Quantification of DNA in biologic scaffold materials, J Surg Res 152(1) (2009) 135-139.

[111] H. Capella-Monsonis, J.Q. Coentro, V. Graceffa, Z. Wu, D.I. Zeugolis, An experimental toolbox for characterization of mammalian collagen type I in biological specimens, Nat Protoc 13(3) (2018) 507-529.

[112] P. Brun, P. Brun, M. Vono, P. Venier, E. Tarricone, V. Deligianni, E. Martines, M. Zuin, S. Spagnolo, R. Cavazzana, R. Cardin, I. Castagliuolo, A. La Gloria Valerio, A. Leonardi, Disinfection of ocular cells and tissues by atmospheric-pressure cold plasma, PLoS One 7(3) (2012) e33245.

[113] T.J. Keane, I.T. Swinehart, S.F. Badylak, Methods of tissue decellularization used for preparation of biologic scaffolds and in vivo relevance, Methods 84 (2015) 25-34.

[114] P.M. Crapo, T.W. Gilbert, S.F. Badylak, An overview of tissue and whole organ decellularization processes, Biomaterials 32(12) (2011) 3233-3243.

[115] T. Pennel, G. Fercana, D. Bezuidenhout, A. Simionescu, T.-H. Chuang, P. Zilla, D. Simionescu, The performance of cross-linked acellular arterial scaffolds as vascular grafts; pre-clinical testing in direct and isolation loop circulatory models, Biomaterials 35(24) (2014) 6311-6322.

[116] R.E. De Filippo, J.J. Yoo, A. Atala, Urethral replacement using cell seeded tubularized collagen matrices, J Urol 168(4, Supplement) (2002) 1789-1793.

[117] D.J. Rosario, G.C. Reilly, E. Ali Salah, M. Glover, A.J. Bullock, S. MacNeil, Decellularization and sterilization of porcine urinary bladder matrix for tissue engineering in the lower urinary tract, Regen Med 3(2) (2008) 145-156.

[118] H. Aubin, A. Kranz, J. Hülsmann, A. Lichtenberg, P. Akhyari, Decellularized whole heart for bioartificial heart, Methods Mol Biol 1036 (2013) 163-178.

[119] P.-F. Lee, E. Chau, R. Cabello, A.T. Yeh, L.C. Sampaio, A.S. Gobin, D.A. Taylor, Inverted orientation improves decellularization of whole porcine hearts, Acta Biomater 49 (2017) 181-191.

[120] A. Weymann, N.P. Patil, A. Sabashnikov, S. Korkmaz, S. Li, P. Soos, R. Ishtok, N. Chaimow, I. Pätzold, N. Czerny, B. Schmack, A.-F. Popov, A.R. Simon, M. Karck, G. Szabo, Perfusion-decellularization of porcine lung and trachea for respiratory bioengineering, Artif Organs 39(12) (2015) 1024-1032.

[121] I. Fathi, H. Elhammady, M. Sakr, A. Nabawi, M. Marei, Rapid hepatic perfusion decellularization: technique and critique, Xenotransplantation 22(6) (2015) 451-457.

[122] Y. Wang, J. Bao, Q. Wu, Y. Zhou, Y. Li, X. Wu, Y. Shi, L. Li, H. Bu, Method for perfusion decellularization of porcine whole liver and kidney for use as a scaffold for clinical-scale bioengineering engrafts, Xenotransplantation 22(1) (2015) 48-61.

[123] D.C. Sullivan, S.-H. Mirmalek-Sani, D.B. Deegan, P.M. Baptista, T. Aboushwareb, A. Atala, J.J. Yoo, Decellularization methods of porcine kidneys for whole organ engineering using a high-throughput system, Biomaterials 33(31) (2012) 7756-7764.

[124] A.K. Nowocin, A. Southgate, S.M. Gabe, T. Ansari, Biocompatibility and potential of decellularized porcine small intestine to support cellular attachment and growth, J Tissue Eng Regen Med 10(1) (2016) E23-33.

[125] J. Zhang, Z.Q. Hu, N.J. Turner, S.F. Teng, W.Y. Cheng, H.Y. Zhou, L. Zhang, H.W. Hu, Q. Wang, S.F. Badylak, Perfusion-decellularized skeletal muscle as a three-dimensional scaffold with a vascular network template, Biomaterials 89 (2016) 114-126.

[126] B.J. Jank, J. Goverman, J.P. Guyette, J.M. Charest, M. Randolph, G.R. Gaudette, J.R. Gershlak, M. Purschke, E. Javorsky, R.M. Nazarian, D.A. Leonard, C.L. Cetrulo, W.G. Austen, H.C. Ott, Creation of a Bioengineered Skin Flap Scaffold with a Perfusable Vascular Pedicle, Tissue Eng Part A 23(13-14) (2017) 696-707.

[127] J. Burk, I. Erbe, D. Berner, J. Kacza, C. Kasper, B. Pfeiffer, K. Winter, W. Brehm, Freeze-thaw cycles enhance decellularization of large tendons, Tissue Eng Part C Methods 20(4) (2014) 276-84.

[128] D.-W. Kang, S.-C. Shin, J.-Y. Jang, H.-Y. Park, J.-C. Lee, S.-G. Wang, B.-J. Lee, Decellularization of human nasal septal cartilage for the novel filler material of vocal fold augmentation, J Voice 31(1) (2017) 127.e1-127.e6.

[129] Y. Xu, G. Zhang, Y. Chang, Y.-x. Qiu, C. Wang, The preparation of acellular dermal matrices by freeze–thawing and ultrasonication process and the evaluation of its antigenicity, Cell Biochem Biophys 73(1) (2015) 27-33.

[130] P.N. Nonaka, J.J. Uriarte, N. Campillo, E. Melo, D. Navajas, R. Farré, L.V.F. Oliveira, Mechanical properties of mouse lungs along organ decellularization by sodium dodecyl sulfate, Respir Physiol Neurobiol 200 (2014) 1-5.

[131] H.-Y. Tuan-Mu, C.-H. Yu, J.-J. Hu, On the decellularization of fresh or frozen human umbilical arteries: Implications for small-diameter tissue engineered vascular grafts, Ann Biomed Eng 42(6) (2014) 1305-1318.

[132] L.K.Y. Chan, V.Y.L. Leung, V. Tam, W.W. Lu, K.Y. Sze, K.M.C. Cheung, Decellularized bovine intervertebral disc as a natural scaffold for xenogenic cell studies, Acta Biomater 9(2) (2013) 5262-5272.

[133] J.-X. Xiang, X.-L. Zheng, R. Gao, W.-Q. Wu, X.-L. Zhu, J.-H. Li, Y. Lv, Liver regeneration using decellularized splenic scaffold: a novel approach in tissue engineering, Hepatobiliary Pancreat Dis Int 14(5) (2015) 502-508.

[134] Q. Wang, C. Zhang, L. Zhang, W. Guo, G. Feng, S. Zhou, Y. Zhang, T. Tian, Z. Li, F. Huang, The preparation and comparison of decellularized nerve scaffold of tissue engineering, J Biomed Mater Res A 102(12) (2014) 4301-8.

[135] M. Parmaksiz, A.E. Elcin, Y.M. Elcin, Decellularization of bovine small intestinal submucosa and its use for the healing of a critical-sized full-thickness skin defect, alone and in combination with stem cells, in a small rodent model, J Tissue Eng Regen Med (2015) n/a-n/a.

[136] J.Y. Oh, M.K. Kim, H.J. Lee, J.H. Ko, W.R. Wee, J.H. Lee, Processing porcine cornea for biomedical applications, Tissue Eng Part C Methods 15(4) (2009) 635-45.

[137] U. Sarig, G.C. Au-Yeung, Y. Wang, T. Bronshtein, N. Dahan, F.Y. Boey, S.S. Venkatraman, M. Machluf, Thick acellular heart extracellular matrix with inherent vasculature: a potential platform for myocardial tissue regeneration, Tissue Eng Part A 18(19-20) (2012) 2125-37.

[138] S.H. Hung, C.H. Su, S.E. Lin, H. Tseng, Preliminary experiences in trachea scaffold tissue engineering with segmental organ decellularization, Laryngoscope 126(11) (2016) 2520-2527.

[139] S.-H. Hung, C.-H. Su, F.-P. Lee, H. Tseng, Larynx decellularization: Combining freeze-drying and sonication as an effective method, J Voice 27(3) (2013) 289-294.

[140] S.H. Kim, Y. Jung, S.H. Kim, A biocompatible tissue scaffold produced by supercritical fluid processing for cartilage tissue engineering, Tissue Eng Part C Methods 19(3) (2013) 181-8.

[141] J.K. Wang, B. Luo, V. Guneta, L. Li, S.E.M. Foo, Y. Dai, T.T.Y. Tan, N.S. Tan, C. Choong, M.T.C. Wong, Supercritical carbon dioxide extracted extracellular matrix material from adipose tissue, Mater Sci Eng C Mater Biol Appl 75 (2017) 349-358.

[142] Y. Sun, V. Lovric, T. Wang, R.A. Oliver, W.R. Walsh, Effects of SCCO2, gamma irradiation, and sodium dodecyl sulfate treatments on the initial properties of tendon allografts, Int J Mol Sci 21(5) (2020).

[143] M. Saghizadeh, M.A. Winkler, A.A. Kramerov, D.M. Hemmati, C.A. Ghiam, S.D. Dimitrijevich, D. Sareen, L. Ornelas, H. Ghiasi, W.J. Brunken, E. Maguen, Y.S. Rabinowitz, C.N. Svendsen, K. Jirsova, A.V. Ljubimov, A simple alkaline method for decellularizing human amniotic membrane for cell culture, PLoS One 8(11) (2013) e79632.

[144] N. Poornejad, L.B. Schaumann, E.M. Buckmiller, N. Momtahan, J.R. Gassman, H.H. Ma, B.L. Roeder, P.R. Reynolds, A.D. Cook, The impact of decellularization agents on renal tissue extracellular matrix, J Biomater Appl 31(4) (2016) 521-533.

[145] B. Mendoza-Novelo, E.E. Avila, J.V. Cauich-Rodríguez, E. Jorge-Herrero, F.J. Rojo, G.V. Guinea, J.L. Mata-Mata, Decellularization of pericardial tissue and its impact on tensile viscoelasticity and glycosaminoglycan content, Acta Biomater 7(3) (2011) 1241-1248.

[146] G. Falke, J.J. Yoo, T.G. Kwon, R. Moreland, A. Atala, Formation of corporal tissue architecture in vivo using human cavernosal muscle and endothelial cells seeded on collagen matrices, Tissue Eng 9(5) (2003) 871-9.

[147] J.A. Bronstein, C.Y.L. Woon, S. Farnebo, A.W. Behn, T. Schmitt, H. Pham, A.B. Castillo, J. Chang, Physicochemical decellularization of composite flexor tendon–bone interface grafts, Plast Reconstr Surg 132(1) (2013) 94-102.

[148] C.R. Deeken, A.K. White, S.L. Bachman, B.J. Ramshaw, D.S. Cleveland, T.S. Loy, S.A. Grant, Method of preparing a decellularized porcine tendon using tributyl phosphate, J Biomed Mater Res B Appl Biomater 96(2) (2011) 199-206.

[149] A.M. Kajbafzadeh, N. Javan-Farazmand, M. Monajemzadeh, A. Baghayee, Determining the optimal decellularization and sterilization protocol for preparing a tissue scaffold of a human-sized liver tissue, Tissue Eng Part C Methods 19(8) (2013) 642-51.

[150] Y. Zou, Y. Zhang, Mechanical evaluation of decellularized porcine thoracic aorta, J Surg Res 175(2) (2012) 359-368.

[151] S.R. Meyer, B. Chiu, T.A. Churchill, L. Zhu, J.R. Lakey, D.B. Ross, Comparison of aortic valve allograft decellularization techniques in the rat, J Biomed Mater Res A 79(2) (2006) 254-62.

[152] H. Ren, X. Shi, L. Tao, J. Xiao, B. Han, Y. Zhang, X. Yuan, Y. Ding, Evaluation of two decellularization methods in the development of a whole-organ decellularized rat liver scaffold, Liver Int 33(3) (2013) 448-58.

[153] S. Goktas, A.M. Matuska, N. Pierre, T.M. Gibson, J.J. Dmytryk, P.S. McFetridge, Decellularization method influences early remodeling of an allogenic tissue scaffold, J Biomed Mater Res A 102(1) (2014) 8-16.

[154] H. Xu, B. Xu, Q. Yang, X. Li, X. Ma, Q. Xia, Y. Zhang, C. Zhang, Y. Wu, Y. Zhang, Comparison of decellularization protocols for preparing a decellularized porcine annulus fibrosus scaffold, PLoS One 9(1) (2014) e86723.

[155] T.W. Hudson, S. Zawko, C. Deister, S. Lundy, C.Y. Hu, K. Lee, C.E. Schmidt, Optimized acellular nerve graft is immunologically tolerated and supports regeneration, Tissue Eng 10(11-12) (2004) 1641-1651.

[156] F. Moroni, T. Mirabella, Decellularized matrices for cardiovascular tissue engineering, Am J Stem Cells 3(1) (2014) 1-20.

[157] L. Gui, A. Muto, S.A. Chan, C.K. Breuer, L.E. Niklason, Development of decellularized human umbilical arteries as small-diameter vascular grafts, Tissue Eng Part A 15(9) (2009) 2665-76.

[158] T. Tsuchiya, J. Mendez, E.A. Calle, G. Hatachi, R. Doi, L. Zhao, T. Suematsu, T. Nagayasu, L.E. Niklason, Ventilation-Based Decellularization System of the Lung, Biores Open Access 5(1) (2016) 118-26.

[159] A.C. Oliveira, I. Garzón, A.M. Ionescu, V. Carriel, J.d.l.C. Cardona, M. González-Andrades, M.d.M. Pérez, M. Alaminos, A. Campos, Evaluation of small intestine grafts decellularization methods for corneal tissue engineering, PLoS One 8(6) (2013) e66538.

[160] E. Yoeruek, T. Bayyoud, C. Maurus, J. Hofmann, M.S. Spitzer, K.-U. Bartz-Schmidt, P. Szurman, Reconstruction of corneal stroma with decellularized porcine xenografts in a rabbit model, Acta Ophthalmol (Copenh) 90(3) (2012) e206-e210.

[161] B.D. Elder, S.V. Eleswarapu, K.A. Athanasiou, Extraction techniques for the decellularization of tissue engineered articular cartilage constructs, Biomaterials 30(22) (2009) 3749-3756.

[162] L.E. Flynn, The use of decellularized adipose tissue to provide an inductive microenvironment for the adipogenic differentiation of human adipose-derived stem cells, Biomaterials 31(17) (2010) 4715-4724.

[163] S. Ponce Márquez, V.S. Martínez, W. McIntosh Ambrose, J. Wang, N.G. Gantxegui, O. Schein, J. Elisseeff, Decellularization of bovine corneas for tissue engineering applications, Acta Biomater 5(6) (2009) 1839-1847.

[164] S.B. Lumpkins, N. Pierre, P.S. McFetridge, A mechanical evaluation of three decellularization methods in the design of a xenogeneic scaffold for tissue engineering the temporomandibular joint disc, Acta Biomater 4(4) (2008) 808-816.

[165] P. Maghsoudlou, F. Georgiades, H. Smith, A. Milan, P. Shangaris, L. Urbani, S.P. Loukogeorgakis, B. Lombardi, G. Mazza, C. Hagen, N.J. Sebire, M. Turmaine, S. Eaton, A. Olivo, J. Godovac-Zimmermann, M. Pinzani, P. Gissen, P. De Coppi, Optimization of liver decellularization maintains extracellular matrix micro-architecture and composition predisposing to effective cell seeding, PLoS One 11(5) (2016) e0155324.

[166] D.M. Giraldo-Gomez, B. Leon-Mancilla, M.L. Del Prado-Audelo, A. Sotres-Vega, J. Villalba-Caloca, D. Garciadiego-Cazares, M.C. Pina-Barba, Trypsin as enhancement in cyclical tracheal decellularization: Morphological and biophysical characterization, Mater Sci Eng C Mater Biol Appl 59 (2016) 930-937.

[167] S.L. Wilson, L.E. Sidney, S.E. Dunphy, H.S. Dua, A. Hopkinson, Corneal decellularization: A method of recycling unsuitable donor tissue for clinical translation?, Curr Eye Res 41(6) (2016) 769-782.

[168] R.-N. Chen, H.-O. Ho, Y.-T. Tsai, M.-T. Sheu, Process development of an acellular dermal matrix (ADM) for biomedical applications, Biomaterials 25(13) (2004) 2679-2686.

[169] H. Abdolghafoorian, P. Farnia, R.S. Sajadi Nia, A. Bahrami, A. Dorudinia, J. Ghanavi, Effect of Heart Valve Decellularization on Xenograft Rejection, Exp Clin Transplant 15(3) (2017) 329-336.

[170] A.R. Gillies, L.R. Smith, R.L. Lieber, S. Varghese, Method for decellularizing skeletal muscle without detergents or proteolytic enzymes, Tissue Eng Part C Methods 17(4) (2011) 383-9.

[171] B.-J. Min, Y.J. Kim, J.-W. Choi, S.Y. Choi, S.H. Kim, H.-G. Lim, Histologic characteristics and mechanical properties of bovine pericardium treated with decellularization and α-galactosidase: A comparative study, Korean J Thorac Cardiovasc Surg 45(6) (2012) 368-379.

[172] J. Nam, S.-Y. Choi, S.-C. Sung, H.-G. Lim, S.-s. Park, S.-H. Kim, Y.J. Kim, Changes of the structural and biomechanical properties of the bovine pericardium after the removal of α-Gal epitopes by decellularization and α-galactosidase treatment, Korean J Thorac Cardiovasc Surg 45(6) (2012) 380-389.

[173] R. Yoshida, P. Vavken, M.M. Murray, Decellularization of bovine anterior cruciate ligament tissues minimizes immunogenic reactions to alpha-gal epitopes by human peripheral blood mononuclear cells, Knee 19(5) (2012) 672-5.

[174] P. Shi, M. Gao, Q. Shen, L. Hou, Y. Zhu, J. Wang, Biocompatible surgical meshes based on decellularized human amniotic membrane, Mater Sci Eng C Mater Biol Appl 54 (2015) 112-9.

[175] S. Park, S.H. Kim, H.-G. Lim, C. Lim, Y.J. Kim, The anti-calcification effect of dithiobispropionimidate, carbodiimide and ultraviolet irradiation cross-linking compared to glutaraldehyde in rabbit implantation models, Korean J Thorac Cardiovasc Surg 46(1) (2013) 1-13.

[176] Y. Hu, L. Liu, W. Dan, N. Dan, Z. Gu, X. Yu, Synergistic effect of carbodiimide and dehydrothermal crosslinking on acellular dermal matrix, Int J Biol Macromol 55 (2013) 221-230.

[177] A.D. Bhrany, C.J. Lien, B.L. Beckstead, N.D. Futran, N.H. Muni, C.M. Giachelli, B.D. Ratner, Crosslinking of an oesophagus acellular matrix tissue scaffold, J Tissue Eng Regen Med 2(6) (2008) 365-372.

[178] Y. Wang, J. Bao, X. Wu, Q. Wu, Y. Li, Y. Zhou, L. Li, H. Bu, Genipin crosslinking reduced the immunogenicity of xenogeneic decellularized porcine whole-liver matrices through regulation of immune cell proliferation and polarization, Sci Rep 6 (2016) 24779.

[179] T. Fujisato, K. Tomihata, Y. Tabata, Y. Iwamoto, K. Burczak, Y. Ikada, Cross-linking of amniotic membranes, J Biomater Sci Polym Ed 10(11) (1999) 1171-1181.

[180] C. Weissenstein, P. Human, D. Bezuidenhout, P. Zilla, Glutaraldehyde detoxification in addition to enhanced amine cross-linking dramatically reduces bioprosthetic tissue calcification in the rat model, J Heart Valve Dis 9(2) (2000) 230-40.

[181] P. Zilla, L. Fullard, P. Trescony, J. Meinhart, D. Bezuidenhout, M. Gorlitzer, P. Human, U. von Oppell, Glutaraldehyde detoxification of aortic wall tissue: a promising perspective for emerging bioprosthetic valve concepts, J Heart Valve Dis 6(5) (1997) 510-20.

[182] J.J. Glynn, E.G. Polsin, M.T. Hinds, Crosslinking decreases the hemocompatibility of decellularized, porcine small intestinal submucosa, Acta Biomater 14 (2015) 96-103.

[183] E. Jorge-Herrero, P. Fernández, J. Turnay, N. Olmo, P. Calero, R. García, I. Freile, J.L. Castillo-Olivares, Influence of different chemical cross-linking treatments on the properties of bovine pericardium and collagen, Biomaterials 20(6) (1999) 539-545.

[184] H.W. Sung, W.H. Chang, C.Y. Ma, M.H. Lee, Crosslinking of biological tissues using genipin and/or carbodiimide, J Biomed Mater Res A 64(3) (2003) 427-38.

[185] F. Everaerts, M. Torrianni, M. Hendriks, J. Feijen, Biomechanical properties of carbodiimide crosslinked collagen: influence of the formation of ester crosslinks, J Biomed Mater Res A 85(2) (2008) 547-55.

[186] J. Leong, A. Munnelly, B. Liberio, L. Cochrane, N. Vyavahare, Neomycin and carbodiimide crosslinking as an alternative to glutaraldehyde for enhanced durability of bioprosthetic heart valves, J Biomater Appl 27(8) (2013) 948-60.

[187] M.J.A. van Luyn, P.B. van Wachem, L. Olde Damink, P.J. Dijkstra, J. Feijen, P. Nieuwenhuis, Relations between in vitro cytotoxicity and crosslinked dermal sheep collagens, J Biomed Mater Res 26(8) (1992) 1091-1110.

[188] S.C. Vasudev, T. Chandy, C.P. Sharma, The anticalcification effect of polyethylene glycol-immobilized on hexamethylene diisocyanate treated pericardium, Artif Cells Blood Substit Immobil Biotechnol 28(1) (2000) 79-94.

[189] D.W. Courtman, B.F. Errett, G.J. Wilson, The role of crosslinking in modification of the immune response elicited against xenogenic vascular acellular matrices, J Biomed Mater Res 55(4) (2001) 576-586.

[190] S. Baiguera, C. Del Gaudio, E. Kuevda, A. Gonfiotti, A. Bianco, P. Macchiarini, Dynamic decellularization and cross-linking of rat tracheal matrix, Biomaterials 35(24) (2014) 6344-6350.

[191] A. Pinheiro, A. Cooley, J. Liao, R. Prabhu, S. Elder, Comparison of natural crosslinking agents for the stabilization of xenogenic articular cartilage, J Orthop Res 34(6) (2016) 1037-1046.

[192] B. Kirking, T. Hedman, J. Criscione, Changes in the interfacial shear resistance of disc annulus fibrosus from genipin crosslinking, J Biomech 47(1) (2014) 10.1016/j.jbiomech.2013.10.019.

[193] W. Zhai, H. Zhang, C. Wu, J. Zhang, X. Sun, H. Zhang, Z. Zhu, J. Chang, Crosslinking of saphenous vein ECM by procyanidins for small diameter blood vessel replacement, J Biomed Mater Res B Appl Biomater 102(6) (2014) 1190-8.

[194] X. Wang, B. Ma, J. Chang, Preparation of decellularized vascular matrix by co-crosslinking of procyanidins and glutaraldehyde, Biomed Mater Eng 26(1-2) (2015) 19-30.

[195] S.C. Roe, B.K. Milthorpe, K. True, G.J. Rogers, K. Schindhelm, The effect of gamma irradiation on a xenograft tendon bioprosthesis, Clin Mater 9(3) (1992) 149-154.

[196] N.R. Bonenfant, D. Sokocevic, D.E. Wagner, Z.D. Borg, M. Lathrop, Y.W. Lam, B. Deng, M. DeSarno, T. Ashikaga, R. Loi, D.J. Weiss, The effects of storage and sterilization on de-cellularized and re-cellularized whole lung, Biomaterials 34(13) (2013) 3231-3245.

[197] E.Y. Elenes, S.A. Hunter, Soft-tissue allografts terminally sterilized with an electron beam are biomechanically equivalent to aseptic, nonsterilized tendons, J Bone Joint Surg Am 96(16) (2014) 1321-6.

[198] A. Jastrzebska, A. Kaminski, E. Grazka, J. Marowska, J. Sadlo, G. Gut, I. Uhrynowska-Tyszkiewicz, Effect of gamma radiation and accelerated electron beam on

stable paramagnetic centers induction in bone mineral: influence of dose, irradiation temperature and bone defatting, Cell Tissue Bank 15(3) (2014) 413-28.

[199] A. Hoburg, S. Keshlaf, T. Schmidt, M. Smith, U. Gohs, C. Perka, A. Pruss, S. Scheffler, High-dose electron beam sterilization of soft-tissue grafts maintains significantly improved biomechanical properties compared to standard gamma treatment, Cell Tissue Bank 16(2) (2015) 219-26.

[200] A. Kaminski, E. Grazka, A. Jastrzebska, J. Marowska, G. Gut, A. Wojciechowski, I. Uhrynowska-Tyszkiewicz, Effect of accelerated electron beam on mechanical properties of human cortical bone: influence of different processing methods, Cell Tissue Bank 13(3) (2012) 375-86.

[201] T. Baldini, K. Caperton, M. Hawkins, E. McCarty, Effect of a novel sterilization method on biomechanical properties of soft tissue allografts, Knee Surg Sports Traumatol Arthrosc 24(12) (2016) 3971-3975.

[202] B. Yang, Y. Zhang, L. Zhou, Z. Sun, J. Zheng, Y. Chen, Y. Dai, Development of a porcine bladder acellular matrix with well-preserved extracellular bioactive factors for tissue engineering, Tissue Eng Part C Methods 16(5) (2010) 1201-11.

[203] B.L. Proffen, G.S. Perrone, B.C. Fleming, J.T. Sieker, J. Kramer, M.L. Hawes, M.M. Murray, Effect of low-temperature ethylene oxide and electron beam sterilization on the in vitro and in vivo function of reconstituted extracellular matrix-derived scaffolds, J Biomater Appl 30(4) (2015) 435-49.

[204] C. Derham, H. Yow, J. Ingram, J. Fisher, E. Ingham, S.A. Korrosis, S. Homer-Vanniasinkam, Tissue engineering small-diameter vascular grafts: preparation of a biocompatible porcine ureteric scaffold, Tissue Eng Part A 14(11) (2008) 1871-82.

[205] L. Zilic, S.P. Wilshaw, J.W. Haycock, Decellularisation and histological characterisation of porcine peripheral nerves, Biotechnol Bioeng 113(9) (2016) 2041-2053.

[206] G. Jones, A. Herbert, H. Berry, J.H. Edwards, J. Fisher, E. Ingham, Decellularization and Characterization of Porcine Superflexor Tendon: A Potential Anterior Cruciate Ligament Replacement, Tissue Eng Part A 23(3-4) (2017) 124-134.

[207] J.C. Kutten, D. McGovern, C.M. Hobson, S.A. Luffy, A. Nieponice, K. Tobita, R.J. Francis, S.D. Reynolds, J.S. Isenberg, T.W. Gilbert, Decellularized tracheal extracellular matrix supports epithelial migration, differentiation, and function, Tissue Eng Part A 21(1-2) (2015) 75-84.

[208] J. Hodde, M. Hiles, Virus safety of a porcine-derived medical device: Evaluation of a viral inactivation method, Biotechnol Bioeng 79(2) (2002) 211-216.

[209] K. Shimizu, H. Yano, E. Nakamura, N. Kaku, Lipid extracted freeze-dried bank bone sterilized with low temperature plasma, Ann Transplant 6(1) (2001) 26-31.

[210] S.D. Ferreira, W.S. Dernell, B.E. Powers, R.A. Schochet, C.A. Kuntz, S.J. Withrow, R.M. Wilkins, Effect of gas-plasma sterilization on the osteoinductive capacity of demineralized bone matrix, Clin Orthop Relat Res 388 (2001) 233-239.

[211] J.H. Edwards, A. Herbert, G.L. Jones, I.W. Manfield, J. Fisher, E. Ingham, The effects of irradiation on the biological and biomechanical properties of an acellular porcine superflexor tendon graft for cruciate ligament repair, J Biomed Mater Res B Appl Biomater 105(8) (2017) 2477-2486.

[212] N.J. Slater, M. van der Kolk, T. Hendriks, H. van Goor, R.P. Bleichrodt, Biologic grafts for ventral hernia repair: a systematic review, Am J Surg 205(2) (2013) 220-30.

[213] K.C. Harth, M.J. Rosen, Major complications associated with xenograft biologic mesh implantation in abdominal wall reconstruction, Surg Innov 16(4) (2009) 324-329.

[214] K.M.F. Itani, M. Rosen, D. Vargo, S.S. Awad, G. DeNoto, C.E. Butler, Prospective study of single-stage repair of contaminated hernias using a biologic porcine tissue matrix: The RICH Study, Surgery 152(3) (2012) 498-505.

[215] C.F. Bellows, P. Shadduck, W.S. Helton, R. Martindale, B.C. Stouch, R. Fitzgibbons, Early report of a randomized comparative clinical trial of Strattice™ reconstructive tissue matrix to lightweight synthetic mesh in the repair of inguinal hernias, Hernia 18(2) (2014) 221-230.

[216] O. Guerra, M.M. Maclin, Non-crosslinked porcine-derived acellular dermal matrix for the management of complex ventral abdominal wall hernias: a report of 45 cases, Hernia 18(1) (2014) 71-79.

[217] D. Golla, C.C. Russo, Outcomes following placement of non–cross-linked porcine-derived acellular dermal matrix in complex ventral hernia repair, Int Surg 99(3) (2014) 235-240.

[218] S.B. Orenstein, Y. Qiao, U. Klueh, D.L. Kreutzer, Y.W. Novitsky, Activation of human mononuclear cells by porcine biologic meshes in vitro, Hernia 14(4) (2010) 401-407.

[219] L.E. de Castro Brás, S. Shurey, P.D. Sibbons, Evaluation of crosslinked and non-crosslinked biologic prostheses for abdominal hernia repair, Hernia 16(1) (2012) 77-89.

[220] M.J. Rosen, G. DeNoto, K.M.F. Itani, C. Butler, D. Vargo, J. Smiell, R. Rutan, Evaluation of surgical outcomes of retro-rectus versus intraperitoneal reinforcement with bio-prosthetic mesh in the repair of contaminated ventral hernias, Hernia 17(1) (2013) 31-35.

[221] F. Catena, L. Ansaloni, F. Gazzotti, S. Gagliardi, S. Di Saverio, L. D'Alessandro, A.D. Pinna, Use of porcine dermal collagen graft (Permacol) for hernia repair in contaminated fields, Hernia 11(1) (2007) 57-60.

[222] M.M. Abdelfatah, N. Rostambeigi, E. Podgaetz, M.G. Sarr, Long-term outcomes (>5-year follow-up) with porcine acellular dermal matrix (Permacol™) in incisional hernias at risk for infection, Hernia 19(1) (2015) 135-140.

[223] Y.W. Novitsky, Biology of biological meshes used in hernia repair, Surg Clin North Am 93(5) (2013) 1211-1215.

[224] D.S. Edelman, J.P. Hodde, Bioactive prosthetic material for treatment of hernias, Surg Technol Int 15 (2006) 104-108.

[225] M. Jacobs, E. Gomez, G. Plasencia, C. Lopez-Penalver, H. Lujan, D. Velarde, T. Jessee, Use of surgisis mesh in laparoscopic repair of hiatal hernias, Surg Laparosc Endosc Percutan Tech 17(5) (2007) 365-8.

[226] L. Ansaloni, F. Catena, L. D'Alessandro, Prospective randomized, double-blind, controlled trial comparing Lichtenstein's repair of inguinal hernia with polypropylene mesh versus Surgisis gold soft tissue graft: preliminary results, Acta Biomed 74(Suppl 2) (2003) 10-14.

[227] M.G. Sarr, N.E. Hutcher, S. Snyder, J. Hodde, B. Carmody, A prospective, randomized, multicenter trial of Surgisis Gold, a biologic prosthetic, as a sublay reinforcement of the fascial closure after open bariatric surgery, Surgery 156(4) (2014) 902-909.

[228] A.H. Annor, M.E. Tang, C.L. Pui, G.C. Ebersole, M.M. Frisella, B.D. Matthews, C.R. Deeken, Effect of enzymatic degradation on the mechanical properties of biological scaffold materials, Surg Endosc 26(10) (2012) 2767-2778.

[229] L. Negron, S. Lun, B.C. May, Ovine forestomach matrix biomaterial is a broad spectrum inhibitor of matrix metalloproteinases and neutrophil elastase, Int Wound J 11(4) (2014) 392-7.

[230] C.A. McDevitt, G.M. Wildey, R.M. Cutrone, Transforming growth factor-beta1 in a sterilized tissue derived from the pig small intestine submucosa, J Biomed Mater Res A 67(2) (2003) 637-40.

[231] J.P. Hodde, D.M.J. Ernst, M.C. Hiles, An investigation of the long-term bioactivity of endogenous growth factor in OASIS Wound Matrix, J Wound Care 14(1) (2005) 23-25.

[232] S.M. Irvine, J. Cayzer, E.M. Todd, S. Lun, E.W. Floden, L. Negron, J.N. Fisher, S.G. Dempsey, A. Alexander, M.C. Hill, A. O'Rouke, S.P. Gunningham, C. Knight, P.F.

Davis, B.R. Ward, B.C.H. May, Quantification of in vitro and in vivo angiogenesis stimulated by ovine forestomach matrix biomaterial, Biomaterials 32(27) (2011) 6351-6361.

[233] C.M.J. Healy, J.G. Boorman, Comparison of E-Z Derm and Jelonet dressings for partial skin thickness burns, Burns 15(1) (1989) 52-54.

[234] P. Vanstraelen, Comparison of calcium sodium alginate (KALTOSTAT) and porcine xenograft (E-Z DERM) in the healing of split-thickness skin graft donor sites, Burns 18(2) (1992) 145-148.

[235] D.W. Raimer, A.R. Group, M.S. Petitt, N. Nosrati, M.L. Yamazaki, N.A. Davis, B.C. Kelly, B.R. Gibson, R.D. Montilla, R.F.W. Jr, Porcine xenograft biosynthetic wound dressings for the management of postoperative Mohs wounds, Dermatol Online J 17(9) (2011).

[236] B. Burkey, W. Davis, P.M. Glat, Porcine xenograft treatment of superficial partial-thickness burns in paediatric patients, J Wound Care 25(Sup2) (2016) S10-S15.

[237] S.J. Kavros, Acellular fetal bovine dermal matrix for treatment of chronic ulcerations of the midfoot associated with Charcot neuroarthropathy, Foot Ankle Spec 5(4) (2012) 230-4.

[238] E. Hayn, Successful treatment of complex traumatic and surgical wounds with a foetal bovine dermal matrix, Int Wound J 11(6) (2014) 675-80.

[239] S.J. Kavros, T. Dutra, R. Gonzalez-Cruz, B. Liden, B. Marcus, J. McGuire, L. Nazario-Guirau, The use of PriMatrix, a fetal bovine acellular dermal matrix, in healing chronic diabetic foot ulcers: a prospective multicenter study, Adv Skin Wound Care 27(8) (2014) 356-62.

[240] J.C. Karr, Retrospective comparison of diabetic foot ulcer and venous stasis ulcer healing outcome between a dermal repair scaffold (PriMatrix) and a bilayered living cell therapy (Apligraf), Adv Skin Wound Care 24(3) (2011) 119-25.

[241] C.E. Witherel, P.L. Graney, D.O. Freytes, M.S. Weingarten, K.L. Spiller, Response of human macrophages to wound matrices in vitro, Wound Repair Regen 24(3) (2016) 514-524.

[242] R.C. Rennert, M. Sorkin, R.K. Garg, M. Januszyk, G.C. Gurtner, Cellular response to a novel fetal acellular collagen matrix: implications for tissue regeneration, Int J Biomater 2013 (2013) 527957.

[243] E.N. Mostow, G.D. Haraway, M. Dalsing, J.P. Hodde, D. King, Effectiveness of an extracellular matrix graft (OASIS Wound Matrix) in the treatment of chronic leg ulcers: A randomized clinical trial, J Vasc Surg 41(5) (2005) 837-843.

[244] J.S. Kim, A.J. Kaminsky, J.B. Summitt, W.P. Thayer, New innovations for deep partial-thickness burn treatment with ACell MatriStem Matrix, Adv Wound Care 5(12) (2016) 546-552.

[245] M. Romanelli, V. Dini, M.S. Bertone, Randomized comparison of OASIS wound matrix versus moist wound dressing in the treatment of difficult-to-heal wounds of mixed arterial/venous etiology, Adv Skin Wound Care 23(1) (2010) 34-8.

[246] D.D. Yeh, R.M. Nazarian, L. Demetri, T. Mesar, S. Dijkink, A. Larentzakis, G. Velmahos, K.W. Sadik, Histopathological assessment of OASIS Ultra on critical-sized wound healing: a pilot study, J Cutan Pathol 44(6) (2017) 523-529.

[247] H. Kimmel, M. Rahn, T.W. Gilbert, The clinical effectiveness in wound healing with extracellular matrix derived from porcine urinary bladder matrix: a case series on severe chronic wounds, J Am Col Certif Wound Spec 2(3) (2010) 55-9.

[248] M. Romanelli, V. Dini, M. Bertone, S. Barbanera, C. Brilli, OASIS wound matrix versus Hyaloskin in the treatment of difficult-to-heal wounds of mixed arterial/venous aetiology, Int Wound J 4(1) (2007) 3-7.

[249] J.A. Niezgoda, C.C. Van Gils, R.G. Frykberg, J.P. Hodde, Randomized clinical trial comparing OASIS Wound Matrix to Regranex Gel for diabetic ulcers, Adv Skin Wound Care 18(5 Pt 1) (2005) 258-66.

[250] R.G. Frykberg, S.M. Cazzell, J. Arroyo-Rivera, A. Tallis, A.M. Reyzelman, F. Saba, L. Warren, B.C. Stouch, T.W. Gilbert, Evaluation of tissue engineering products for the management of neuropathic diabetic foot ulcers: an interim analysis, J Wound Care 25(Sup7) (2016) S18-S25.

[251] M. Martinson, N. Martinson, A comparative analysis of skin substitutes used in the management of diabetic foot ulcers, J Wound Care 25(Sup10) (2016) S8-S17.

[252] B.A. Liden, B.C. May, Clinical outcomes following the use of ovine forestomach matrix (endoform dermal template) to treat chronic wounds, Adv Skin Wound Care 26(4) (2013) 164-7.

[253] J.H. Alexander, D.A. Yeager, D.S. Stern, C.A. Messina, B.J. Griffeth, E. Pacocha, M. Barakat, Equine pericardium as a biological covering for the treatment of diabetic foot wounds, J Am Podiatr Med Assoc 102(5) (2012) 352-358.

[254] C.K. Yang, T.O. Polanco, J.C. Lantis, 2nd, A Prospective, Postmarket, Compassionate Clinical Evaluation of a Novel Acellular Fish-skin Graft Which Contains Omega-3 Fatty Acids for the Closure of Hard-to-heal Lower Extremity Chronic Ulcers, Wounds 28(4) (2016) 112-8.

[255] J.J. Kim, G.R.D. Evans, Applications of biomaterials in plastic surgery, Clin Plast Surg 39(4) (2012) 359-376.

[256] J.A. Cavallo, N. Gangopadhyay, J. Dudas, A.A. Roma, M.S. Jasielec, J. Baty, S. Baalman, M.M. Frisella, M.M. Tenenbaum, T.M. Myckatyn, B.D. Matthews, C.R. Deeken, Remodeling characteristics and collagen distributions of biologic scaffold materials biopsied from postmastectomy breast reconstruction sites, Ann Plast Surg 75(1) (2015) 74-83.

[257] E. Kocak, T.W. Nagel, J.H. Hulsen, 3rd, K.H. Carruthers, S.P. Povoski, C.J. Salgado, A.H. Chao, Biologic matrices in oncologic breast reconstruction after mastectomy, Expert Rev Med Devices 11(1) (2014) 65-75.

[258] M.Y. Nahabedian, Implant-based breast reconstruction: Strategies to achieve optimal outcomes and minimize complications, J Surg Oncol 113(8) (2016) 895-905.

[259] T. Eisenberg, Implant exposure through a breast augmentation incision repaired with porcine acellular dermal matrix (StratticeTM): A technique to ensure graft take, Aesthetic Plast Surg 35(4) (2011) 681-683.

[260] I. Himsl, V. Drinovac, M. Lenhard, D. Stöckl, T. Weissenbacher, D. Dian, The use of porcine acellular dermal matrix in silicone implant-based breast reconstruction, Arch Gynecol Obstet 286(1) (2012) 187-192.

[261] J.N. Pozner, J.B. White, M.I. Newman, Use of porcine acellular dermal matrix in revisionary cosmetic breast augmentation, Aesthet Surg J 33(5) (2013) 681-690.

[262] V.L. Negenborn, J.M. Smit, R.E.G. Dikmans, H.A.H. Winters, J.W.R. Twisk, P.Q. Ruhé, M.A.M. Mureau, S. Tuinder, Y. Eltahir, N.A.S. Posch, J.M. van Steveninck-Barends, R.R.W.J. van der Hulst, M.J.P.F. Ritt, M.B. Bouman, M.G. Mullender, Short-term cost-effectiveness of one-stage implant-based breast reconstruction with an acellular dermal matrix versus two-stage expander-implant reconstruction from a multicentre randomized clinical trial, Br J Surg 106(5) (2019) 586-595.

[263] R.E.G. Dikmans, V.L. Negenborn, M.-B. Bouman, H.A.H. Winters, J.W.R. Twisk, P.Q. Ruhé, M.A.M. Mureau, J.M. Smit, S. Tuinder, Y. Eltahir, N.A. Posch, J.M. van Steveninck-Barends, M.A. Meesters-Caberg, R.R.W.J. van der Hulst, M.J.P.F. Ritt, M.G. Mullender, Two-stage implant-based breast reconstruction compared with immediate one-stage implant-based breast reconstruction augmented with an acellular dermal matrix: an open-label, phase 4, multicentre, randomised, controlled trial, Lancet Oncol 18(2) (2017) 251-258.

[264] F. Lohmander, J. Lagergren, P.G. Roy, H. Johansson, Y. Brandberg, C. Eriksen, J. Frisell, Implant based breast reconstruction with acellular dermal matrix: Safety data from

an open-label, multicenter, randomized, controlled trial in the setting of breast cancer treatment, Ann Surg 269(5) (2019) 836-841.

[265] D. Gschwantler-Kaulich, P. Schrenk, V. Bjelic-Radisic, K. Unterrieder, C. Leser, A. Fink-Retter, M. Salama, C. Singer, Mesh versus acellular dermal matrix in immediate implant-based breast reconstruction - A prospective randomized trial, Eur J Surg Oncol 42(5) (2016) 665-71.

[266] R. Endress, M.S. Choi, G.K. Lee, Use of fetal bovine acellular dermal xenograft with tissue expansion for staged breast reconstruction, Ann Plast Surg 68(4) (2012) 338-41.

[267] R. Ohkuma, K.J. Buretta, R. Mohan, G.D. Rosson, A.N. Rad, Initial experience with the use of foetal/neonatal bovine acellular dermal collagen matrix (SurgiMend™) for tissue-expander breast reconstruction, J Plast Reconstr Aesthet Surg 66(9) (2013) 1195-1201.

[268] H. Headon, A. Kasem, A. Manson, C. Choy, A.R. Carmichael, K. Mokbel, Clinical outcome and patient satisfaction with the use of bovine-derived acellular dermal matrix (SurgiMend™) in implant based immediate reconstruction following skin sparing mastectomy: A prospective observational study in a single centre, Surg Oncol 25(2) (2016) 104-110.

[269] M.M. Mofid, M.S. Meininger, M.S. Lacey, Veritas(R) bovine pericardium for immediate breast reconstruction: a xenograft alternative to acellular dermal matrix products, Eur J Plast Surg 35(10) (2012) 717-722.

[270] A. Gubitosi, G. Docimo, D. Parmeggiani, R. Pirozzi, C. Vitiello, P. Schettino, M. Avellino, G. Casalino, M. Amato, R. Ruggiero, L. Docimo, Acellular bovine pericardium dermal matrix in immediate breast reconstruction after Skin Sparing Mastectomy, Int J Surg 12 Suppl 1 (2014) S205-8.

[271] A.M. Simpson, K.K. Higdon, M.S. Kilgo, D.G. Tepper, K. Alizadeh, P.M. Glat, J.P. Agarwal, Porcine acellular peritoneal matrix in immediate breast reconstruction: A multicenter, prospective, single-arm trial, Plast Reconstr Surg 143(1) (2019) 10e-21e.

[272] J.H. Leonard, A.J. Cohen, Use of the tarSys® for posterior lamellar grafting for lower eyelid malposition, Eur J Plast Surg 36(12) (2013) 733-738.

[273] S.L. Liao, Y.H. Wei, Correction of lower lid retraction using TarSys bioengineered grafts for graves ophthalmopathy, Am J Ophthalmol 156(2) (2013) 387-392.e1.

[274] B.T. Ambro, J. Zimmerman, M. Rosenthal, E.A. Pribitkin, Nasal septal perforation repair with porcine small intestinal submucosa, Arch Facial Plast Surg 5(6) (2003) 528-529.

[275] J.P. Iannotti, M.J. Codsi, Y.W. Kwon, K. Derwin, J. Ciccone, J.J. Brems, Porcine small intestine submucosa augmentation of surgical repair of chronic two-tendon rotator cuff tears. A randomized, controlled trial, J Bone Joint Surg Am 88(6) (2006) 1238-44.

[276] W.P. Phipatanakul, S.A. Petersen, Porcine small intestine submucosa xenograft augmentation in repair of massive rotator cuff tears, Am J Orthop (Belle Mead NJ) 38(11) (2009) 572-575.

[277] D. Bryant, R. Holtby, K. Willits, R. Litchfield, D. Drosdowech, A. Spouge, D. White, G. Guyatt, A randomized clinical trial to compare the effectiveness of rotator cuff repair with or without augmentation using porcine small intestine submucosa for patients with moderate to large rotator cuff tears: a pilot study, J Shoulder Elbow Surg 25(10) (2016) 1623-1633.

[278] M.H. Zheng, J. Chen, Y. Kirilak, C. Willers, J. Xu, D. Wood, Porcine small intestine submucosa (SIS) is not an acellular collagenous matrix and contains porcine DNA: possible implications in human implantation, J Biomed Mater Res B Appl Biomater 73(1) (2005) 61-7.

[279] J.M. Chen, C. Willers, J. Xu, A. Wang, M.H. Zheng, Autologous tenocyte therapy using porcine-derived bioscaffolds for massive rotator cuff defect in rabbits, Tissue Eng 13(7) (2007) 1479-91.

[280] A. Jimenez-Martin, F.J. Santos-Yubero, F.J. Najarro-Cid, S. Navarro-Martinez, M. Zurera-Carmona, S. Perez-Hidalgo, Use of grafts in rotator cuff re-rupture, Rev Esp Cir Ortop Traumatol 60(5) (2016) 286-95.

[281] H. Xu, H. Wan, W. Zuo, W. Sun, R.T. Owens, J.R. Harper, D.L. Ayares, D.J. McQuillan, A porcine-derived acellular dermal scaffold that supports soft tissue regeneration: removal of terminal galactose-alpha-(1,3)-galactose and retention of matrix structure, Tissue Eng Part A 15(7) (2009) 1807-19.

[282] H. Xu, M. Sandor, S. Qi, J. Lombardi, J. Connor, D.J. McQuillan, J.P. Iannotti, Implantation of a porcine acellular dermal graft in a primate model of rotator cuff repair, J Shoulder Elbow Surg 21(5) (2012) 580-588.

[283] S.P. Badhe, T.M. Lawrence, F.D. Smith, P.G. Lunn, An assessment of porcine dermal xenograft as an augmentation graft in the treatment of extensive rotator cuff tears, J Shoulder Elbow Surg 17(1) (2008) S35-S39.

[284] A.K. Gupta, K. Hug, B. Boggess, M. Gavigan, A.P. Toth, Massive or 2-tendon rotator cuff tears in active patients with minimal glenohumeral arthritis, Am J Sports Med 41(4) (2013) 872-879.

[285] Y. Ono, D.A. Dávalos Herrera, J.M. Woodmass, R.S. Boorman, G.M. Thornton, I.K.Y. Lo, Can grafts provide superior tendon healing and clinical outcomes after rotator cuff repairs?: A meta-analysis, Orthop J Sports Med 4(12) (2016) 2325967116674191.

[286] C. Rucker, H. Kirch, O. Pullig, H. Walles, Strategies and first advances in the development of prevascularized bone implants, Curr Mol Biol Rep 2(3) (2016) 149-157.

[287] S. Meyer, T. Floerkemeier, H. Windhagen, Histological osseointegration of Tutobone®: first results in human, Arch Orthop Trauma Surg 128(6) (2008) 539-544.

[288] S.K. Prakash, N. Mukerji, F.P. Nath, Is tutobone an efficient alternative to other implants used in anterior cervical discectomy and fusion surgeries?, Br J Neurosurg 31(3) (2017) 340-344.

[289] V. Campana, G. Milano, E. Pagano, M. Barba, C. Cicione, G. Salonna, W. Lattanzi, G. Logroscino, Bone substitutes in orthopaedic surgery: from basic science to clinical practice, J Mater Sci Mater Med 25(10) (2014) 2445-61.

[290] M. Abuelnaga, N. Elbokle, M. Khashaba, Evaluation of custom made xenogenic bone grafts in mandibular alveolar ridge augmentation versus particulate bone graft with titanium mesh, J Oral Maxillofac Surg 9(2) (2018) 62-73.

[291] R. Ferracini, A. Bistolfi, R. Garibaldi, V. Furfaro, A. Battista, G. Perale, Composite xenohybrid bovine bone-derived scaffold as bone substitute for the treatment of tibial plateau fractures, Appl Sci 9(13) (2019) 2675.

[292] I. Sallent, H. Capella-Monsonís, P. Procter, I.Y. Bozo, R.V. Deev, D. Zubov, R. Vasyliev, G. Perale, G. Pertici, J. Baker, P. Gingras, Y. Bayon, D.I. Zeugolis, The few who made it: Commercially and clinically successful innovative bone grafts, Front Bioeng Biotechnol 8(952) (2020).

[293] T. Starch-Jensen, H. Aludden, M. Hallman, C. Dahlin, A.E. Christensen, A. Mordenfeld, A systematic review and meta-analysis of long-term studies (five or more years) assessing maxillary sinus floor augmentation, Int J Oral Maxillofac Surg 47(1) (2018) 103-116.

[294] M.P. Ramírez Fernández, S.A. Gehrke, C. Pérez Albacete Martinez, J.L. Calvo Guirado, P.N. de Aza, SEM-EDX study of the degradation process of two xenograft materials used in sinus lift procedures, Materials (Basel) 10(5) (2017) 542.

[295] C. Rombouts, C. Jeanneau, J. Camilleri, P. Laurent, I. About, Characterization and angiogenic potential of xenogeneic bone grafting materials: Role of periodontal ligament cells, Dent Mater J 35(6) (2016) 900-907.

[296] A. Figueiredo, P. Coimbra, A. Cabrita, F. Guerra, M. Figueiredo, Comparison of a xenogeneic and an alloplastic material used in dental implants in terms of physico-

chemical characteristics and in vivo inflammatory response, Mater Sci Eng C Mater Biol Appl 33(6) (2013) 3506-13.

[297] V.M. Festa, F. Addabbo, L. Laino, F. Femiano, R. Rullo, Porcine-derived xenograft combined with a soft cortical membrane versus extraction alone for implant site development: A clinical study in humans, Clin Implant Dent Relat Res 15(5) (2013) 707-713.

[298] H.C. Aludden, A. Mordenfeld, M. Hallman, C. Dahlin, T. Jensen, Lateral ridge augmentation with Bio-Oss alone or Bio-Oss mixed with particulate autogenous bone graft: a systematic review, Int J Oral Maxillofac Surg 46(8) (2017) 1030-1038.

[299] E. Poulias, H. Greenwell, M. Hill, D. Morton, R. Vidal, B. Shumway, T.L. Peterson, Ridge preservation comparing socket allograft alone to socket allograft plus facial overlay xenograft: A clinical and histologic study in humans, J Periodontol 84(11) (2013) 1567-1575.

[300] B. Wessing, I. Urban, E. Montero, W. Zechner, M. Hof, J. Alández Chamorro, N. Alández Martin, G. Polizzi, S. Meloni, M. Sanz, A multicenter randomized controlled clinical trial using a new resorbable non-cross-linked collagen membrane for guided bone regeneration at dehisced single implant sites: interim results of a bone augmentation procedure, Clin Oral Implants Res 28(11) (2017) e218-e226.

[301] S. Arunjaroensuk, S. Panmekiate, A. Pimkhaokham, The stability of augmented bone between two different membranes used for guided bone regeneration simultaneous with dental implant placement in the esthetic zone, Int J Oral Maxillofac Implants 33(1) (2018) 206-216.

[302] S. Ghanaati, Non-cross-linked porcine-based collagen I–III membranes do not require high vascularization rates for their integration within the implantation bed: A paradigm shift, Acta Biomater 8(8) (2012) 3061-3072.

[303] Z. Mosala Nezhad, A. Poncelet, L. de Kerchove, P. Gianello, C. Fervaille, G. El Khoury, Small intestinal submucosa extracellular matrix (CorMatrix®) in cardiovascular surgery: a systematic review, Interact Cardiovasc Thorac Surg 22(6) (2016) 839-850.

[304] M.S. Khan, M.R. Yeager, R. Bryant, A. Lorts, D.L.S. Morales, Coronary artery reconstruction using a bioengineered patch and epicardial tunnel, Ann Thorac Surg 101(1) (2016) 363-365.

[305] A. Adeel, B. Tyler, R. Brian, Repair of complete atrioventricular septal defects with decellularized extracellular matrix: Initial and midterm outcomes, World J Pediatr Congenit Heart Surg 8(3) (2017) 310-314.

[306] M.A. Padalino, B. Castaldi, M. Fedrigo, M. Gallo, F. Zucchetta, V.L. Vida, O. Milanesi, A. Angelini, G. Stellin, Porcine intestinal submucosa (CorMatrix) for semilunar valve repair in children: A word of caution after midterm results, Semin Thorac Cardiovasc Surg 28(2) (2016) 436-445.

[307] T.M. Kelley, M. Kashem, H. Wang, J. McCarthy, N.D. Carroll, G.W. Moser, T.S. Guy, Anterior leaflet augmentation with CorMatrix porcine extracellular matrix in twenty-five patients: Unexpected patch failures and histologic analysis, Ann Thorac Surg 103(1) (2017) 114-120.

[308] J.S. Woo, M.C. Fishbein, B. Reemtsen, Histologic examination of decellularized porcine intestinal submucosa extracellular matrix (CorMatrix) in pediatric congenital heart surgery, Cardiovasc Pathol 25(1) (2016) 12-17.

[309] G. Strange, C. Brizard, T.R. Karl, L. Neethling, An evaluation of Admedus' tissue engineering process-treated (ADAPT) bovine pericardium patch (CardioCel) for the repair of cardiac and vascular defects, Expert Rev Med Devices 12(2) (2015) 135-41.

[310] M. Sobieraj, E. Cudak, W. Mrowczynski, T.K. Nalecz, P. Westerski, M. Wojtalik, Application of the CardioCel bovine pericardial patch - a preliminary report, Kardiochir Torakochirurgia Pol 13(3) (2016) 210-212.

[311] C. Pavy, G. Michielon, J.L. Robertus, F. Lacour-Gayet, O. Ghez, Initial 2-year results of CardioCel® patch implantation in children, Interact Cardiovasc Thorac Surg (2017) ivx295-ivx295.

[312] A.J. Kovalic, D.K. Beattie, A.H. Davies, Outcome of ProCol, a bovine mesenteric vein graft, in infrainguinal reconstruction, Eur J Vasc Endovasc Surg 24(6) (2002) 533-4.

[313] J. Schmidli, H. Savolainen, G. Heller, M.K. Widmer, U. Then-Schlagau, I. Baumgartner, T.P. Carrel, Bovine mesenteric vein graft (ProCol) in critical limb ischaemia with tissue loss and infection, Eur J Vasc Endovasc Surg 27(3) (2004) 251-3.

[314] J.I. Spark, S. Yeluri, C. Derham, Y.T. Wong, D. Leitch, Incomplete cellular depopulation may explain the high failure rate of bovine ureteric grafts, Br J Surg 95(5) (2008) 582-585.

[315] F. Boccafoschi, M. Botta, L. Fusaro, F. Copes, M. Ramella, M. Cannas, Decellularized biological matrices: an interesting approach for cardiovascular tissue repair and regeneration, J Tissue Eng Regen Med 11(5) (2017) 1648-1657.

[316] D.Y. Cheung, B. Duan, J.T. Butcher, Current progress in tissue engineering of heart valves: multiscale problems, multiscale solutions, Expert Opin Biol Ther 15(8) (2015) 1155-1172.

[317] D.M. Pineda, M.J. Dougherty, M.C. Wismer, C. Carroll, S. Tyagi, D.A. Troutman, K.D. Calligaro, Bovine carotid artery xenografts for hemodialysis access, J Vasc Surg 65(6) (2017) 1729-1734.

[318] P. Lindsey, A. Echeverria, M. Cheung, E. Kfoury, C.F. Bechara, P.H. Lin, Lower extremity bypass using bovine carotid artery graft (Artegraft): An analysis of 124 cases with long-term results, World J Surg 42(1) (2018) 295-301.

[319] S. Pashneh-Tala, S. MacNeil, F. Claeyssens, The Tissue-Engineered Vascular Graft-Past, Present, and Future, Tissue Eng Part B Rev 22(1) (2016) 68-100.

[320] J.E. Bavaria, N.D. Desai, A. Cheung, M.R. Petracek, M.A. Groh, M.A. Borger, H.V. Schaff, The St Jude Medical Trifecta aortic pericardial valve: results from a global, multicenter, prospective clinical study, J Thorac Cardiovasc Surg 147(2) (2014) 590-7.

[321] T. Bourguignon, A.-L. Bouquiaux-Stablo, P. Candolfi, A. Mirza, C. Loardi, M.-A. May, R. El-Khoury, M. Marchand, M. Aupart, Very long-term outcomes of the Carpentier-Edwards Perimount valve in aortic position, Ann Thorac Surg 99(3) (2015) 831-837.

[322] R.J.M. Klautz, A.P. Kappetein, R. Lange, F. Dagenais, L. Labrousse, V. Bapat, M. Moront, M. Misfeld, C. Zeng, J.F. Sabik Iii, P. Investigators, Safety, effectiveness and haemodynamic performance of a new stented aortic valve bioprosthesis, Eur J Cardiothorac Surg 52(3) (2017) 425-431.

[323] J. Ennker, A. Albert, I.C. Ennker, Stentless aortic valves. Current aspects, HSR Proc Intensive Care Cardiovasc Anesth 4(2) (2012) 77-82.

[324] B.N. Shultz, T. Timek, A.T. Davis, J. Heiser, E. Murphy, C. Willekes, R. Hooker, A propensity matched analysis of outcomes and long term survival in stented versus stentless valves, J Cardiothorac Surg 12(1) (2017) 45-45.

[325] O. Fouquet, C. Baufreton, A. Tassin, F. Pinaud, J.-P. Binuani, S. DangVan, F. Prunier, F. Rouleau, S. Willoteaux, J.-L. De Brux, A. Furber, Influence of stentless versus stented valves on ventricular remodeling assessed at 6 months by magnetic resonance imaging and long-term follow-up, J Cardiol 69(1) (2017) 264-271.

[326] J.R. Etnel, L.C. Elmont, E. Ertekin, M.M. Mokhles, H.J. Heuvelman, J.W. Roos-Hesselink, P.L. de Jong, W.A. Helbing, A.J. Bogers, J.J. Takkenberg, Outcome after aortic valve replacement in children: A systematic review and meta-analysis, J Thorac Cardiovasc Surg 151(1) (2016) 143-52 e1-3.

[327] M. Namiri, M.K. Ashtiani, O. Mashinchian, M.M. Hasani-Sadrabadi, M. Mahmoudi, N. Aghdami, H. Baharvand, Engineering natural heart valves: possibilities and challenges, J Tissue Eng Regen Med 11(5) (2017) 1675-1683.

[328] M.C. VeDepo, M.S. Detamore, R.A. Hopkins, G.L. Converse, Recellularization of decellularized heart valves: Progress toward the tissue-engineered heart valve, J Tissue Eng 8 (2017) 2041731417726327.

[329] M.R. Labrosse, R. Jafar, J. Ngu, M. Boodhwani, Planar biaxial testing of heart valve cusp replacement biomaterials: Experiments, theory and material constants, Acta Biomater 45 (2016) 303-320.

[330] A.V. Vashi, J.F. White, K.M. McLean, W.M. Neethling, D.I. Rhodes, J.A. Ramshaw, J.A. Werkmeister, Evaluation of an established pericardium patch for delivery of mesenchymal stem cells to cardiac tissue, J Biomed Mater Res A 103(6) (2015) 1999-2005.

[331] C.P. Brizard, J. Brink, S.B. Horton, G.A. Edwards, J.C. Galati, W.M. Neethling, New engineering treatment of bovine pericardium confers outstanding resistance to calcification in mitral and pulmonary implantations in a juvenile sheep model, J Thorac Cardiovasc Surg 148(6) (2014) 3194-201.

[332] A. Salameh, W. Greimann, D. Vondrys, M. Kostelka, Calcification or not. This is the question. A 1-year study of bovine pericardial vascular patches (CardioCel) in minipigs, Semin Thorac Cardiovasc Surg (2017).

[333] C.R. Deeken, B.J. Eliason, M.D. Pichert, S.A. Grant, M.M. Frisella, B.D. Matthews, Differentiation of biologic scaffold materials through physicomechanical, thermal, and enzymatic degradation techniques, Ann Surg 255(3) (2012) 595-604.

[334] Y.W. Novitsky, S.B. Orenstein, D.L. Kreutzer, Comparative analysis of histopathologic responses to implanted porcine biologic meshes, Hernia 18(5) (2014) 713-721.

[335] R. Garcia-Pumarino, G. Pascual, M. Rodriguez, B. Perez-Kohler, J.M. Bellon, Do collagen meshes offer any benefits over preclude(R) ePTFE implants in contaminated surgical fields? A comparative in vitro and in vivo study, J Biomed Mater Res B Appl Biomater 102(2) (2014) 366-75.

[336] E.D. Jenkins, L. Melman, C.R. Deeken, S.C. Greco, M.M. Frisella, B.D. Matthews, Evaluation of fenestrated and non-fenestrated biologic grafts in a porcine model of mature ventral incisional hernia repair, Hernia 14(6) (2010) 10.1007/s10029-010-0684-x.

[337] K.P. Shea, M.B. McCarthy, F. Ledgard, C. Arciero, D. Chowaniec, A.D. Mazzocca, Human tendon cell response to 7 commercially available extracellular matrix materials: an in vitro study, Arthroscopy 26(9) (2010) 1181-8.

[338] H.D. Toeg, O. Abessi, T. Al-Atassi, L. de Kerchove, G. El-Khoury, M. Labrosse, M. Boodhwani, Finding the ideal biomaterial for aortic valve repair with ex vivo porcine

left heart simulator and finite element modeling, J Thorac Cardiovasc Surg 148(4) (2014) 1739-1745 e1.

[339] T.F. Deering, C. Chang, C. Snyder, S.K. Natarajan, R. Matheny, Enhanced antimicrobial effects of decellularized extracellular matrix (CorMatrix) with added vancomycin and gentamicin for device implant protection, Pacing Clin Electrophysiol 40(6) (2017) 615-623.

[340] N.A. Kouris, J.M. Squirrell, J.P. Jung, C.A. Pehlke, T. Hacker, K.W. Eliceiri, B.M. Ogle, A nondenatured, noncrosslinked collagen matrix to deliver stem cells to the heart, Regen Med 6(5) (2011) 569-582.

[341] Z. Mosala Nezhad, A. Poncelet, L. de Kerchove, C. Fervaille, X. Banse, X. Bollen, J.-P. Dehoux, G. El Khoury, P. Gianello, CorMatrix valved conduit in a porcine model: long-term remodelling and biomechanical characterization†, Interact Cardiovasc Thorac Surg 24(1) (2017) 90-98.

[342] R.M. Jacob, C.H. Matthew, S.L. Timothy, P.L. Christopher, B.S. Richard, S. Mark, A. Mark, K. Attila, G.M. Robert, E. Pirooz, J.D. Ralph, S.B. Umar, Pulmonary valve replacement with small intestine submucosa-extracellular matrix in a porcine model, World J Pediatr Congenit Heart Surg 7(4) (2016) 475-483.

[343] Z. Mosala Nezhad, A. Poncelet, C. Fervaille, L. de Kerchove, P. Gianello, Experimental Aortic Valve Cusp Extension with CorMatrix in a Porcine Model, Thorac Cardiovasc Surg 65(3) (2017) 206-210.

[344] H.E. Mewhort, J.D. Turnbull, A. Satriano, K. Chow, J.A. Flewitt, A.C. Andrei, D.G. Guzzardi, D.A. Svystonyuk, J.A. White, P.W. Fedak, Epicardial infarct repair with bioinductive extracellular matrix promotes vasculogenesis and myocardial recovery, J Heart Lung Transplant 35(5) (2016) 661-70.

[345] W. Johnson, J. Inamasu, B. Yantzer, C. Papangelou, B. Guiot, Comparative in vitro biomechanical evaluation of two soft tissue defect products, J Biomed Mater Res B Appl Biomater (2007) n/a-n/a.

[346] F.A. Barber, M.A. Herbert, D.A. Coons, Tendon augmentation grafts: biomechanical failure loads and failure patterns, Arthroscopy 22(5) (2006) 534-8.

[347] S.F. Badylak, J.E. Valentin, A.K. Ravindra, G.P. McCabe, A.M. Stewart-Akers, Macrophage phenotype as a determinant of biologic scaffold remodeling, Tissue Eng Part A 14(11) (2008) 1835-42.

[348] J.E. Valentin, J.S. Badylak, G.P. McCabe, S.F. Badylak, Extracellular matrix bioscaffolds for orthopaedic applications: A comparative histologic study, J Bone Joint Surg 88(12) (2006) 2673-2686.

[349] M. Street, A. Thambyah, M. Dray, S. Amirapu, D. Tuari, K.E. Callon, J.D. McIntosh, K. Burkert, P.R. Dunbar, B. Coleman, J. Cornish, D.S. Musson, Augmentation with an ovine forestomach matrix scaffold improves histological outcomes of rotator cuff repair in a rat model, J Orthop Surg Res 10 (2015) 165.

[350] J. Troy, R. Karlnoski, K. Downes, K.S. Brown, C.W. Cruse, D.J. Smith, W.G. Payne, The use of EZ Derm® in partial-thickness burns: An institutional review of 157 patients, Eplasty 13 (2013) e14.

[351] S. Magnusson, B.T. Baldursson, H. Kjartansson, O. Rolfsson, G.F. Sigurjonsson, Regenerative and antibacterial properties of acellular fish skin grafts and human amnion/chorion membrane: Implications for tissue preservation in combat casualty care., Mil Med 182(S1) (2017) 383-388.

[352] H. Kjartansson, I.H. Olafsson, S. Karason, H. Thorisson, B.T. Baldursson, E. Gunnarsson, E. Jorundsson, G.F. Sigurjonsson, Use of acellular fish skin for dura repair in an ovine model: A pilot study, Open J Mod Neurosurg 05(04) (2015) 124-136.

[353] B.T. Baldursson, H. Kjartansson, F. Konradsdottir, P. Gudnason, G.F. Sigurjonsson, S.H. Lund, Healing rate and autoimmune safety of full-thickness wounds treated with fish skin acellular dermal matrix versus porcine small-intestine submucosa: a noninferiority study, Int J Low Extrem Wounds 14(1) (2015) 37-43.

[354] E.A. Rommer, M. Peric, A. Wong, Urinary bladder matrix for the treatment of recalcitrant nonhealing radiation wounds, Adv Skin Wound Care 26(10) (2013) 450-5.

[355] J. LeCheminant, C. Field, Porcine urinary bladder matrix: a retrospective study and establishment of protocol, J Wound Care 21(10) (2012) 476-482.

[356] W.N. Sivak, E.J. Ruane, S.J. Hausman, J.P. Rubin, A.M. Spiess, Decellularized matrix and supplemental fat grafting leads to regeneration following traumatic fingertip amputation, Plast Reconstr Surg 4(10) (2016) e1094.

[357] A. Gupta, S. Francis, R. Stewart, D. Hobson, K.V. Meriwether, Repair of colonic neovaginal stenosis using a biological graft in a male-to-female transgender patient, Int Urogynecol J 30(4) (2019) 661-663.

[358] A.M. Pearlman, V. Mujumdar, K.E. McAbee, R.P. Terlecki, Outcomes of adult urethroplasty with commercially available acellular matrix, Ther Adv Urol 10(11) (2018) 351-355.

[359] N.S. Hillberg, P.I. Ferdinandus, R.E.G. Dikmans, B. Winkens, J. Hommes, R. van der Hulst, Is single-stage implant-based breast reconstruction (SSBR) with an acellular matrix safe?: Strattice or Meso Biomatrix(R) in SSBR, Eur J Plast Surg 41(4) (2018) 429-438.

[360] K.M. Kulig, X. Luo, E.B. Finkelstein, X.-H. Liu, S.M. Goldman, C.A. Sundback, J.P. Vacanti, C.M. Neville, Biologic properties of surgical scaffold materials derived from dermal ECM, Biomaterials 34(23) (2013) 5776-5784.

[361] C.C. Petro, A.S. Prabhu, L. Liu, A. Majumder, J.M. Anderson, M.J. Rosen, An in vivo analysis of Miromesh—a novel porcine liver prosthetic created by perfusion decellularization, J Surg Res 201(1) (2016) 29-37.

[362] E.S. Nihsen, D.A. Zopf, D.M. Ernst, A.D. Janis, M.C. Hiles, C. Johnson, Absorption of bioactive molecules into OASIS wound matrix, Adv Skin Wound Care 20(10) (2007) 541-8.

[363] W. Mari, S. Younes, J. Naqvi, A.A. Issa, T.L. Oroszi, D.R. Cool, J.B. Travers, R. Simman, Use of a natural porcine extracellular matrix with negative pressure wound therapy hastens the healing rate in stage 4 rressure ulcers, Wounds 31(5) (2019) 117-122.

[364] J.G. Fleischli, T.J. Laughlin, J.W. Fleischli, Equine pericardium collagen wound dressing in the treatment of the neuropathic diabetic foot wound, J Am Podiatr Med Assoc 99(4) (2009) 301-305.

[365] T. Arca, J. Proffitt, P. Genever, Analysis of human mesenchymal stem cells on a cross-linked collagen-based surgical implant material, Biomed Mater Eng 22(5) (2012) 261-76.

[366] F. Spelzini, S. Manodoro, M. Frigerio, G. Nicolini, D. Maggioni, E. Donzelli, L. Altomare, S. Fare, F. Veneziano, F. Avezza, G. Tredici, R. Milani, Stem cell augmented mesh materials: an in vitro and in vivo study, Int Urogynecol J 26(5) (2015) 675-83.

[367] T.M. MacLeod, A. Cambrey, G. Williams, R. Sanders, C.J. Green, Evaluation of Permacol™ as a cultured skin equivalent, Burns 34(8) (2008) 1169-1175.

[368] S. Chaudhury, C. Holland, M.S. Thompson, F. Vollrath, A.J. Carr, Tensile and shear mechanical properties of rotator cuff repair patches, J Shoulder Elbow Surg 21(9) (2012) 1168-1176.

[369] S. Lucke, A. Hoene, U. Walschus, A. Kob, J.W. Pissarek, M. Schlosser, Acute and chronic local inflammatory reaction after implantation of different extracellular porcine dermis collagen matrices in rats, Biomed Res Int 2015 (2015) 938059.

[370] T.M. Macleod, G. Williams, R. Sanders, C.J. Green, Histological evaluation of Permacol™ as a subcutaneous implant over a 20-week period in the rat model, Br J Plast Surg 58(4) (2005) 518-532.

[371] F.S. Ayubi, P.J. Armstrong, M.S. Mattia, D.M. Parker, Abdominal wall hernia repair: a comparison of Permacol® and Surgisis® grafts in a rat hernia model, Hernia 12(4) (2008) 373-378.

[372] M. Kalin, S. Kuru, K. Kismet, A.M. Barlas, Y.A. Akgun, H.M. Astarci, H. Ustun, E. Ertas, The effectiveness of porcine dermal collagen (Permacol(®)) on wound healing in the rat model, Indian J Surg 77(Suppl 2) (2015) 407-411.

[373] G.P. Nicholson, G.J. Breur, D. Van Sickle, J.Q. Yao, J. Kim, C.R. Blanchard, Evaluation of a cross-linked acellular porcine dermal patch for rotator cuff repair augmentation in an ovine model, J Shoulder Elbow Surg 16(5) (2007) S184-S190.

[374] J.W. Tsai, F.S. Ayubi, R.D. Rice, Z. Zhang, P.J. Armstrong, Permacol (porcine dermal collagen) and Alloderm (acellular cadaveric dermis) as a vascular patch repair for common carotid arteriotomy in a rabbit model, Ann Vasc Surg 23(3) (2009) 374-381.

[375] T.E. Simon, R.J. Johnson, A.L. Naig, J.R. Brockmeyer, B.M. Prasad, P.W. White, Permacol interposition graft as an alternative to vein in contaminated wounds using a rabbit model, Ann Vasc Surg 29(6) (2015) 1307-1314.

[376] P. Wille-Jørgensen, B. Pilsgaard, P. Møller, Reconstruction of the pelvic floor with a biological mesh after abdominoperineal excision for rectal cancer, Int J Colorectal Dis 24(3) (2009) 323-325.

[377] S. Wahed, M. Ahmad, K. Mohiuddin, M. Katory, M. Mercer-Jones, Short-term results for laparoscopic ventral rectopexy using biological mesh for pelvic organ prolapse, Colorectal Dis 14(10) (2012) 1242-1247.

[378] C.-H. Cho, S.-M. Lee, Y.-K. Lee, H.-K. Shin, Mini-open suture bridge repair with porcine dermal patch augmentation for massive rotator cuff tear: Surgical technique and preliminary results, Clin Orthop Surg 6(3) (2014) 329-335.

[379] L. Knabben, G. Kanagalingam, S. Imboden, A.R. Günthert, Acellular dermal matrix (Permacol(®)) for heterologous immediate breast reconstruction after skin-sparing mastectomy in patients with breast cancer: A single-institution experience and a review of the literature, Front Med (Lausanne) 3 (2017) 72-72.

[380] T.A. Gurney, D.W. Kim, Applications of porcine dermal collagen (ENDURAGen) in facial plastic surgery, Facial Plast Surg Clin North Am 15(1) (2007) 113-21, viii.

[381] C. McCord, F.R. Nahai, M.A. Codner, F. Nahai, T.R. Hester, Use of porcine acellular dermal matrix (Enduragen) grafts in eyelids: a review of 69 patients and 129 eyelids, Plast Reconstr Surg 122(4) (2008) 1206-13.

[382] A. Barmettler, M. Heo, A prospective, randomized comparison of lower eyelid retraction repair with autologous auricular cartilage, bovine acellular dermal matrix (Surgimend), and porcine acellular dermal matrix (Enduragen) spacer grafts, Ophthal Plast Reconstr Surg 34(3) (2018) 266-273.

[383] G. Pascual, S. Sotomayor, F. Adel, B. Perez-Kohler, M. Rodriguez, A. Cifuentes, J.M. Bellon, Remodeling of noncrosslinked acellular dermal matrices in a rabbit model of ventral hernia repair, Eur Surg Res 56(1-2) (2016) 32-48.

[384] W.Q. Sun, H. Xu, M. Sandor, J. Lombardi, Process-induced extracellular matrix alterations affect the mechanisms of soft tissue repair and regeneration, J Tissue Eng 4 (2013) 2041731413505305.

[385] E.N. Fahrenbach, C. Qi, O. Ibrahim, J.Y. Kim, M. Alam, Resistance of acellular dermal matrix materials to microbial penetration, JAMA Dermatol 149(5) (2013) 571-5.

[386] G.A. Monteiro, N.L. Rodriguez, A.I. Delossantos, C.T. Wagner, Short-term in vivo biological and mechanical remodeling of porcine acellular dermal matrices, J Tissue Eng 4 (2013) 2041731413490182.

[387] B.D. Powell, S.A. Cofer, J.J. Garcia, In vivo Durability and Safety of Rolled Acellular Dermis in a Submucosal Pocket in Pigs, Laryngoscope 121(S5) (2011) S346-S346.

[388] G. Pascual, B. Pérez-Köhler, M. Rodríguez, S. Sotomayor, J.M. Bellón, Postimplantation host tissue response and biodegradation of biologic versus polymer meshes implanted in an intraperitoneal position, Surg Endosc 28(2) (2014) 559-569.

[389] L. Ansaloni, P. Cambrini, F. Catena, S. Di Saverio, S. Gagliardi, F. Gazzotti, J.P. Hodde, D.W. Metzger, L. D'Alessandro, A.D. Pinna, Immune response to small intestinal submucosa (Surgisis) implant in humans: preliminary observations, J Invest Surg 20(4) (2007) 237-241.

[390] J.H. Koetje, T. Irvine, S.K. Thompson, P.G. Devitt, S.D. Woods, A. Aly, G.G. Jamieson, D.I. Watson, Quality of life following repair of large hiatal hernia is improved but not influenced by use of mesh: Results from a randomized controlled trial, World J Surg 39(6) (2015) 1465-1473.

[391] L.K. Papatheodorou, B.G. Williams, D.G. Sotereanos, Preliminary results of recurrent cubital tunnel syndrome treated with neurolysis and porcine extracellular matrix nerve wrap, J Hand Surg Am 40(5) (2015) 987-92.

[392] M.T. Wilson, S.-K. Chuang, V.B. Ziccardi, Lingual nerve microsurgery outcomes using 2different conduits: A retrospective cohort study, J Oral Maxillofac Surg 75(3) (2017) 609-615.

[393] L. Song, R.E. Olsen, J.P. Spalazzi, T. Davisson, Biomechanical evaluation of acellular collagen matrix augmented Achilles tendon repair in sheep, J Foot Ankle Surg 49(5) (2010) 438-41.

[394] E.R. Guerzon, B.P. Pereira, K. Bhavanam, Z.A. Khin, S.S. Nathan, Collagen membranes for host-graft integration: an animal study, J Orthop Surg (Hong Kong) 19(2) (2011) 151-6.

Chapter 2

Decellularised porcine peritoneum as a tendon barrier biomaterial

Part of this chapter has been published:

Capella-Monsonís, H., Kelly, J., Kearns, S., & Zeugolis, D. I. (2019). *Decellularised porcine peritoneum as a tendon protector sheet*. **Biomedical Materials**, 14(4), 044102.

2.1. Introduction

In recent years, although significant strides have been achieved in biomaterials processing [1], we are still not able to develop implantable devices that closely imitate native tissue architecture and composition [2, 3]. To this end, tissue grafts are favoured for biomedical applications, as they preserve tissue architecture and composition and, as a result, they offer superior biofunctionality [4, 5]. Autografts and allografts [5] are extensively used for tissue engineering applications, however, their limited availability triggered investigation into the use of xenografts [6]. Advancements in decellularisation methods enabled development of implantable devices with reduced risk of immune reaction [7-10], whilst still preserve the characteristics of native tissues (e.g. tendon [11, 12], tendon-bone interface [13], cornea [14, 15], heart valve [16, 17]) and organs (e.g. lung [18, 19], liver [20, 21], kidney [22, 23]).

Decellularised tissue grafts are extensively used in hernia and wound healing [24-29]. Augmentation [30] and wrapping [31] devices for tendon are also used to reinforce tendon tissues and prevent scar formation, respectively. Augmentation systems include synthetic (e.g. Sportmesh™), xenogeneic (e.g. Permacol™) and allogeneic (e.g. GraftJacket®) devices, which are intended to promote remodelling and provide mechanical support during the healing [30]. Current augmentation systems have been shown to provide superior functional recovery than conventional primary repairs and are characterised by adequate mechanical properties [30, 32, 33]. Decellularised pericardium [34] and a cell seeded PGA scaffold [35] have also shown promise as tendon sheaths. These wrapping systems must limit adhesions formation and promote gliding of tendon tissue [36]. However, complications derive from the disruption of the tendon sheath still represent a major burden in orthopaedic surgery and no optimal option seems to be available [31]. TenoGlide®, a collagen type I and glycosaminoglycans (GAG) scaffold, is clinically available as a means to reduce the risk of adhesions and to promote gliding [37]. Although promising results in reducing adhesions *in vivo* [38] are available, no clinical data support its use as a tendon sheath substitute.

In this study, we ventured to assess the biochemical, biophysical and biological properties of decellularised porcine peritoneum (XenoMEM™, Viscus Biologics LLC, Ohio, USA) and to correlate them to a commercially available tendon wrapping collagen matrix (TenoGlide®, Integra Lifesciences, New Jersey, USA) to test its potential as antiadhesion barrier.

2.2. Materials and methods

2.2.1. Materials

The decellularised porcine peritoneum (XenoMEM™) was provided by Viscus Biologics LLC (Ohio, USA) in freeze-dried state. The collagen matrix (TenoGlide®) was purchased from Integra Lifesciences (New Jersey, USA) and was delivered in wet state in phosphate buffered saline (PBS). All chemical and consumables were purchased from Sigma-Aldrich (Ireland), unless otherwise stated.

2.2.2. Solubility analysis

To assess the presence of soluble collagen, solubility assay was carried out, as has been described previously [39]. Briefly, samples were incubated at 1 mg dry weight of material per ml of extraction solution in 0.5 M acetic acid or in 1 mg / ml pepsin (P6687, Sigma-Aldrich) in 0.5 M acetic acid overnight at 4 ^{0}C under agitation. Then samples were analysed by SDS-PAGE and stained with SilverQuest™ Silver Staining kit (ThermoFisher Scientific), purified bovine collagen type I (CBP2US, Symatese) was used as control

2.2.3. Free amine analysis

Ninhydrin assay was employed to quantify free amines, as has been described previously [39]. Samples were weighed and incubated with 4 % ninhydrin in 2-ethoxyethanol and citric acid 200 mM in 0.16 % tin II chloride (pH 5.00), ratio 1:1, at 100 °C for 15 min. The reaction was then stopped by adding 50 % 2-propanol. Absorbance was then measured using a plate reader (VarioSkan Flash Spectral Scanning Multimode Reader, Thermo Scientific, Ireland) at 570 nm and the amount of free amines was calculated.

2.2.4. Thermal analysis

In order to study the thermal properties of the materials, differential scanning calorimetry (DSC) analysis was performed, as has been described previously [39, 40]. Samples were incubated in PBS overnight and following blotting on filter paper to remove non-bound surface PBS, they were placed in DSC aluminium pans. The denaturation temperature was determined using the DSC-60/60A, Shimadzu Scientific Instruments (UK). Heating was carried out at a constant temperature ramp of 5 ºC / min in the temperature range 25 to 100 °C. An empty aluminium pan was used as reference. Thermal denaturation was recorded as a typical peak, and the onset and peak temperatures were recorded, along with the transition enthalpy.

2.2.5. Collagenase degradation assay

Resistance to enzymatic (collagenase) degradation was assessed as has been described previously [39, 41]. Biological degradation of both materials by the collagenases MMP-8 (17101015, Gibco®) and MMP-1 (C5138, Sigma-Aldrich) was analysed. Degradation was assessed by weight loss after 4, 8, 12 and 24 h of incubation in MMP-1 and MMP-8 degradation buffer. In summary, 5 mg of dry samples were incubated in MMP-1 and MMP-8 at 50 U / ml in tris-HCl 0.1 M (pH 7.40) at 37 °C and continuous agitation at 150 rpm for the different time points. Then, samples were centrifuged at 3,500 g at room temperature for 10 min and the pellets freeze dried overnight. After freeze drying, weight was recorded for each sample and relative weight loss was calculated.

2.2.6. Mechanical properties

The mechanical properties were assessed by tensile uniaxial test, as has been described previously [42]. Briefly, 1 x 5 cm strips for each material were incubated overnight in PBS. The following date, the strips were quickly blotted on filter paper to remove non-bound surface PBS. A Z009 Zwick Tensile Tester (Zwick Roell, Ireland) was used. All tests were carried out at 20 mm / min with a 0.1 N pre-load until the sample broke. Correct clamping, absence of slippage and breakage in the middle of the sample was ensured thorough the test.

2.2.7. Histology and immunohistochemistry

Samples were fixed in Tissue Freezing Medium® (Leica Biosystems, Ireland) at -80 °C for at least 12 h. subsequently, transverse cryosections of 5 μm were obtained using the CM1850 Cryostat (Leica Biosystems, Ireland). The samples were then stained with haematoxylin and eosin, Picrosirius red and Masson's trichrome [43] and mounted using DPX mountant (06522, Sigma-Aldrich, Ireland).

Immunohistochemistry of the sections was carried out for collagen type I (ab90395, Abcam, USA), collagen type III (ab7778, Abcam, USA), collagen type IV (ab6586, Abcam, USA), elastin (ab21610, Abcam, USA), laminin (L939, Sigma-Aldrich, Ireland) and fibronectin (F7387, Sigma-Aldrich, Ireland), as has been described previously [43], with slight modifications. Sections were blocked for 1 h at room temperature in 5 % normal goat serum (NGS) and 0.1 % Triton X-100 in PBS. Then, the sections were incubated with the primary antibodies diluted in blocking buffer at 1:100 overnight at 4 °C, followed by 3 washes in PBS. Subsequently, secondary antibody solutions at 1:500

were added (Alexa Fluor 488 goat anti rabbit and Alexa Fluor 555 goat anti mouse, Life Technologies, Ireland) for 1 h at room temperature, followed by 3 washes in PBS. Nuclei were stained with Hoechst (H1399, Invitrogen, Ireland) at 1:5000 in PBS for 5 min at room temperature. Finally, sections were mounted with Fluoromount™ Aqueous Mounting Medium (F4680, Sigma-Aldrich, Ireland), left for 2 h at room temperature and then stored at 4 °C. Images were taken with an inverted fluorescence microscope (IX81, Olympus, UK).

2.2.8. Scanning electron microscopy and atomic force microscopy analysis

Topography of both sides of XenoMEM™ and TenoGlide® was analysed after freeze drying. SEM analysis was conducted using the Hitachi S-4700 scanning electron microscope (Hitachi, UK) at 5.0 kV after gold-coating of the samples (Emitech K-550X Sputter Coater, Emitech, UK). AFM analysis was conducted using the Dimension 3100 (Veeco Instruments Inc., USA) and images were captured and analysed at 0.5 Hz of scan frequency and 1.0 V of amplitude set point.

2.2.9. Coefficient of friction

Tribological analysis was carried out to assess the coefficient of friction of both layers of XenoMEM™ and of TenoGlide®. Samples incubated in PBS overnight, were wrapped around a tube that was fixed with an in-house designed tribometer (CSM Manufactured Systems, UK) and analysis was carried out as previously described for soft tissue using glass as static reference [44]. The samples remained hydrated throughout the analysis.

2.2.10. Cell response analysis

Primary adult dermal fibroblasts (DFs, ATCC®, UK) were expanded in Dulbecco's minimum essential medium (DMEM) high glucose with L-glutamine supplemented with 10 % foetal bovine serum (FBS) and 1 % penicillin / streptomycin (P / S) at 37 °C and 5 % CO_2. Cells were seeded at passage 4, when they had reached 90-95 % confluence. Indirect cell cytotoxicity was assessed with conditioned media (CM) from each material. XenoMEM™ and TenoGlide® were incubated at 2 ml / cm^2 for 1, 3 and 7 days with complete medium; at each time point the media were collected and acted as CM (CM1, CM3 and CM7 for day 1, 3 and 7, respectively). DFs were then incubated for 1, 3 and 7 days with each of the different CM and assessment of metabolic activity, viability and proliferation were carried out with alamarBlue® (ThermoFisher, Ireland), LIVE / DEAD® (ThermoFisher, Ireland) and Quant-iT PicoGreen® dsDNA (ThermoFisher,

Ireland) assays, respectively (**Figure 2.1**). For cell seeding on the materials, pieces of 1 cm^2 of both XenoMEM™ and TenoGlide® were sterilized with 70 % ethanol for 30 min and washed in PBS for 3 times. Then, they were placed at the bottom of the wells of a 24-well plate and kept in place using a silicone ring (Z504165, Sigma-Aldrich, Ireland). DFs were then seeded on both sides of the peritoneum and on TenoGlide® at 50,000 cells / well and incubated at 37 °C and 5 % CO_2. Medium was replaced every 3 days and cells were cultured for 3, 7 and 14 days. Metabolic activity and viability were assessed with alamarBlue® (ThermoFisher, Ireland) and LIVE / DEAD® (ThermoFisher, Ireland) assays, respectively. For morphology analysis, cells and samples were fixed in 4 % paraformaldehyde (PFA, 158127, Sigma-Aldrich, Ireland) in PBS for 15 min, then washed with PBS and stained with rhodamine-phalloidin (R415, Life Technologies, Ireland) in PBS at 1:500 for 1 h. After washing with PBS, nuclei were stained with Hoechst solution (see section 2.7) and the samples were imaged. Cell proliferation was assessed through nuclei counting with ImageJ (NIH, USA) and was also employed to normalise metabolic activity. Alignment was quantified through Fast Fourier Transform (FFT) and 90 ° correction of the image, whereas manual measurement of individual DFs degree was employed to quantify the distribution of aligned cells.

Human tenocytes (TCs) were obtained from human flexor tendon, using the migration approach. After expansion in complete medium, they were seeded at passage 4 on both sides of XenoMEM™ and on TenoGlide® following the same procedure and assessments described above.

Both XenoMEM™ and TenoGlide® were seeded with DFs and TCs for 14 days, fixed in 4 % PFA, cryosectioned as described above and stained with DAPI to assess cell penetration.

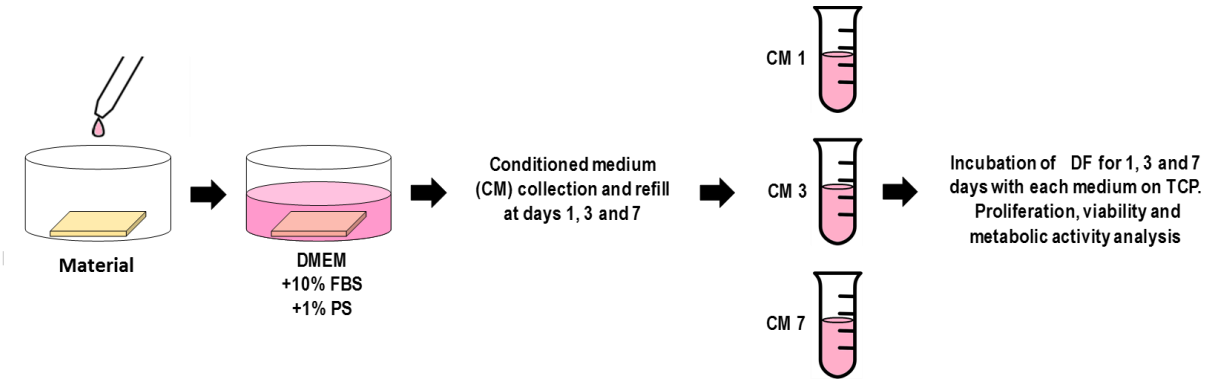

Figure 2.1. Schematic experimental design for materials conditioned media (CM) analysis.

2.2.11. Immune response *in vitro* analysis

Immune response was assessed as has been described previously [42]. Monocyte-like cells (THP-1, ATCC, UK) were expanded in RPMI-1640 medium supplemented with 10 % FBS and 1 % P / S (Sigma-Aldrich, Ireland). Cells were seeded in 48-well plates for CM inflammatory response assessment or on the materials at 25,000 cells/cm^2. To induce the macrophage phenotype, cells were treated with phorbol 12-myristate 13-acetate (PMA, P8139, Sigma-Aldrich, Ireland) at 100 ng / ml for 6 h at 37 °C and 5 % CO_2. Non-attached cells were washed with PBS. The cells on the well plates were incubated with 2 days CM [45, 46] produced as described above for 1 and 2 days, whereas cells attached on the materials were incubated with complete RPMI-1640 medium. As positive control, cells were treated with lipopolysaccharides (LPS) from *E. Coli* (L2637, Sigma-Aldrich, Ireland) at 100 ng / ml to induce inflammatory response. Metabolic activity was assessed with alamarBlue® assay and normalised to proliferation, whilst proliferation was assessed by nuclei counting after fixation in 4 % PFA and Hoechst staining. To assess the immune response *in vitro*, morphology of the cells was analysed after imaging cells with an inverted microscope (CKX41, Olympus, UK) in the case of CM-incubated cells or after rhodamine-phalloidin staining and imaging for THP-1 cells attached to the materials. Images were analysed with ImageJ and the relative number of elongated cells was calculated. The shape of the cells was described manually and the aspect ratio, circumference and roundness were measured. Those cells with an aspect ratio inferior to 3.0 and a circumference and roundness superior to 0.5 were considered as round cells, meanwhile the rest were considered as elongated. The formation of clusters was also assessed, were only those containing 5 or more cells were considered.

To quantify the production of pro-inflammatory cytokines by THP-1 cells, media from each condition at days 1 and 2 were collected and stored at -80 °C. ELISA analysis of cytokines was carried out employing DuoSet ELISA kits for human TNF-α and IL-6 (DY210 and DY206, respectively, R&D Systems, UK) on Nunc MaxiSorp™ 96-well ELISA plates (ThermoFisher, Ireland) as per manufacturer's instructions. Briefly, capture antibody solution was incubated in the wells of the ELISA plate overnight at room temperature. Then, 3 washing steps with 0.05 % Tween®20 in PBS and a blocking step for 1 h with 1 % BSA in PBS were carried out. After other 3 washes, 100 μl of thawed medium samples were added and incubated 1 h at room temperature. Samples were then washed and the diluted detection antibody was pipetted on the samples. After 1 h incubation, other 3 washing steps were carried out followed by an incubation with

streptavidin-HRP solution for 20 min and further 3 washes were conducted. Subsequently, substrate solution (1-Step™ Ultra TMB-ELISA, ThermoFisher, Ireland) was added and allowed to develop for 20 min. 2 N sulfuric acid solution was added to stop the reaction. Absorbance was read at 450 nm with correction at 540 nm.

2.2.12. Epithelium formation *in vitro* analysis

Mesothelial cells (MeT-5A, ATCC, UK) were expanded in M199 medium supplemented with 10 % FBS, 1 % P / S, 20 mM HEPES, 3.3 nM epidermal growth factor (EGF), 400 nM hydrocortisone and 870 nM bovine insulin (Sigma-Aldrich, Ireland). Cells were seeded in 12 mm trans-well inserts with a polyester membrane of 4 μm pore size (CLS3460, Sigma-Aldrich, Ireland). XenoMEM™ (samples for both BM and CT sides) and TenoGlide® were cut in 12 mm diameter pieces with a biopsy punch and placed at the bottom of the trans-well insert, fixed with a silicone O-ring (Z504165, Sigma-Aldrich, Ireland) and cells were seeded in complete M199 medium at 25,000 cells / cm2; cells seeded on the trans-well membrane were used as control. Medium was collected and replaced every 3-4 days. At days 7, 14 and 21, the production of tissue plasminogen activator (tPA) and plasminogen activator inhibitor (PAI) was analysed with ELISA (DY7449 and DY1786 respectively, R&D Systems, UK). At the same time points, cells were fixed in 4 % PFA, stained with rhodamine phalloidin and Hoechst and imaged. Seeded materials at the same time points were further processed in a tissue processor (Excelsior AS, ThermoFisher, Ireland), embedded in paraffin blocks and transverse sections of 5 μm were stained with haematoxylin and eosin to assess the morphology of the cell layer formed.

2.2.13. Flexor tendon barrier model in vivo

A model to test the potential of XenoMEM in vivo was developed through a pilot study on adult New Zealand White rabbits, based in previous established models. All the procedures were carried out under ethical approval of the Animal Care Research Ethics Committee of the National University of Ireland Galway (NUI Galway). Briefly, animals were anaesthetised with ketamine at 35 mg / kg and the digits of both hind paws were shaved, cleaned and sterilised. An incision on the zone II of the 2nd and 3rd digits of the paws was practised and the flexor digitorum profundus tendon was identified and fully sectioned with a scalpel proximally to the vincula. The tendon was then repaired with a modified Kessler core suture using 5-0 braided polyester. The repair area was wrapped employing either XenoMEM with the CT or BM facing the tendon, or with TenoGlide®,

and the skin was sutured. PBS was applied after the repair in the negative control. The same treatment was applied in all surgery areas (4 per animal) of each rabbit, with n=3 per treatment. The paws of the animals were then casted employing a metal splint for one week and a soft cast for the next week. For the rest of the study the paws were not casted, allowing free movement of the digits. This protocol was supervised by orthopaedic surgeons to better imitate the clinical practice of initial restraint and gradual gain of movement. Animals were euthanised after 8 weeks and fingers were collected and employed either for mechanical analysis or histology. Mechanical analysis consisted of tendon excursion, degree of flexion and uniaxial tensile tests. Fingers for mechanical tests were fixed through the bone, and flexor tendon excursion distance and degree of flexion in the proximal interphalangeal (PIP) joint were measured after applying a constant force of 2 N on the flexor tendon and 0.5 N on the extensor tendon to ensure initial straightness of the finger, by suturing the sectioned end of the tendon to the correspondent weight. For tensile uniaxial test, flexor tendon was carefully excised from the finger and analysis was carried out with a Z009 Zwick Tensile Tester (Zwick Roell, Ireland) at 20 mm / min until breakage with a reading load cell of 100 N, where the tendons where fixed with a hydraulic clamp system and maintained wet throughout the analysis. Force, stress and strain at breakage were recorded, and Young's modulus was calculated. For histology, fingers were fixed in 4 % PFA for 48 h and decalcified in 12 % EDTA and 2 % PFA solution for 2 weeks. Then, fingers were processed through sequential steps of dehydration in ethanol, xylene and paraffin in a tissue processor (Excelsior AS, ThermoFisher Scientific, UK). Paraffin blocks containing the finger surgery area were then sectioned and stained for haematoxylin and eosin.

2.2.14. Statistical analysis

Data were analysed using the IBM SPSS Statistics (IBM Analytics, USA) software. Student's t-test and one-way analysis of variance (ANOVA) followed by Fisher's post-hoc test were employed after confirming normal distribution from each sample population (Kolmogorov-Smirnov normality test) and equality of variances (Levine's test for homogeneity of variance). For non-normal distributions or different variance, Mann-Whitney U test and Kruskal-Wallis test were employed to assess significant differences. Significant difference was accepted at $p < 0.05$.

2.3. Results

2.3.1. Solubility, thermal, free amine and resistance to enzymatic degradation analysis

TenoGlide® was completely insoluble in both acetic acid and acetic acid / pepsin, whilst XenoMEM™ was soluble, mainly in acetic acid / pepsin (**Figure 2.2A**). TenoGlide® exhibited significantly higher ($p < 0.01$) denaturation temperature than XenoMEM™ (**Figure 2.2B**). TenoGlide® exhibited significantly lower ($p < 0.05$) free amine content than XenoMEM™ (**Figure 2.2C**). TenoGlide® exhibited significantly higher ($p < 0.05$) resistance to MMP-8 (**Figure 2.2D**) and MMP-1 (**Figure 2.2E**) than XenoMEM™. Enzymatic degradation results were qualitatively confirmed through SDS-PAGE of the supernatants (**Figure 2.3**).

2.3.2. Mechanical properties analysis

Tensile uniaxial test analysis revealed that the stress at break, strain at break and modules at 2 % strain values of TenoGlide® were significantly lower ($p < 0.01$) than those of XenoMEM™ (**Figure 2.4A**). Both TenoGlide® (**Figure 2.4B**) and XenoMEM™ (**Figure 2.4C**) exhibited a j-shape strain curve, characterised by a small toe region, a region of sharply rising stress and a long region of constant gradient up to fracture. TenoGlide® (**Figure 2.4B**) exhibited a sharply reduced stress at break, whilst XenoMEM™ (**Figure 2.4C**) exhibited a delayed reduced stress at break.

2.3.3. Histology and immunohistochemistry analysis

Histology analysis (**Figure 2.5**) revealed a loose structure for TenoGlide® and a dense structure for XenoMEM™. H&E, Picrosirius Red and Masson's trichrome stains showed that both TenoGlide® and XenoMEM™ were comprised of collagen and H&E and Masson's trichrome staining indicated no residual nuclei in XenoMEM™.

Immunohistochemistry analysis (**Figure 2.6**) made apparent that TenoGlide® was comprised of collagen type I, collagen type III and fibronectin (no collagen type IV, laminin and elastin were detectable), whilst XenoMEM™ was made up of collagen type I, collagen type III, collagen type IV (at the basement membrane site), fibronectin, laminin (at the basement membrane site) and elastin. DAPI staining confirmed the absence of nuclei at XenoMEM™ and TenoGlide®.

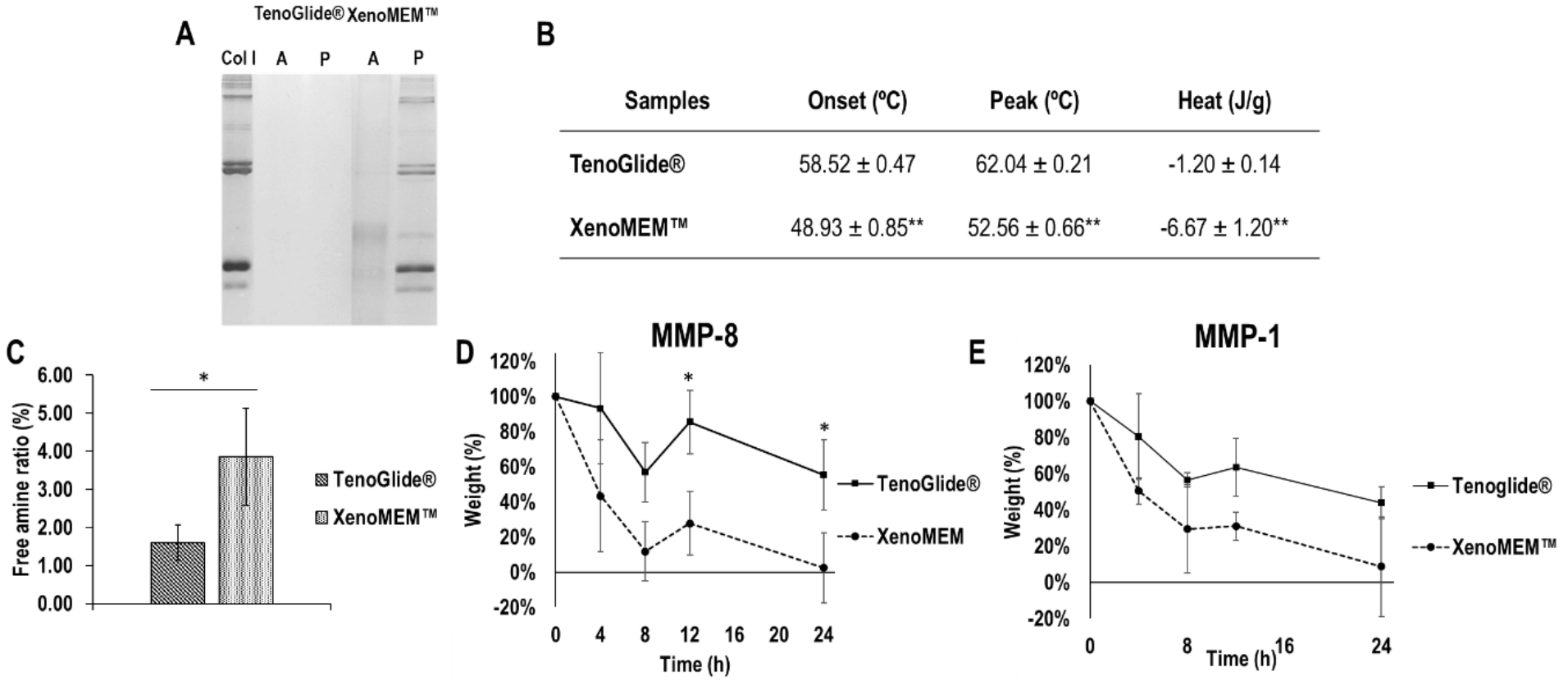

Figure 2.2. SDS-PAGE after acetic acid (A) and pepsin (P) extractions revealed that XenoMEM™ contained soluble collagen type I; no bands were observed in TenoGlide® (**A**). DSC analysis showed a higher denaturation temperature for TenoGlide® rather than for XenoMEM™ (n=5) (**B**). Free amines quantification revealed a lower crosslinking ratio of porcine peritoneum than TenoGlide® (n=6) (C). XenoMEM™ degraded faster by MMP-8 (**D**) and MMP-1 (**E**) than TenoGlide® (n=3). Data presented as mean ± standard deviation. A significant difference of $p < 0.05$ between samples is indicated as *, whereas ** implies $p < 0.01$.

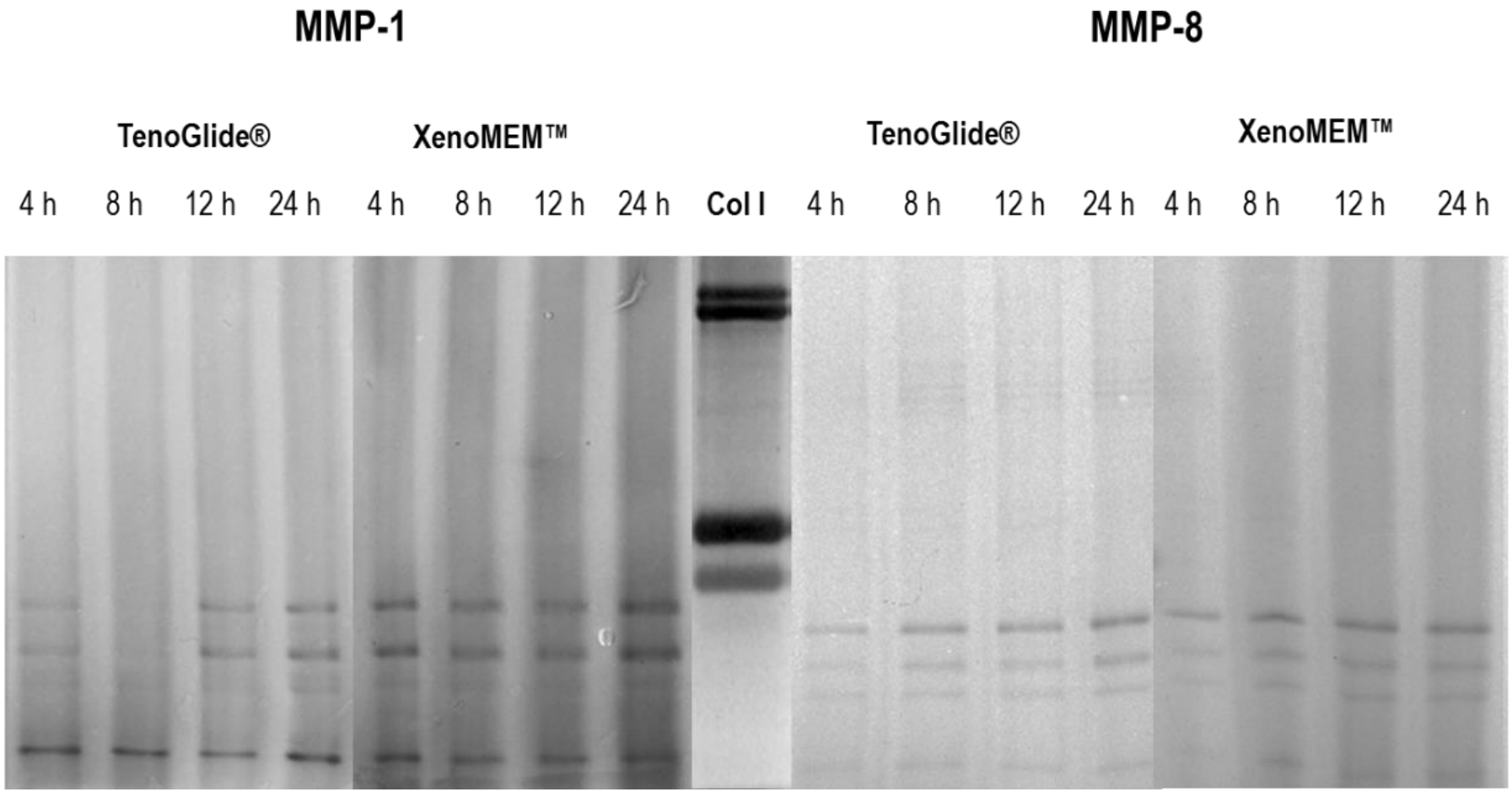

Figure 2.3. SDS-PAGE of enzymatic degradation supernatants qualitatively showed an increase in the concentration of collagen type, which was higher in XenoMEM™. Also, the bands size of approximately one third of native collage chains, confirmed cleavage from the MMP.

A

	Stress at break (MPa)	Strain at break (%)	Modules at 2% (MPa)
TenoGlide®	0.18 ± 0.02	6.20 ± 0.23	0.43 ± 0.01
XenoMEM™	34.79 ± 16.69**	19.61 ± 5.84**	3.59 ± 1.23**

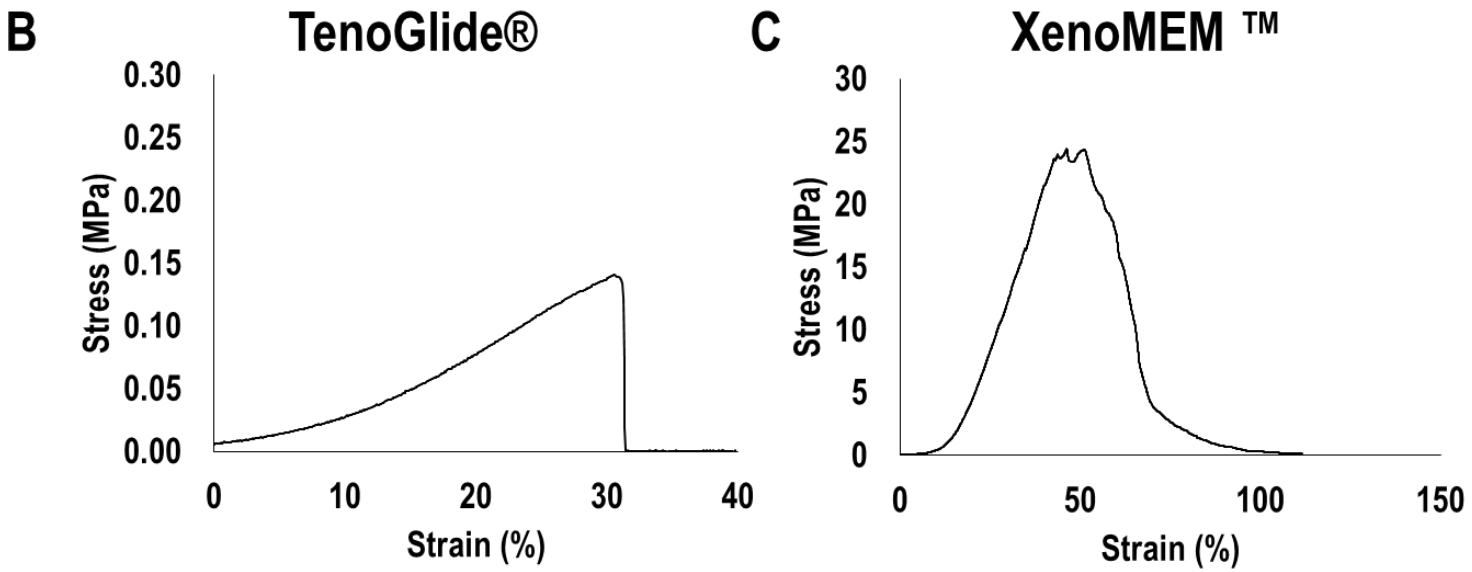

Figure 2.4. Tensile uniaxial test of TenoGlide® (n=5) and XenoMEM™ (n=3) showed higher stress at break, strain at break and module at 2 % for XenoMEM™ (**A**). Data presented as mean ± standard deviation. A significant difference of $p < 0.01$ between samples is indicated as **. Both TenoGlide® and XenoMEM™ exhibited typical J-shape stress / strain curves of collagenous materials (**B**).

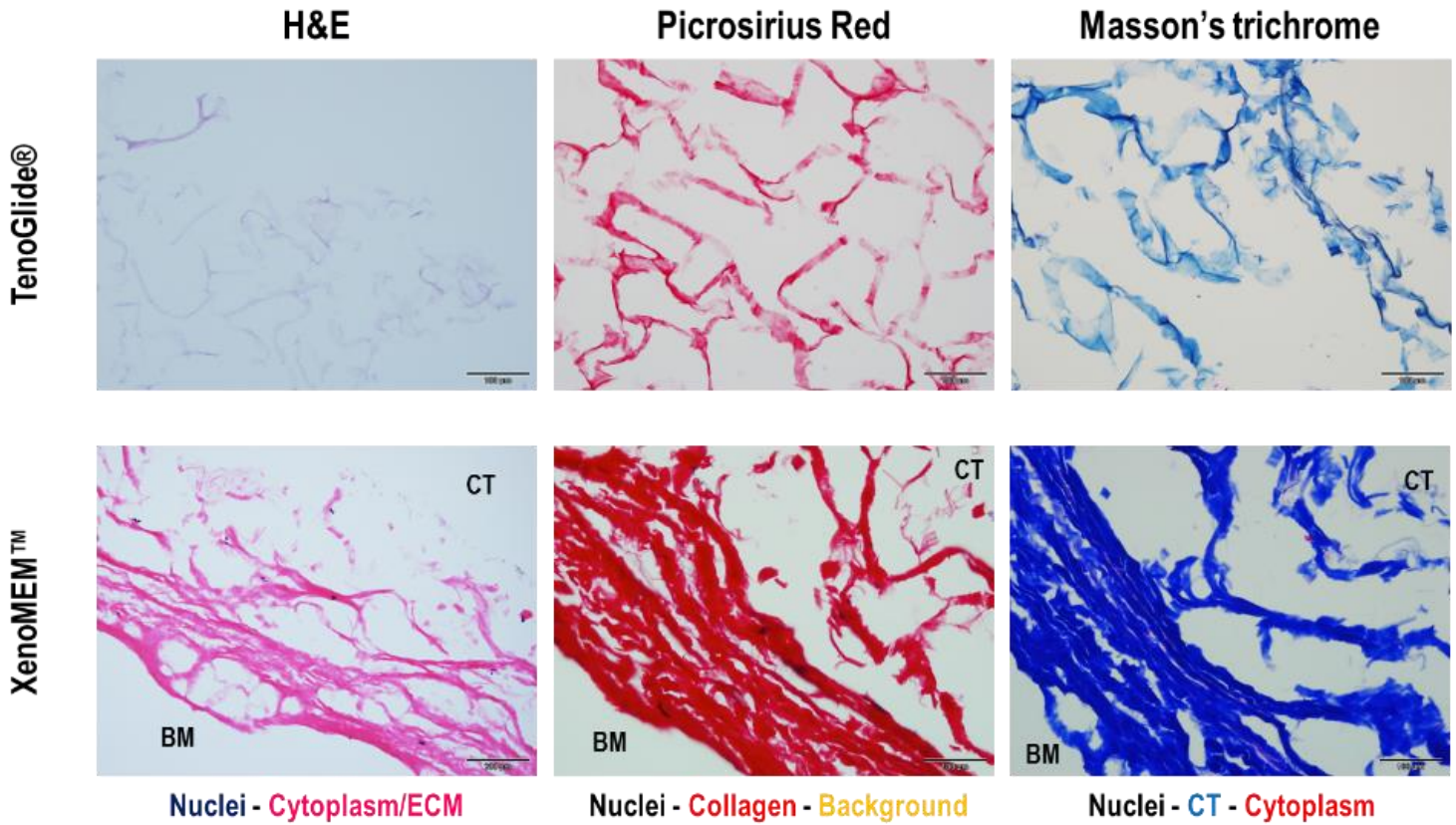

Figure 2.5. Histology analysis of cryosections revealed the acellular structure of TenoGlide® and XenoMEM™ and made apparent the architectural differences between the two materials. BM refers to the Basal Membrane side, CT refers to the Connective Tissue side of XenoMEM™. Scale bar 100 μm.

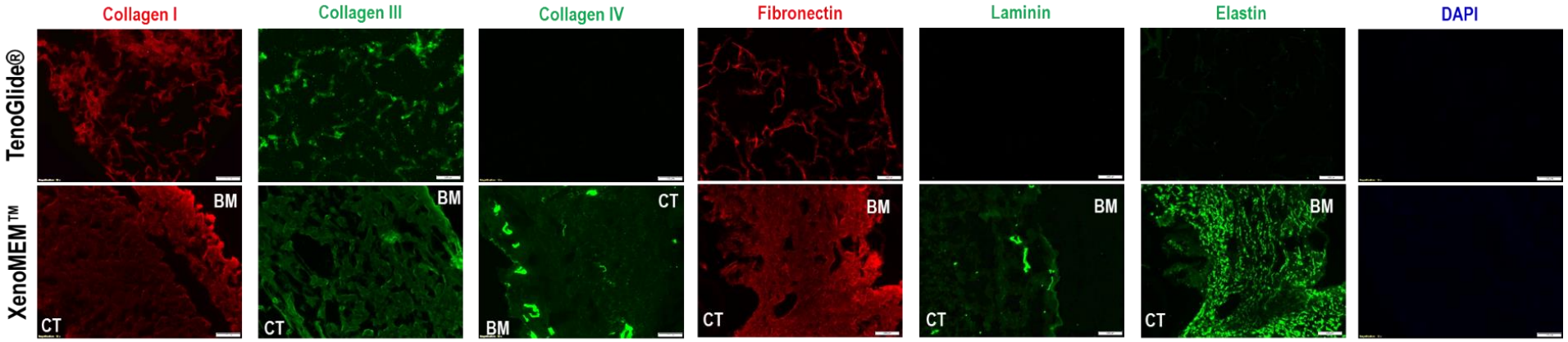

Figure 2.6. Collagen type I, collagen type III and fibronectin were observed by immunohistochemistry in cryosections of both TenoGlide® and XenoMEM™. Collagen type IV, laminin and elastin were only observed in XenoMEM™. No signal was detected with DAPI staining. BM refers to the Basal Membrane side, CT refers to the Connective Tissue side of XenoMEM™. Scale bar 100 μm.

2.3.4. SEM and AFM analysis

SEM analysis revealed that the freeze-dried TenoGlide® exhibited a collapsed porous structure, whilst the freeze-dried XenoMEM™ showed a smooth topography from the basement membrane site and a fibrous topography from the connective tissue site (**Figure 2.7A**). Quantitative analysis of AFM micrographs (**Figure 2.7B**) revealed that the freeze-dried TenoGlide® exhibited the lowest surface roughness ($p < 0.01$) (**Figure 2.7C**).

2.3.5. Coefficient of friction analysis

TenoGlide® exhibited a higher coefficient of friction than XenoMEM™ ($p < 0.01$), whilst the connective tissue site of XenoMEM™ exhibited the lowest ($p < 0.01$) coefficient of friction (**Figure 2.7D**).

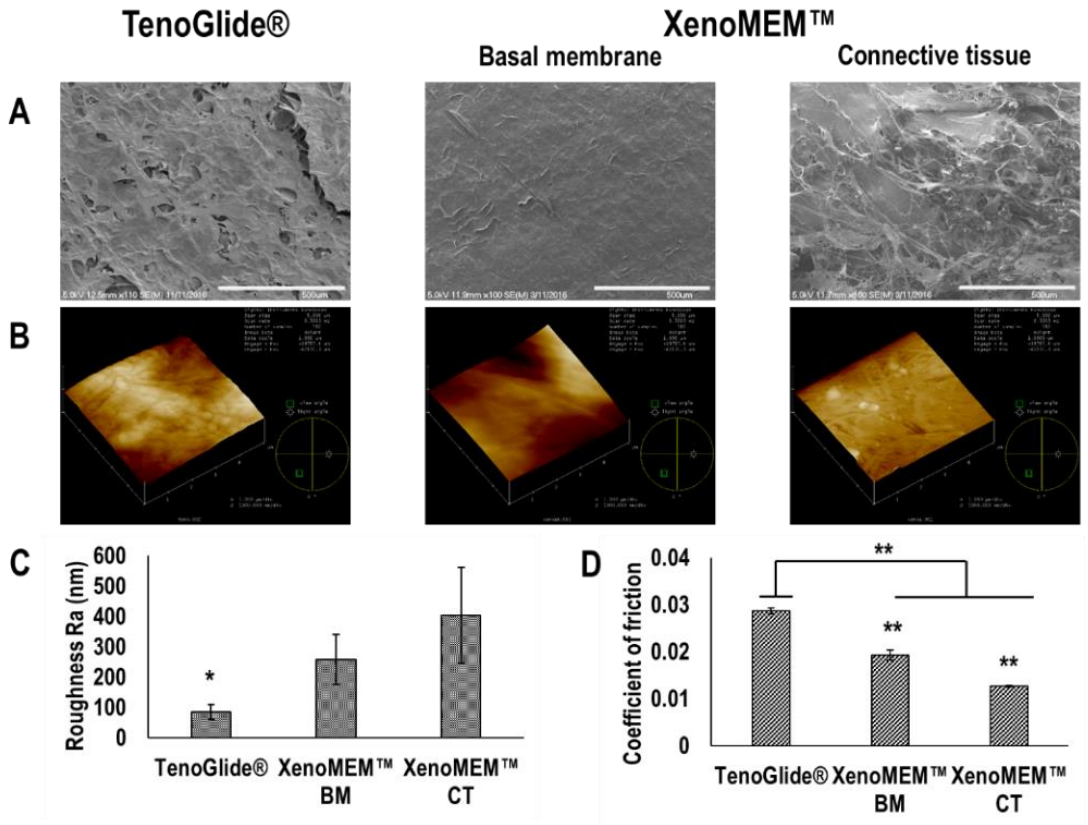

Figure 2.7. (**A**) SEM showed different topographies between both sides of XenoMEM™. (**B**) AFM images also revealed such differences in XenoMEM™. (**C**) Quantification of AFM images revealed a higher roughness in both sides of XenoMEM™ than that observed in TenoGlide®. (**D**) Contrary, both sides of XenoMEM™ presented a lower coefficient of friction in wet state against glass than TenoGlide®. BM indicates Basal membrane and CT connective tissue sides of XenoMEM™. A significant difference of *p*

< 0.05 between samples is indicated as *, meanwhile a difference of $p < 0.01$ between samples is indicated as ** (n=3).

2.3.6. Cell response analysis

Culture of DFs with CM from TenoGlide® and XenoMEM™ did not appear to affect cell viability, metabolic activity and proliferation (**Figure 2.8**).

Direct culture of TenoGlide® and XenoMEM™ with DFs did not appear to significantly ($p > 0.05$) affect cell viability (**Figure 2.9A**), metabolic activity (**Figure 2.9B**) and proliferation (**Figure 2.9C**) by day 14. Qualitative rhodamine-phalloidin staining revealed a rather bidirectional cytoskeleton orientation on the connective tissue side of XenoMEM™ (**Figure 2.9D**), which was confirmed after image analysis and quantification of aligned cells (**Figure 2.10**).

No difference was observed in cell viability at any time point between TenoGlide® and XenoMEM™, when they were seeded with TCs (**Figure 2.11A**). However, TenoGlide® exhibited the highest ($p < 0.05$) metabolic activity per cell at days 3 and 14 (**Figure 2.11B**) and lowest proliferation ($p < 0.01$) (**Figure 2.11C**) at day 7 and day 14. Also, the metabolic activity on XenoMEM™ BM was lower ($p < 0.05$) than the control at day 14, although proliferation was higher at days 7 ($p < 0.05$) and 14 ($p < 0.01$). Qualitative rhodamine-phalloidin staining confirmed the rather low TCs attachment and proliferation on TenoGlide® (**Figure 2.11D**).

DAPI staining after sectioning of the materials seeded with DFs and TCs showed that the cells were able to penetrate TenoGlide®, whereas they proliferated with no infiltration into XenoMEM™ when seeded on either side (**Figure 2.12**).

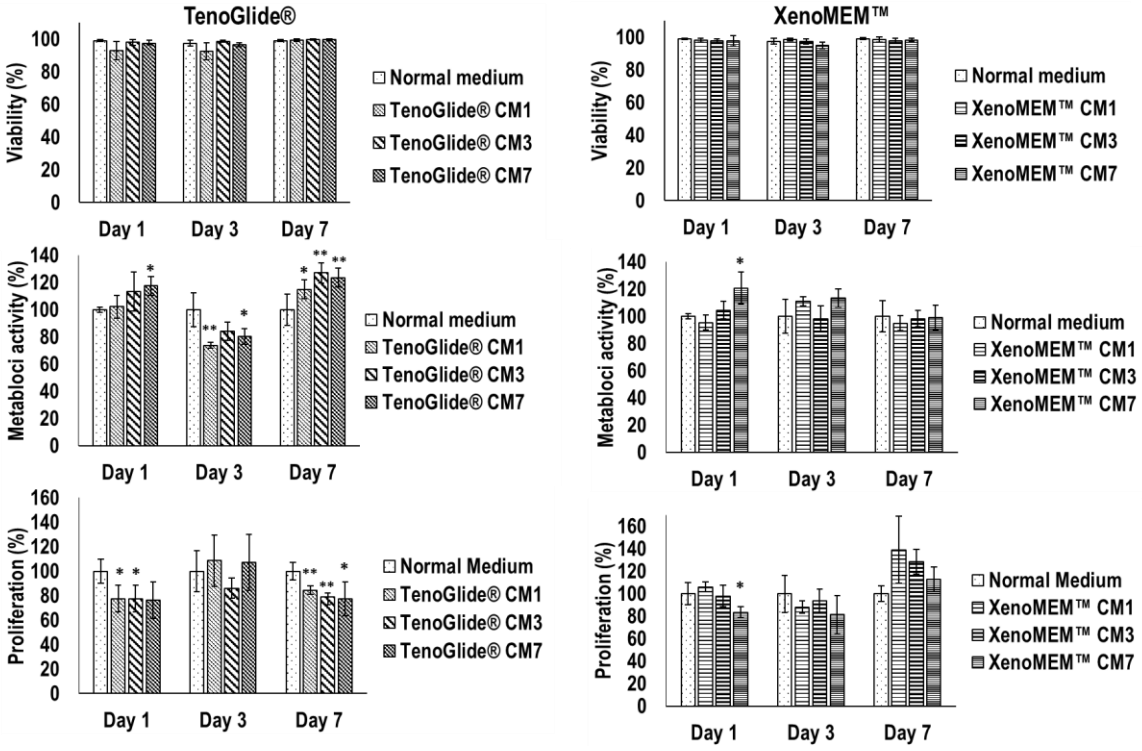

Figure 2.8. *In vitro* cell response of DFs to media conditioned with XenoMEM™ and TenoGlide® for 1 (CM1), 3 (CM3) and 7 (CM7) days. No significant effect was observed in any of the conditions on cell viability, metabolic activity (normalised to DNA content) nor proliferation. Data normalised to control and presented as mean ± standard deviation. A statistically significant difference of $p < 0.05$ with the control is indicated as *, whereas ** implies $p < 0.01$ (n=6).

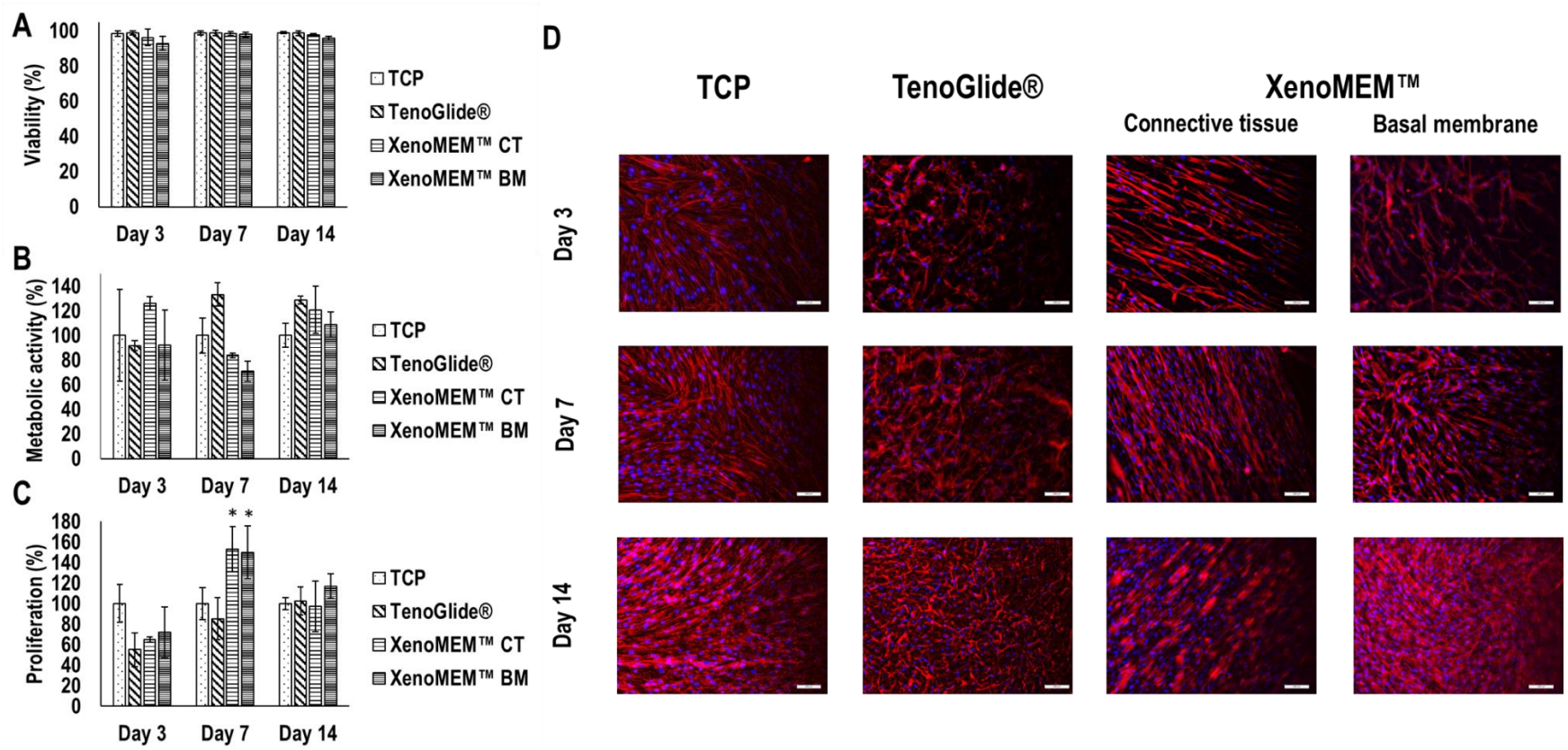

Figure 2.9. DFs viability (**A**), metabolic activity normalised to cell count (**B**) and proliferation (**C**) showed no significant differences when seeded on TenoGlide® and on both sides of XenoMEM™. Data normalised to control and presented as mean ± standard deviation (n=3). A statistically significant difference of $p < 0.05$ with the control is indicated as *, whereas ** implies $p < 0.01$. (D) Cytoskeleton (red) and nuclei (blue) staining confirmed previous results and showed a bidirectional alignment of cells in the connective tissue side of XenoMEM™. Scale bar 100 μm (**D**).

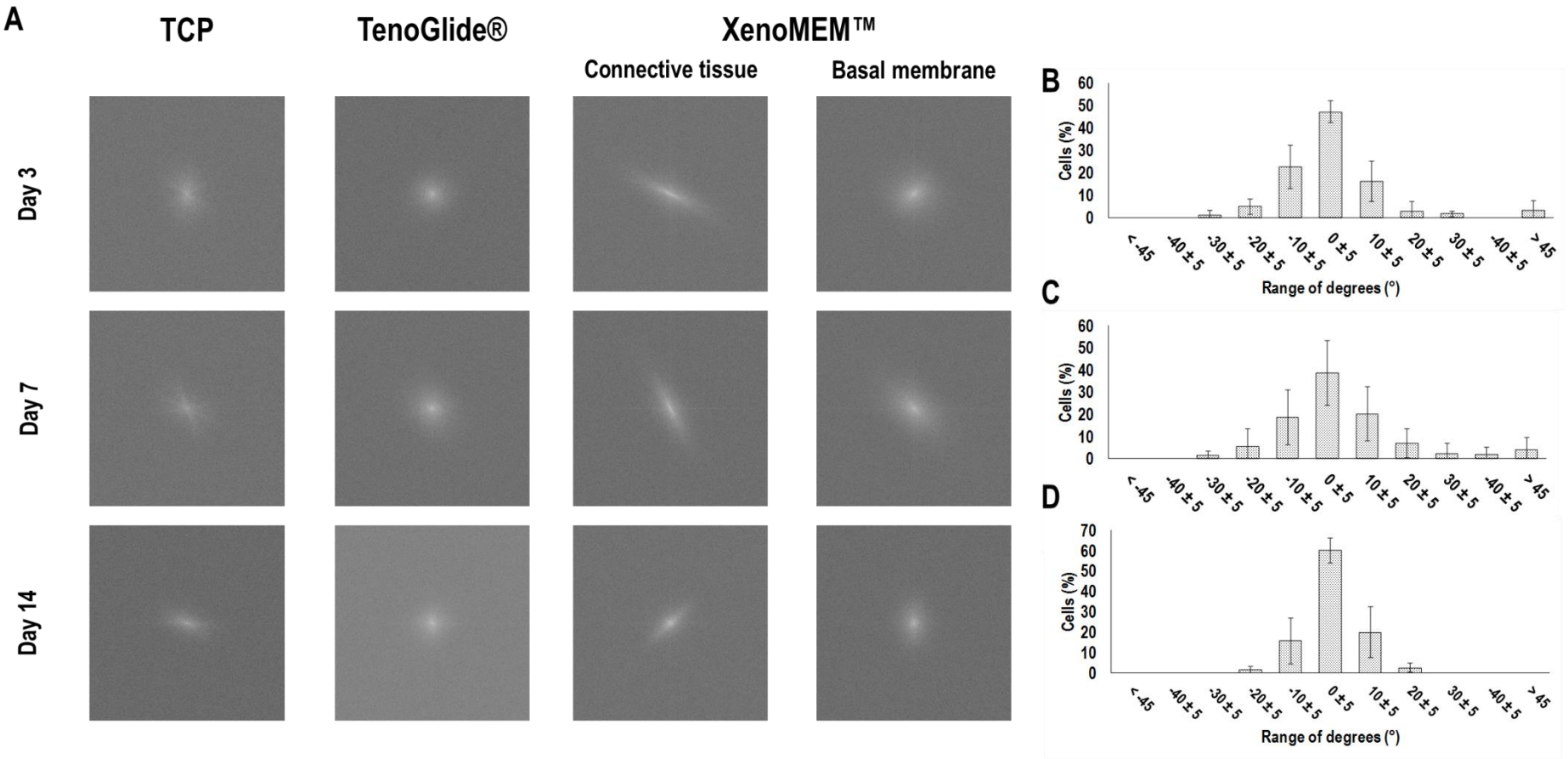

Figure 2.10. (A) FFT analysis after 90 ° correction of stained DF cytoskeleton images on the different materials showed a bidirectional alignment only in the connective tissue of XenoMEM™. (**B, C, D**) This alignment was confirmed after quantification of the DFs among different degrees of alignment on the connective tissue side of XenoMEM™ at days 3, 7 and 14. Data presented as mean ± standard deviation (n=3).

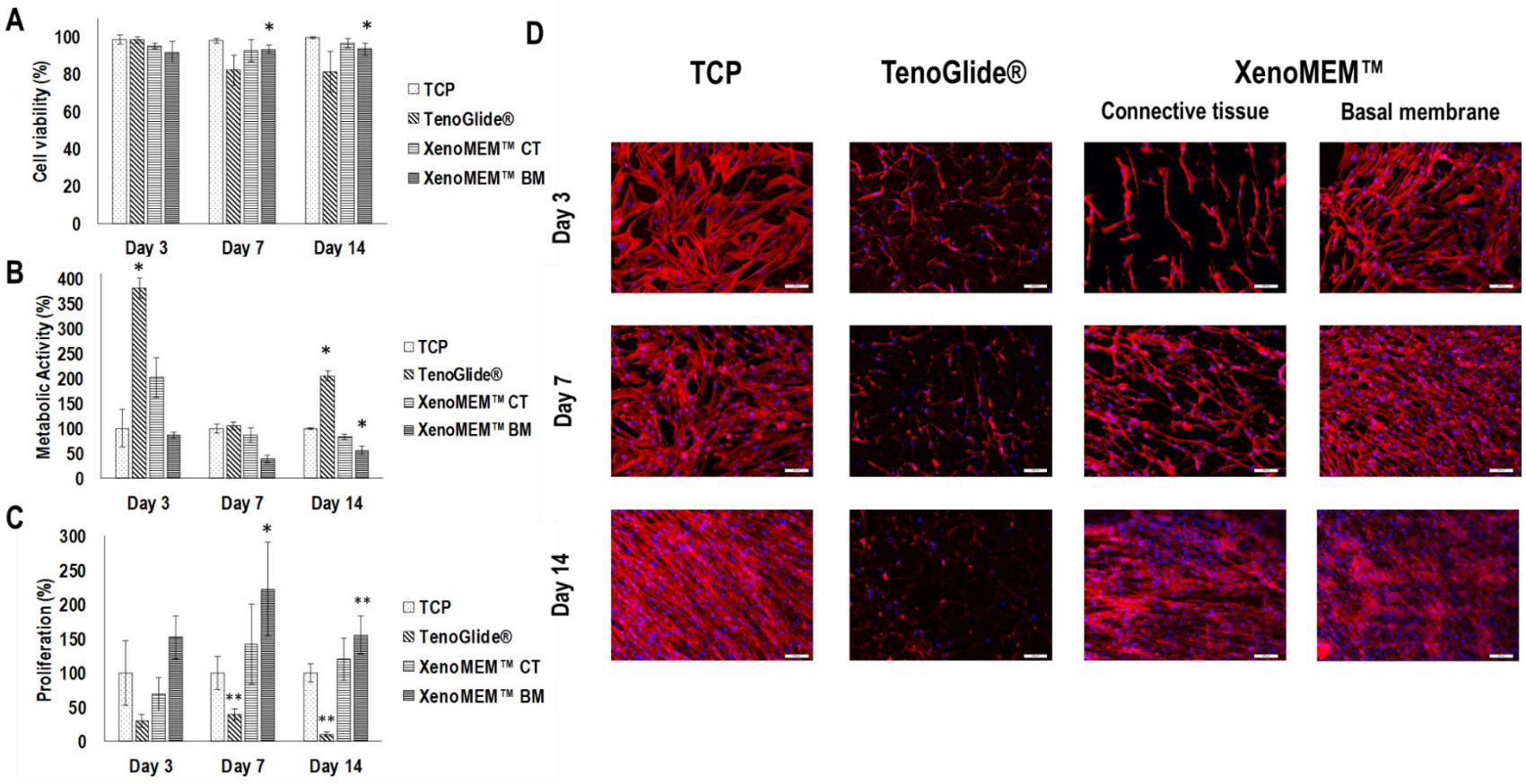

Figure 2.11. (**A**) TCs viability showed no differences among groups. (**B, C**) Contrary, normalised metabolic activity was higher, and proliferation was lower than control on TenoGlide®, whereas both sides of XenoMEM™ showed no significant difference. Data normalised to control and presented as mean ± standard deviation (n=3). A significant difference of $p < 0.05$ with the control is indicated as (*), whereas (**) implies $p < 0.01$. (**D**) Immunofluorescence images of TCs of the cytoskeleton (red) and nuclei (blue) confirmed previous findings. Scale bar 100 μm.

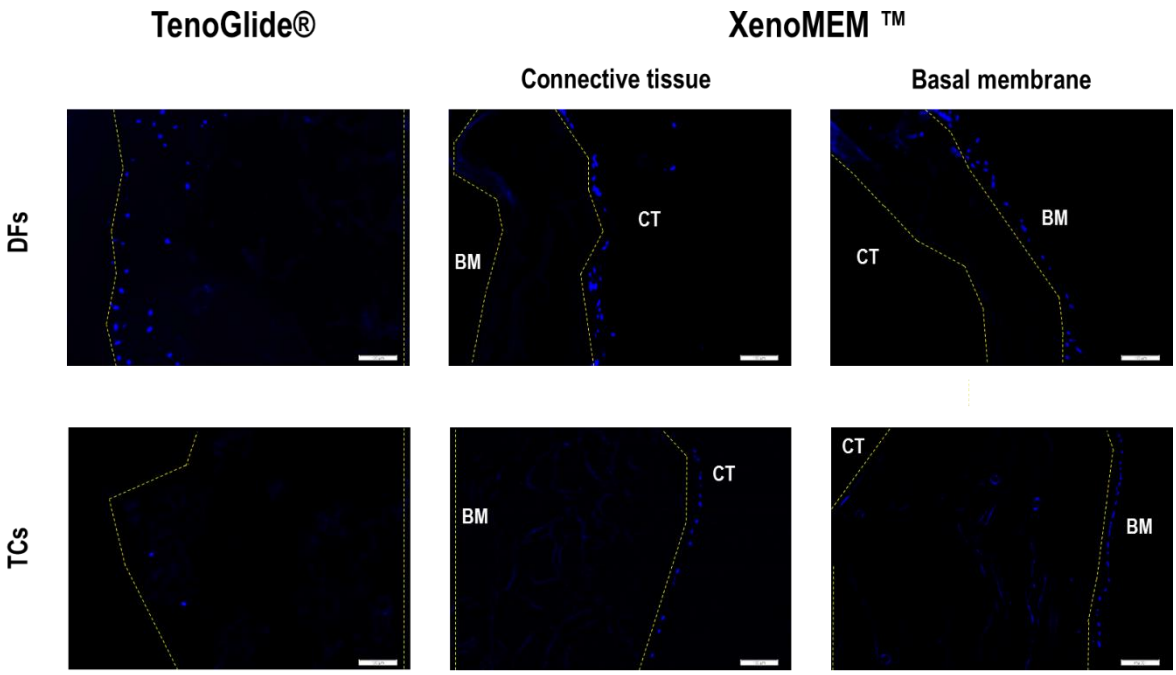

Figure 2.12. Transverse sections of TenoGlide® showed infiltration of DFs and TCs after nuclei staining, whereas XenoMEM™ did not allow cell penetration. Yellow dash-line indicates the limits of the material. Scale bar 100 μm.

2.3.7. Immune response *in vitro* analysis

THP-1 cells seeded with the different CM showed a heterogeneous population of rounded and elongated cells in all conditions, where the elongated cells were more prominent in LPS and TenoGlide® CM at both time points. Clusters were observed more frequently in the LPS and TenoGlide® CM at days 1 and 2 and, in a lower extent, in XenoMEM™ CM. The presence of clusters in normal medium was rare (**Figure 2.13A**). No significant differences ($p > 0.05$) in metabolic activity (**Figure 2.13B**) and proliferation (**Figure 2.13C**) were observed between the different conditions.

Quantification of the proportion of elongated cells confirmed the higher number of elongated cells in LPS and TenoGlide® CM at both time points ($p < 0.01$) and also revealed a slightly higher proportion of elongated cells in XenoMEM™ CM at day 1 ($p < 0.05$). Normal medium and XenoMEM™ CM elicited lower ($p < 0.01$) number of elongated cells than the LPS (**Figure 2.13D**). Quantitative analysis revealed a reduction in the number of elongated cells at day 2 in all conditions (**Figure 2.13D**). THP-1 cells seeded with LPS and TenoGlide® CM, when compared to cells grown in normal medium, showed significantly ($p < 0.01$) higher production of TNF-α at both time points, whereas XenoMEM™ CM showed no significant ($p > 0.05$) differences (**Figure 2.13E**). At both

time points, all conditions (normal medium, TenoGlide® CM, XenoMEM™ CM) showed significantly ($p < 0.01$) lower amounts of TNF-α than LPS (**Figure 2.13E**). IL-6 (**Figure 2.13F**) was only detected in TenoGlide® CM at both days, but with no significant differences ($p > 0.05$).

The assessment of the immune response *in vitro* on the materials revealed a lower number of cells attached on both materials, principally on TenoGlide®. In addition, elongated cells were observed in the LPS condition and, in lower proportion, in the rest of the conditions. Clusters were found in LPS and on XenoMEM™ (**Figure 2.14A**). On TenoGlide®, THP-1 showed higher metabolic activity at day 1 ($p < 0.05$) and day 2 (**Figure 2.14B**), and lower proliferation ($p < 0.01$) at both time points (**Figure 2.14C**) compared to TCP. No significant differences ($p < 0.01$) in the metabolic activity (**Figure 2.14B**) on XenoMEM™ were observed. Elongation quantification (**Figure 2.14D**) revealed a higher ($p < 0.05$) number in LPS and on TenoGlide® at day 2. When compared to LPS, a lower ($p < 0.05$) number of elongated cells was observed on TCP and on the basement membrane of XenoMEM™ (**Figure 2.14D**).

Cells seeded on TenoGlide® showed significantly ($p < 0.05$) higher amounts of TNF-α than cells seeded on TCP at both tie points (**Figure 2.14E**). Both sides of showed significantly ($p < 0.05$) higher amounts of TNF-α than cells seeded on TCP at day 1, but no significant ($p > 0.05$) differences were observed at day 2 (**Figure 2.14E**). XenoMEM™ and TenoGlide® elicited significantly ($p < 0.05$) lower production of TNF-α than LPS at both time points (**Figure 2.14E**). At day 2, TenoGlide® elicited significantly ($p < 0.05$) higher production of TNF-α than either side of XenoMEM™ (**Figure 2.14E**). A higher production of IL-6 (**Figure 2.14F**) by THP-1 cells was observed when seeded on TenoGlide® after 2 days ($p < 0.05$).

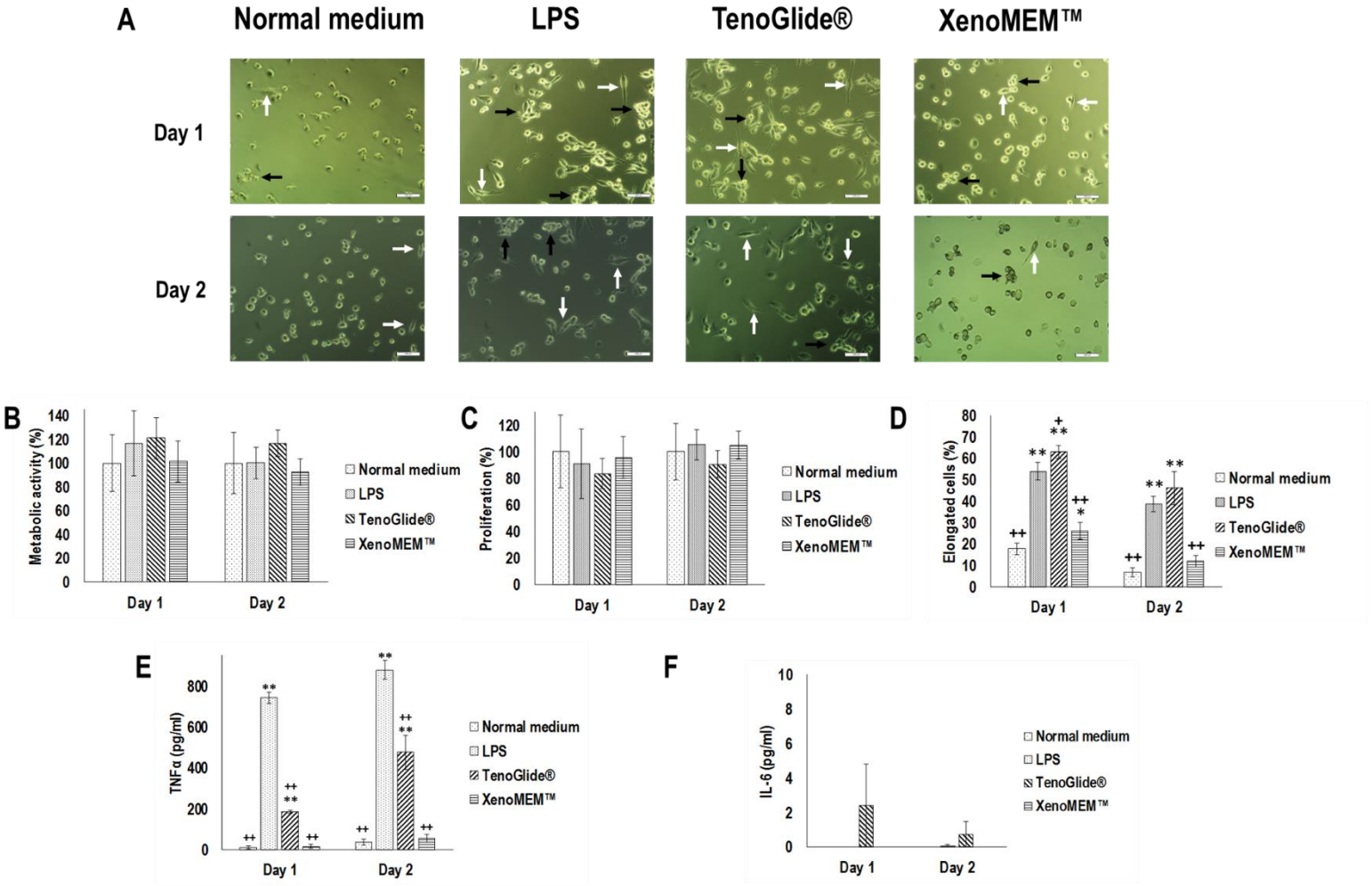
A
Normal medium
LPS
TenoGlide®
XenoMEM™
Day 1
Day 2
B
Metabolic activity (%)
Normal medium
LPS
TenoGlide®
XenoMEM™
Day 1
Day 2
C
Proliferation (%)
D
Elongated cells (%)
E
TNFα (pg/ml)
F
IL-6 (pg/ml)

Figure 2.13. (**A**) THP-1 differentiated with PMA at 100 ng / ml showed a higher proportion of elongated cells (white arrows) and clusters (black arrows) in LPS (100 ng / ml) and TenoGlide® CM groups than those observed in normal medium and XenoMEM™ CM. (**B, C**) Metabolic activity and proliferation of macrophages showed no differences among conditions. Data normalised to control and presented as mean ± standard deviation (n=6). (**D**) Quantification of the proportion of elongated cells confirmed a higher proportion of elongated macrophages in LPS and TenoGlide® CM conditions. (**E, F**) ELISA analysis also showed a higher production of the inflammatory cytokine TNF-α in TenoGlide® CM and LPS conditions whereas no differences were found in IL-6 release. Data presented as mean ± standard deviation (n=6). A significant difference of $p < 0.05$ with the normal medium condition is indicated as *, whereas ** implies $p < 0.01$. A significant difference of $p<0.05$ with the LPS condition is indicated as +, whereas ++ denotes $p < 0.01$.

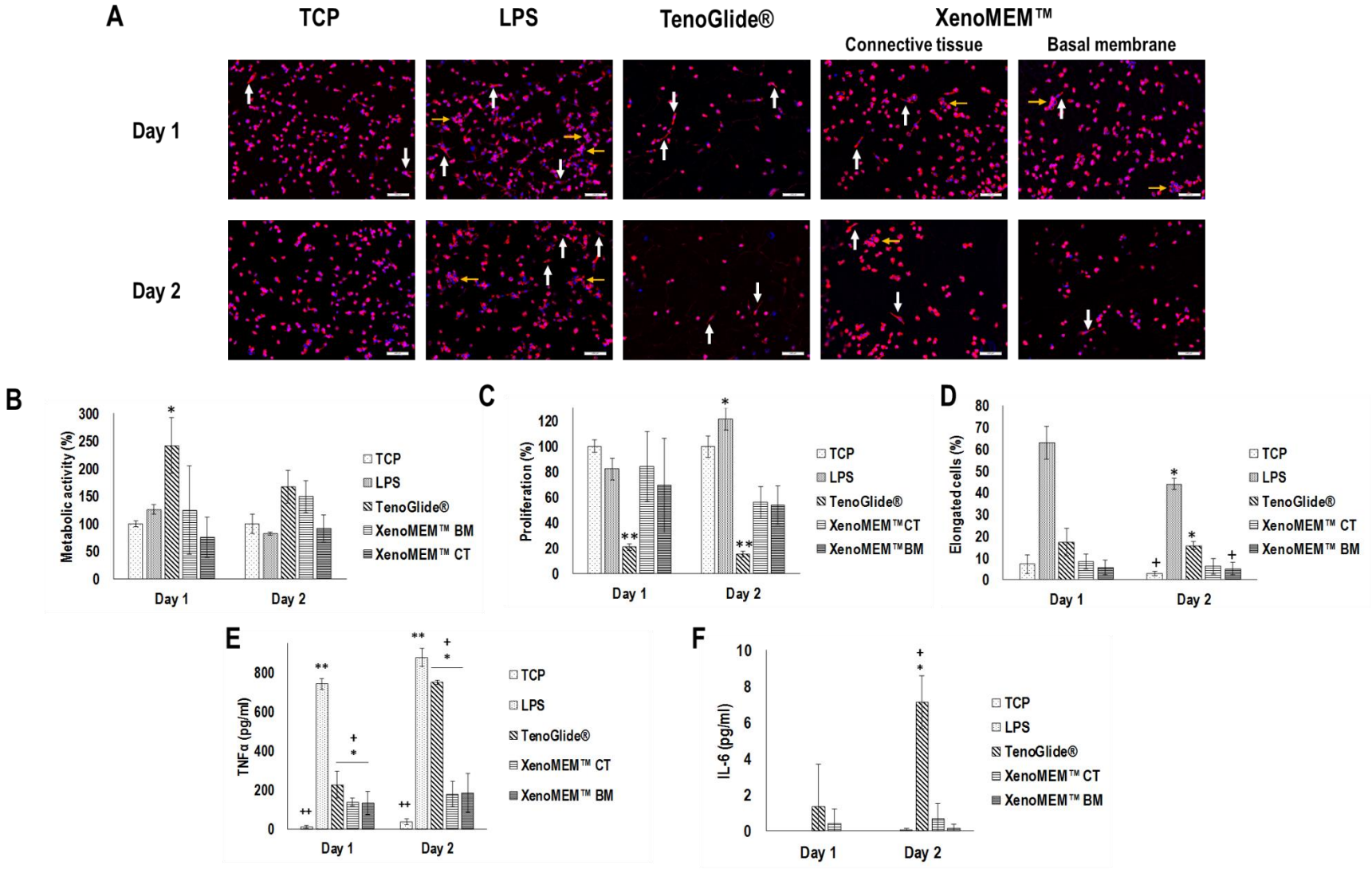
A
TCP
LPS
TenoGlide®
XenoMEM™
Connective tissue
Basal membrane
Day 1
Day 2
B
Metabolic activity (%)
TCP
LPS
TenoGlide®
XenoMEM™ BM
XenoMEM™ CT
Day 1
Day 2
C
Proliferation (%)
TCP
LPS
TenoGlide®
XenoMEM™CT
XenoMEM™BM
Day 1
Day 2
D
Elongated cells (%)
TCP
LPS
TenoGlide®
XenoMEM™ CT
XenoMEM™ BM
Day 1
Day 2
E
TNFα (pg/ml)
TCP
LPS
TenoGlide®
XenoMEM™ CT
XenoMEM™ BM
Day 1
Day 2
F
IL-6 (pg/ml)
TCP
LPS
TenoGlide®
XenoMEM™ CT
XenoMEM™ BM
Day 1
Day 2

Figure 2.14. (A) THP-1 cells immunofluorescence of cytoskeleton (red) and nuclei (blue) showed a lower proliferation of cells on both TenoGlide® and XenoMEM™ in direct contact. Also, a mixed population of elongated (white arrows) and round cells, with some aggregates (yellow arrows) were observed in LPS and materials conditions. Scale bar 100 μm. (**B, C**) Macrophages showed significantly higher metabolic activity and lower proliferation in TenoGlide® after 2 days. On XenoMEM™, both metabolic activity and proliferation were lower after 2 days but without significant differences. (D) Quantification of elongated cells showed a significantly higher proportion of elongated cells in TenoGlide® and LPS conditions. (**E, F**) ELISA analysis of inflammatory cytokines revealed a higher production of TNF-α in TenoGlide® and LPS conditions, meanwhile IL-6 was only detected in direct contact with TenoGlide®. Data presented as mean ± standard deviation (n=3). A significant difference of $p < 0.05$ with the normal medium condition is indicated as *, whereas ** denotes $p < 0.01$. A significant difference of $p < 0.05$ with the LPS condition is indicated as +, whereas ++ indicates $p < 0.01$.

2.3.8. Formation of an epithelium *in vitro*

Mesothelial cells were able to attach and proliferate in all conditions (**Figure 2.15A**). On the trans-well membrane control, TenoGlide® and CT side of XenoMEM™ cells formed several layers and materials topography guided their structure, whereas a monolayer was observed on BM side of XenoMEM™. The ratio between PAI / tPA, antifibrinolytic and fibrinolytic molecules respectively, did not show any differences between conditions after days 7 (**Figure 2.15B**) and 14 (**Figure 2.15C**), whereas after 21 days (**Figure 2.15D**) the BM side of XenoMEM™ promoted a lower ratio ($p < 0.05$).

Histology of seeded materials (**Figure 2.16**) showed a layer of one / few cell(s) on the CT and BM sides of XenoMEM™, whereas on TenoGlide® some cells also penetrated the inner layers of the material.

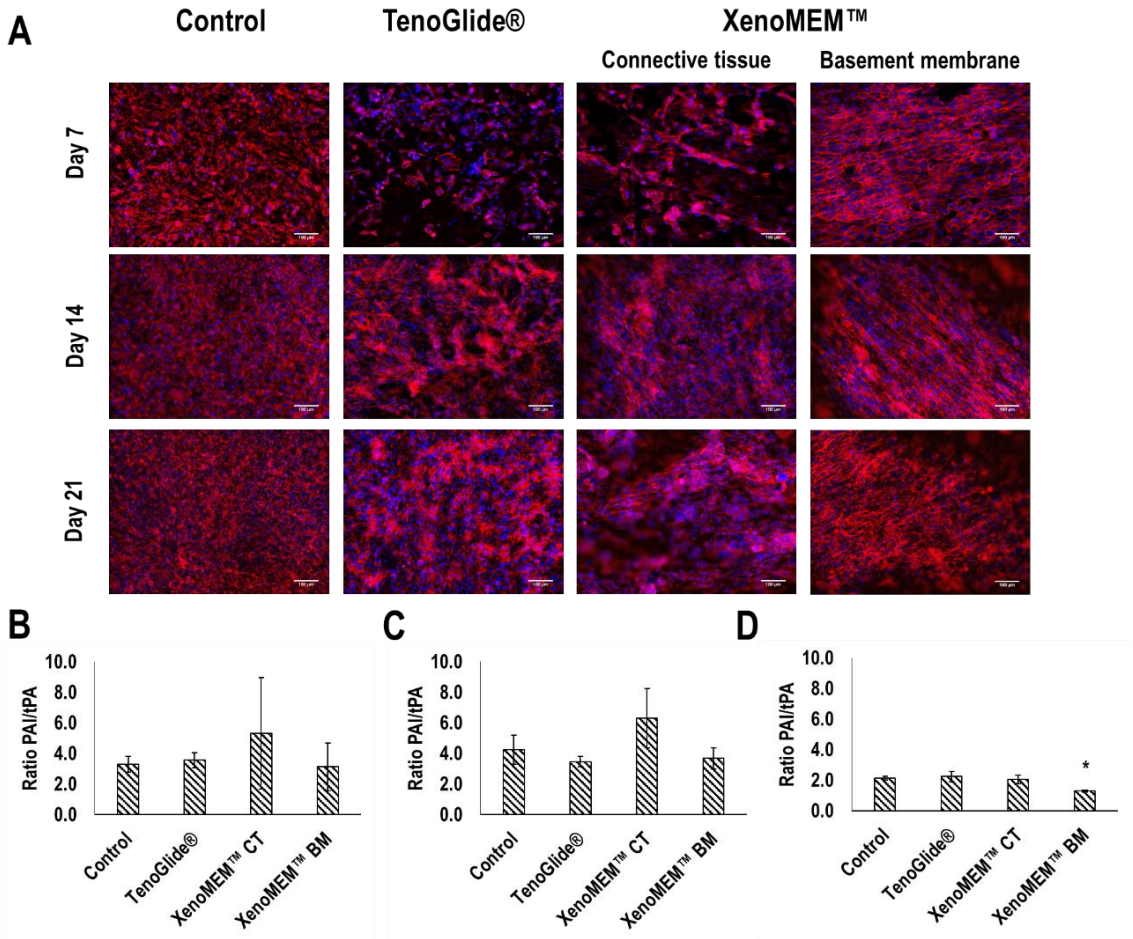

Figure 2.15. Mesothelial cells grew on the trans-well, TenoGlide® and both sides of XenoMEM™ in supplemented M199 medium without EGF, although a monolayer epithelial-like was only observed on BM side of XenoMEM™. (**B**,**C**) After 7 and 14 days, the ratio between PAI and tPA showed no differences between conditions and after 21 days (**D**) a lower ratio was observed on BM side of XenoMEM™.

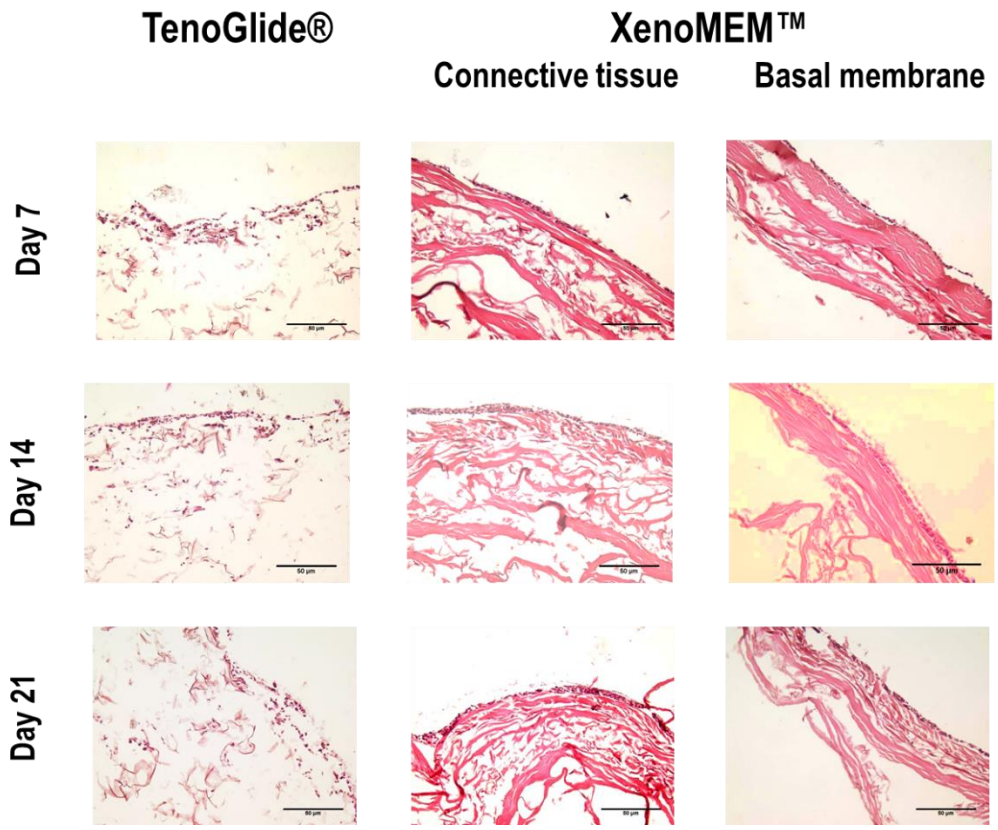

Figure 2.16. Histology of materials seeded with mesothelial cells showed a cell layer of few cells on XenoMEM™ CT and BM, whereas TenoGlide® allowed the penetration of cells in the material. Scale bars 50 μm.

2.3.9. Flexor tendon model in vivo

A pilot study with 12 New Zealand white rabbits was carried out to develop a model for testing the potential of XenoMEM as tendon barrier in vivo. Macroscopic observation of the fingers after 8 weeks showed the formation of adhesions in all the conditions (**Figure 2.17**). Mechanical analysis showed how both tendon excursion (**Figure 2.18A**) and degree of flexion (**Figure 2.18B**) were much lower ($p < 0.01$) in all the conditions when compared to healthy tendon. Tensile uniaxial test also revealed lower ($p < 0.01$) force at break (**Figure 2.18C**), maximum stress (**Figure 2.18D**), and Young's modulus (**Figure 2.18F**) in all the groups compared to the healthy tendon, with no differences among treatments. Strain at break (**Figure 2.18E**) showed significantly ($p < 0.01$) lower value in TenoGlide®-treated tendons Histology analysis (**Figure 2.19)** confirmed the presence of adhesions in all the conditions.

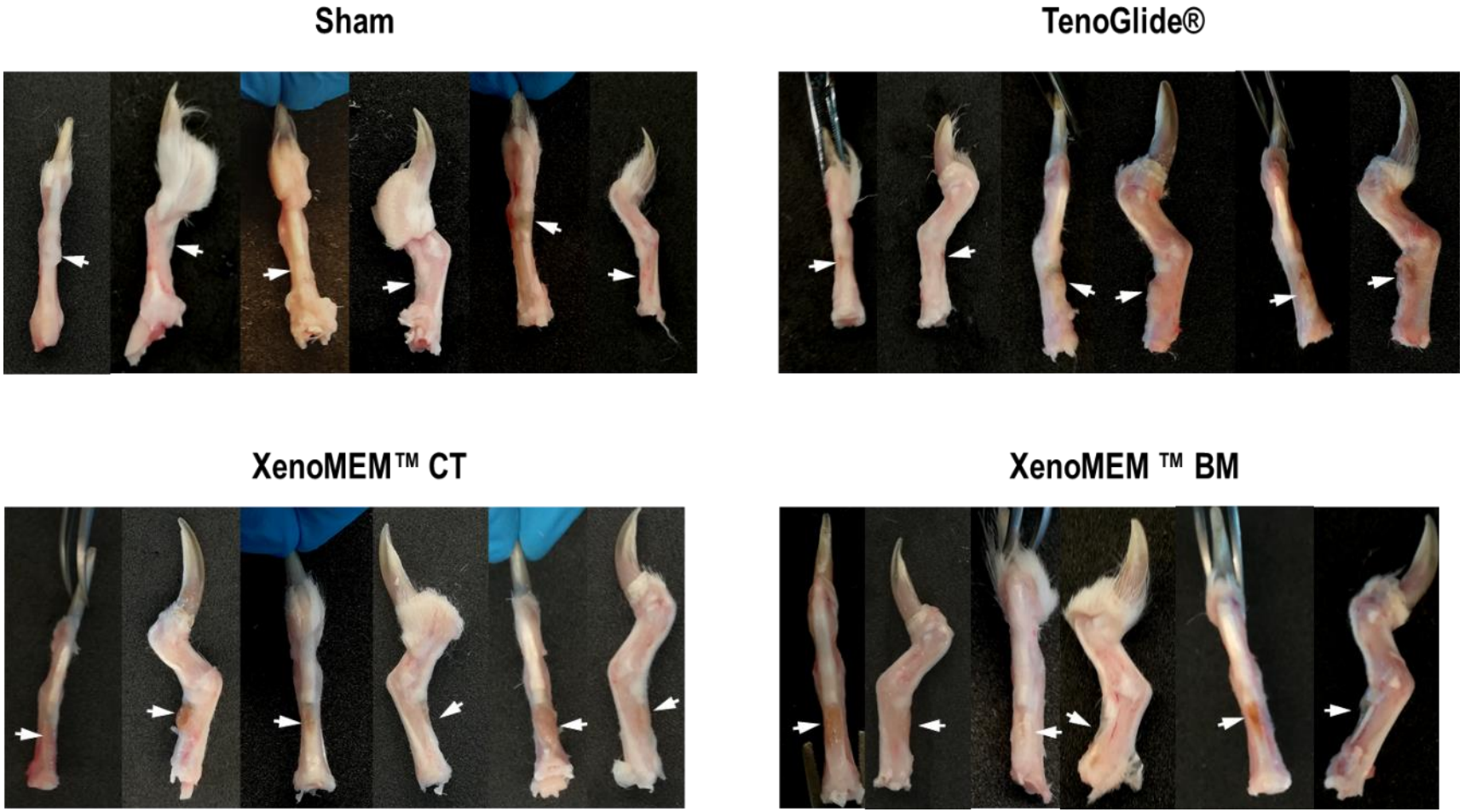

Figure 2.17. Macroscopic observation of repaired fingers showed the formation of adhesions (white arrows) in all conditions.

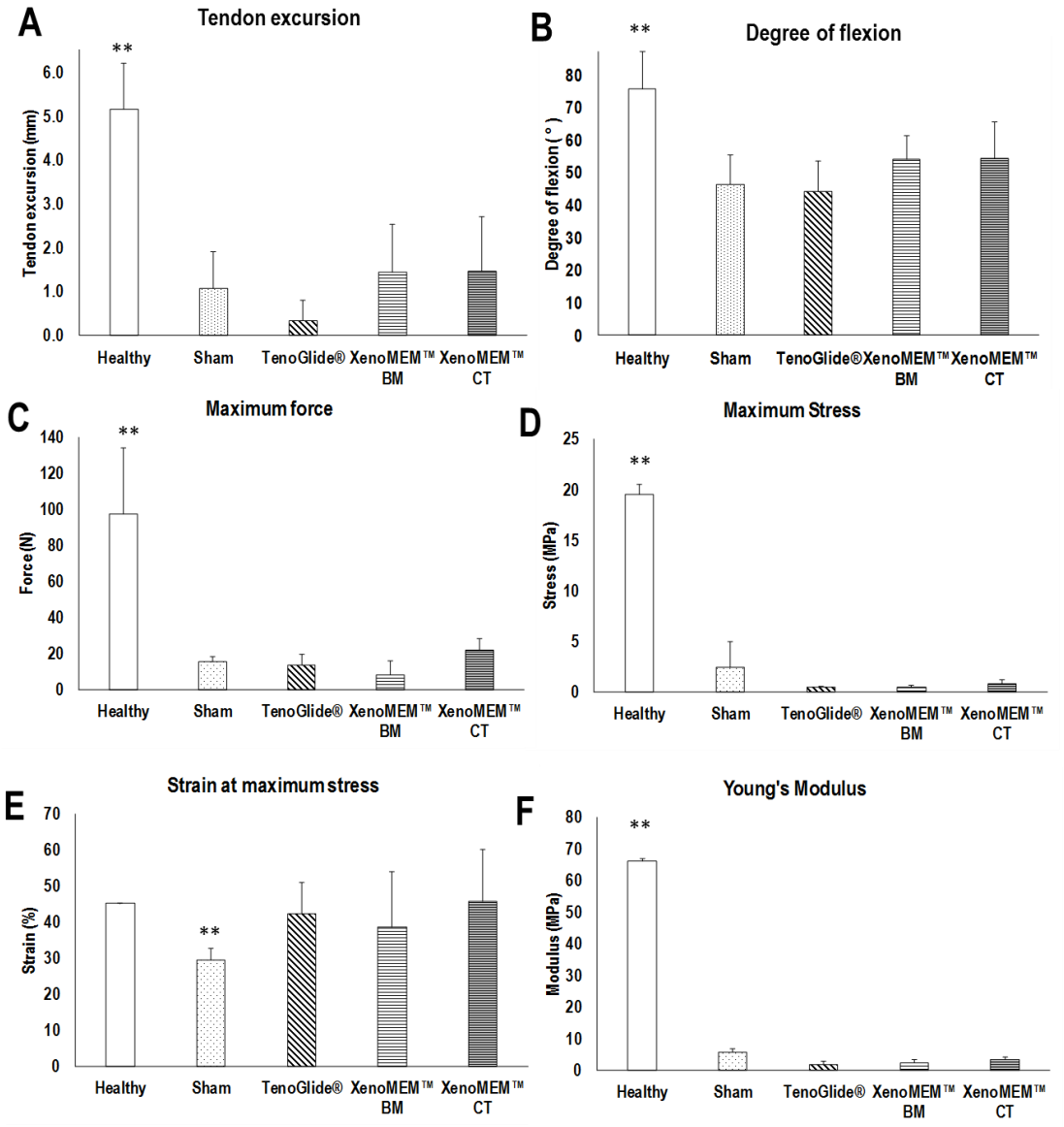

Figure 2.18. Mechanical analysis of flexor tendons after 8 weeks showed a higher excursion distance (**A**), degree of flexion (**B**), force at break (**C**), stress at break (**D**), and modulus (**F**) in the healthy tendon compared to treatment groups, where no significant difference was found. Strain at break (**E**) showed similar values among groups, except for the sham which seemed lower. Data expressed as average ± standard deviation (n=3). ** $p < 0.01$.

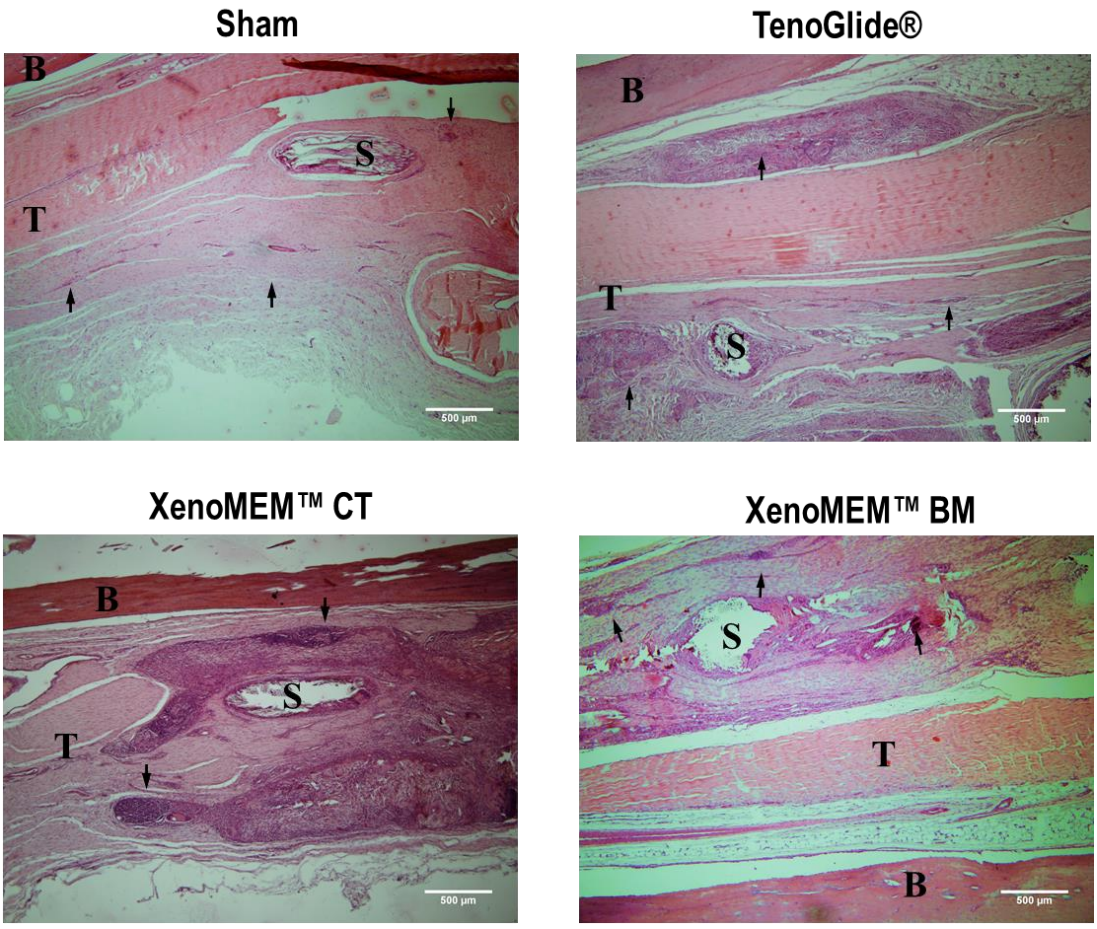

Figure 2.19. Haematoxylin and eosin staining of sectioned fingers after 8 weeks. T: Tendon, B: Bone, S: Suture. Arrows indicate adhesion areas. Scale bar 500 μm.

2.4. Discussion

Decellularised porcine peritoneum has shown promise in wound healing applications [47-51]. The present study investigated the potential of a decellularised porcine peritoneum matrix (XenoMEM™) for tendon tissue engineering applications, considering that it was compared to TenoGlide®, a commercially available product that acts as a tendon protector sheet.

SDS-PAGE analysis revealed that XenoMEM™ was composed of collagen types I and V; this was more obvious in the acid / pepsin samples, considering that pepsin increases the yield in collagen extractions [52, 53]. However, extensive exogenous cross-linking provides resistance against the action of proteolytic enzymes [42, 54], which could be related to the absence of collagen bands after both extractions of TenoGlide®. This is supported by the less free amine and higher thermal properties of TenoGlide® in comparison to XenoMEM™. The high cross-linking density of TenoGlide® justifies its higher than XenoMEM™ resistance to enzymatic degradation, which is also in agreement with other studies with collagen scaffolds [42] and decellularised tissue grafts [41]. Considering that highly cross-linked materials are associated with inflammation and poor remodelling [55-57], the lower, but adequate cross-linking density of XenoMEM™ may be proven beneficial in *in vivo* setting.

The mechanical properties of TenoGlide® were much lower than those of XenoMEM™, considering that mechanical integrity is lost during collagen extraction and scaffold fabrication [2, 3, 58]. Collagen-based scaffolds, even after extensive cross-linking, are unable to mimic the native tissue mechanical features, contrary to decellularised tissue grafts that still retain a large portion of the original tissue mechanical integrity.

The mechanical features of XenoMEM™ were similar to those observed previously for decellularised peritoneum tissues [48, 49, 51], with previous studies showing that processing minimally affects its mechanical properties [49]. Although high mechanical properties may not seem relevant for tendon barriers, a high mechanical resilience facilitates the usage of a device in the clinical scenario. In addition, the mechanical properties of porcine peritoneum pose a high potential for XenoMEM™ in other tendon clinical applications (*i.e.* as augmentation device).

Detailed SEM analysis revealed that XenoMEM™ had a fibrous-like topography from the connective tissue side and a rather smooth topography from the basement membrane side, typical of the peritoneum tissue [47, 48]. TenoGlide® had a porous structure, possibly attributed to the freeze drying. Roughness analysis through AFM showed significant lower values in TenoGlide® than in XenoMEM™, however these differences

did not translate into a higher friction coefficient, but an inverse trend was observed. This is not surprising, considering that other factors have a major influence than the roughness on the friction, such as the presence of molecules, which promote the gliding (e.g. hyaluronic acid (HA) or lubricin [44]). The presence of components that promote the gliding on XenoMEM™ would be expected, since one of the functions of peritoneum is to promote gliding between organs [59]. This feature could be beneficial as a tendon sheath, which promotes the gliding after surgery, a desirable characteristic particularly in flexor tendon operations [44]. However, one must keep in mind the limitations of this analysis, since the coefficient of friction is a characteristic of both surfaces tested and different results could be observed when testing the material against tendon.

Histological and immunohistochemistry analyses not only confirmed the complete removal of cellular materials, but also demonstrated that the native composition of the major ECM components (a laminar flat structure containing collagen types I and III, fibronectin, prominent fibres of elastin and basement membrane markers in blood vessels and basal membrane side [59-61]) had not been affected during processing. A slight damage on the basal membrane was observed due to decellularisation, freeze drying or sectioning processes, as it has been reported in other studies [48]. TenoGlide® contained only collagen types I and III and fibronectin in a homogeneous sponge-like distribution, a typical composition of processed collagen sponges.

In vitro biological response was first assessed using DFs. In general, DFs adhered and grew well in both TenoGlide® and XenoMEM™. Cells grown with the CM of XenoMEM™ showed a slight increment in metabolic activity and proliferation as a function of time in culture, as has been observed previously [48]. This can be attributed to the preservation of the biofunctional molecules, such as vascular endothelial growth factor (VEGF), fibroblastic growth factor (FGF) and transforming growth factor β (TGF-β), which promote the production of VGEF by human foreskin fibroblast *in vitro* [48]. The fibrous structure of the connective tissue side of XenoMEM™ also induced cellular alignment, as has been observed previously with human foreskin fibroblasts [48].

TCs seeded on TenoGlide® exhibited the lowest proliferation rate, which could be related to the presence of soluble cross-linking remnants. Indeed, chemically cross-linked collagen scaffolds have been repeatedly reported to induce negative effects on cells *in vitro* [58, 62]. Although this low affinity of TenoGlide® with TCs may promote the confinement of TCs within tendon after surgery and decrease adhesions [63], if it is due to the cytotoxic effect of TenoGlide®, undesirable effects such as inflammation and fibrotic encapsulation, may come up after prolonged implantation studies. TCs grew well

on both layers of XenoMEM™, with the basal membrane enhancing a faster growth. Non-cross-linked biological materials, similar to XenoMEM™, have been shown previously to promote TC growth [64, 65]. Neither DFs nor TCs penetrated XenoMEM™. This inhibition of cellular migration into the bulk of the material could be beneficial for tendon wrapping applications, as it would effectively isolate the tendon from surrounding fibroblasts and confine the TCs promoting its intrinsic healing [66-68], although such hypothesis must be confirmed in further *in vivo* studies. In addition, the epithelial proliferation on XenoMEM™ could prevent the fibrin and further adhesions deposition due to the presence of a functional epithelium [69]. On the other hand, TenoGlide® allowed the penetration of the cells, which could be related to the presence of adhesions after 21 days in a flexor tendon model defect in chicken [38, 63].

THP-1 cells are used extensively to assess immune response *in vitro*; M1 (inflammatory) or M2 (remodelling) phenotypes can be differentiated via cell morphology analysis (M1: round morphology, M2: elongated morphology, foreign body response: cell aggregates) and LPS treatment is an established control to induce M1 phenotype [70, 71]. In this study, LPS triggered the highest proportion of elongated cells, which has also been reported previously [72], whereas macrophages on normal medium adopted a more rounded shape. XenoMEM™ elicited lower number of elongated cells than LPS, but higher than normal medium, whilst TenoGlide® induced more elongated cells than normal medium and presented similar proportion than those in LPS. Cell clusters were found in LPS, TenoGlide® and XenoMEM™ by descending order in number of clusters observed. TenoGlide® showed a significant lower proliferation rate, in comparison to the control groups, which has been previously reported as an indication of inflammatory response [73]. Furthermore, ELISA analysis of pro-inflammatory cytokines TNF-α and IL-6, produced by THP-1 cells, showed significantly higher amounts in LPS and TenoGlide®, which is indicative of a shift to M1 phenotype in macrophages [72]. This differential response can be attributed to the different cross-linking density, stiffness and topography of the materials, as all of these have been shown to play a crucial role in the morphology of macrophages [42, 71, 74].

Mesothelial cells play a vital role in adhesions resolution in peritoneum, where the balance between PAI and tPA, antifibrinolytic and fibrinolytic molecules, is critical [68, 75]. We observed that, in absence of EGF supplementation, the BM side of XenoMEM™ promoted the formation of a mesothelial cell layer, as shown by immunocytochemistry and histology. Although histology showed similar morphology of the epithelium in the CT side of XenoMEM™, the PAI / tPA ratio was lower only in the BM side after 21 days,

characteristic of a healthy epithelium [76], which prevents adhesion formation and also relates to the tendon environment [68]. The TenoGlide® allowed the penetration of cells rather than an epithelial formation, and elicited similar levels of PAI / tPA to the control. Such response on XenoMEM™ BM side is likely related to its composition rich in BM markers, such as collagen type IV and laminin, which can govern epithelial behaviour [77-79].

A model for flexor tendon repair in rabbits was also developed in this study. No significant differences nor conclusions could be drawn, since during the optimisation progress different regimes of immobilisation and casting were applied. This makes the analysis negligible, since movement of the digits (physiotherapy) highly affects the formation of adhesions in tendon [68]. Nonetheless, the differences observed between the healthy tendon and sham and treatments support the employment of this model to validate the hypothesis formulated in this study.

2.5. Conclusion

The present work assessed the suitability and potential of decellularised porcine peritoneum (XenoMEM™) as a tendon tissue engineering material. Structural, compositional, biomechanical and biological (using dermal fibroblasts, tenocytes, THP-1 macrophages and mesothelial cells) analyses advocate the use of non-cross-linked decellularised porcine peritoneum (XenoMEM™) as a potential tendon wrapping device.

2.6. References

[1] M.W. Tibbitt, C.B. Rodell, J.A. Burdick, K.S. Anseth, Progress in material design for biomedical applications, Proc Natl Acad Sci U S A 112(47) (2015) 14444-14451.

[2] N. Davidenko, T. Gibb, C. Schuster, S.M. Best, J.J. Campbell, C.J. Watson, R.E. Cameron, Biomimetic collagen scaffolds with anisotropic pore architecture, Acta Biomater 8(2) (2012) 667-676.

[3] B.D. Walters, J.P. Stegemann, Strategies for directing the structure and function of 3D collagen biomaterials across length scales, Acta Biomater 10(4) (2014) 1488-1501.

[4] S. Geraghty, J.Q. Kuang, D. Yoo, M. LeRoux-Williams, C.T. Vangsness, Jr., A. Danilkovitch, A novel, cryopreserved, viable osteochondral allograft designed to augment marrow stimulation for articular cartilage repair, J Orthop Surg Res 10 (2015) 66.

[5] F.M. Chen, X. Liu, Advancing biomaterials of human origin for tissue engineering, Prog Polym Sci 53 (2016) 86-168.

[6] P. Mahmut, D. Arin, O. Sedat, A.E. Elçin, Y.M. Elçin, Clinical applications of decellularized extracellular matrices for tissue engineering and regenerative medicine, Biomed Mater 11(2) (2016) 022003.

[7] T.W. Gilbert, T.L. Sellaro, S.F. Badylak, Decellularization of tissues and organs, Biomaterials 27(19) (2006) 3675-3683.

[8] S.S. Raghavan, C.Y. Woon, A. Kraus, K. Megerle, M.S. Choi, B.C. Pridgen, H. Pham, J. Chang, Human flexor tendon tissue engineering: decellularization of human flexor tendons reduces immunogenicity in vivo, Tissue Eng Part A 18(7-8) (2012) 796-805.

[9] R. Yoshida, P. Vavken, M.M. Murray, Decellularization of bovine anterior cruciate ligament tissues minimizes immunogenic reactions to alpha-gal epitopes by human peripheral blood mononuclear cells, Knee 19(5) (2012) 672-675.

[10] T.W. Hudson, S. Zawko, C. Deister, S. Lundy, C.Y. Hu, K. Lee, C.E. Schmidt, Optimized acellular nerve graft is immunologically tolerated and supports regeneration, Tissue Eng 10(11-12) (2004) 1641-1651.

[11] M. Bottagisio, A.F. Pellegata, F. Boschetti, M. Ferroni, M. Moretti, A.B. Lovati, A new strategy for the decellularisation of large equine tendons as biocompatible tendon substitutes, Eur Cell Mater 32 (2016) 58-73.

[12] S. Xing, C. Liu, B. Xu, J. Chen, D. Yin, C. Zhang, Effects of various decellularization methods on histological and biomechanical properties of rabbit tendons, Exp Ther Med 8(2) (2014) 628-634.

[13] K. Xu, L.A. Kuntz, P. Foehr, K. Kuempel, A. Wagner, J. Tuebel, C.V. Deimling, R.H. Burgkart, Efficient decellularization for tissue engineering of the tendon-bone interface with preservation of biomechanics, PLoS One 12(2) (2017) e0171577.

[14] S.L. Wilson, L.E. Sidney, S.E. Dunphy, H.S. Dua, A. Hopkinson, Corneal decellularization: A method of recycling unsuitable donor tissue for clinical translation?, Curr Eye Res 41(6) (2016) 769-782.

[15] S. Ponce Márquez, V.S. Martínez, W. McIntosh Ambrose, J. Wang, N.G. Gantxegui, O. Schein, J. Elisseeff, Decellularization of bovine corneas for tissue engineering applications, Acta Biomater 5(6) (2009) 1839-1847.

[16] S. Cebotari, I. Tudorache, T. Jaekel, A. Hilfiker, S. Dorfman, W. Ternes, A. Haverich, A. Lichtenberg, Detergent decellularization of heart valves for tissue engineering: Toxicological effects of residual detergents on human endothelial cells, Artif Organs 34(3) (2010) 206-210.

[17] B.T. Yu, W.T. Li, B.Q. Song, Y.L. Wu, Comparative study of the Triton X-100-sodium deoxycholate method and detergent-enzymatic digestion method for decellularization of porcine aortic valves, Eur Rev Med Pharmacol Sci 17(16) (2013) 2179-84.

[18] P. Maghsoudlou, F. Georgiades, A. Tyraskis, G. Totonelli, S.P. Loukogeorgakis, G. Orlando, P. Shangaris, P. Lange, J.-M. Delalande, A.J. Burns, A. Cenedese, N.J. Sebire, M. Turmaine, B.N. Guest, J.F. Alcorn, A. Atala, M.A. Birchall, M.J. Elliott, S. Eaton, A. Pierro, T.W. Gilbert, P. De Coppi, Preservation of micro-architecture and angiogenic potential in a pulmonary acellular matrix obtained using intermittent intra-tracheal flow of detergent enzymatic treatment, Biomaterials 34(28) (2013) 6638-6648.

[19] A.P. Price, L.M. Godin, A. Domek, T. Cotter, J. D'Cunha, D.A. Taylor, A. Panoskaltsis-Mortari, Automated decellularization of intact, human-sized lungs for tissue engineering, Tissue Eng Part C Methods 21(1) (2015) 94-103.

[20] G. Mazza, K. Rombouts, A. Rennie Hall, L. Urbani, T. Vinh Luong, W. Al-Akkad, L. Longato, D. Brown, P. Maghsoudlou, A.P. Dhillon, B. Fuller, B. Davidson, K. Moore, D. Dhar, P. De Coppi, M. Malago, M. Pinzani, Decellularized human liver as a natural 3D-scaffold for liver bioengineering and transplantation, Sci Rep 5 (2015) 13079.

[21] H. Ren, X. Shi, L. Tao, J. Xiao, B. Han, Y. Zhang, X. Yuan, Y. Ding, Evaluation of two decellularization methods in the development of a whole-organ decellularized rat liver scaffold, Liver Int 33(3) (2013) 448-58.

[22] A. Schmitt, R. Csiki, A. Tron, B. Saldamli, J. Tubel, K. Florian, S. Siebenlist, E. Balmayor, R. Burgkart, Optimized protocol for whole organ decellularization, Eur J Med Res 22(1) (2017) 31.

[23] D.C. Sullivan, S.-H. Mirmalek-Sani, D.B. Deegan, P.M. Baptista, T. Aboushwareb, A. Atala, J.J. Yoo, Decellularization methods of porcine kidneys for whole organ engineering using a high-throughput system, Biomaterials 33(31) (2012) 7756-7764.

[24] M.M. Abdelfatah, N. Rostambeigi, E. Podgaetz, M.G. Sarr, Long-term outcomes (>5-year follow-up) with porcine acellular dermal matrix (Permacol™) in incisional hernias at risk for infection, Hernia 19(1) (2015) 135-140.

[25] A.M. Ibrahim, C.R. Vargas, S. Colakoglu, J.T. Nguyen, S.J. Lin, B.T. Lee, Properties of meshes used in hernia repair: a comprehensive review of synthetic and biologic meshes, J Reconstr Microsurg 31(2) (2015) 83-94.

[26] M.J. Rosen, G. DeNoto, K.M.F. Itani, C. Butler, D. Vargo, J. Smiell, R. Rutan, Evaluation of surgical outcomes of retro-rectus versus intraperitoneal reinforcement with

bio-prosthetic mesh in the repair of contaminated ventral hernias, Hernia 17(1) (2013) 31-35.

[27] E.N. Mostow, G.D. Haraway, M. Dalsing, J.P. Hodde, D. King, O.V.U.S. Group, Effectiveness of an extracellular matrix graft (OASIS Wound Matrix) in the treatment of chronic leg ulcers: a randomized clinical trial, J Vasc Surg 41(5) (2005) 837-43.

[28] H. Kimmel, M. Rahn, T.W. Gilbert, The clinical effectiveness in wound healing with extracellular matrix derived from porcine urinary bladder matrix: a case series on severe chronic wounds, J Am Col Certif Wound Spec 2(3) (2010) 55-9.

[29] C.K. Yang, T.O. Polanco, J.C. Lantis, A prospective, postmarket, compassionate clinical evaluation of a novel acellular fish-skin graft which contains omega-3 fatty acids for the closure of hard-to-heal lower extremity chronic ulcers, Wounds 28(4) (2016) 112-118.

[30] U.G. Longo, A. Lamberti, N. Maffulli, V. Denaro, Tendon augmentation grafts: A systematic review, Br Med Bull (2010) ldp051.

[31] G. Meier Bürgisser, J. Buschmann, History and performance of implant materials applied as peritendinous antiadhesives, J Biomed Mater Res B Appl Biomater 103(1) (2015) 212-228.

[32] T. Thangarajah, C.J. Pendegrass, S. Shahbazi, S. Lambert, S. Alexander, G.W. Blunn, Augmentation of rotator cuff repair with soft tissue scaffolds, Orthop J Sports Med 3(6) (2015) 2325967115587495.

[33] D.P. Ferguson, M.R. Lewington, T.D. Smith, I.H. Wong, Graft Utilization in the augmentation of large-to-massive rotator cuff repairs: A systematic review, Am J Sports Med 44(11) (2016) 2984-2992.

[34] K. Megerle, C. Woon, A. Kraus, S. Raghavan, H. Pham, J. Chang, Flexor tendon sheath engineering using decellularized porcine pericardium, Plast Reconstr Surg 138(4) (2016) 630e-41e.

[35] L. Xu, D. Cao, W. Liu, G. Zhou, W.J. Zhang, Y. Cao, In vivo engineering of a functional tendon sheath in a hen model, Biomaterials 31(14) (2010) 3894-3902.

[36] P.C. Amadio, Gliding resistance and modifications of gliding surface of tendon: clinical perspectives, Hand Clin 29(2) (2013) 159-66.

[37] B. Elhassan, Lower trapezius transfer for shoulder external rotation in patients with paralytic shoulder, J Hand Surg Am 39(3) (2014) 556-62.

[38] J.B. Turner, R.L. Corazzini, T.J. Butler, D.S. Garlick, B.D. Rinker, Evaluating adhesion reduction efficacy of type I/III collagen membrane and collagen-GAG

resorbable matrix in primary flexor tendon repair in a chicken model, Hand (N Y) 10(3) (2015) 482-8.

[39] H. Capella-Monsonis, J.Q. Coentro, V. Graceffa, Z. Wu, D.I. Zeugolis, An experimental toolbox for characterization of mammalian collagen type I in biological specimens, Nat Protoc 13(3) (2018) 507-529.

[40] D.I. Zeugolis, M. Raghunath, The physiological relevance of wet versus dry differential scanning calorimetry for biomaterial evaluation: A technical note, Polym Int 59(10) (2010) 1403-1407.

[41] A.L. Helling, E.K. Tsekoura, M. Biggs, Y. Bayon, A. Pandit, D.I. Zeugolis, In vitro enzymatic degradation of tissue grafts and collagen biomaterials by matrix metalloproteinases: Improving the collagenase assay, ACS Biomater Sci Eng (2016).

[42] L.M. Delgado, K. Fuller, D.I. Zeugolis, Collagen cross-linking: Biophysical, biochemical, and biological response analysis, Tissue Eng Part A 23(19-20) (2017) 1064-1077.

[43] A. Satyam, P. Kumar, X. Fan, A. Gorelov, Y. Rochev, L. Joshi, H. Peinado, D. Lyden, B. Thomas, B. Rodriguez, M. Raghunath, A. Pandit, D. Zeugolis, Macromolecular crowding meets tissue engineering by self-assembly: a paradigm shift in regenerative medicine, Adv Mater 26(19) (2014) 3024-34.

[44] P.S. Theobald, D. Dowson, I.M. Khan, M.D. Jones, Tribological characteristics of healthy tendon, J Biomech 45(11) (2012) 1972-8.

[45] K.M. Kulig, X. Luo, E.B. Finkelstein, X.-H. Liu, S.M. Goldman, C.A. Sundback, J.P. Vacanti, C.M. Neville, Biologic properties of surgical scaffold materials derived from dermal ECM, Biomaterials 34(23) (2013) 5776-5784.

[46] J.K. McDade, E.P. Brennan-Pierce, M.B. Ariganello, R.S. Labow, J. Michael Lee, Interactions of U937 macrophage-like cells with decellularized pericardial matrix materials: Influence of crosslinking treatment, Acta Biomater 9(7) (2013) 7191-7199.

[47] Z. Wu, Y. Tang, H. Fang, Z. Su, B. Xu, Y. Lin, P. Zhang, X. Wei, Decellularized scaffolds containing hyaluronic acid and EGF for promoting the recovery of skin wounds, J Mater Sci Mater Med 26(1) (2015) 5322.

[48] D.M. Hoganson, G.E. Owens, E.M. O'Doherty, C.M. Bowley, S.M. Goldman, D.O. Harilal, C.M. Neville, R.T. Kronengold, J.P. Vacanti, Preserved extracellular matrix components and retained biological activity in decellularized porcine mesothelium, Biomaterials 31(27) (2010) 6934-6940.

[49] M. van Steenberghe, T. Schubert, Y. Guiot, C. Bouzin, X. Bollen, P. Gianello, Enhanced vascular biocompatibility of decellularized xeno-/allogeneic matrices in a rodent model, Cell Tissue Bank 18(2) (2017) 249-262.

[50] Z. Su, H. Ma, Z. Wu, H. Zeng, Z. Li, Y. Wang, G. Liu, B. Xu, Y. Lin, P. Zhang, X. Wei, Enhancement of skin wound healing with decellularized scaffolds loaded with hyaluronic acid and epidermal growth factor, Mater Sci Eng C Mater Biol Appl 44(Supplement C) (2014) 440-8.

[51] P.C. Tsai, Z. Zhang, C. Florek, B.B. Michniak-Kohn, Constructing human skin equivalents on porcine acellular peritoneum extracellular matrix for in vitro irritation testing, Tissue Eng Part A 22(1-2) (2016) 111-22.

[52] L.M. Delgado, N. Shologu, K. Fuller, D.I. Zeugolis, Acetic acid and pepsin result in high yield, high purity and low macrophage response collagen for biomedical applications, Biomed Mater 12(6) (2017) 065009.

[53] D.I. Zeugolis, R.G. Paul, G. Attenburrow, Factors influencing the properties of reconstituted collagen fibers prior to self-assembly: animal species and collagen extraction method, J Biomed Mater Res A 86(4) (2008) 892-904.

[54] E.K. Tsekoura, A.L. Helling, J.G. Wall, Y. Bayon, D.I. Zeugolis, Battling bacterial infection with hexamethylene diisocyanate cross-linked and Cefaclor-loaded collagen scaffolds, Biomed Mater 12(3) (2017) 035013.

[55] Y.W. Novitsky, S.B. Orenstein, D.L. Kreutzer, Comparative analysis of histopathologic responses to implanted porcine biologic meshes, Hernia 18(5) (2014) 713-721.

[56] N. Bryan, H. Ashwin, N.J. Smart, S. Wohlert, Y. Bayon, J.A. Hunt, Characterisation and comparison of the host response of 6 tissue-based surgical implants in a subcutaneous in vivo rat model, J Appl Biomater Funct Mater 13(1) (2015) 35-42.

[57] S. Lucke, A. Hoene, U. Walschus, A. Kob, J.W. Pissarek, M. Schlosser, Acute and chronic local inflammatory reaction after implantation of different extracellular porcine dermis collagen matrices in rats, Biomed Res Int 2015 (2015) 938059.

[58] N. Reddy, R. Reddy, Q. Jiang, Crosslinking biopolymers for biomedical applications, Trends Biotechnol 33(6) (2015) 362-9.

[59] T. Jasna, N. D, L. Z, O. Miljana, B. G, S. Biljana, Histological characteristics of healthy animal peritoneum, Acta Vet Brno 56(5-6) (2006) 405-412.

[60] C.A. Witz, I.A. Montoya-Rodriguez, S. Cho, V.E. Centonze, L.F. Bonewald, R.S. Schenken, Composition of the extracellular matrix of the peritoneum, J Soc Gynecol Investig 8(5) (2001) 299-304.

[61] S.C. Blackburn, M.P. Stanton, Anatomy and physiology of the peritoneum, Semin Pediatr Surg 23(6) (2014) 326-330.

[62] M.A. Awang, M.A. Firdaus, M.B. Busra, S.R. Chowdhury, N.R. Fadilah, W.K. Wan Hamirul, M.Y. Reusmaazran, M.Y. Aminuddin, B.H. Ruszymah, Cytotoxic evaluation of biomechanically improved crosslinked ovine collagen on human dermal fibroblasts, Biomed Mater Eng 24(4) (2014) 1715-24.

[63] D. Bhavsar, D. Shettko, M. Tenenhaus, Encircling the tendon repair site with collagen-GAG reduces the formation of postoperative tendon adhesions in a chicken flexor tendon model, J Surg Res 159(2) (2010) 765-71.

[64] K.P. Shea, M.B. McCarthy, F. Ledgard, C. Arciero, D. Chowaniec, A.D. Mazzocca, Human tendon cell response to 7 commercially available extracellular matrix materials: an in vitro study, Arthroscopy 26(9) (2010) 1181-8.

[65] R.D. Smith, A. Carr, S.G. Dakin, S.J. Snelling, C. Yapp, O. Hakimi, The response of tenocytes to commercial scaffolds used for rotator cuff repair, Eur Cell Mater 31 (2016) 107-18.

[66] P.B. Voleti, M.R. Buckley, L.J. Soslowsky, Tendon healing: repair and regeneration, Annu Rev Biomed Eng 14 (2012) 47-71.

[67] S. Thomopoulos, W.C. Parks, D.B. Rifkin, K.A. Derwin, Mechanisms of tendon injury and repair, J Orthop Res 33(6) (2015) 832-9.

[68] H. Capella-Monsonis, S. Kearns, J. Kelly, D.I. Zeugolis, Battling adhesions: from understanding to prevention, BMC Biomed Eng 1(1) (2019) 5.

[69] S.H. Taylor, S. Al-Youha, T. Van Agtmael, Y. Lu, J. Wong, D.A. McGrouther, K.E. Kadler, Tendon is covered by a basement membrane epithelium that is required for cell retention and the prevention of adhesion formation, PLoS One 6(1) (2011) e16337.

[70] A. Yahyouche, X. Zhidao, J.T. Czernuszka, A.J.P. Clover, Macrophage-mediated degradation of crosslinked collagen scaffolds, Acta Biomater 7(1) (2011) 278-286.

[71] F.Y. McWhorter, T. Wang, P. Nguyen, T. Chung, W.F. Liu, Modulation of macrophage phenotype by cell shape, Proc Natl Acad Sci U S A 110(43) (2013) 17253-8.

[72] D.Y. Vogel, J.E. Glim, A.W. Stavenuiter, M. Breur, P. Heijnen, S. Amor, C.D. Dijkstra, R.H. Beelen, Human macrophage polarization in vitro: maturation and activation methods compared, Immunobiology 219(9) (2014) 695-703.

[73] K.P. Fuller, D. Gaspar, L.M. Delgado, A. Pandit, D.I. Zeugolis, Influence of porosity and pore shape on structural, mechanical and biological properties of poly -caprolactone electro-spun fibrous scaffolds, Nanomedicine 11(9) (2016) 1031-40.

[74] S.F. Badylak, J.E. Valentin, A.K. Ravindra, G.P. McCabe, A.M. Stewart-Akers, Macrophage phenotype as a determinant of biologic scaffold remodeling, Tissue Eng Part A 14(11) (2008) 1835-42.

[75] S.P. Wilshaw, D. Burke, J. Fisher, E. Ingham, Investigation of the antiadhesive properties of human mesothelial cells cultured in vitro on implantable surgical materials, J Biomed Mater Res B Appl Biomater 88(1) (2009) 49-60.

[76] A.K. Ghosh, D.E. Vaughan, PAI-1 in tissue fibrosis, J Cell Physiol 227(2) (2012) 493-507.

[77] J. Kruegel, N. Miosge, Basement membrane components are key players in specialized extracellular matrices, Cell Mol Life Sci 67(17) (2010) 2879-95.

[78] W. Halfter, P. Oertle, C.A. Monnier, L. Camenzind, M. Reyes-Lua, H. Hu, J. Candiello, A. Labilloy, M. Balasubramani, P.B. Henrich, M. Plodinec, New concepts in basement membrane biology, FEBS J 282(23) (2015) 4466-79.

[79] V.S. LeBleu, B. Macdonald, R. Kalluri, Structure and function of basement membranes, Exp Biol Med (Maywood) 232(9) (2007) 1121-9.

Chapter 3

Porcine mesothelium matrix as a biomaterial for wound healing applications

Part of this chapter has been published:

Capella-Monsonís, H., Tilbury M. A., Wall J. G., & Zeugolis, D. I. (2020). *Porcine mesothelium matrix as a biomaterial for wound healing applications*. **Materials Today Bio** 7, 100057

3.1. Introduction

Wound healing represents a substantial financial burden in current healthcare systems with estimated annual healthcare expenditure in excess of $50 billion in the United States alone [1]. The estimated global prevalence is over 3.5 per 100,000 people, which continuously raises, as life expectancy and disease associated non-healing conditions (e.g. diabetes) increase [2, 3]. It is thus urgent and imperative to develop functional therapies for wound healing applications.

Decellularised xenografts have shown promise in wound healing management [4-8], overcoming disadvantages of human grafts (e.g. low availability, donor site morbidity) and synthetic biomaterials (e.g. foreign body response). Yet again, there is no consensus on the ideal xenograft, considering the scattered therapeutic efficacy and efficiency (e.g. the porcine dermal matrix Permacol™ in hernia [9, 10] repair, the porcine small intestine submucosa CorMatrix® in paediatric cardiovascular surgery [11, 12] and the porcine dermal matrix Strattice® in breast reconstruction [13, 14] have shown both positive and negative results).

Porcine mesothelium is a tissue rich in connective tissue (e.g. collagens type I and III, elastin, fibronectin) and basement membrane (e.g. collagen type IV and laminin) proteins and growth factors (e.g. FGF-2, TGF-β, VEGF) [15-17]. These extracellular matrix (ECM) components present recognition motifs that promote the attachment and proliferation of cells [18-20], contributing to the high cytocompatibility and low immunogenicity *in vitro* of porcine mesothelium [21, 22] and allowing re-epithelisation *in vitro*, promoted by its basement membrane components [22, 23]. Further, growth factors retained within the porcine mesothelium matrix promote wound healing events, such as cell proliferation and angiogenesis *in vivo* [22, 24, 25]. Such features clearly illustrate their potential in the wound healing scenario, where cell proliferation, re-epithelisation and angiogenesis are desirable events to be promoted. Despite all these advantages, commercially available porcine mesothelium grafts have only been used in breast [13], cartilage [26] and nasal [27] reconstruction and as a tendon protector sheet [21].

Herein, we compared the biochemical and biological properties of the only two commercially available porcine mesothelium grafts (Meso Biomatrix® and Puracol® Ultra ECM / XenoMEM™) to traditionally used wound healing grafts (Endoform™, ovine forestomach [28] and MatriStem®, porcine urinary bladder [29, 30]) and biomaterials (Promogran™, oxidised regenerated cellulose / collagen [31-34]) that have all also shown efficiency and efficacy in wound healing clinical trials.

3.2. Materials and methods

3.2.1. Materials

The products assessed in this study are provided in **Table 3.1**. All chemicals and consumables were purchased from Sigma-Aldrich (Ireland), unless otherwise stated.

Table 3.1. Commercially available products that were assessed in this study.

Product Description & Name
Collagen / Oxidised regenerated cellulose, Promogran™ (CORC-PG), Acelity™, USA
Ovine forestomach, Endoform™ (OF-EF), Hollister Wound Care, USA
Porcine urinary bladder, MatriStem® (PUB-MS), ACell®, USA
Porcine mesothelium, Meso Biomatrix® (PM-MB), DSM Biomedical, Netherlands
Porcine mesothelium, Puracol® Ultra ECM / XenoMEM™ (PM-PC), Medline Industries, USA

3.2.2. SDS-PAGE

The presence of soluble collagen type I was assessed with sodium dodecyl sulphate-polyacrylamide gel electrophoresis (SDS-PAGE) [35]. Briefly, small pieces of each material were cut, weighed and incubated in 1 mg / ml pepsin (P6687, Sigma-Aldrich, Ireland) in 0.5 M acetic acid overnight at 4 ºC under continuous agitation (1 mg of material per 1 ml of pepsin / acetic acid solution). Solutions were then centrifuged (Heraeus Fresco 17 Centrifuge, ThermoFisher, Ireland) at 13,000 rpm and 4 ºC for 15 min, supernatants were recovered and loaded onto a Mini-Protean 3 SDS-PAGE unit (Bio-Rad Laboratories, UK). 3 % stacking and 5 % separation gels were used. Purified collagen type I (CBP2US, Symatese, France) was used as standard. Gels were stained using the SilverQuest™ Silver Staining kit, as per manufacturer's protocol (ThermoFisher, Ireland).

3.2.3. Elastin and collagen quantification

Elastin content was quantified using the Fastin™ Elastin Kit (Biocolor, UK), as per manufacturer's protocol. The total amount of collagen in each material was analysed by hydroxyproline assay [35]. Briefly, 5 mg of each sample were hydrolysed in 6 M HCl at

110 ºC overnight. The hydrolysates were then centrifuged (Heraeus Pico 17 Centrifuge, ThermoFisher, Ireland) at 15,000 g and room temperature for 10 min and 10x, 50x and 100x dilutions of the supernatants were prepared. 110 μl of these dilutions were transferred to a microcentrifuge tube and 176 μl of chloramine-T reagent were added. The samples were then mixed and incubated for 10 min at room temperature. After incubation, 460 μl of Ehrlich's reagent were added, the samples were vortexed (Fisherbrand™ Classic Vortex Mixer, ThermoFisher, Ireland) for 30 sec and incubated at 70 ºC for 10 min. Then, 200 μl of each sample were transferred to a well of a 96-well plate and absorbance (VarioSkan Flash Spectral Multimode Reader, ThermoFisher, Ireland) was measured at 555 nm. The hydroxyproline corresponding to the elastin (1 % wt / wt) was subtracted from the total hydroxyproline content. The remaining hydroxyproline amount was employed to calculate the collagen content by diving by 0.135 (13.5 % wt / wt) [35].

3.2.4. Growth factor quantification

The content of growth factors was assessed using ELISA [22]. Briefly, samples were weighed and proteins were extracted employing a radioimmunoprecipitation assay (RIPA) extraction buffer (R0278, Sigma-Aldrich, Ireland) with a protease inhibitor cocktail (P9599, Sigma-Aldrich, Ireland). To each sample, 1 ml of extraction buffer was added and samples were incubated in a tissue homogenizer (TissueLyser LT, Qiagen, UK) overnight at 50 rpm and 4 ºC. Samples were then centrifuged (Heraeus Fresco 17 Centrifuge, ThermoFisher, Ireland) at 13,000 rpm and 4 ºC for 15 min. Supernatants were then concentrated using Pierce™ 3K Concentrators (ThermoFisher, Ireland) and FGF-basic, VEGF and TGF-β1 content was measured using ELISA DuoSet® kits (DY233, DY293B and DY240, respectively; R&D Systems, UK), as per manufacturer's protocols.

3.2.5. Histology and immunohistochemistry analysis

For further compositional analysis, samples were cut in 1 cm^2 pieces, hydrated for 2 h in phosphate buffered saline (PBS) at room temperature and then stored at -80 ºC in Tissue Freezing Medium® (Leica Biosystems, Ireland). Transverse cryosections of 5 μm thickness were obtained using a CM1850 Cryostat (Leica Biosystems, Ireland) operating at -20 ºC. The cryo-sections were subsequently stained with haematoxylin / eosin, Picrosirius red and Masson's trichrome using DPX mountant (06522, Sigma-Aldrich, Ireland) [36].

Immunohistochemistry analysis was carried out for collagen type I (ab90395, Abcam, USA), collagen type III (ab7778, Abcam, USA), collagen type IV (ab6586, Abcam,

USA), elastin (ab21610, Abcam, USA), laminin (L939, Sigma-Aldrich, Ireland) and fibronectin (F7387, Sigma-Aldrich, Ireland) [36]. Cryosections were blocked at room temperature with 5 % normal goat serum (NGS) and 0.1 % Triton X-100 in PBS for 1 h. The sections were then incubated with the primary antibodies diluted in blocking buffer overnight at 4 ºC, followed by 3 washes in PBS at room temperature. Subsequently, secondary antibodies at 1:500 in blocking buffer were added (Alexa Fluor 488 goat anti rabbit and Alexa Fluor 555 goat anti mouse, Life Technologies, Ireland) for 1 h at room temperature, followed by 3 washes in PBS at room temperature. To assess whether any cellular remnants had remained, sections were stained with Hoechst (H1399, Invitrogen, Ireland) at 1:5000 in PBS for 5 min at room temperature. Sections were then mounted with Fluoromount™ Aqueous Mounting Medium (F4680, Sigma-Aldrich, Ireland), left for 2 h at room temperature and then stored at 4 ºC. Images were taken with an inverted fluorescence microscope (IX81, Olympus, UK).

3.2.6. Enzymatic degradation

Resistance to collagenase [35] and elastase [37] degradation was also assessed. Briefly, 5 mg pieces of each material were cut and placed into Eppendorf tubes. 1 ml of Tris-HCl buffer pH 7.40 containing 50 U / ml of MMP-8 (17101015, Gibco®, Ireland) or Tris buffer pH 8.5 containing 0.1 U / ml of elastase (E7885, Sigma-Aldrich, Ireland) was added. The samples were then incubated at 37 °C under agitation in an orbital shaker (MaxQ 4000, ThermoFisher, Ireland) at 150 rpm for 2, 4, 8, 12 and 24 h. The solubilized portion was discarded after centrifugation (Heraeus Pico 17 Centrifuge, ThermoFisher, Ireland) at 13,000 rpm and room temperature for 10 min and the remaining pellets where weighed after overnight freeze drying (FreeZone Plus 4.5, Labconco, ThermoFisher, Ireland). The % weight loss over time was subsequently calculated for each material and enzyme.

3.2.7. Swelling ratio analysis

Pieces from all the materials were cut with an 8 mm diameter biopsy punch and were weighed with a laboratory scale (MH-124, Fisherbrand, UK). The materials were then incubated in PBS overnight at room temperature. After blotting excess PBS with Whatman filter paper, their weight was recorded. Swelling (%) was calculated as (wet weight – dry weigh) / dry weight %.

3.2.8. Bacterial penetration assay

Microbial analysis was conducted using *Escherichia coli* (*E. coli*, BL21(DE3), Invitrogen, Ireland) [38, 39]. To assess the effect of the different materials on bacterial growth, bacteria were seeded on Lysogenic Broth (LB) agar petri dishes at 10^{10} CFU / ml and allowed to dry for 10 min at room temperature. Then, 6 mm discs of each material were soaked in sterile PBS for 20 min, placed on the agar plates, incubated at 37 °C for 24 h and the inhibition growth area was measured employing ImageJ (NIH, USA). Filter paper discs loaded with 50 μg of ampicillin sodium salt (A9518, Sigma-Aldrich, Ireland) were used as control. To assess the penetration of bacteria in the materials, trans-well constructs attached to a silicone sheet were used. The silicone sheet between the inner and outer layer was perforated with a 6 mm biopsy punch, and 13 mm discs of each materials were fixed on the silicone sheet using glue. The hole was covered and the materials formed the only barrier between the chambers; care was taken so the glue was not deposited in the hole / material area. The constructs were sterilised under UV for 1 h and 70 % ethanol for 30 min, followed by 3 washes of PBS. A single colony of *E. coli* from an agar plate was used to inoculate 50 ml LB and grown with continuous agitation at 37 °C until the culture reached an OD_{600} of 0.7-0.8. The culture was centrifuged (Heraeus Pico 17 Centrifuge, ThermoFisher, Ireland) at 6,000 rpm for 5 min at room temperature, the pellet was resuspended in sterile PBS, and 0.5 ml of the suspension containing 10^{10} CFU / ml *E. coli* was added to the inner chamber of the trans-well. In the outer chamber, 1 ml of sterile PBS was placed, and aliquots of 50 μl were taken after incubation for 1, 2 and 4 h at 37 °C with mild agitation. Aliquots were then serially diluted and plated on LB agar plates at 10^{-1}, 10^{-5} and 10^{-8} dilutions and the number of CFU were counted after incubation at 37 °C for 24 h. In a pilot study, it was confirmed that the industrial glue and system employed did not affect the viability of the bacteria or the ability of the unperforated silicone sheet without perforation to contain the microorganisms. After 24 h incubation, the materials were fixed in 4 % paraformaldehyde (PFA, 158127, Sigma-Aldrich, Ireland) and cryosections were prepared as described in section 2.4. Cryosections were stained with DAPI to qualitatively assess the localisation of the bacteria within the material.

3.2.9. Dermal fibroblast response analysis

Cytocompatibility was assessed using primary adult dermal fibroblasts (PCS-201-012, ATCC®, UK). CORC-PG, OF-EF, PUB-MS and PM-MB and PM-PC were cut in 1 cm^2 pieces, placed of at the bottom 24-wellplates and fixed with a silicone O-ring (Z504165,

Sigma-Aldrich, Ireland). Then, they were sterilized with 70 % ethanol for 30 min at room temperature and washed 3 times with PBS. Dulbecco's Modified Eagle Medium (DMEM) supplemented with 10 % of foetal bovine serum (FBS) and 1 % penicillin / streptomycin (P / S) containing 15,000 cells / ml was gently poured on top of the CORC-PG, both sides of the OF-EF [serosa (SR) and papillae (PL)] and both sides of the PUB-MS, PM-MB and PM-PC [connective tissue (CT) and basal membrane (BM)] and incubated at 37 °C and 5 % CO_2 for 3, 7 and 14 days. Media were changed every 3 days. Cell morphology was evaluated after fixation with 4 % PFA for 15 min at room temperature and rhodamine / phalloidin (R415, Life Technologies, Ireland) and Hoechst (62249, ThermoFisher, Ireland) staining. Images were taken with an inverted fluorescence microscope (IX81, Olympus, UK). Nuclei counting was used to assess cell proliferation. Cell metabolic activity and viability were evaluated at each time point with alamarBlue® (ThermoFisher, Ireland) and LIVE/DEAD® (ThermoFisher, Ireland) assays, respectively. Metabolic activity was first normalised to cell number and then expressed relatively to the control TCP. Cell proliferation was expressed relatively to the control TCP.

3.2.10. Monocyte response analysis

Immune response was assessed using monocyte-like cells (THP-1, TIB-202, ATCC®, UK) [21]. Briefly, cells were expanded in suspension in RPMI-1640 medium with 10 % FBS and 1 % P / S (Sigma-Aldrich, Ireland). Then, THP-1 cells were seeded on the materials at 25,000 cells / cm^2. To induce macrophage phenotype, cells were treated with phorbol 12-myristate 13-acetate (PMA, P8139, Sigma-Aldrich, Ireland) at 100 ng / ml for 24 h at 37 ºC and 5 % CO_2. Non-attached cells were washed with PBS and seeded cells were incubated with complete RPMI-1640 medium. As positive inflammatory control, cells were treated with lipopolysaccharides (LPS) from *E. Coli* (L2637, Sigma-Aldrich, Ireland) at 100 ng / ml. All conditions were in culture for 1 and 2 days. Cell metabolic activity, viability, proliferation and morphology of cells were assessed as described in section 2.7. Released TNF-α in the medium was quantified using an ELISA assay (DY210, R&D Systems, UK). Same experiments were also performed on THP-1 attached to TCP and then treated with conditioned media, which were prepared by incubating media with each material for 48 h at 37 ºC under continuous agitation, and subsequent filtering with a 0.2 μm Millipore filter.

3.2.11. Scratch assay

The *in vitro* angiogenic potential of all materials was assessed using the scratch assay [40]. Human umbilical vein endothelial cells (HUVECs, C2517A, Lonza, UK) were expanded in specific medium (EGM™-2, Lonza, Ireland). When they reached 85-90 % confluence, they were seeded in 48-wellplates and incubated at 37 ºC and 5 % CO_2 until confluent (2 days). Using a sterile pipette tip, 1 mm wide gap was created at the cell monolayer. The cells were then washed 3 times with PBS to remove cellular debris and treated with medium conditioned with each material. Conditioned media was created by incubating supplemented with 2 % FBS and 1 % P / S DMEM with each of the materials at 20 mg / ml overnight at 37 °C under continuous agitation in an incubated orbital shaker (MaxQ 4000, ThermoFisher, Ireland) at 150 rpm. These mixtures were then sterile filtered and poured on the cell monolayer with the gap. DMEM with 2 % FBS and 1 % P / S and endothelial growth medium (EGM™-2, Lonza, Ireland) were used as negative and positive controls, respectively. Images were taken at 4, 8, 12 and 24 h and the area fold change in the monolayer moving into the scratch zone with respect to the area at time 0 was calculated for each material.

3.2.12. Rat aortic ring assay

The aortic ring assay was carried out to compare the impact on angiogenesis of the different materials in an *ex vivo* model [40]. The preclinical work was conducted as per NUI Galway's rules and regulations governing preclinical assessment, following the internationally established 3Rs principles. Animals were used from the study with approval number 17Apr01 (Animal Care Research Ethics Committee, NUI Galway). Briefly, 3 adult (12 weeks) female Sprague Dawley rats were housed with water and food *ad libitum*. The rats were euthanised by isoflurane overdose and decapitation. The aortas were dissected, cleaned and sectioned into 2 mm thick sections. Remaining biological waste was frozen, sterilised and disposed according to NUI Galway's biological waste management policies. 500 μL of the different conditioned media (see section 2.9), containing fibrinogen (F4883, Sigma-Aldrich, Ireland) at 3 mg / ml, were used to cover the aortic rings in a 24-well plate. Then, thrombin (T1063, Sigma-Aldrich, Ireland) at 1 U/ml was added to form a hydrogel. Gels were set overnight at 37 °C and 5 % CO_2 and then 500 μL of the correspondent conditioned media was gently poured over the gels. DMEM supplemented with 2 % FBS and 1 % P / S was used as negative control, whereas DMEM supplemented with 100 ng / ml of VEGF (AF-100-20, PeproTech, UK) was used as positive control. The aorta rings in the gels were then incubated at 37 °C and 5 % CO_2,

and images were taken at 4x magnification after 3 and 5 days using an inverted microscope (EVOS® Image System, ThermoFisher, Ireland). ImageJ (NIH, USA) was used to measure the megapixels of the new micro-vessels formed by creating masks.

3.2.13. Statistical analysis

Data were analysed using the IBM SPSS Statistics software (IBM Analytics, USA). Student's t-test and one-way analysis of variance (ANOVA) followed by Fisher's post-hoc test were employed after confirming normal distribution of the populations (Kolmogorov-Smirnov) and the equality of variances (Levine's test for homogeneity of variance). For non-normal distributions or different variances Mann-Whitney U test and Kruskal-Wallis test were employed to assess significant differences. Statistical significance was accepted at $p < 0.05$.

3.3. Results

3.3.1. SDS-PAGE, content of collagen, elastin and growth factors

SDS-PAGE analysis (**Figure 3.1A**) revealed the presence of soluble collagen in OF-EF, PM-MB (highest amount) and PM-PC after acetic acid and pepsin extraction, whereas no soluble collagen was observed in any extraction of the CORC-PG and PUB-MS. Hydroxyproline assay (**Figure 3.1B**) showed OF-EF, PUB-MS and PM-PC to contain similar levels between them ($p > 0.05$) and all of them significantly higher levels ($p < 0.01$) than CORC-PG and PM-MB of collagen. OF-EF and PM-PC showed significantly higher ($p < 0.05$) elastin content than PUB-MS and PM-MB, whereas no elastin was detected at the CORC-PG (**Figure 3.1C**). PUB-MS exhibited the highest ($p < 0.001$) amounts of FGF-basic (**Figure 3.1D**). PM-MB had the highest ($p < 0.001$) amounts of TGF-β1 (**Figure 3.1E**) and VEGF (**Figure 3.1F**). No growth factors were detected at the CORC-PG (**Figure 3.1D**, **Figure 3.1E** and **Figure 3.1F**).

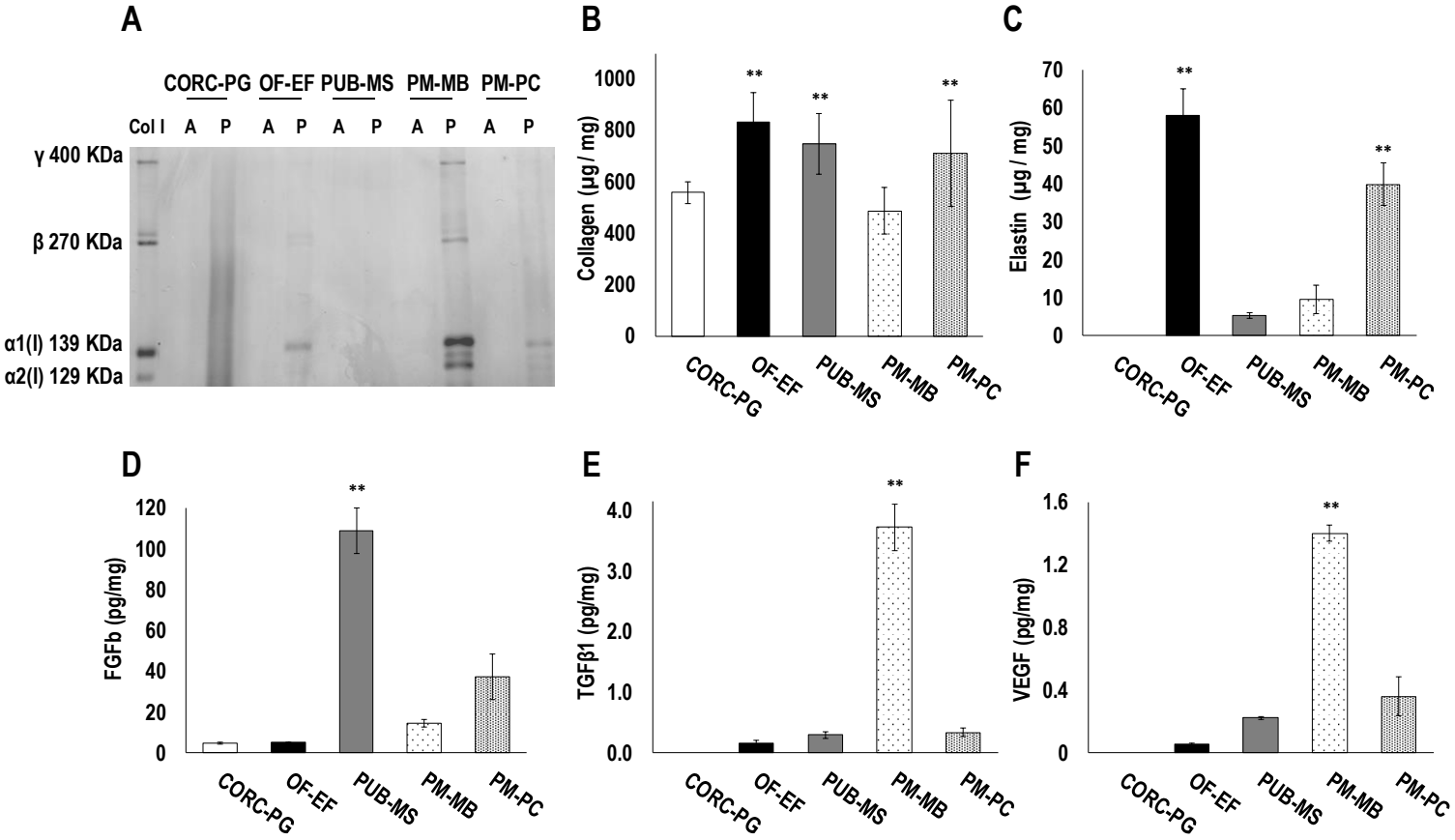

Figure 3.1. SDS-PAGE analysis of acetic acid (A) and acetic acid / pepsin (P) showed soluble collagen in OF-EF, PUB-MS, PM-MB and PM-PC (**A**). Hydroxyproline assay revealed that the OF-EF, PUB-MS and PM-PC had the highest (**) collagen content (**B**). OF-EF and PM-PC showed the highest (**) elastin content (**C**). The PUB-MS had the highest (**) FGF-basic (**D**) content. The PM-MB had the highest (**) TGF-β1 (E) and VEGF (**F**) content. Data expressed as average ± standard deviation (n=3). ** indicates statistically higher ($p < 0.01$) groups.

3.3.2. Histology and immunohistochemistry

Histological analysis (**Figure 3.2**) revealed a loose structure for the CORC-PG product (**Figure 3.2A-C**), whilst all tissue grafts products exhibited a denser, tissue-like structure (**Figure 3.2D-O**). Among the tissue grafts, the PUB-MS showed the least dense structure (**Figure 3.2G-I**), whilst the OF-EF showed the highest preservation of tissue architecture (**Figure 3.2D-F**). In PM-MB (**Figure 3.2J-L**) and PM-PC (**Figure 3.2M-O**) some cavities were observed, probably related to processing. Picrosirius red staining confirmed a dense collagenous network in all tissue grafts, especially in OF-EF (**Figure 3.2E**), PM-MB (**Figure 3.2K**) and PM-PC (**Figure 3.2N**) products. Masson's Trichrome staining revealed a red staining in OF-EF (**Figure 3.2F**) and PUB-MS (**Figure 3.2I**), which could correspond to residual cellular material or fibronectin.

Immunohistochemistry analysis (**Figure 3.3**) revealed the presence of collagen types I, III and fibronectin in all the tissue grafts products; collagen type IV was detected in OF-EF (**Figure 3.3B3**), PUB-MS (**Figure 3.3C3**) and PM-PC (**Figure 3.3E3**); laminin was detected in PUB-MS (**Figure 3.3C5**) and PM-PC (**Figure 3.3E5**); and elastin was detected in PM-PC (**Figure 3.3E6**), PM-MS (**Figure 3.3D6**) and OF-EF (**Figure 3.3B6**). DAPI stained residual cellular material in OF-EF (**Figure 3.3B7**), particularly in the serosa side, in PM-MB (**Figure 3.3D7**), and in some samples of PUB-MS, and PM-PC. CORC-PG showed very slight signals of collagen types I (**Figure 3.3A1**) and III (**Figure 3.3A2**) only.

3.3.3. Enzymatic degradation

The CORC-PG showed the highest resistance to collagenase degradation ($p < 0.05$), whereas the PUB-MS, PM-MB and PM-PC showed intermediate resistance and the OF-EF showed the lowest resistance to collagenase digestion (**Figure 3.4A**). The CORC-PG showed the lowest resistance to elastase ($p < 0.05$), whilst the OF-EF, PUB-MS, PM-MB and PM-PC showed similar high resistance to elastase degradation (**Figure 3.4B**).

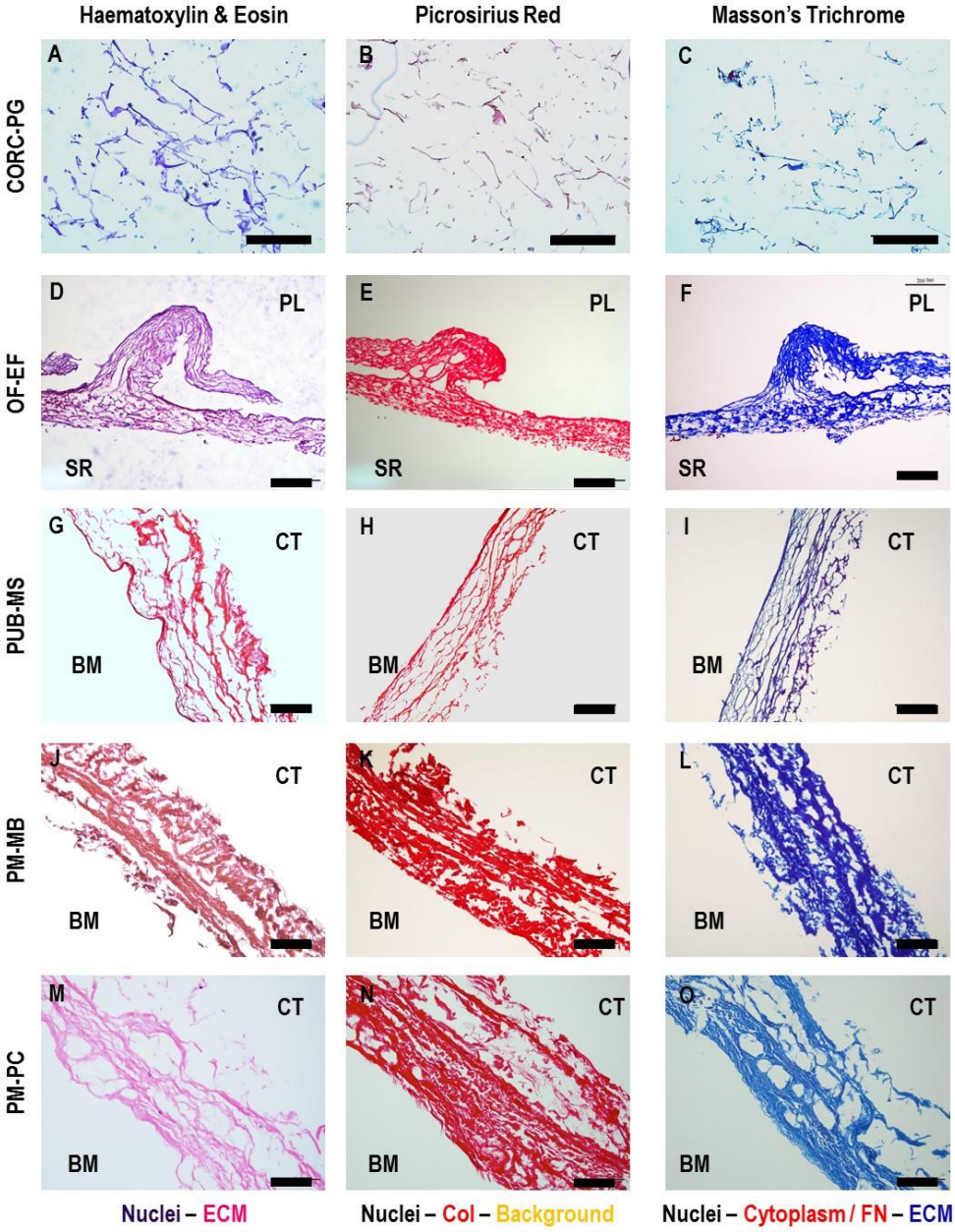

Figure 3.2. Histology analysis with haematoxylin / eosin, picrosirius red and Masson's trichrome of CORC-PG, OF-EF, PUB-MS, PM-MB and PM-PC revealed a loose structure for the CORC-PG and a dense structure for the tissue graft materials. SR: serosa side; PL: papillae side; CT: connective tissue side; BM: basement membrane side. Scale bars 200 μm.

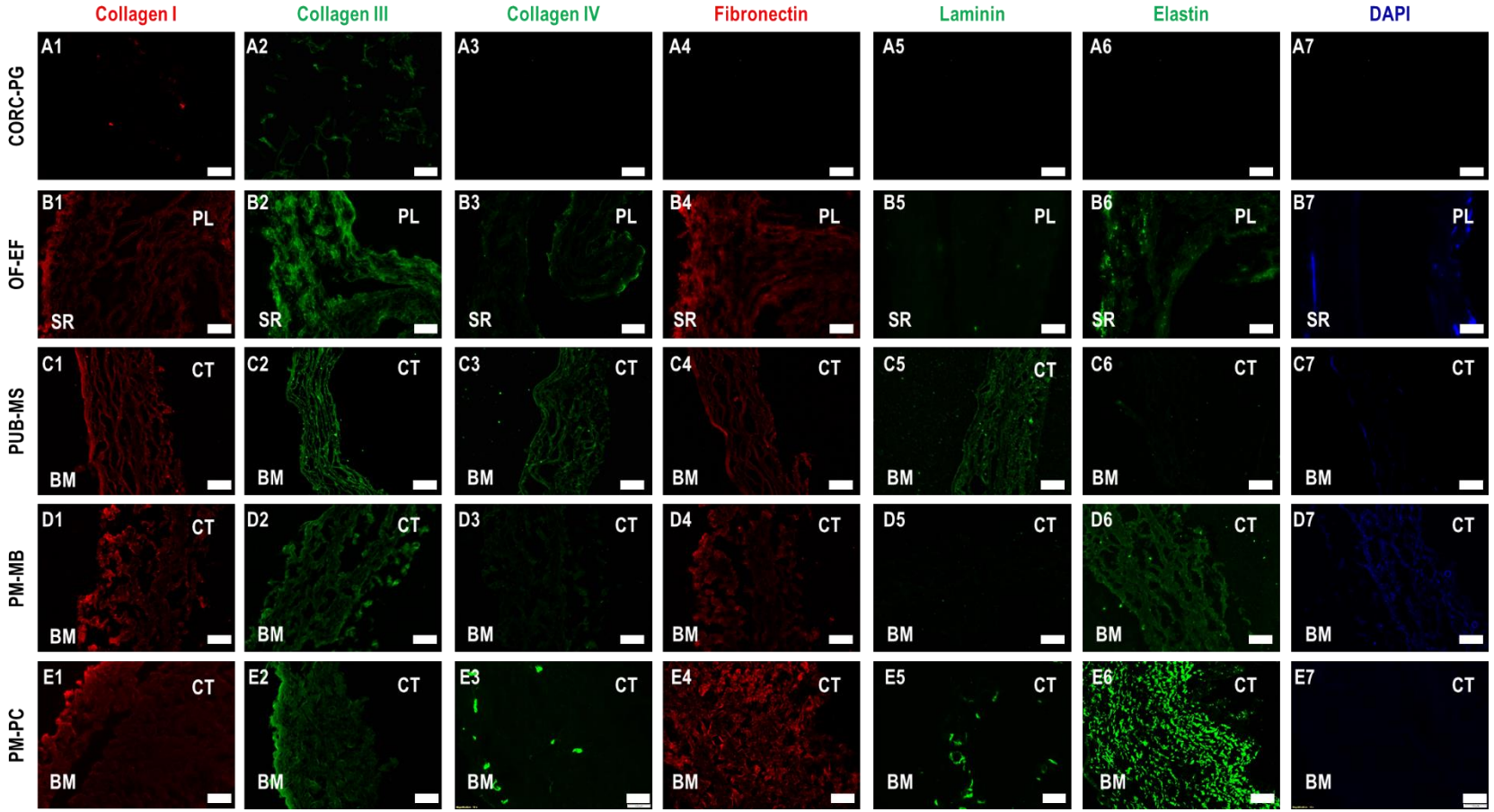

Figure 3.3. Immunohistochemistry analysis made apparent the presence collagen type I, collagen type III and fibronectin in all tissue grafts; collagen type IV in OF-EF, PUB-MS and PM-PC; laminin in PUB-MS and PM-PC and elastin in OF-EF, PM-MB and PM-PC. Remaining cellular material was found in OF-EF and PM-MB. SR: serosa side; PL: papillae side; CT: connective tissue side; BM: basement membrane side. Scale bars 100 μm.

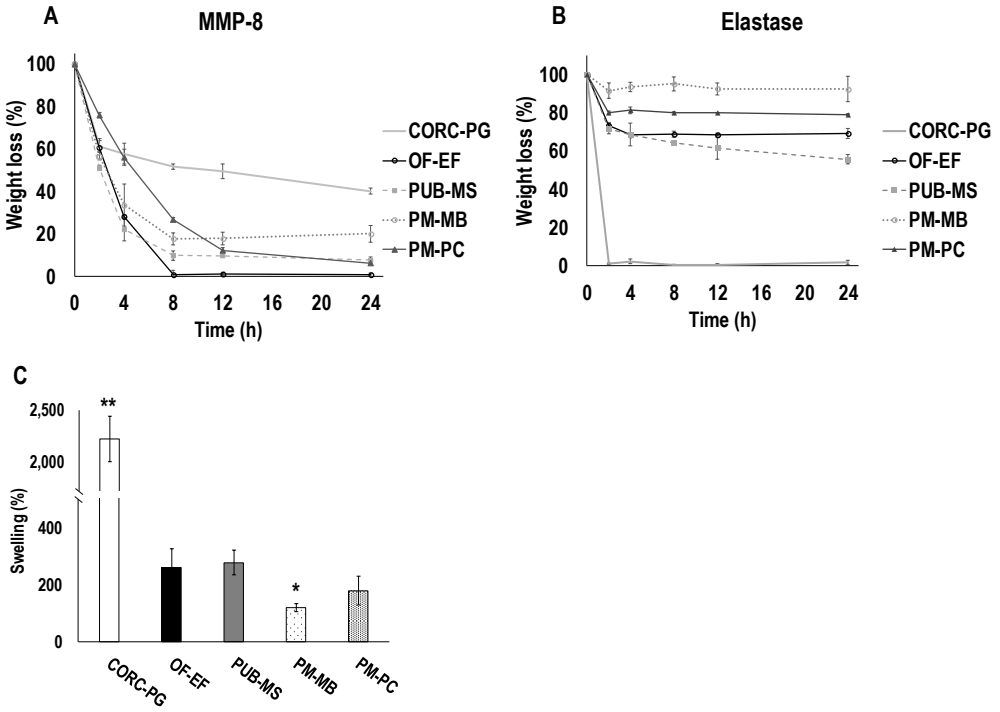

Figure 3.4. The CORC-PG showed the highest resistance to collagenase digestion (**A**) and the lowest resistance to elastase digestion (**B**). Among the tissue grafts, the PM-MB showed the highest resistance to collagenase (**A**) and elastase (**B**) digestion. The CORC-PG exhibited the highest the PM-MB the lowest swelling capacity (**C**). Data expressed as average ± standard deviation (n=3). ** indicates statistically higher ($p < 0.01$) groups, * indicates statistically lower ($p < 0.05$) groups.

3.3.4. Swelling analysis

Among the materials analysed, the CORC-PG exhibited the highest ($p < 0.01$) swelling capacity and the PM-MB showed the lowest ($p < 0.05$) swelling capacity (**Figure 3.4C**).

3.3.5. Bacterial penetration assay

Bacterial penetration was studied employing an in-house developed trans-well system (**Figure 3.5A**). From all products tested, only the positive antibiotic control and the CORC-PG showed bacteria growth inhibition (**Figure 3.5B**). The CORC-PG showed the highest ($p < 0.05$) CFU number at all times and the lowest ($p < 0.05$) CFU number was detected for the OF-EF and PM-PC after 1 h, the PM-PC after 2 h and PUB-MS and PM-PC after 4 h (**Figure 3.5C**). Immunohistochemistry of transverse sections of the materials after 24 h of bacterial incubation showed accumulation of bacteria only at the interface with the PM-MB and PM-PC, whilst bacterial colonisation at the inner layers of CORC-PG, OF-EF and PUB-MS products was observed (**Figure 3.5D**).

A

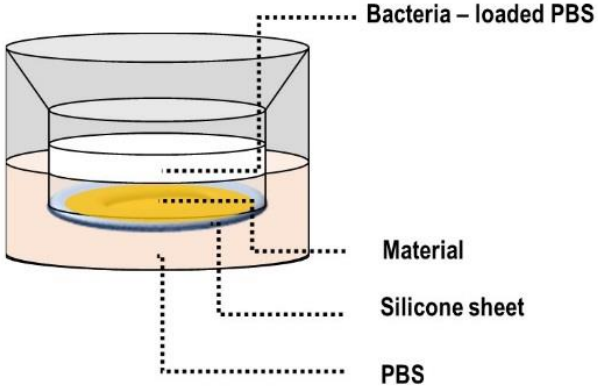

B

	Antibiotic	CORC-PG	OF-EF	PUB-MS	PM-MB	PM-PC
Area (cm^2)	5.88 ± 1.15	0.52 ± 0.08	-	-	-	-

C

		CORC-PG	OF-EF	PUB-MS	PM-MB	PM-PC
Thickness (mm)		2.73 ± 0.18	0.19 ± 0.02	0.21 ± 0.04	0.27 ± 0.05	0.32 ± 0.07
Density (mg/mm^3)		0.01 ± 0.00	0.14 ± 0.01	0.23 ± 0.02	0.21 ± 0.03	0.23 ± 0.02
1 h	1	2.80 E+08	-	1.00 E+06	9.20 E+03	-
	2	3.00 E+08	-	-	3.40 E+03	-
	3	1.76 E+08	-	-	4.00 E+03	-
2 h	1	6.72 E+11	6.72 E+04	3.60 E+07	2.96 E+08	9.00 E+01
	2	5.36 E+11	8.20 E+07	-	1.64 E+08	-
	3	5.84 E+11	6.56 E+04	1.50 E+04	2.12 E+08	-
4 h	1	4.96 E+11	8.00 E+07	6.60 E+07	3.56 E+08	2.87 E+05
	2	8.56 E+11	1.12 E+08	-	3.92 E+08	2.00 E+06
	3	5.60 E+11	2.80 E+08	6.00 E+06	4.76 E+08	-

D

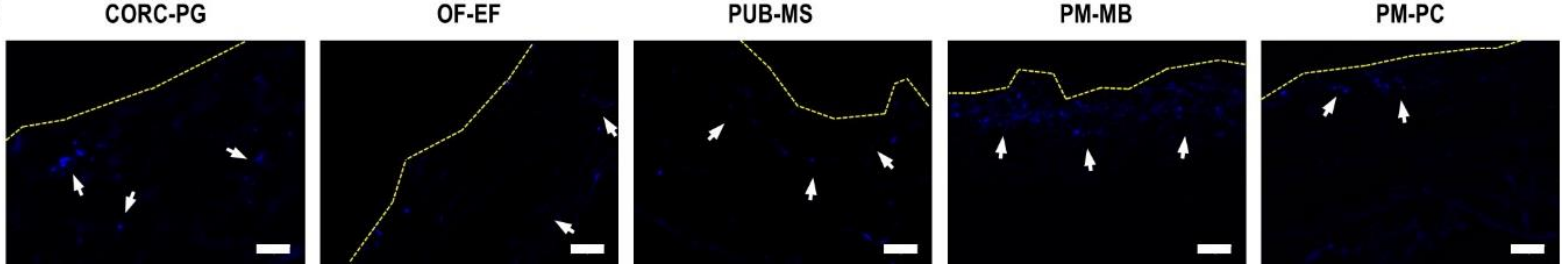

Figure 3.5. Bacterial penetration assay was carried out using an in-house trans-well system (**A**). Among the groups, only the CORC-PG showed bacteria growth inhibition (**B**). The CORC-PG showed the highest CFU number at all time points (**C**). Immunohistochemistry analysis of transverse sections after 24 h of bacterial incubation revealed bacterial colonisation at the inner layers of the CORC-PG, OF-EF and PUB-MS products (**D**). Area, thickness and density data are expressed as average ± standard deviation (n=4 for growth inhibition assay, n=3 for thickness and density). Manual count of CFUs is represented with the value of each replicate; '-' indicates the absence of colonies. Scale bars 50 μm.

3.3.6. Dermal fibroblast response analysis

In comparison to the control TCP, the lowest ($p < 0.05$) dermal fibroblast proliferation (**Figure 3.6A** and **Figure 3.7**) was detected for the CORC-PG, both sides of OF-EF and PUB-MS, connective tissue side of PM-MB and both sides of PM-PC at day 3; the CORC-PG, serosa side of OF-EF and connective tissue side of PUB-MS at day 7; and the CORC-PG, serosa side of OF-EF and connective tissue side of PM-PC at day 14. The highest ($p < 0.05$) dermal fibroblast proliferation (**Figure 3.6A**) was detected for the basement membrane side of the PUB-MS at day 7 and the basement membrane sides of the PUB-MS and PM-MB at day 14.

In comparison to the control TCP, the highest ($p < 0.05$) dermal fibroblast metabolic activity (**Figure 3.6B**) was detected for the CORC-PG at day 3 and day 7; and the CORC-PG, papillae side of OF-EF and both sides of PM-PC at day 14.

In comparison to the control TCP, the lowest ($p < 0.05$) dermal fibroblast viability (**Figure 3.6C** and **Figure 3.8**) was detected for the CORC-PG, serosa side of OF-EF and basement membrane side of PM-PC at day 3 and for the serosa side of OF-EF, basement membrane side of PUB-MS, and basement membrane side of PM-MB at day 14.

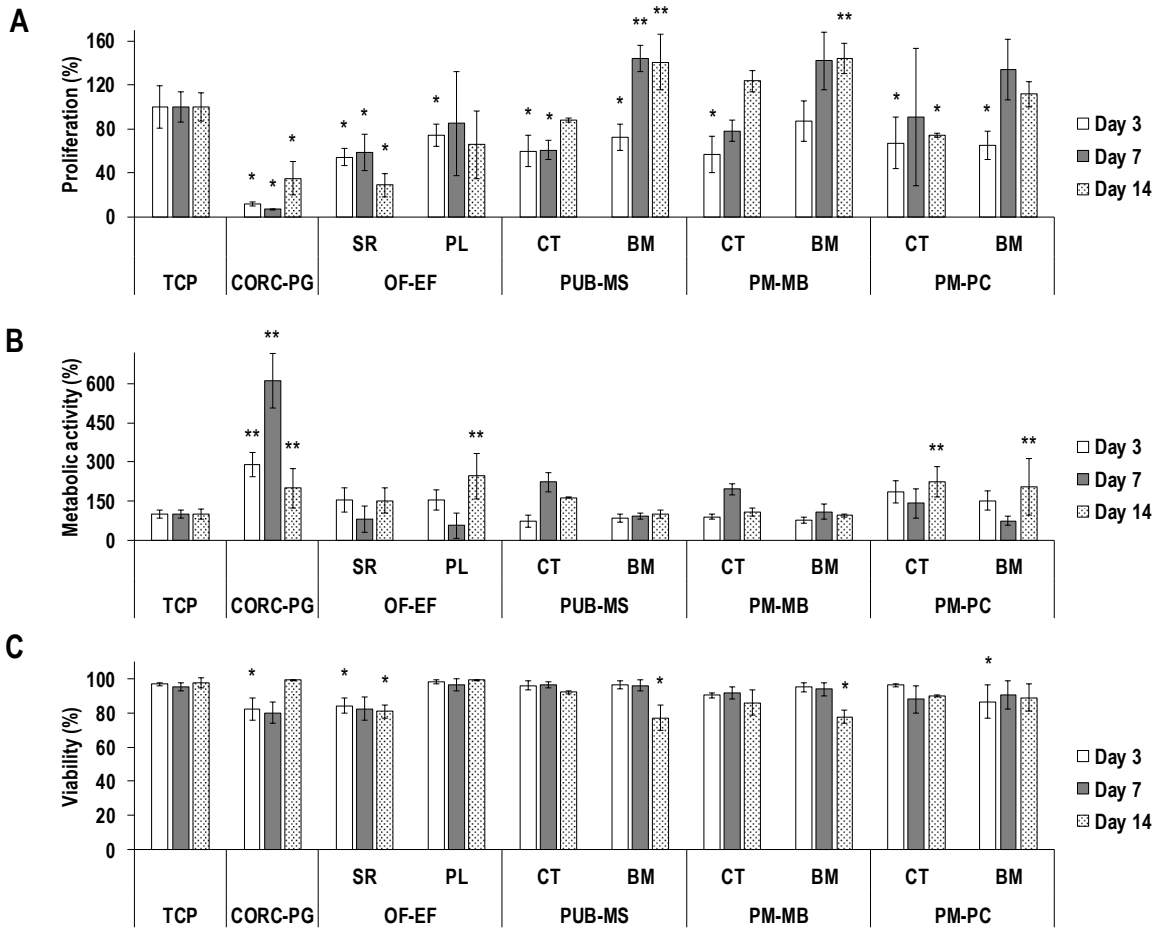

Figure 3.6. By day 14, the lowest (*, $p < 0.05$) dermal fibroblast proliferation was detected for the CORC-PG, serosa (SR) side of the OF-EF and the connective tissue (CT) side of the PM-PC, whilst the highest (**, $p < 0.05$) dermal fibroblast proliferation was detected for the basement membrane (BM) sides of the PUB-MS and PM-MB (**A**). By day 14, the CORC-PG, the papillae (PL) side of the OF-EF and both sides of PM-PC exhibited the highest (**, $p < 0.05$) dermal fibroblast metabolic activity (**B**). By day 14, the SR side of the OF-EF, the BM side of the PUB-MS and the MB side of the PM-MB showed the lowest (*, $p < 0.05$) dermal fibroblast viability, although all groups exhibited viability higher than 75 % (**C**). Data expressed as average ± standard deviation (n=3). Samples were compared to the control tissue culture plate (TCP) at a given time point. SR: serosa side; PL: papillae side; CT: connective tissue side; BM: basement membrane side.

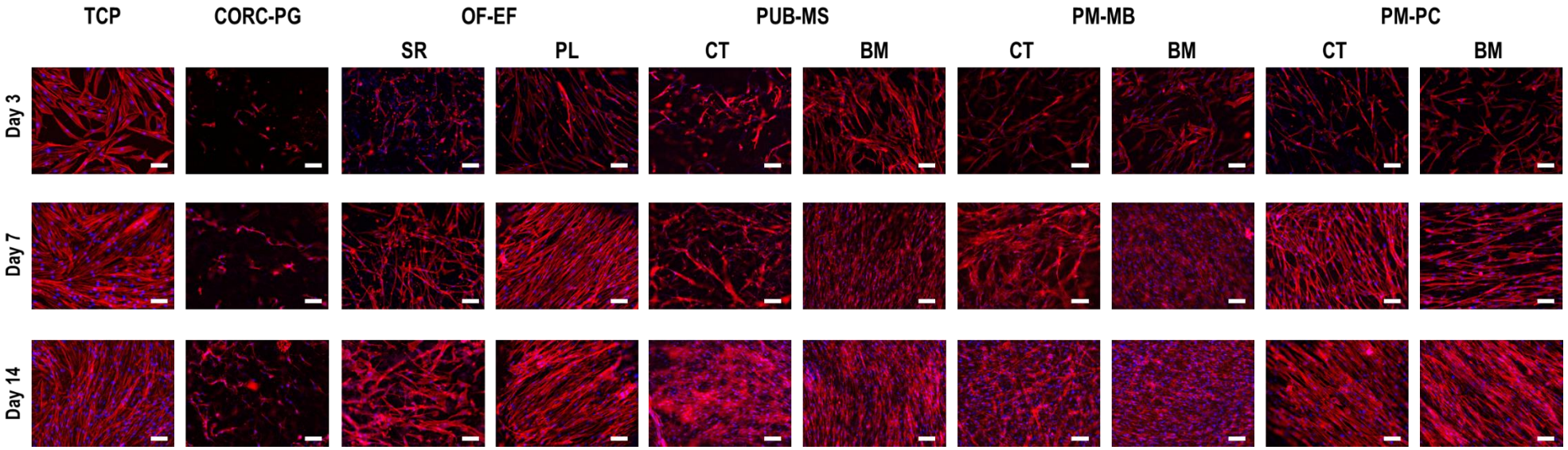

Figure 3.7. Immunocytochemistry analysis [cytoskeleton with rhodamine (red) and nuclei with Hoechst (blue)] made apparent a very low dermal fibroblast proliferation rate on CORC-PG. Scale bars 100 μm. SR: serosa side; PL: papillae side; CT: connective tissue side; BM: basement membrane side.

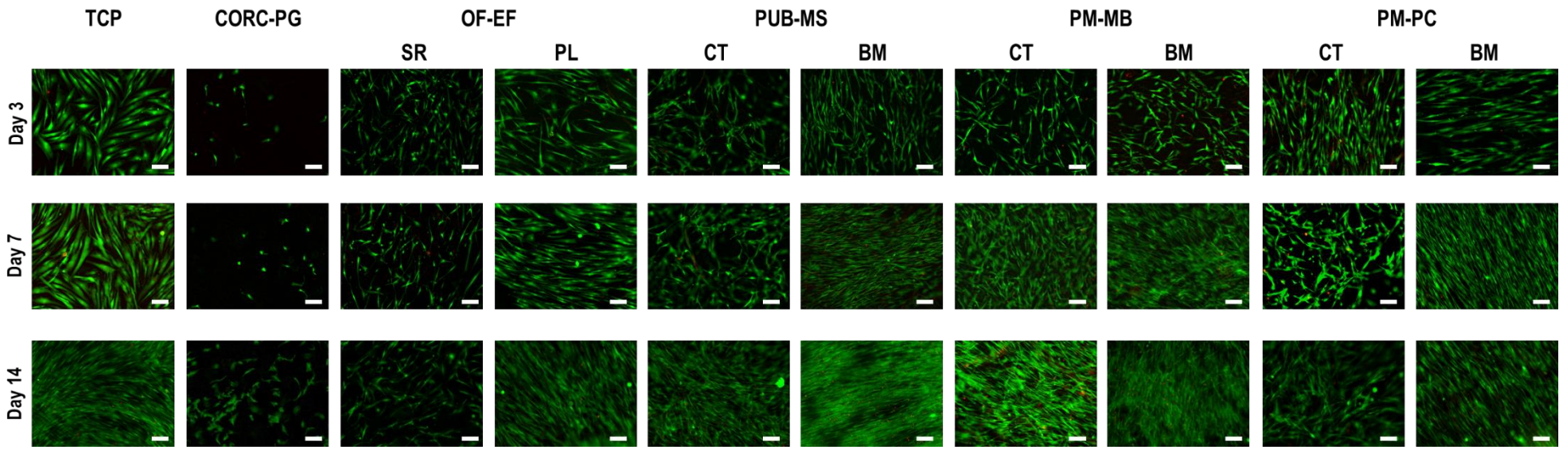

Figure 3.8. Immunocytochemistry analysis for alive (calcein AM, green) and dead (ethidium homodimer, red) dermal fibroblasts on the various materials and time points. Scale bars 100 µm. SR: serosa side; PL: papillae side; CT: connective tissue side; BM: basement membrane side.

3.3.7. Monocyte response analysis

In comparison to the control, the lowest ($p < 0.05$) monocyte proliferation (**Figure 3.9A** and **Figure 3.10**) was detected for the CORC-PG at day 1 and day 2, papillae side of the OF-EF at day 1 and day 2, the basement membrane side of PM-MB at day 1 and day 2 and the basement membrane side of PM-PC at day 2.

In comparison to the control, the highest ($p < 0.05$) monocyte metabolic activity (**Figure 3.9B**) was detected for the CORC-PG at day 1 and day 2, the papillae side of the OF-EF at day 1 and day 2 and the basement membrane side of PM-MB at day 1.

In comparison to the control, the lowest ($p < 0.05$) monocyte viability (**Figure 3.9C** and **Figure 3.11**) the basement membrane side of PM-MB at day 1. In comparison to the control, the highest ($p < 0.01$) TNF-α production (**Figure 3.9D**) was observed for the LPS group at day 1 and day 2. Further, in comparison to the control, the lowest ($p < 0.05$) TNF-α production (**Figure 3.9D**) was detected for the connective tissue side of PUB-MS at day 2; whilst the highest ($p < 0.05$) TNF-α production (**Figure 3.9D**) was observed for the CORC-PG at day 1, the papillae side of the OF-EF at day 1, the basement membrane side of the PUB-MS at day 1, the basement membrane side of the PM-MB at day 1 and the basement membrane side of PM-PC at day 1.

Immunocytochemistry analysis of the cytoskeleton revealed that all treatments resulted in rounded cell morphology, although some elongated cells were detected in the LPS (day 1 and day 2), serosa side of OF-EF at day 2, basement membrane side of PUB-MS at day 1, connective tissue side of PM-PC at day 1 and 2, and basement membrane side of PM-PC at day 1. Some cell clusters (> than 5 cells) were also observed in the LPS (day 1 and day 2), serosa side of OF-EF at day 2, basement membrane side of PUB-MS at day 1 and connective tissue and basement membrane sides at day 2 of PUB-MS, connective tissue and basement membrane sides of PM-PC at day 1 and basement membrane side of PM-PC at day 2 (**Figure 3.10**).

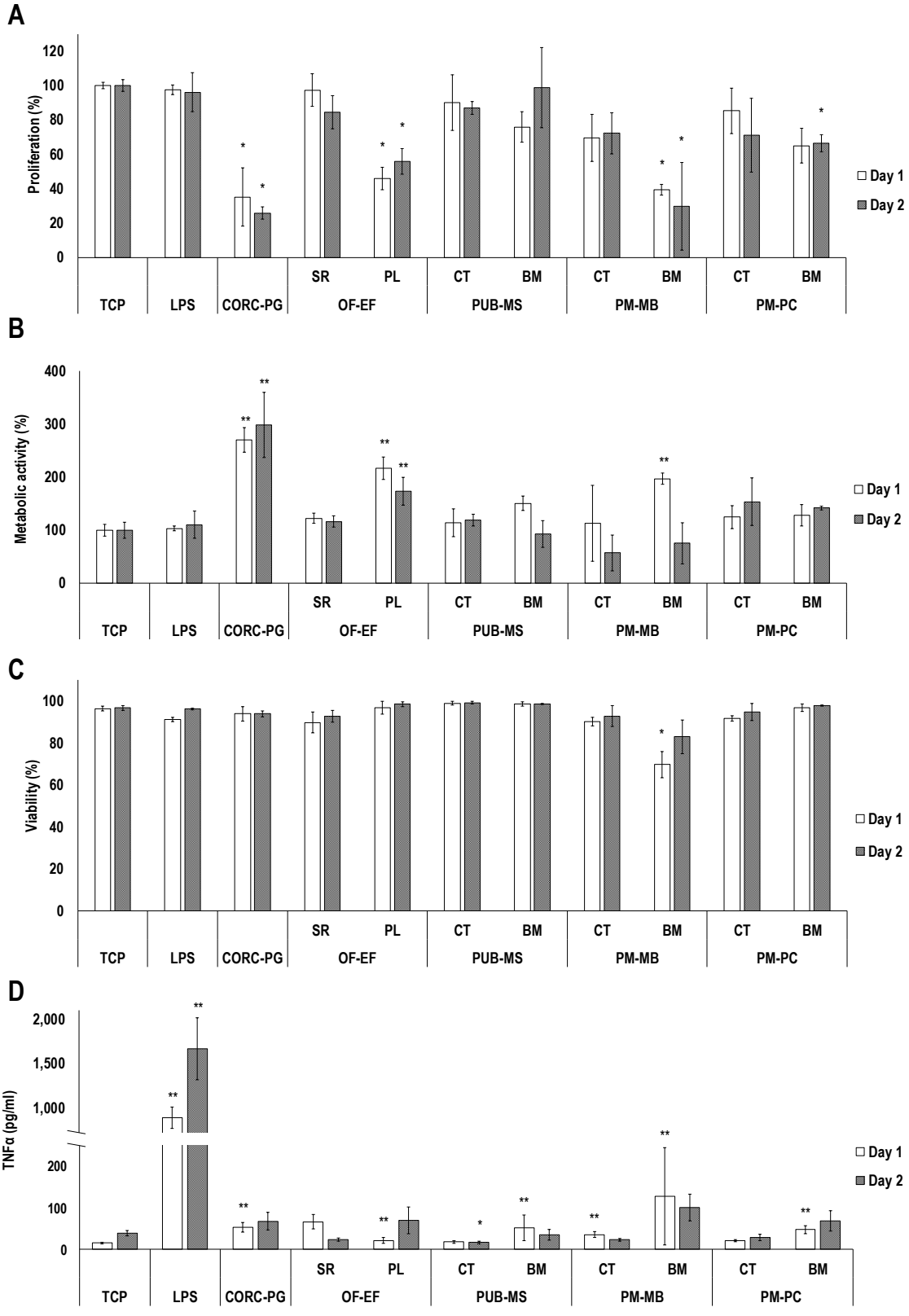
A
Proliferation (%)
120
100
80
60
40
20
0
Day 1
Day 2
TCP
LPS
CORC-PG
OF-EF
SR
PL
PUB-MS
CT
BM
PM-MB
PM-PC
B
Metabolic activity (%)
400
300
200
100
0
C
Viability (%)
D
TNFα (pg/ml)
2,000
1,500
1,000
200
100

Figure 3.9. THP-1 response *in vitro* assessment revealed the lowest (*, $p < 0.05$) proliferation on CORC-PG, papillae (PL) side of OF-EF and basement membrane (BM) side of PM-MB at both time points (**A**). The highest (**, $p < 0.05$) THP-1 metabolic activity was observed for the CORC-PG and the PL side of OF-EF at both time points (**B**). all groups exhibited similar ($p > 0.05$) THP-1 viability at day 2 (**C**). Pro-inflammatory cytokine TNF-α analysis showed the highest (**, $p < 0.01$) production by THP-1 cells in LPS group (**D**). Among the test groups, higher TNF-α production (**, $p < 0.05$) was observed on CORC-PG, PL side of OF-EF and BM sides of PUB-PM, PM-MB and PM-PC at day 1, although far from LPS levels (D). Data expressed as average ± standard deviation (n=3). Samples were compared to the monocytes cultured on tissue culture plate (TCP) with normal medium at a given time point. SR: serosa side; PL: papillae side; CT: connective tissue side; BM: basement membrane side.

When THP-1 were treated with the materials' conditioned media, in comparison to the control, the highest ($p < 0.05$) proliferation at day 1 was detected for the CORC-PG, OF-EF, PM-MB and PMPC and no differences were observed between the groups at day 2 (**Figure 3.12A**). In comparison to the control, the lowest ($p < 0.05$) THP-1 metabolic activity was found when they were treated with conditioned media of CORC-PG at day 1 and with conditioned media of PUB-MS, PMMB and PM-PC at day 2 (**Figure 3.12B**). In comparison to the control, the conditioned media of all materials induced significantly lower ($p < 0.05$) THP-1 viability at day 2 (**Figure 3.12C**). TNF-α production by LPS was the highest ($p < 0.01$) at day 1 and day 2 and no significant differences ($p > 0.05$) were observed between the control and THP-1 cells treated with any of the materials' conditioned media (**Figure 3.12D**).

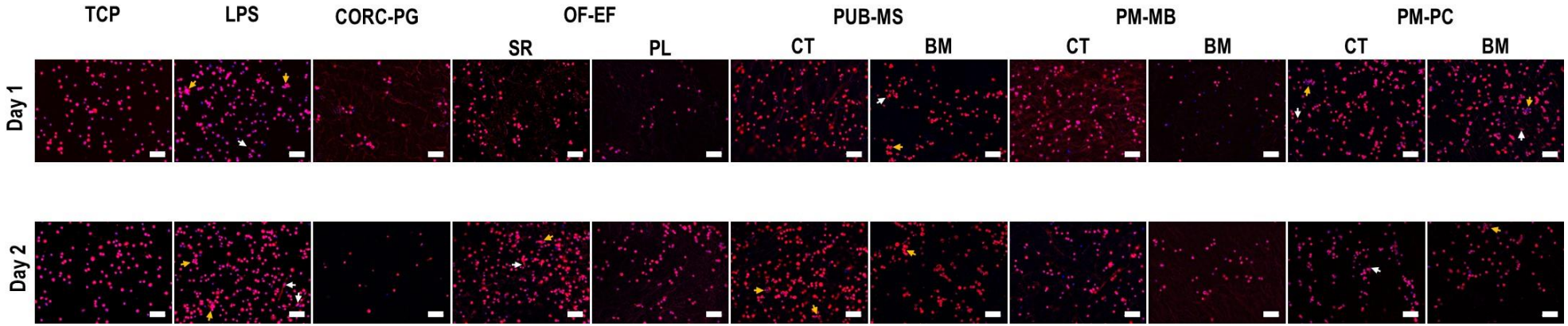

Figure 3.10. Immunocytochemistry (red: cytoskeleton; blue: nuclei) analysis of THP-1 revealed the presence of elongated cells (white arrows; LPS at day 1 and day 2, serosa (SR) side of OF-EF at day 2, BM side of PUB-MS at day 1, connective tissue (CT) side of PM-PC at day 1 and 2 and BM side of PM-PC at day 1) and cell clusters (yellow arrows; LPS at day 1 and day 2, SR side of OF-EF at day 2, BM side of PUB-MS at day 1 and both sides at day 2, both sides of PM-PC at day 1 and BM side of PM-PC at day 2). Scale bars 100 μm. SR: serosa side; PL: papillae side; CT: connective tissue side; BM: basement membrane side.

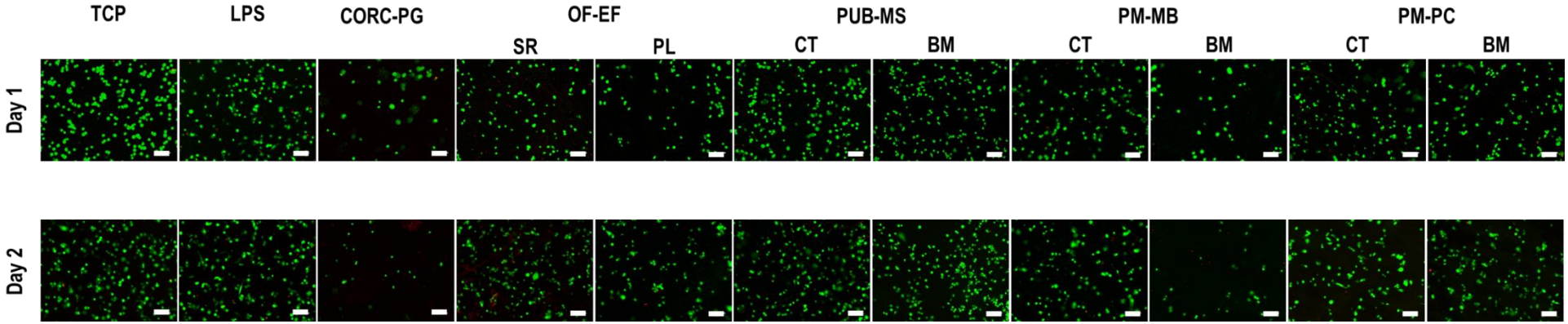

Figure 3.11. Immunocytochemistry analysis for alive (calcein AM, green) and dead (ethidium homodimer, red) THP-1 monocytes on the various materials and time points. Scale bars 100 μm. SR: serosa side; PL: papillae side; CT: connective tissue side; BM: basement membrane side.

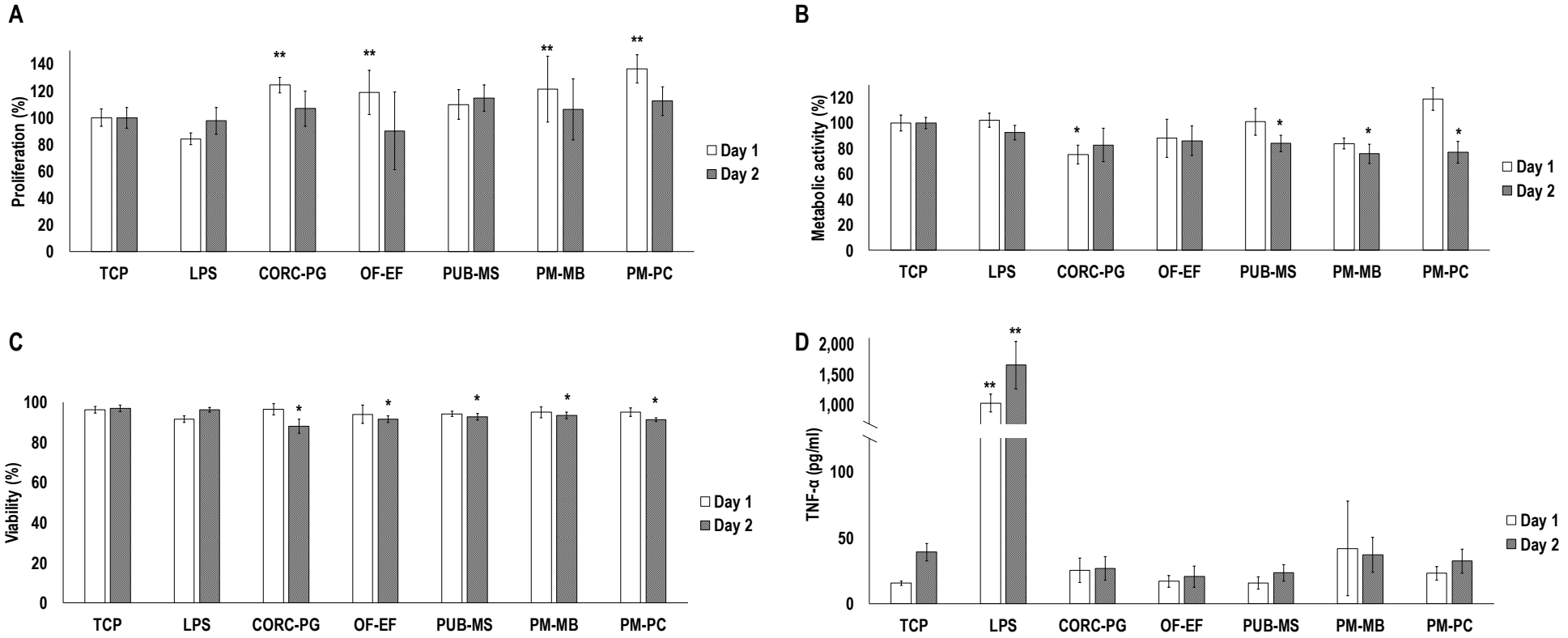

Figure 3.12. Quantification of THP-1 proliferation, metabolic activity, cell viability and TNF-α production under materials conditioned media incubation for 2 days. Data showed as average ± standard deviation (n=5).

3.3.8. Scratch and rat aortic ring assays

In comparison to DMEM control, the EGM2 was significantly higher ($p < 0.01$) in monolayer area fold change at all time points (**Figure 3.13A**, **Figure 3.14**). Further, in comparison to the DMEM control, the highest ($p < 0.05$) monolayer area fold change was observed for the CORC-PG, OF-EF and PM-PC groups at 4 h, the OF-EF and PM-PC groups at 8 h, the CORC-PG, OF-EF and PM-PC groups at 12 h and all the groups at 24 h (**Figure 3.13A, Figure 3.14**).

Microscopy analysis of sectioned aorta rings revealed that only the CORC-PG group was not able to produce micro-vessels and also resulted in media discolouration, indicative of low pH (**Figure 3.13B**).

Micro-vessel quantification (**Figure 3.13C**) revealed that, in comparison to DMEM control, VEGF micro-vessel area was significantly higher ($p < 0.05$) at day 3 and day 5. Further, in comparison to DMEM control, the lowest ($p < 0.05$) micro-vessel area was found in CORC-PG at day 5, whilst the highest ($p < 0.05$) micro-vessel area was observed in PUB-MS and PM-PC groups at day 5.

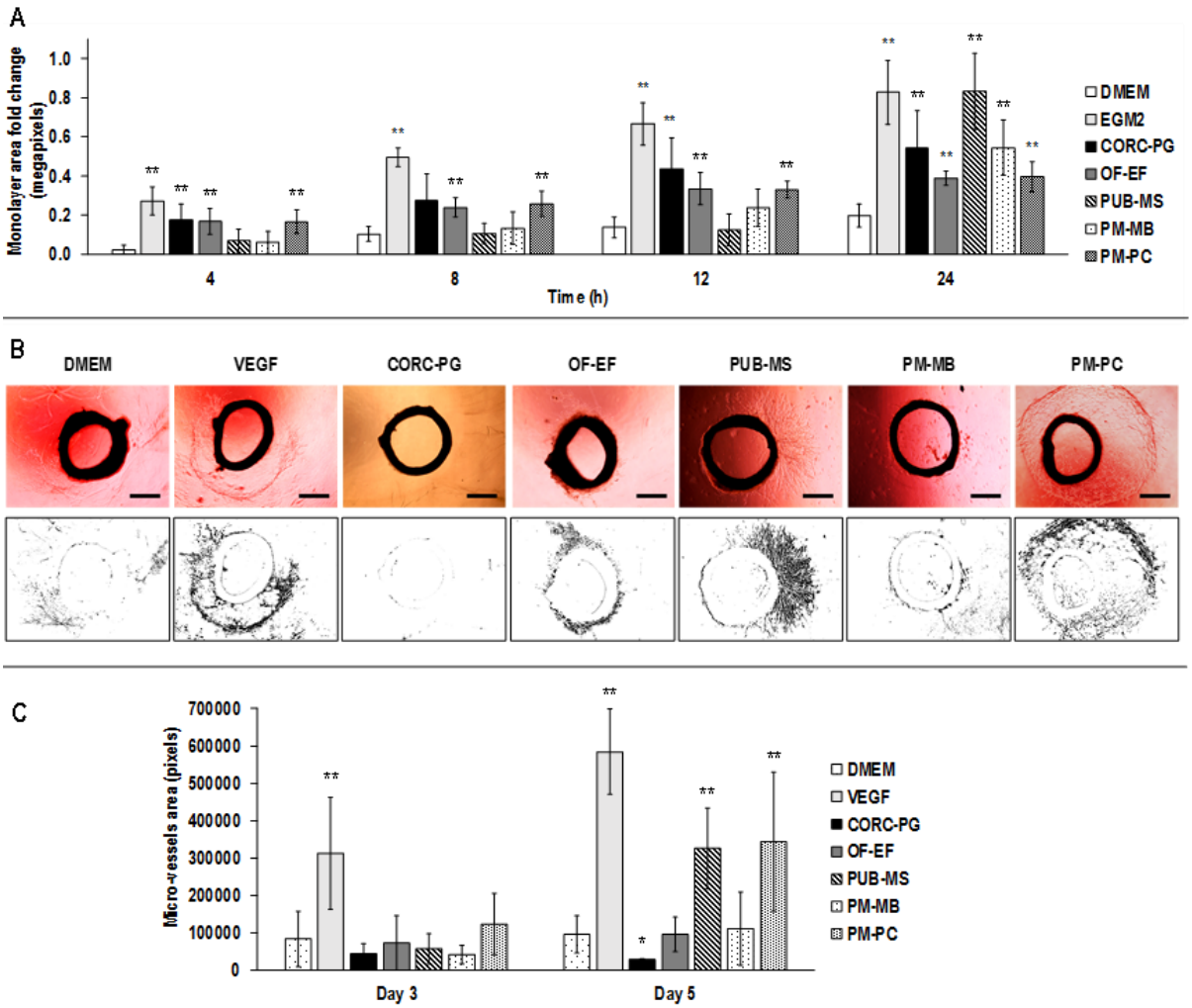

Figure 3.13. HUVECs scratch assay analysis revealed that after 24 h, all groups demonstrated significantly higher (**) monolayer area fold change (**A**). Representative images and binary masks of aortic rings at day 5 showed formation of micro-vessels in all conditions except CORC-PG (**B**). At day 5, the VEGF, PUB-MS and PM-PC showed the highest (**) and the CORC-PG the lowest (*) micro-vessels area quantification (**C**). Scale bars 50 μm. Data are expressed as average ± standard deviation (n=5 for scratch assay, n=3 for aortic ring assay). Statistically significant: $p < 0.05$.

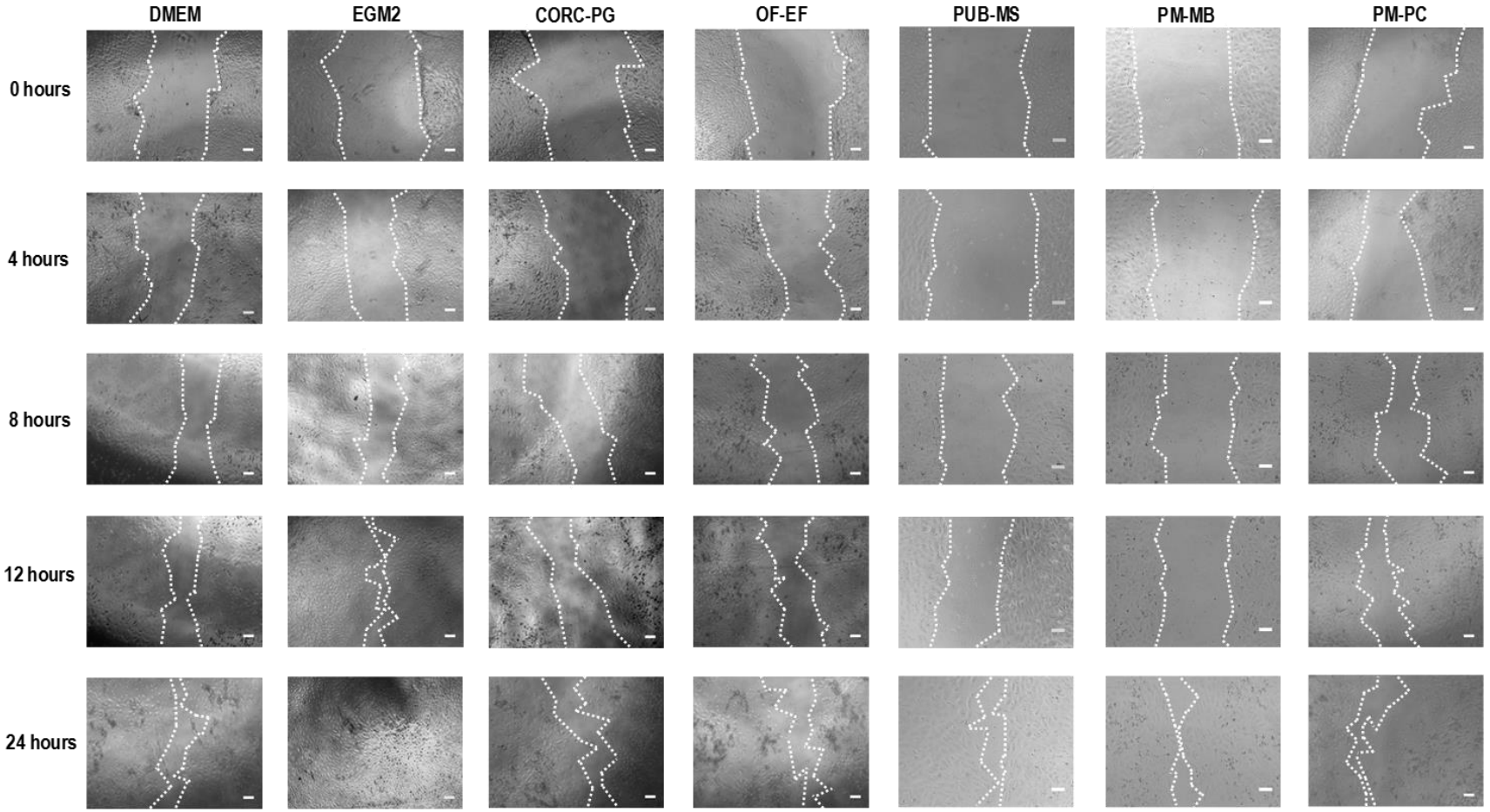

Figure 3.14. Microscopy images of the scratch assay with HUVECs in media conditioned with different materials, where white dashed line indicates the front of cells. Scale bars 100 μm.

3.4. Discussion

Although porcine mesothelium has structural, compositional and biological properties potentially beneficial for wound healing applications [15-17, 21, 22], to-date, it has been used only for breast [13], cartilage [26] and nasal [27] reconstruction and as tendon protector sheet [21]. To assess whether porcine mesothelium grafts are indeed good candidates for wound healing applications, herein, we compared the properties of the only two commercially available decellularised porcine mesothelium xenografts (Meso Biomatrix®; PM-MB and Puracol® Ultra ECM; PM-PC) to traditionally used wound healing xenografts (Endoform™, ovine forestomach; OF-EF and MatriStem®, porcine urinary bladder; PUB-MS) and biomaterials (Promogran™, oxidised regenerated cellulose / collagen; CORC-PG). In addition to the different tissue sources, the tissue grafts used herein were also processed differently, which also impacts on their features and biological response. For instance, OF-EF and PM-PC are processed with detergents and osmotic solutions and are sterilised with ethylene oxide and gamma irradiation, respectively. The PUB-MS is processed with peracetic acid and ethanol and sterilised with electron beam irradiation. The PM-MS is processed using the OPTRIX™ Tissue Process protocol, which gently disinfects tissues, inactivates viruses, removes cells and retains native tissue composition. However, the details of the individual processing conditions remain confidential / trade secret and as such their correlation to their final characteristics is elusive.

SDS-PAGE of acid / pepsin treated materials revealed soluble collagen only in PM-MB, PM-PC and OF-EF materials, whilst hydroxyproline assay revealed that all materials were comprised of collagen. Elastin quantification revealed no elastin in CORC-PG biomaterial, which is not surprising considering that it is produced from extracted collagen, and among the tissue grafts, the OF-EF and the PM-PC had the highest elastin content. The observed differences among the various grafts can be attributed to the different processing [41-43] and cross-linking density, which is species, age and tissue dependent [20, 44-49].

Growth factors such as FGF-basic, VEGF and TGF-β1 can be retained in the ECM after decellularisation [19, 50-52] and are known to promote key events in would healing, such as cell proliferation and migration and angiogenesis [24, 53]. In this study, all three growth factors were detected in the porcine grafts, as has been reported previously [22, 54]. OF-EF also preserved VEGF and TGF-β1, but to a lower extent than the porcine materials. Previous work has shown OF-EF to contain FGF-basic, but in amounts below the background detection of this study [55]. On the other hand, PM-MB contained higher

amounts of TGF-β1 and VEGF than the rest of the materials tested, which could enhance wound healing events *in vivo*. However, high levels TGF-β1 could also trigger fibrosis events [56]. Such differences in growth factor content among the products may be attributed to their diverse range of tissue and/or processing. As expected, growth factors were undetected in CORC-PG biomaterial.

Histology and immunohistochemistry analyses confirmed the maintenance of tissue structure and presence of fundamental components (e.g. collagen type I, collagen type III, fibronectin) in the ECM products, as it has been reported previously [16, 17, 22, 55, 57]. The CORC-PG biomaterial exhibited a loose, sponge-like structure, as it has been described before [58], largely attributed to its lyophilisation manufacturing process. Tissue grafts presented a laminar and fibrous structure, closely imitating the native (pre-processing) tissue structure. Decellularisation protocols and further processing can affect the structure, integrity and composition of tissue grafts [22, 59], which explains the observed differences in tissue preservation, as revealed by histology and immunohistochemistry analyses) among the different tissue graft products. The presence of elastin was much more intense in the PM-PC compared to PM-MB and PUB-MS, matching the colorimetric quantification results, conversely to OF-EF, which staining was expected to be more intense. Such differences could be due to the specificity of the immunohistochemistry antibody between species, considering that the presence of elastin in OF-EF has been previously documented [55]. DAPI staining revealed residual cellular material in OF-EF and PM-MB products, which has been related to immune reactions *in vivo* [60].

MMPs play a crucial role in the wound healing [61] and their modulation is a desirable and characteristic feature of collagen-based biomaterials [62]. CORC-PG showed the highest resistance to MMP-8 degradation; however, the collagen component of this material (55 %) was completely degraded within the first 4 h, indicating that the cellulose component (45 %) was responsible for the resistance to enzymatic degradation and that collagen acted as a sacrificial substrate [63], which would decrease the activity of MMPs in the wound environment [64]. The resistance to porcine pancreatic elastase, which keeps similar substrate specificity with human neutrophil elastase [65], was also assessed. The CORC-PG biomaterial was completely degraded in 2 h, as has been observed in previous studies [63], where CORC-PG acted as substrate for neutrophil elastase, thereby reducing its activity in wound fluid. The tissue grafts showed a proportional resistance to enzymatic degradation; less than 20 % remained after 24 h of MMP-8 incubation and more than 60 % remained after 24 h elastase incubation, both of which can be explained considering

their compositional analysis. Observed differences among them could be attributed to their heterogeneous composition, donor variability and processing. In any case, their higher resistance to proteolytic degradation than collagen-based biomaterials could translate to a slower resorption rate and the need of fewer applications, which would ultimately reduce healthcare costs [3].

Exudates uptake from the wound and maintenance of the appropriate moisture is a desirable characteristic of a wound dressing [66]. The CORC-PG biomaterials swelled the most due to its rather 'simple' (in comparison to the tissue grafts) composition and highly-porous structure (in comparison to the laminar, fibrous and less porous structure of the tissue grafts), as observed in this study by histological analysis and in previous studies with scanning electron microscopy analysis of CORC-PG [58], OF-EF [55], PUB-MS [59, 67], PM-MB [68] and PM-PC [21]. PM-MB exhibited the lowest swelling, probably due to differences in structure, processing and/or crosslinking density [69].

Infection is a major complication in wound healing [70], where ECM products have been shown to be an effective alternative to synthetic materials [10, 71]. In a wound healing scenario, tissue grafts and biomaterials applied on the wound become the only barrier to pathogen penetration into the wound when it is exposed (e.g. during re-application) [72]. We therefore utilised a model to evaluate the potential of these materials as microbial barrier, based on previous studies [38, 39]. It is worth noting that although this *in vitro* model does not recapitulate the *in vivo* bacterial penetration in a wound setting (i.e. higher pathogen concentration, longer exposure time), it can act as an effective screening tool for material selection / screening to proceed to preclinical assessment. As per previous reports [73, 74], in the absence of any antibiotic, none of the tissue grafts inhibited bacterial growth, considering that collagen type IV, fibronectin and laminin have been shown to bind and aggregate bacteria [75]. The CORC-PG presented a slight bacterial inhibition, which has been previously attributed to the oxidized regenerated cellulose component [76]; however, its porous structure allowed immediate bacterial invasion. Among the tissue grafts, the PM-PC showed the lowest bacteria colonisation / penetration capacity, possibly attributed to its denser structure. This is in accordance to previous publications where lower porosity and/or basement membrane preservation have been shown to inhibit bacterial colonisation / penetration [39, 77].

Cytocompatibility analysis with dermal fibroblasts showed that all tissue grafts were capable of supporting cell growth, as has been observed in previous studies [21-23]. Although some statically significant differences were observed between the groups, all exhibited >75 % dermal fibroblast viability, which, in general, is not considered as

biologically significant. The papillae and the basement membrane sides of the grafts showed higher cell growth than the serosa and the connective sides, respectively, largely attributed to higher amounts of collagen type IV, laminin and/or fibronectin that have been shown to promote cellular growth [78-80], albeit with variable degree of cell specificity [81] and attachment and spreading [82]. Cells on CORC-PG showed the lowest proliferation and the highest metabolic activity among the tested samples, which could be due to the fast loss of the collagen and lower cytocompatibility of the oxidised regenerated cellulose. In fact, CORC-PG has previously been shown to support the attachment of 3T3 fibroblasts, but with limited growth [58].

The CORC-PG, the papillae side of OF-EF and the basement membrane side of the PM-MB and PM-PC showed the lowest proliferation and the CORC-PG and papillae side of OF-EF showed the highest metabolic activity at both time points when seeded with THP-1, which could be related to an inflammatory response [21]. However, for all materials the production of TNF-α was far lower from the levels observed in LPS group, which matches previous studies with cellulose scaffolds [83], urinary bladder matrix [57, 84] and porcine mesothelium [21]. Although some elongated cells and cell clusters were observed in some conditions, we cannot conclusively corelate these observations to THP-1 polarisation, as cell morphology of differentiated THP-1 can be influenced by the surface (e.g. topographical features) and bulk (e.g. substrate elasticity) properties of the under investigation scaffolds [85, 86]. However, TNF-α analysis indicated M2 or combined M1/M2 polarisation, as per previous studies of decellularised grafts [57, 84], which could promote remodelling *in vivo*. The higher TNF-α production in the basement membrane side, as opposed to the connective tissue side, of the porcine grafts may be related to their higher laminin and fibronectin content [15, 87-91]. When cells were treated with materials' conditioned media no particular differences were observed, indicating that the effects observed in direct contact are not related to materials' soluble factors and degradation products.

In the scratch test, all materials promoted higher migration than the negative control after 24 h. In the case of CORC-PG, this phenomenon may be due to the solubilisation of the collagenous fraction, which has been shown to promote cell migration of endothelial cells [92, 93]. The observed high migration of the tissue grafts may be attributed to the release of soluble factors that promote angiogenesis, such as FGF-basic, TGF-β1 and VEGF [24, 53]. The aortic ring assay showed only the PUB-MS and PM-PC products to promote micro-vessel formation when compared to DMEM control, whilst the CORC-PG did not allow the formation of micro-vessels. This is in contrast to previous studies, where OF-

EF showed an angiogenic effect on rat aorta rings [40], which may account for batch-to-batch variability or differences in the protocol, since in this study the FBS may have masked the effect on the angiogenesis of OF-EF [94]. Also, despite the higher presence of VEGF and TGF-β1 in PM-MB, the higher total amount and combination of growth factors in PUB-MS and PM-PC could have triggered a higher synergistic effect on the angiogenesis [95]. Nonetheless, these results provide evidence for the angiogenic effect of porcine mesothelium tissues similarly to the porcine urinary bladder that its angiogenic effect has been reported previously [96].

3.5. Conclusion

Xenografts are extensively used in biomedicine due to their abundant availability, structural features, biochemical composition and biological properties. Herein, we demonstrated that porcine mesothelium grafts (e.g. Meso Biomatrix® and Puracol® Ultra ECM / XenoMEM™), although previously not designed for wound healing applications, they have similar or even superior properties to traditionally used wound healing xenografts (e.g. Endoform™ and MatriStem®) and biomaterials (e.g. Promogran™). Considering that there is no widely accepted tissue graft or biomaterial therapy for wound healing applications, this study paves the way for diversification of already clinically available materials, thus reducing the timeframe to bedside.

3.6. References

[1] L.J. Gould, Topical collagen-based biomaterials for chronic wounds: Rationale and clinical application, Adv Wound Care (New Rochelle) 5(1) (2016) 19-31.

[2] E.R. Zielins, D.A. Atashroo, Z.N. Maan, D. Duscher, G.G. Walmsley, M. Hu, K. Senarath-Yapa, A. McArdle, R. Tevlin, T. Wearda, K.J. Paik, C. Duldulao, W.X. Hong, G.C. Gurtner, M.T. Longaker, Wound healing: an update, Regen Med 9(6) (2014) 817-30.

[3] C. Lindholm, R. Searle, Wound management for the 21st century: combining effectiveness and efficiency, Int Wound J 13 Suppl 2(S2) (2016) 5-15.

[4] E.N. Mostow, G.D. Haraway, M. Dalsing, J.P. Hodde, D. King, Effectiveness of an extracellular matrix graft (OASIS Wound Matrix) in the treatment of chronic leg ulcers: A randomized clinical trial, J Vasc Surg 41(5) (2005) 837-843.

[5] M. Martinson, N. Martinson, A comparative analysis of skin substitutes used in the management of diabetic foot ulcers, J Wound Care 25(Sup10) (2016) S8-S17.

[6] M. Romanelli, V. Dini, M. Bertone, S. Barbanera, C. Brilli, OASIS wound matrix versus Hyaloskin in the treatment of difficult-to-heal wounds of mixed arterial/venous aetiology, Int Wound J 4(1) (2007) 3-7.

[7] J. LeCheminant, C. Field, Porcine urinary bladder matrix: a retrospective study and establishment of protocol, J Wound Care 21(10) (2012) 476-482.

[8] B. Burkey, W. Davis, P.M. Glat, Porcine xenograft treatment of superficial partial-thickness burns in paediatric patients, J Wound Care 25(Sup2) (2016) S10-S15.

[9] F. Catena, L. Ansaloni, F. Gazzotti, S. Gagliardi, S. Di Saverio, L. D'Alessandro, A.D. Pinna, Use of porcine dermal collagen graft (Permacol) for hernia repair in contaminated fields, Hernia 11(1) (2007) 57-60.

[10] M.M. Abdelfatah, N. Rostambeigi, E. Podgaetz, M.G. Sarr, Long-term outcomes (>5-year follow-up) with porcine acellular dermal matrix (Permacol™) in incisional hernias at risk for infection, Hernia 19(1) (2015) 135-140.

[11] A. Adeel, B. Tyler, R. Brian, Repair of complete atrioventricular septal defects with decellularized extracellular matrix: Initial and midterm outcomes, World J Pediatr Congenit Heart Surg 8(3) (2017) 310-314.

[12] T.M. Kelley, M. Kashem, H. Wang, J. McCarthy, N.D. Carroll, G.W. Moser, T.S. Guy, Anterior leaflet augmentation with CorMatrix porcine extracellular matrix in twenty-five patients: Unexpected patch failures and histologic analysis, Ann Thorac Surg 103(1) (2017) 114-120.

[13] N.S. Hillberg, P.I. Ferdinandus, R.E.G. Dikmans, B. Winkens, J. Hommes, R.R.W.J. van der Hulst, Is single-stage implant-based breast reconstruction (SSBR) with an acellular matrix safe?: Strattice™ or Meso Biomatrix® in SSBR, Eur J Plast Surg 41(4) (2018) 429-438.

[14] C.A. Salzberg, C. Dunavant, N. Nocera, Immediate breast reconstruction using porcine acellular dermal matrix (Strattice®): Long-term outcomes and complications, J Plast Reconstr Aesthet Surg 66(3) (2013) 323-328.

[15] S.C. Blackburn, M.P. Stanton, Anatomy and physiology of the peritoneum, Semin Pediatr Surg 23(6) (2014) 326-330.

[16] C.A. Witz, I.A. Montoya-Rodriguez, S. Cho, V.E. Centonze, L.F. Bonewald, R.S. Schenken, Composition of the extracellular matrix of the peritoneum, J Soc Gynecol Investig 8(5) (2001) 299-304.

[17] T. Jasna, N. D, L. Z, O. Miljana, B. G, S. Biljana, Histological characteristics of healthy animal peritoneum, Acta Vet Brno 56(5-6) (2006) 405-412.

[18] D.A. Taylor, L.C. Sampaio, Z. Ferdous, A.S. Gobin, L.J. Taite, Decellularized matrices in regenerative medicine, Acta Biomater 74 (2018) 74-89.

[19] A.K. Nowocin, A. Southgate, S.M. Gabe, T. Ansari, Biocompatibility and potential of decellularized porcine small intestine to support cellular attachment and growth, J Tissue Eng Regen Med 10(1) (2016) E23-33.

[20] A. Sorushanova, L.M. Delgado, Z. Wu, N. Shologu, A. Kshirsagar, R. Raghunath, A.M. Mullen, Y. Bayon, A. Pandit, M. Raghunath, D.I. Zeugolis, The collagen suprafamily: From biosynthesis to advanced biomaterial development, Adv Mater (2018).

[21] H. Capella-Monsonís, J. Kelly, S. Kearns, D.I. Zeugolis, Decellularised porcine peritoneum as a tendon protector sheet, Biomed Mater 14(4) (2019) 044102.

[22] D.M. Hoganson, G.E. Owens, E.M. O'Doherty, C.M. Bowley, S.M. Goldman, D.O. Harilal, C.M. Neville, R.T. Kronengold, J.P. Vacanti, Preserved extracellular matrix components and retained biological activity in decellularized porcine mesothelium, Biomaterials 31(27) (2010) 6934-6940.

[23] P.C. Tsai, Z. Zhang, C. Florek, B.B. Michniak-Kohn, Constructing human skin equivalents on porcine acellular peritoneum extracellular matrix for in vitro irritation testing, Tissue Eng Part A 22(1-2) (2016) 111-22.

[24] S. Werner, R. Grose, Regulation of wound healing by growth factors and cytokines, Physiol Rev 83(3) (2003) 835-870.

[25] L.E. Tracy, R.A. Minasian, E.J. Caterson, Extracellular matrix and dermal fibroblast function in the healing wound, Adv Wound Care (New Rochelle) 5(3) (2016) 119-136.

[26] Q. Meng, X. Hu, H. Huang, Z. Liu, L. Yuan, Z. Shao, Y. Jiang, J. Zhang, X. Fu, X. Duan, Y. Ao, Microfracture combined with functional pig peritoneum-derived acellular matrix for cartilage repair in rabbit models, Acta Biomater 53 (2017) 279-292.

[27] A. Bramos, D.P. Perrault, A.N. Fedenko, G.H. Kim, S. Bougioukli, J.R. Lieberman, J.W. Calvert, A.K. Wong, Porcine mesothelium-wrapped diced cartilage grafts for nasal reconstruction, Tissue Eng Part A 24(7-8) (2018) 672-681.

[28] B.A. Liden, B.C. May, Clinical outcomes following the use of ovine forestomach matrix (endoform dermal template) to treat chronic wounds, Adv Skin Wound Care 26(4) (2013) 164-7.

[29] J.S. Kim, A.J. Kaminsky, J.B. Summitt, W.P. Thayer, New innovations for deep partial-thickness burn treatment with ACell MatriStem Matrix, Adv Wound Care (New Rochelle) 5(12) (2016) 546-552.

[30] R.G. Frykberg, S.M. Cazzell, J. Arroyo-Rivera, A. Tallis, A.M. Reyzelman, F. Saba, L. Warren, B.C. Stouch, T.W. Gilbert, Evaluation of tissue engineering products for the management of neuropathic diabetic foot ulcers: an interim analysis, J Wound Care 25(Sup7) (2016) S18-S25.

[31] R. Lobmann, C. Zemlin, M. Motzkau, K. Reschke, H. Lehnert, Expression of matrix metalloproteinases and growth factors in diabetic foot wounds treated with a protease absorbent dressing, J Diabetes Complications 20(5) (2006) 329-335.

[32] A. Veves, P. Sheehan, H.T. Pham, S. For the Promogran Diabetic Foot Ulcer, A randomized, controlled trial of promogran (a collagen/oxidized regenerated cellulose dressing) vs standard treatment in the management of diabetic foot ulcers, Arch Surg 137(7) (2002) 822-827.

[33] O. Ghatnekar, M. Willis, U. Persson, Cost-effectiveness of treating deep diabetic foot ulcers with Promogran in four European countries, J Wound Care 11(2) (2002) 70-74.

[34] D.D. Kakagia, K.J. Kazakos, K.C. Xarchas, M. Karanikas, G.S. Georgiadis, G. Tripsiannis, C. Manolas, Synergistic action of protease-modulating matrix and autologous growth factors in healing of diabetic foot ulcers. A prospective randomized trial, J Diabetes Complications 21(6) (2007) 387-391.

[35] H. Capella-Monsonis, J.Q. Coentro, V. Graceffa, Z. Wu, D.I. Zeugolis, An experimental toolbox for characterization of mammalian collagen type I in biological specimens, Nat Protoc 13(3) (2018) 507-529.

[36] A. Satyam, P. Kumar, X. Fan, A. Gorelov, Y. Rochev, L. Joshi, H. Peinado, D. Lyden, B. Thomas, B. Rodriguez, M. Raghunath, A. Pandit, D. Zeugolis, Macromolecular crowding meets tissue engineering by self-assembly: a paradigm shift in regenerative medicine, Adv Mater 26(19) (2014) 3024-34.

[37] Q. Lu, K. Ganesan, D.T. Simionescu, N.R. Vyavahare, Novel porous aortic elastin and collagen scaffolds for tissue engineering, Biomaterials 25(22) (2004) 5227-5237.

[38] C.H. Woo, Y.C. Choi, J.S. Choi, H.Y. Lee, Y.W. Cho, A bilayer composite composed of TiO2-incorporated electrospun chitosan membrane and human extracellular matrix sheet as a wound dressing, J Biomater Sci Polym Ed 26(13) (2015) 841-854.

[39] S. Yaghobee, N. Samadi, A. Khorsand, R. Ghahroudi Amir Ali, M. Kadkhodazadeh, Comparison of the penetration and passage of Streptococcus mutans and Aggregatibacter actinomycetemcomitans through membranes loaded with tetracycline, amoxicillin, and chlorhexidine: an in vitro study, J Basic Clin Physiol Pharmacol, 2014, p. 87.

[40] S.M. Irvine, J. Cayzer, E.M. Todd, S. Lun, E.W. Floden, L. Negron, J.N. Fisher, S.G. Dempsey, A. Alexander, M.C. Hill, A. O'Rouke, S.P. Gunningham, C. Knight, P.F. Davis, B.R. Ward, B.C.H. May, Quantification of in vitro and in vivo angiogenesis stimulated by ovine forestomach matrix biomaterial, Biomaterials 32(27) (2011) 6351-6361.

[41] K. Schenke-Layland, O. Vasilevski, F. Opitz, K. König, I. Riemann, K.J. Halbhuber, T. Wahlers, U.A. Stock, Impact of decellularization of xenogeneic tissue on extracellular matrix integrity for tissue engineering of heart valves, J Struct Biol 143(3) (2003) 201-208.

[42] L. Partington, N.J. Mordan, C. Mason, J.C. Knowles, H.W. Kim, M.W. Lowdell, M.A. Birchall, I.B. Wall, Biochemical changes caused by decellularization may compromise mechanical integrity of tracheal scaffolds, Acta Biomater 9(2) (2013) 5251-5261.

[43] T.W. Gilbert, T.L. Sellaro, S.F. Badylak, Decellularization of tissues and organs, Biomaterials 27(19) (2006) 3675-3683.

[44] S. Debeer, J.-B. Le Luduec, D. Kaiserlian, P. Laurent, J.-F. Nicolas, B. Dubois, J. Kanitakis, Comparative histology and immunohistochemistry of porcine versus human skin, Eur J Dermatol 23(4) (2013) 456-466.

[45] A. Kurtz, S.-J. Oh, Age related changes of the extracellular matrix and stem cell maintenance, Prev Med 54, Supplement (2012) S50-S56.

[46] Y. Hosoda, K. Kawano, F. Yamasawa, T. Ishii, T. Shibata, S. Inayama, Age-dependent changes of collagen and elastin content in human aorta and pulmonary artery, Angiology 35(10) (1984) 615-621.

[47] D.J. Cannon, P.F. Davison, Aging, and crosslinking in mammalian collagen, Exp Aging Res 3(2) (1977) 87-105.

[48] N. Reddy, R. Reddy, Q. Jiang, Crosslinking biopolymers for biomedical applications, Trends Biotechnol 33(6) (2015) 362-369.

[49] B.D. Walters, J.P. Stegemann, Strategies for directing the structure and function of 3D collagen biomaterials across length scales, Acta Biomater 10(4) (2014) 1488-1501.

[50] W. Erdbrugger, W. Konertz, P.M. Dohmen, S. Posner, H. Ellerbrok, O.E. Brodde, H. Robenek, D. Modersohn, A. Pruss, S. Holinski, M. Stein-Konertz, G. Pauli, Decellularized xenogenic heart valves reveal remodeling and growth potential in vivo, Tissue Eng 12(8) (2006) 2059-68.

[51] J.P. Hodde, D.M.J. Ernst, M.C. Hiles, An investigation of the long-term bioactivity of endogenous growth factor in OASIS Wound Matrix, J Wound Care 14(1) (2005) 23-25.

[52] C.A. McDevitt, G.M. Wildey, R.M. Cutrone, Transforming growth factor-beta1 in a sterilized tissue derived from the pig small intestine submucosa, J Biomed Mater Res A 67(2) (2003) 637-40.

[53] B. Behm, P. Babilas, M. Landthaler, S. Schreml, Cytokines, chemokines and growth factors in wound healing, J Eur Acad Dermatol Venereol 26(7) (2012) 812-820.

[54] S.Y. Chun, G.J. Lim, T.G. Kwon, E.K. Kwak, B.W. Kim, A. Atala, J.J. Yoo, Identification and characterization of bioactive factors in bladder submucosa matrix, Biomaterials 28(29) (2007) 4251-4256.

[55] S. Lun, S.M. Irvine, K.D. Johnson, N.J. Fisher, E.W. Floden, L. Negron, S.G. Dempsey, R.J. McLaughlin, M. Vasudevamurthy, B.R. Ward, B.C.H. May, A functional extracellular matrix biomaterial derived from ovine forestomach, Biomaterials 31(16) (2010) 4517-4529.

[56] J.Q. Coentro, E. Pugliese, G. Hanley, M. Raghunath, D.I. Zeugolis, Current and upcoming therapies to modulate skin scarring and fibrosis, Adv Drug Del Rev (2018).

[57] K. Sadtler, S.D. Sommerfeld, M.T. Wolf, X. Wang, S. Majumdar, L. Chung, D.S. Kelkar, A. Pandey, J.H. Elisseeff, Proteomic composition and immunomodulatory properties of urinary bladder matrix scaffolds in homeostasis and injury, Semin Immunol 29 (2017) 14-23.

[58] J.C. Karr, A.R. Taddei, S. Picchietti, G. Gambellini, A.M. Fausto, F. Giorgi, A morphological and biochemical analysis comparative study of the collagen products Biopad, Promogram, Puracol, and Colactive, Adv Skin Wound Care 24(5) (2011) 208-16.

[59] D.M. Faulk, C.A. Carruthers, H.J. Warner, C.R. Kramer, J.E. Reing, L. Zhang, A. D'Amore, S.F. Badylak, The effect of detergents on the basement membrane complex of a biologic scaffold material, Acta Biomater 10(1) (2014) 183-193.

[60] T.J. Keane, R. Londono, N.J. Turner, S.F. Badylak, Consequences of ineffective decellularization of biologic scaffolds on the host response, Biomaterials 33(6) (2012) 1771-1781.

[61] M.G. Rohani, W.C. Parks, Matrix remodeling by MMPs during wound repair, Matrix Biol 44-46 (2015) 113-121.

[62] S. Chattopadhyay, R.T. Raines, Collagen-based biomaterials for wound healing, Biopolymers 101(8) (2014) 821-833.

[63] B. Cullen, R. Smith, E. McCulloch, D. Silcock, L. Morrison, Mechanism of action of PROMOGRAN, a protease modulating matrix, for the treatment of diabetic foot ulcers, Wound Repair Regen 10(1) (2002) 16-25.

[64] S. Wu, A.J. Applewhite, J. Niezgoda, R. Snyder, J. Shah, B. Cullen, G. Schultz, J. Harrison, R. Hill, M. Howell, M. Speyrer, H. Utra, J. de Leon, W. Lee, T. Treadwell, Oxidized regenerated cellulose/collagen dressings: Review of evidence and recommendations, Adv Skin Wound Care 30(11S Suppl 1) (2017) S1-S18.

[65] W. Bode, E. Meyer, J.C. Powers, Human leukocyte and porcine pancreatic elastase: x-ray crystal structures, mechanism, substrate specificity, and mechanism-based inhibitors, Biochemistry 28(5) (1989) 1951-1963.

[66] H.S. Kim, X. Sun, J.H. Lee, H.W. Kim, X. Fu, K.W. Leong, Advanced drug delivery systems and artificial skin grafts for skin wound healing, Adv Drug Del Rev 146 (2019) 209-239.

[67] M.T. Wolf, S. Ganguly, T.L. Wang, C.W. Anderson, K. Sadtler, R. Narain, C. Cherry, A.J. Parrillo, B.V. Park, G. Wang, F. Pan, S. Sukumar, D.M. Pardoll, J.H. Elisseeff, A biologic scaffold-associated type 2 immune microenvironment inhibits tumor formation and synergizes with checkpoint immunotherapy, Sci Transl Med 11(477) (2019).

[68] M.J. Cronce, R.A. Faulknor, I. Pomerantseva, X.H. Liu, S.M. Goldman, E.C. Ekwueme, O. Mwizerwa, C.M. Neville, C.A. Sundback, In vivo response to decellularized mesothelium scaffolds, J Biomed Mater Res B Appl Biomater 106(2) (2018) 716-725.

[69] L.M. Delgado, K. Fuller, D.I. Zeugolis, Collagen cross-linking: Biophysical, biochemical, and biological response analysis, Tissue Eng Part A 23(19-20) (2017) 1064-1077.

[70] I. Ludolph, F.W. Fried, K. Kneppe, A. Arkudas, M. Schmitz, R.E. Horch, Negative pressure wound treatment with computer-controlled irrigation/instillation decreases bacterial load in contaminated wounds and facilitates wound closure, Int Wound J 15(6) (2018) 978-984.

[71] B. Pérez-Köhler, Y. Bayon, J.M. Bellón, Mesh infection and hernia repair: A review, Surg Infect (Larchmt) 17(2) (2015) 124-137.

[72] E.N. Fahrenbach, C. Qi, O. Ibrahim, J.Y. Kim, M. Alam, Resistance of acellular dermal matrix materials to microbial penetration, JAMA Dermatology 149(5) (2013) 571-575.

[73] Y. Chen, N. Dan, W. Dan, X. Liu, L. Cong, A novel antibacterial acellular porcine dermal matrix cross-linked with oxidized chitosan oligosaccharide and modified by in situ synthesis of silver nanoparticles for wound healing applications, Mater Sci Eng C Mater Biol Appl 94 (2019) 1020-1036.

[74] H.Y. Zhou, J. Zhang, R.L. Yan, Q. Wang, L.Y. Fan, Q. Zhang, W.J. Wang, Z.Q. Hu, Improving the antibacterial property of porcine small intestinal submucosa by nano-silver supplementation: A promising biological material to address the need for contaminated defect repair, Ann Surg 253(5) (2011) 1033-1041.

[75] G. Vercellotti, J. McCarthy, P. Lindholm, P. Peterson, H. Jacob, L. Furcht, Extracellular matrix proteins (fibronectin, laminin, and type IV collagen) bind and aggregate bacteria, Am J Pathol 120(1) (1985) 13-21.

[76] J. Vytrasova, A. Tylsova, I. Brozkova, L. Cervenka, M. Pejchalova, P. Havelka, Antimicrobial effect of oxidized cellulose salts, J Ind Microbiol Biotechnol 35(11) (2008) 1247.

[77] L. Steukers, S. Glorieux, A.P. Vandekerckhove, H.W. Favoreel, H.J. Nauwynck, Diverse microbial interactions with the basement membrane barrier, Trends Microbiol 20(3) (2012) 147-155.

[78] V.S. LeBleu, B. MacDonald, R. Kalluri, Structure and function of basement membranes, Exp Biol Med 232(9) (2007) 1121-1129.

[79] D. Olivero, L. Furcht, Type IV collagen, laminin, and fibronectin promote the adhesion and migration of rabbit lens epithelial cells in vitro, Invest Ophthalmol Vis Sci 34(10) (1993) 2825-2834.

[80] D. Woodley, K. Wynn, E. O'Keefe, Type IV collagen and fibronectin enhance human keratinocyte thymidine incorporation and spreading in the absence of soluble growth factors, J Invest Dermatol 94(1) (1990) 139-143.

[81] M. Kubo, M. Kan, M. Isemura, I. Yamane, H. Tagami, Effects of extracellular matrices on human keratinocyte adhesion and growth and on its secretion and deposition of fibronectin in culture, J Invest Dermatol 88(5) (1987) 594-601.

[82] D. Bissell, S. Stamatoglou, M. Nermut, R. Hughes, Interactions of rat hepatocytes with type IV collagen, fibronectin and laminin matrices. Distinct matrix-controlled modes of attachment and spreading, Eur J Cell Biol 40(1) (1986) 72-78.

[83] A. Svensson, E. Nicklasson, T. Harrah, B. Panilaitis, D.L. Kaplan, M. Brittberg, P. Gatenholm, Bacterial cellulose as a potential scaffold for tissue engineering of cartilage, Biomaterials 26(4) (2005) 419-431.

[84] L. Huleihel, J.L. Dziki, J.G. Bartolacci, T. Rausch, M.E. Scarritt, M.C. Cramer, T. Vorobyov, S.T. LoPresti, I.T. Swineheart, L.J. White, B.N. Brown, S.F. Badylak, Macrophage phenotype in response to ECM bioscaffolds, Semin Immunol 29 (2017) 2-13.

[85] R. Sridharan, B. Cavanagh, A.R. Cameron, D.J. Kelly, F.J. O'Brien, Material stiffness influences the polarization state, function and migration mode of macrophages, Acta Biomater 89 (2019) 47-59.

[86] J.E. Rayahin, R.A. Gemeinhart, Activation of macrophages in response to biomaterials, in: M. Kloc (Ed.), Macrophages: Origin, Functions and Biointervention, Springer International Publishing, Cham, 2017, pp. 317-351.

[87] T. Huard, H. Malinoff, M. Wicha, Macrophages express a plasma membrane receptor for basement membrane laminin, Am J Pathol 123(2) (1986) 365-370.

[88] J. Chen, J. Cárcamo, O. Bórquez-Ojeda, H. Erdjument-Bromage, P. Tempst, D. Golde, The laminin receptor modulates granulocyte-macrophage colony-stimulating factor receptor complex formation and modulates its signaling, Proc Natl Acad Sci U S A 100(24) (2003) 14000-14005.

[89] K. Ohki, O. Kohashi, Laminin promotes proliferation of bone marrow-derived macrophages and macrophage cell lines, Cell Struct Funct 19(2) (1994) 63-71.

[90] G. Digiacomo, I. Tusa, M. Bacci, M. Cipolleschi, P. Dello Sbarba, E. Rovida, Fibronectin induces macrophage migration through a SFK-FAK/CSF-1R pathway, Cell Adh Migr 11(4) (2017) 327-337.

[91] H. Abdolghafoorian, P. Farnia, R.S. Sajadi Nia, A. Bahrami, A. Dorudinia, J. Ghanavi, Effect of heart valve decellularization on xenograft rejection, Exp Clin Transplant (2016).

[92] M. Sgarioto, P. Vigneron, J. Patterson, F. Malherbe, M.-D. Nagel, C. Egles, Collagen type I together with fibronectin provide a better support for endothelialization, C R Biol 335(8) (2012) 520-528.

[93] P.A. Underwood, F.A. Bennett, The effect of extracellular matrix molecules on the in vitro behavior of bovine endothelial cells, Exp Cell Res 205(2) (1993) 311-319.

[94] I. Kimura, S. Yanagita, S. Kobayshi, M. Fukuta, M. Okabe, Vascular endothelial growth factor-and platelet-derived growth factor-angiogenesis depressed but fetal bovine serum-angiogenesis enhanced choroidal tissue cultures of, Int Angiol 19(1) (2000) 26.

[95] R. Castellon, H.K. Hamdi, I. Sacerio, A.M. Aoki, M. Cristina Kenney, A.V. Ljubimov, Effects of angiogenic growth factor combinations on retinal endothelial cells, Exp Eye Res 74(4) (2002) 523-535.

[96] E.K. Akpek, M. Alkharashi, F.S. Hwang, S.M. Ng, K. Lindsley, Artificial corneas versus donor corneas for repeat corneal transplants, Cochrane Database of Systematic Reviews 11 (2014) CD009561-CD009561.

Chapter 4

Decellularised porcine peritoneum biomaterial as adipose derived stem cell delivery vehicle in wound healing

Part of this chapter has been published:

Capella-Monsonís, H., De Pieri, A., Peixoto, R., Korntner, S. & Zeugolis D.I. (2020) *Extracellular matrix-based biomaterials as adipose derived stem cell delivery vehicles in wound healing: A comparative study between a collagen scaffold and two xenografts*. **Stem Cell Research & Therapy**, 11, 510

4.1. Introduction

Stem cell-based therapies emerged as the pinnacle of regenerative medicine and as the most promising therapeutic solution to a broad spectrum of injuries and degenerative conditions. With global revenue of over US$1 billion per annum, thousands of products on the market and many more at advanced phases of clinical trials and industrial pipeline (1), the therapeutic application of stem cells in regenerative medicine in undeniable. Despite the high prospects and considerable advances of stem cell-based therapies, many limitations still need to be addressed for their efficient use in clinic, including poor cell engraftment at the implantation side and the large number of cells required for therapeutic effect (2).

Biomaterials, by providing stem cell anchoring sites, can be employed as stem cell carriers to maximise their retention at the side of implantation. The ideal stem cell biomaterial carrier must be cytocompatible, provide mechanical support, ensure cell function after transplantation, promote autologous cell infiltration and be resorbable. In the quest of the ideal stem cell biomaterial carrier, extracellular matrix (ECM)-based biomaterials (e.g. extracted collagen scaffolds and decellularised tissue grafts) are favoured due to their inherent cytocompatibility, low immunogenicity and tunable mechanical properties. In particular, decellularised tissue grafts hold great promise, largely attributed to the multifunctional composition of their preserved ECM that no man-made device will ever match. Unfortunately, the ideal tissue graft for soft tissue repair and regeneration remains elusive, considering their scattered clinical outcomes (e.g. Permacol™ in hernia repair (3, 4), CorMatrix® in paediatric cardiovascular surgery (5, 6) and Strattice® in breast reconstruction (7, 8) have shown both positive and negative results).

Appropriately decellularised and processed porcine peritoneum contains a broad range of ECM molecules (e.g. collagen type I, collagen type III, collagen type IV, fibronectin, elastin, laminin) and growth factors [e.g. vascular endothelial growth factor (VEGF), fibroblast growth factor 2 (FGF-2)] (9-12), which are well-known stem cell function regulators (e.g. promote stem cell adhesion, proliferation, migration and differentiation) (13, 14) and wound healing promoters (e.g. promote cell proliferation and angiogenesis *in vivo*) (15, 16). Further, it has a well-established high cytocompatibility and low immunogenicity *in vitro* (17, 18) and high cell proliferation and low immune response *in vivo* (19). Despite all these positive attributes, porcine peritoneum has neither been assessed in wound healing context nor as a stem cell carrier.

Herein, we ventured to assess the potential of decellularised porcine peritoneum (XenoMEM™; alone and) as a human adipose derived stem cell carrier in a splinted nude mouse wound healing model, investigating also the effect that its components (connective tissue and basement membrane layers) may have on this application. As controls (in addition to sham and cells alone), we used a commercially available, also bilayer, decellularised porcine urinary bladder graft (MatriStem™) and a collagen / glycosaminoglycan (GAG) scaffold (Integra™ Matrix Wound Dressing; both alone and with cells), as they have an established clinical history even in challenging wound healing incidents (e.g. burn treatment: MatriStem™ (20), Integra™ Matrix Wound Dressing (21)).

4.2. Materials and methods

Conditions, study design and experimental procedure are summarised in **Figure 4.1**.

4.2.1. Materials

The decellularised porcine peritoneum (XenoMEM™) was provided by Viscus Biologics LLC (USA) in freeze-dried state. The decellularised porcine urinary bladder (MatriStem™) was purchased from ACell® (USA) in a freeze-dried state. The collagen / GAG scaffold (Integra™ Matrix Wound Dressing) was purchased from Integra Life Sciences Corporation (USA) in wet state in phosphate buffered saline (PBS). Human adipose derived stem cells were purchased from Lonza (UK). All chemical and consumables were purchased from Sigma-Aldrich (Ireland), unless otherwise stated.

4.2.2. *In vitro* cytocompatibility assessment

Human adipose derived stem cells (hADSC, PT-5006, Lonza, UK) were expanded in alpha-Minimal Essential Medium (α-MEM) GlutaMAX™ medium (Gibco, Ireland) supplemented with 10 % foetal bovine serum (FBS), 1 % penicillin / streptomycin (P / S) and 5 ng/ml FGF-2 (PromoCell, Ireland) at 5 % CO_2 and 37 ºC. Cells were used to passage 5 for all *in vitro* experiments and were seeded on the materials following standard protocols. Briefly, materials were cut in 1 cm^2 pieces, placed at the bottom of 24-well plates and fixed with silicone O-rings to prevent their floating. Materials were then sterilised with 70 % ethanol for 30 min and washed with PBS 3 times. ADSC were seeded on the Integra™ scaffolds and on both connective tissue (CT) and basement membrane (BM) sides of MatriStem™ and XenoMEM™ at a density of 25,000 cells / cm^2 in α-MEM with 10 % FBS and 1 % P / S and incubated at 5 % CO_2 and 37 ºC for 3, 7 and 14

days, replacing the media every 3 days and using tissue culture plastic (TCP) as control. At each time point, cell viability and metabolic activity were assessed employing LIVE/DEAD® (ThermoFisher, Ireland) and alamarBlue® (ThermoFisher, Ireland) assays, respectively, as per manufacturer's protocols. Proliferation and morphology were assessed by fixation of the cells with 4 % paraformaldehyde (PFA) for 20 min at room temperature and subsequent staining of the cytoskeleton with 1:500 rhodamine-phalloidin (Life Technologies, Ireland) for 1 h and of the nuclei with 1:2000 Hoechst (Invitrogen, Ireland) for 5 min. Images of the stained cells were taken using an inverted fluorescence microscope (IX81, Olympus, UK) and nuclei were counted with ImageJ (NIH, USA) to quantify the proliferation of cells on the materials and TCP.

4.2.3. Flow cytometry analysis

hADSCs were seeded at 25,000 cells / cm^2 density on TCP, on the Integra™ scaffold and on both sides of the MatriStem™ and the XenoMEM™ as described above and cultured for 14 and 21 days in α-MEM with 10 % FBS and 1 % P / S at 5 % CO_2 and 37 ºC, replacing the media every 3 days. At each time point, cells were detached with 0.25% trypsin / ethylenediaminetetraacetic acid (EDTA) solution, filtered through a 40 μm cell strainer (ThermoFisher, Ireland), centrifuged at 300 g for 5 min, resuspended at 10^6 cells / ml with 2 % FBS and 0.05 % sodium azide in PBS and kept on ice. 100 μl of each cell suspension (~10^5 cells) were incubated with fluorescence labelled antibodies for the mesenchymal stem cells markers $CD90^+$, $CD73^+$, $CD44^+$ (respective product codes: 51-9007657, 51-9007649, 51-9007656, BD Bioscience, Ireland) and $CD45^-$ (product code: 46-0459-41, ThermoFisher, Ireland) and their correspondent isotype controls ($CD90^+$, $CD73^+$, $CD44^+$ isotype cocktails, product codes: 51-9007664, 51-9007655 , BD Bioscience, Ireland; $CD45^-$ isotype, product code: 46-4714-80, ThermoFisher, Ireland) for 30 min at 4 ºC in dark. The cell suspensions were then centrifuged at 300 g for 5 min, washed in 2 ml of 2 % FBS and 0.05 % sodium azide solution and centrifuged as above. The supernatants were discarded by decantation and the cell pellets were resuspended in the remaining FBS and sodium azide solution with a vortex, and 5 μl of Sytox™ Blue (ThermoFisher, Ireland) were added to stain dead cells. Cell suspensions were then analysed using a BD FACS Canto™ II flow cytometer (BD Biosciences, Ireland). Analysis was carried out until 10,000 counts were reached and data were processed with the software FlowJo™ v10 (FlowJo™ LLC, USA).

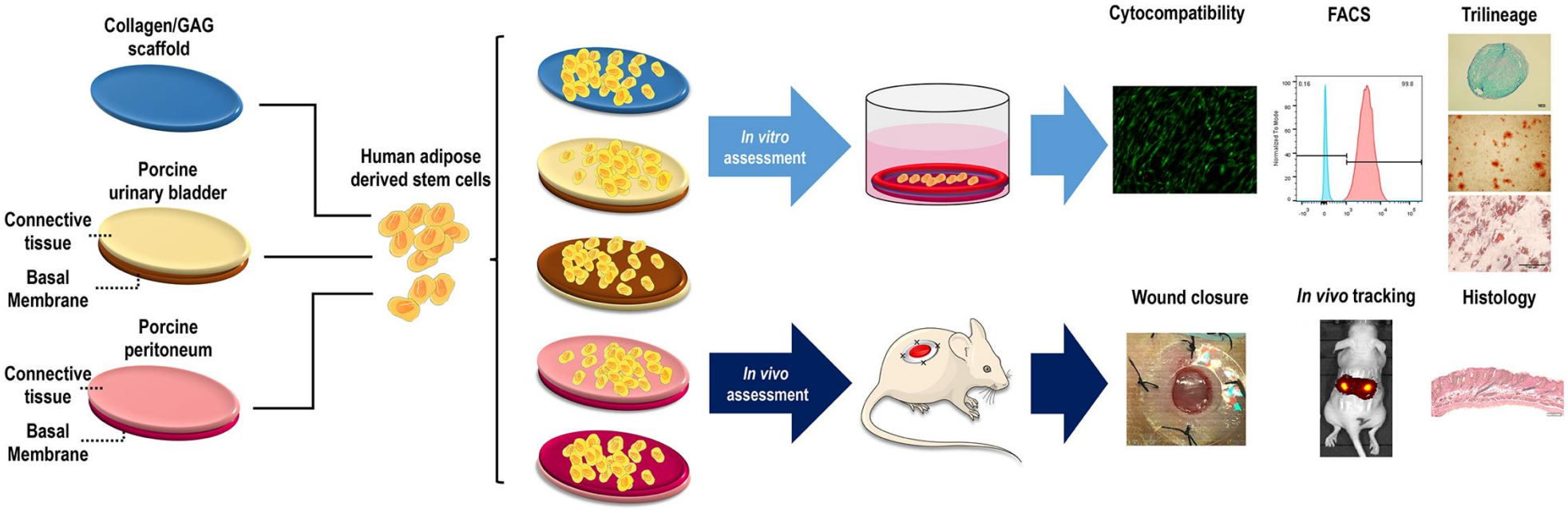

Figure 4.1. Study design graphical abstract. Comparative analysis of a collagen scaffold (Integra™ Matrix Wound Dressing) and two tissue grafts [decellularised porcine peritoneum (XenoMEM™) and porcine urinary bladder (MatriStem™)] as human adipose derived stem cells carriers.

4.2.4. Trilineage differentiation analysis

For trilineage differentiation, 25,000 hADSCs per cm^2 were seeded on TCP, on the Integra™ scaffold and on both sides of the MatriStem™ and the XenoMEM™ as described above and were incubated at 5 % CO_2 and 37 ºC in α-MEM with 10 % FBS and 1 % P / S for 3 days. Osteogenic, adipogenic and chondrogenic differentiations were conducted following established protocols.

For osteogenic differentiation, cells on TCP and on the different materials were treated with α-MEM supplemented with 10 % FBS, 1 % P / S, 100 nM dexamethasone, 50 μM ascorbic acid 2-phospate and 10 mM β-glycerophosphate disodium salt hydrate. The osteogenic media were replaced every 3 days. At days 7, 14 and 21, cells on TCP and the different materials were washed with PBS, treated with 0.5 M HCl and disrupted by scratching with a pipette tip. The solution was then collected, incubated overnight at 4 ºC under agitation, centrifuged at 500 g to discard cell debris and the calcium of the supernatant was quantified with a calcium colorimetric assay (MAK022, Sigma-Aldrich, Ireland). Treated cells on TCP were also stained with 2 % alizarin red solution after fixation with methanol as positive control of differentiation and images were taken with an inverted microscope (CKX41, Olympus, UK).

For adipogenic differentiation, cells on TCP and on the different materials were treated for 3 days with adipogenic induction media (Dulbecco's Modified Eagle Medium, DMEM, high-glucose supplemented with 10 % FBS, 1 % P / S, 1 μM dexamethasone, 1 μM rosiglitazone, 0.5 mM 3-isobutyl-1-methyl-xanthine, 10 μg/ml insulin) and for 3 subsequent days with adipogenic maintenance media (10 % FBS, 1 % P / S, 10 μg/ml insulin) in repeating cycles for 7, 14 and 21 days. At each time point, cells were washed in PBS and fixed with 4 % PFA. All conditions were stained with oil red O staining solution for 5 min, washed with 60 % propanol and washed 3 times with distilled water. Images of the stained cells on TCP were taken with an inverted microscope (CKX41, Olympus, UK); as quality control of differentiation. 99 % propanol was poured on the samples to extract the oil red O stain, the solution was transferred to Eppendorf tubes and centrifuged at 500 g for 5 min to remove cell debris. Optical density (OD) at 520 nm was read to measure the quantity of released stain in the solution. Blanks with only materials were run to subtract any noise signal.

For chondrogenic differentiation, cells on TCP and on the different materials were treated with chondrogenic media [DMEM high glucose supplemented with 1 % P / S, 100 nM dexamethasone, 1x ITS+1 liquid media supplement (insulin, transferrin, sodium selenite, linoleic-bovine serum albumin), 40 μg/ml L-proline, 50 μg/ml ascorbic acid 2-phosphate

and 10 ng/ml transforming growth factor β3 (TGF-β3, R&D Systems, UK)] for 7, 14 and 21 days, changing the media every 3 days. To form pellets, 5 x 10^5 cells were suspended in chondrogenic media, centrifuged at 300 g for 5 min and incubated as the rest of conditions. At each time points, sulphated glycosaminoglycans (GAGs) where quantified using a colorimetric kit (Blyscan™, Biocolor, UK) as per manufacturer's protocol. Pellets at 7, 14 and 21 days were fixed with 4 % PFA for 1 h at 4 ºC and incubated in 15 % and 30 % sucrose for 1 h in each solution at 4 ºC under mild agitation. The pellets were then embedded in OCT™ compound (Tissue-Tek®, Sakura®, The Netherlands), snap-frozen and cryosectioned (CM1850 Cryostat, Leica BioSystems, UK). Cryosections (~ 7 μm in thickness) were stained with Alcian Blue and Nuclear Fast Red solution and imaged with inverted microscope (CKX41, Olympus, UK).

4.2.5. *In vivo* stem cell delivery in a splinted wound model

Animal studies were carried out under approval of the Animal Care Research Ethics Committee of the NUI Galway (Approval number 15/DEC/07). A well-established in the literature splinted nude mouse wound healing model for cell transplantation was used (22-24). In brief, 50-60 days old athymic mice were anaesthetised with isoflurane, the skin of the dorsal area was disinfected with iodine and two full thickness wounds of 5 mm in diameter were created using a punch biopsy. Silicone splints of 6 mm internal diameter and 12 mm external diameter were fixed around each wound with superglue and secured to the skin with 6-0 nylon suture stiches (Ethicon, Ireland) to prevent skin contraction. Animals (n=6 for each group) were randomly assigned to one treatment in both wounds as follows: no treatment control (sham), topical application of 10^6 hADSC in 50 μl of PBS, each one of the materials alone (in tissue grafts, both the CT and the BM were placed facing the exterior of the wound) and each of the materials loaded with hADSCs (in tissue grafts, both the CT and the BM were loaded with cells and placed facing the exterior of the wound). All materials were applied as discs of 5 mm in diameter in wet state. As the tissue grafts were provided in freeze-dried state, they were incubated in sterile PBS for 30 min at room temperature prior to application. hADSCs were seeded on the materials 24 h before implantation at a density of 2.6 x 10^6 cells / cm^2 and, at the surgery, 5 mm in diameter pieces were carrying approximately 5 x 10^5 cells. Cell-loaded materials were applied to the wounds with the cell-loaded side facing the exterior of the wound. In both cells alone and cell-loaded materials groups, cells were stained with fluorescent solution (Vybrant™ DiD, ThermoFisher, Ireland) for 20 min at 37 ºC prior to implantation or seeding, respectively, for their fluorescent tracking *in vivo* (25). After application of the

treatment, wounds were protected with the securement dressing Tegaderm™ (3M, USA) and a cast was applied for the full duration of the study.

4.2.6. *In vivo* cell tracking

At days 3, 7, 10 and 14, animals treated with cells were anaesthetised with isoflurane and fluorescent tracking of the cells was carried out using an *in vivo* imaging system (IVIS® Lumina III, PerkinElmer, UK). The Living Image® software (IVIS® Lumina, PerkinElmer, UK) was used to calculate the intensity of the fluorescence of labelled cells at the wound areas.

4.2.7. Wound closure rate analysis

Animals were anaesthetised with isoflurane and pictures of the wounds were taken at days 3, 7, 10 and 14 with an iPad Pro (Apple, USA). Images were analysed and wound area was accurately calculated using the WoundWiseIQ (Med-Compliance IQ Inc, USA) software. The wound closure rate was calculated using the following equation: % Wound closure = [(Day 0 wound area – Day X wound area) / Day 0 wound area] x 100.

4.2.8. Histology analysis

At day 14, animals were euthanised by CO_2 overdose and tissue samples were harvested with an 8 mm biopsy punch and fixed in 4 % PFA for 24 h at 4 ºC. Cross-sections of 5 μm in thickness were prepared from paraffin blocks after processing of the tissue in a tissue processor (Excelsior AS, ThermoFisher, Ireland). The sections were deparaffinised in xylene and hydrated in descending concentrations of ethanol. Slides were stained using standard protocols for haematoxylin-eosin, Masson's Goldner trichrome and picrosirius red. The sections were then dehydrated in ascending solutions of ethanol and xylene and mounted on DPX mounting medium. Images were captured with an Olympus VS120 digital scanner using the OlyVIA software (both Olympus Corporation, UK). For picrosirius red, an Olympus BX51-microscope (Olympus, UK) was used equipped with a circular light polariser (Olympus, UK) to obtain polarised-light images.

Masson's trichrome and haematoxylin/eosin images were used to calculate the wound gap, scar index and epidermal thickness. Briefly, 4 non-consecutive sections with a separation of 2 sections between them were used per sample to analyse the wound gap with ImageJ (NIH, USA) software using the line tool and measuring its length. Scar index was calculated in 4 non-consecutive sections with a separation of 2 sections between them; the scar tissue was outlined using the polygonal outline tool in ImageJ (NIH, USA)

and the area was then measured. Dermal thickness was estimated by drawing a line to the skin orientation and measuring its length; 4 dermal thickness values were obtained per image in 4 non-consecutive sections, with a separation of 2 sections between them. The scar index was calculated by dividing the wound area between the average dermal thickness. The thickness of neo-formed epidermis was evaluated using ImageJ line tool (NIH, USA); 3 high-power fields per sample and 5 measurements of the epidermal thickness per field were obtained.

Picrosirius red images in 4 non-consecutive sections, with a separation of 2 sections between them were used to measure total collagen and mature collagen deposition. Briefly, bright field images were used to calculate the section area with ImageJ (NIH, USA) and total collagen was calculated by measuring the area of polarised images after applying the correspondent threshold. Using the channel split tool of ImageJ (NIH, USA), the area of the red channel, related to deposited mature collagen, was normalised to the correspondent total deposited collagen; 3 sections were analysed per sample.

4.2.9. Immunohistochemistry analysis

Immunohistochemistry of paraffin embedded sections was carried out to assess the formation of blood vessels and the presence of hADSCs in the wound area. Briefly, sections were processed through heat antigen retrieval with citrate buffer at pH 6.5 in a pressure cooker for 3 min after dewaxing in xylene and re-hydration in descending ethanol solutions. For angiogenesis assessment, sections were incubated in blocking buffer, consisting of PBS with 5 % of normal goal serum and 0.01 % of Triton X-100, for 1 h at room temperature. After 3 washes in PBS, samples were incubated with rabbit anti-CD31 antibody (ab28364, Abcam, UK) for 30 min at room temperature at a 1:50 dilution in blocking buffer. After further 3 washes with PBS, sections were incubated with an Alexa Fluor 488 goat anti-rabbit antibody (A11008, ThermoFisher, Ireland) in blocking buffer at 1:200 dilution for 1 h at room temperature, washed 3 more times in PBS and mounted with ProLong™ Gold antifade mountant with DAPI (ThermoFisher, Ireland). Images of the sections were taken with an inverted fluorescence microscope (IX81, Olympus, UK) and analysed with ImageJ (NIH, USA) by counting the cells and measuring the area of formed blood vessels, which were normalised to the section area.

4.2.10. Statistical analysis

Data were analysed using the IBM SPSS Statistics (IBM Analytics, USA) software. One-way analysis of variance (ANOVA), followed by Fisher's post-hoc test, was employed

after confirming normal distribution (Kolmogorov-Smirnov normality test) and equality of variances (Levine's test for homogeneity of variance). For non-normal distributions or different variance, Mann-Whitney U test and Kruskal-Wallis test were employed. Significant difference was accepted at $p < 0.05$.

4.3. Results

4.3.1. Cytocompatibility analysis

Qualitative cell morphology, proliferation (**Figure 4.2**) and viability (**Figure 4.3**) analyses revealed that hADSCs attached, spread and proliferated in higher rates on either side of both tissue grafts than on TCP and the Integra™ scaffold. Quantitative proliferation analysis (**Figure 4.4A**) revealed that, in comparison to the control TCP, the Integra™ scaffold induced the lowest ($p < 0.01$) hADSCs proliferation at day 7 and day 14, whilst the highest ($p < 0.05$) hADSC proliferation was induced on both sides of MatriStem™ at day 3, on the BM sides of both tissue grafts at day 7 and on the BM side of MatriStem™ and both sides of XenoMEM™ at day 14. hADSCs metabolic activity analysis (**Figure 4.4B**) revealed no significant ($p > 0.05$) differences between the groups at day 3 and day 7 and at day 14, the Integra™ scaffold induced the highest ($p < 0.05$) metabolic activity among all groups, whilst no significant ($p > 0.05$) differences were observed between the TCP and either side of both tissue grafts and between the tissue grafts. hADSCs viability analysis (**Figure 4.4C**) revealed no significant ($p > 0.05$) differences between the groups at any timepoint.

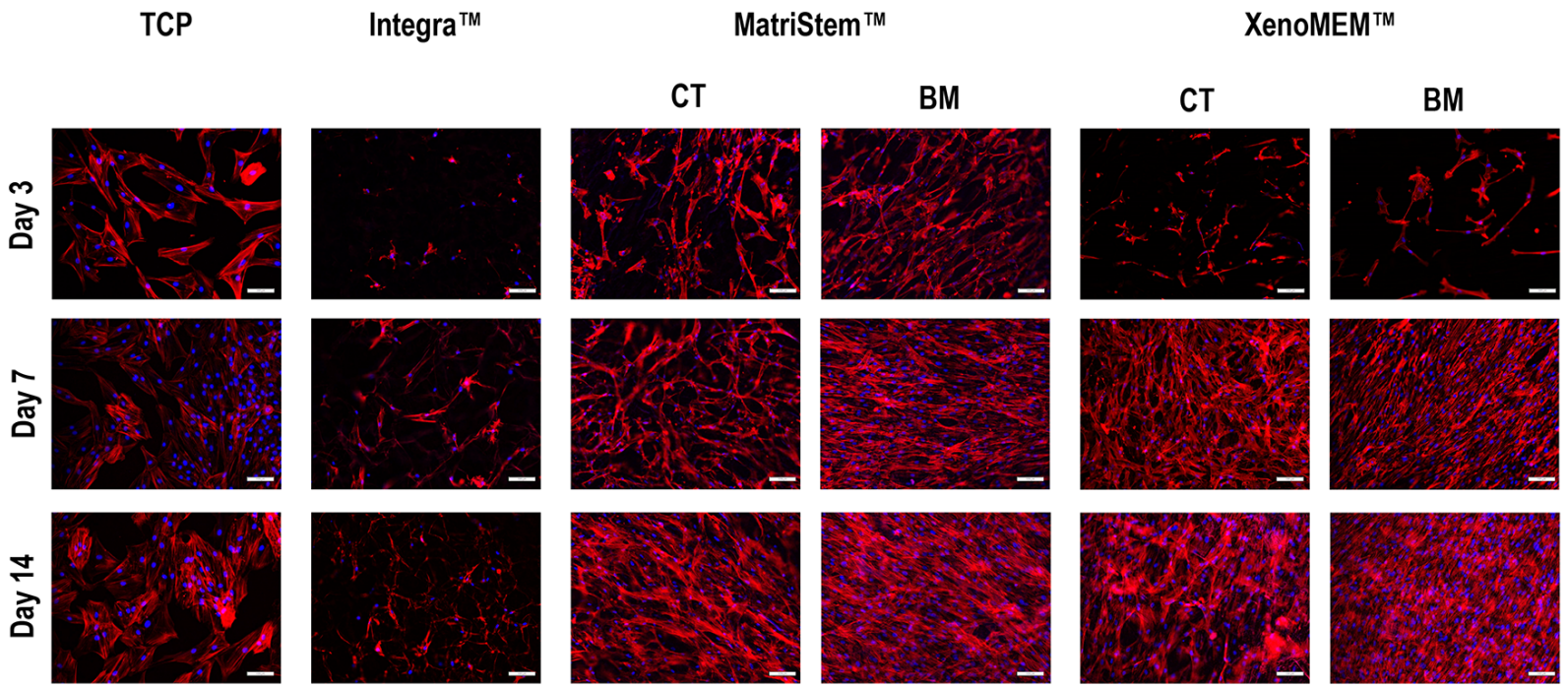

Figure 4.2. Cytoskeleton (red) and nuclei (blue) staining of human ADSCs showed the lower proliferation of cells on Integra™ Matrix Wound Dressing, whilst on the tissue grafts it appeared to be higher, particularly on their BM sides. Scale bars 100 μm.

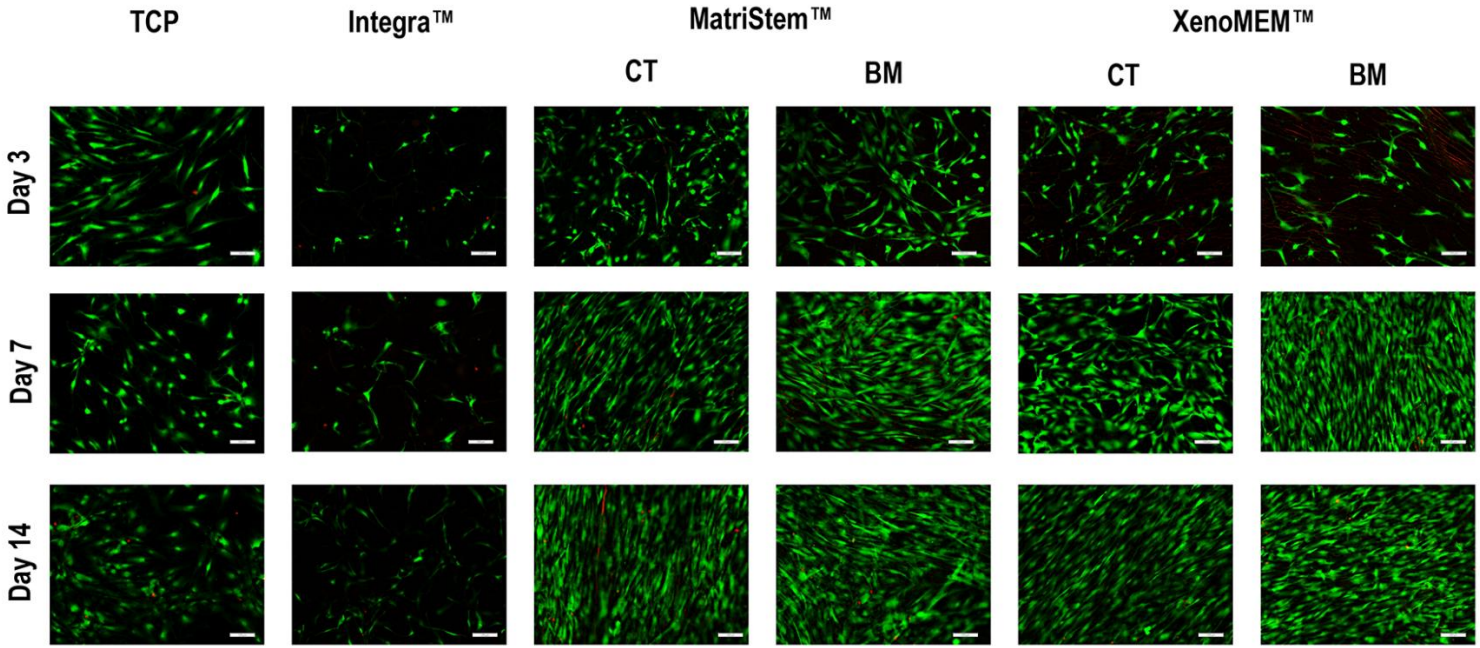

Figure 4.3. Calcein (green) and ethidium homodimer (red) staining of alive and dead cells, respectively, revealed human ADSCs viability to be unaffected in any of the conditions and time points. Scale bars 100 μm.

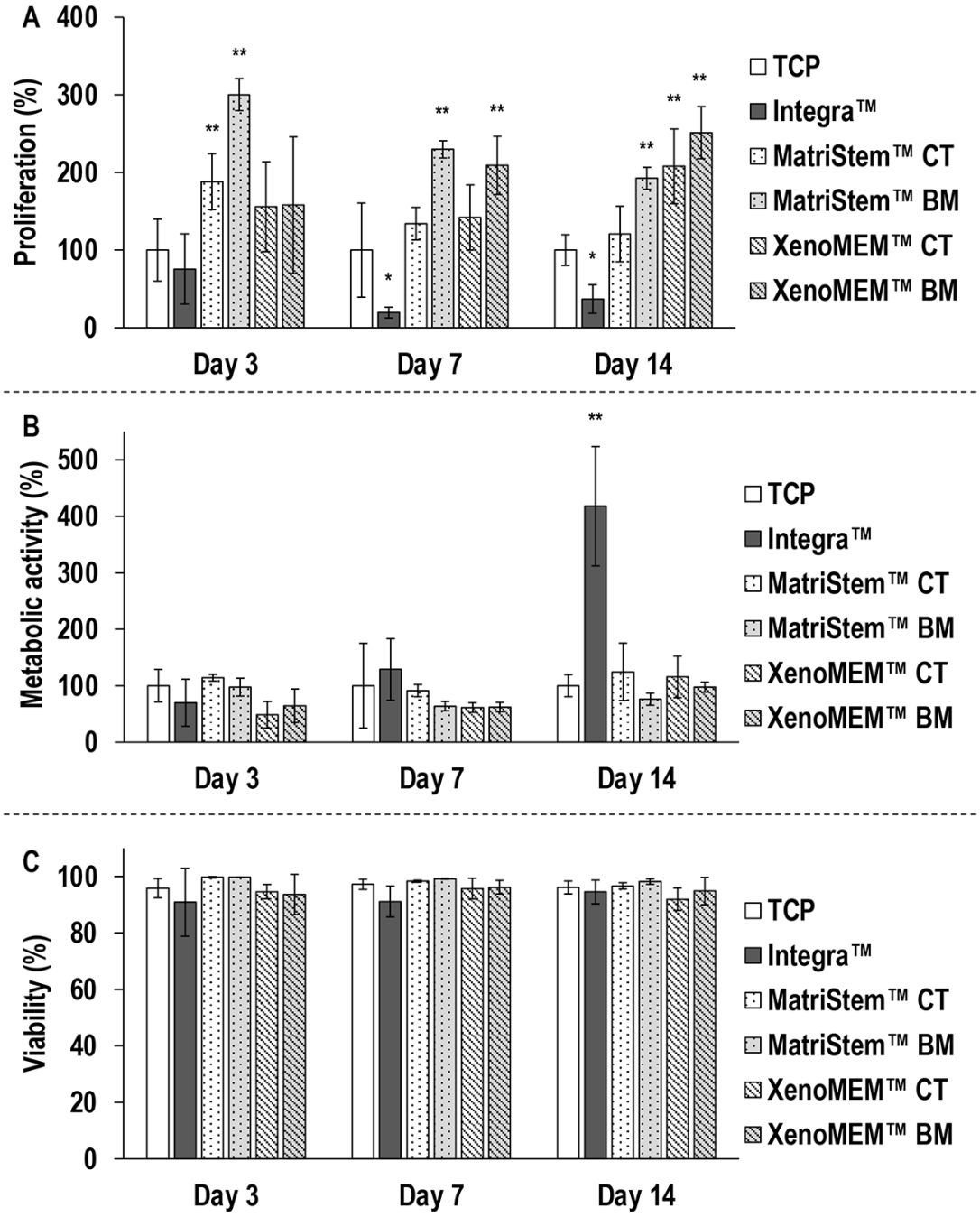

Figure 4.4. hADSC proliferation (**A**) was significantly higher on tissue grafts (in particularly on their basement membrane side) after 7 and 14 days than on TCP and on the collagen / GAG scaffold. hADSC metabolic activity (**B**) was significantly higher on the collagen / GAG scaffold after 14 days than on TCP and on the tissue grafts. hADSC cell viability (**C**) was not affected as a function of the different materials at any timepoint. Data presented as average ± standard deviation (n=3). * indicates a significantly ($p < 0.05$) lower value than the TCP control, ** indicates a significantly ($p < 0.05$) higher value than TCP.

4.3.2. Flow cytometry and trilineage differentiation analyses

Flow cytometry analysis (**Figure 4.5**) revealed that most (> 99 %) hADSCs on all groups expressed CD73, CD44 and CD90 and did not express CD45. Quantification of calcium deposition after osteogenic induction of the hADSCs (**Figure 4.6**) revealed that, at all timepoints, the Integra™ scaffold and both tissue grafts exhibited significantly ($p < 0.05$) higher calcium deposition than the TCP. Oil red OD quantification after adipogenic induction of the hADSCs (**Figure 4.7**) revealed that at day 7, the Integra™ scaffold exhibited the highest ($p < 0.05$) adipogenic potential and at days 14 and 21, the TCP and the Integra™ scaffold were significantly ($p < 0.05$ at day 14 and $p < 0.01$ at day 21) more adipogenic than both tissue grafts.

GAGs quantification after chondrogenic induction of the hADSCs (**Figure 4.8**) revealed that at day 7, all conditions induced significantly ($p < 0.05$) higher chondrogenesis than TCP; at day 14, the CT side of XenoMEM™ induced the highest ($p < 0.05$) chondrogenesis; and at day 21, the pellet and the BM sides of MatriStem™ and XenoMEM™ induced the highest ($p < 0.05$) chondrogenesis.

4.3.3. *In vivo* cell tracking analysis

Macroscopic analysis of fluorescent-labelled hADSCs (**Figure 4.9A**) revealed that the cells of the cell-injection group were dispersed around the dorsal area, whilst the cells that were delivered with the Integra™ scaffold and both tissue grafts were localised within the wounds. Further, for all groups, a gradual loss of signal was observed as a function of time (**Figure 4.9A**). Quantification of radiance efficiency within the wounds (**Figure 4.9B**) revealed that at days 10 and 14 the Integra™ scaffold delivered hADSCs group exhibited significantly ($p < 0.05$) lower than the injected hADSCs group radiance efficiency within the wounds (at days 3 and 7, although radiance efficiency within the wounds was also lower, it was not significant). hADSCs that were delivered from the CT side of the XenoMEM™ (**Figure 4.9B**) also showed significantly ($p < 0.05$) lower than the injected hADSCs group radiance efficiency within the wounds at day 3 (at days 7, 10 and 14, although radiance efficiency within the wounds was also lower, it was not significant). As a function of time, the radiance efficiency within the wounds was significantly ($p < 0.05$) reduced for all groups.

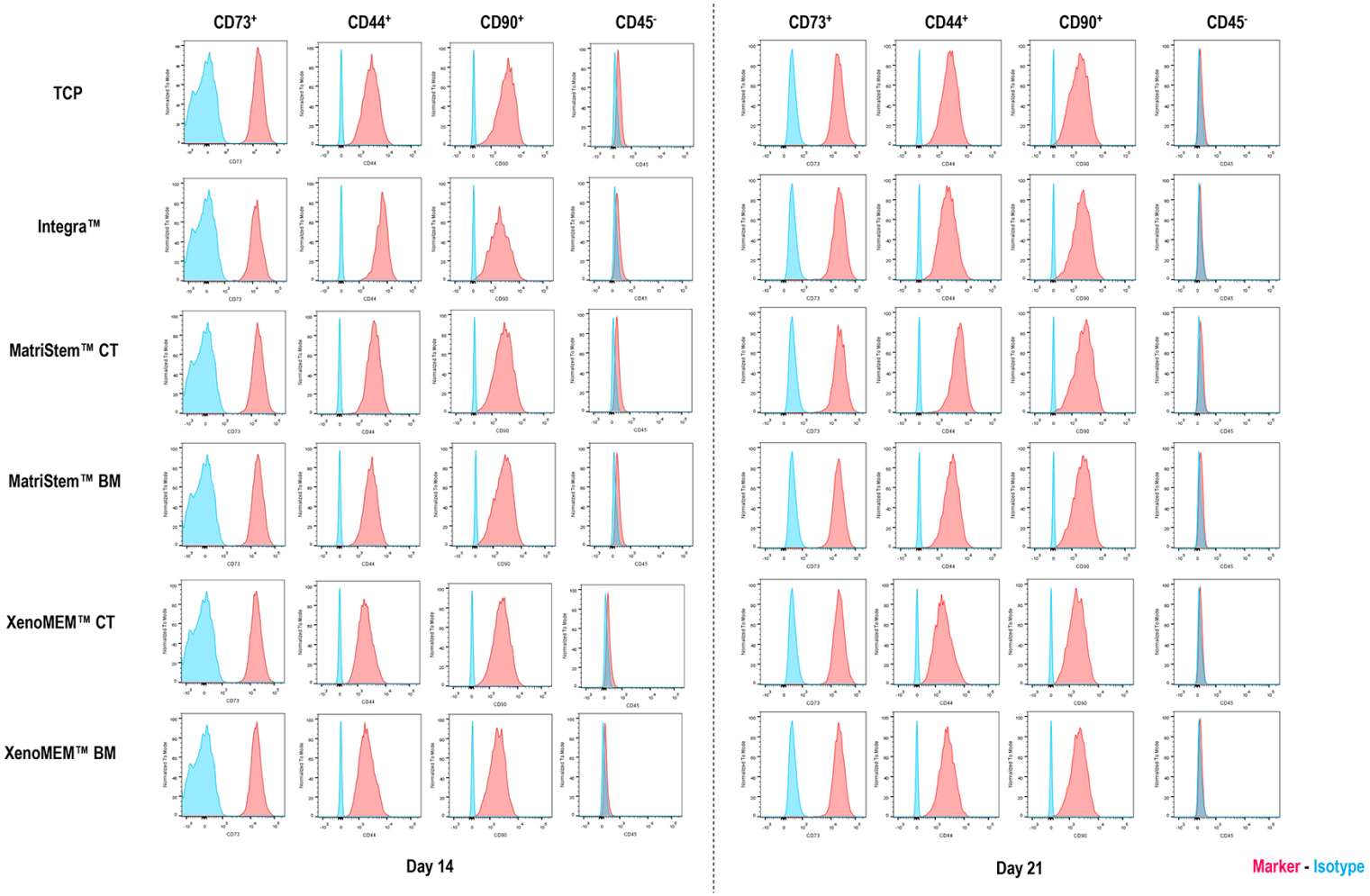

Figure 4.5. Flow cytometry analysis revealed that most (> 99 %) of the human ADSCs were positive for the CD90, CD44 and CD73 markers and negative for the CD45 marker independently of the condition and at both timepoints.

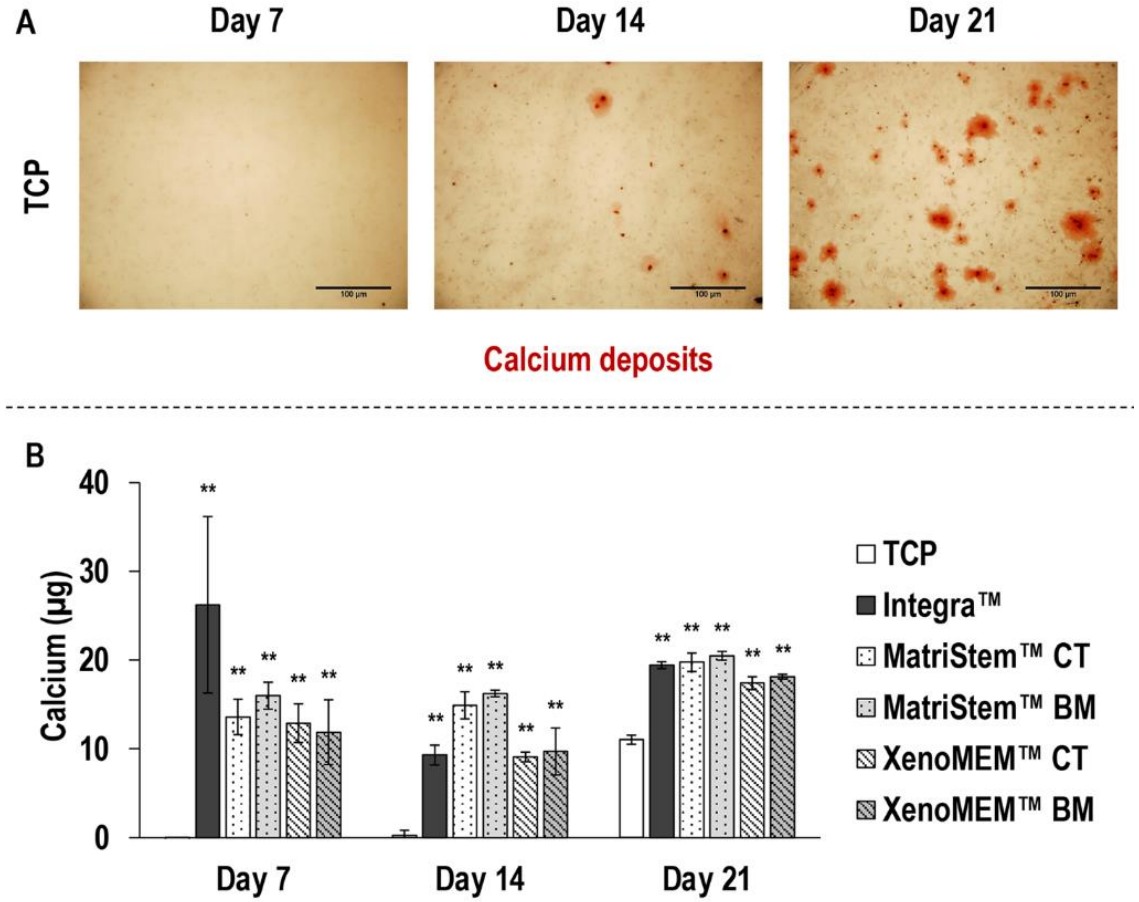

Figure 4.6. Alizarin red staining of human ADSCs on TCP (**A**) after osteogenic differentiation showed deposition of calcium after 14 and 21 days, confirming the suitability of the differentiation protocol. Quantification of deposited calcium (**B**) showed a significantly increase of calcium deposition after 21 days in all conditions, although it was not significant on the Integra™ Matrix Wound Dressing. Scale bars 100 μm. ** indicates a significantly ($p < 0.05$) higher value than the TCP group.

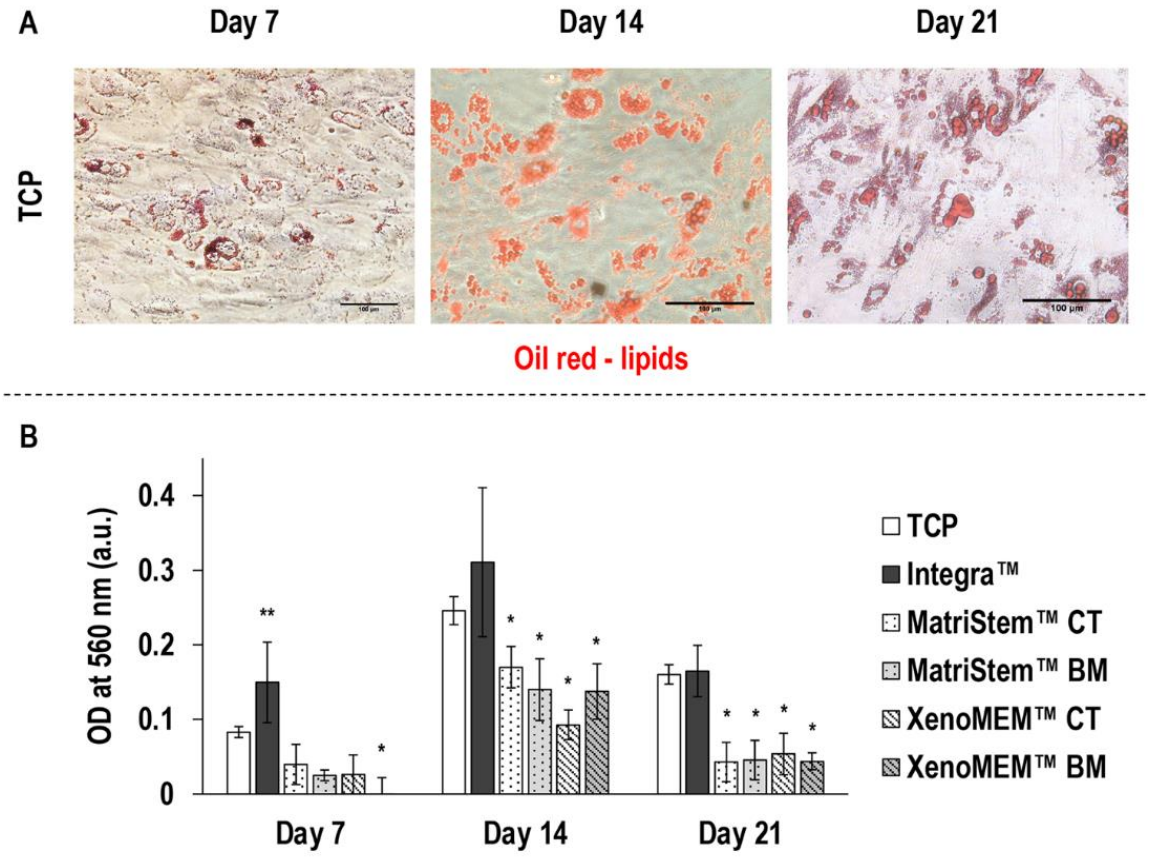

Figure 4.7. Oil red staining of human ADSCs on TCP (**A**) after adipogenic differentiation showed the accumulation of lipids after 7, 14 and 21 days, confirming the suitability of the differentiation protocol. Analysis of released lipids by OD (**B**) revealed a significant increase of lipids deposition in all conditions after 14 days, although this was not significant on the Integra™ Matrix Wound Dressing. Scale bars 100 μm. Data presented as average ± standard deviation (n=3). * indicates a significantly ($p < 0.05$) lower value than the TCP group, ** indicates a significantly ($p < 0.05$) higher value than the TCP group.

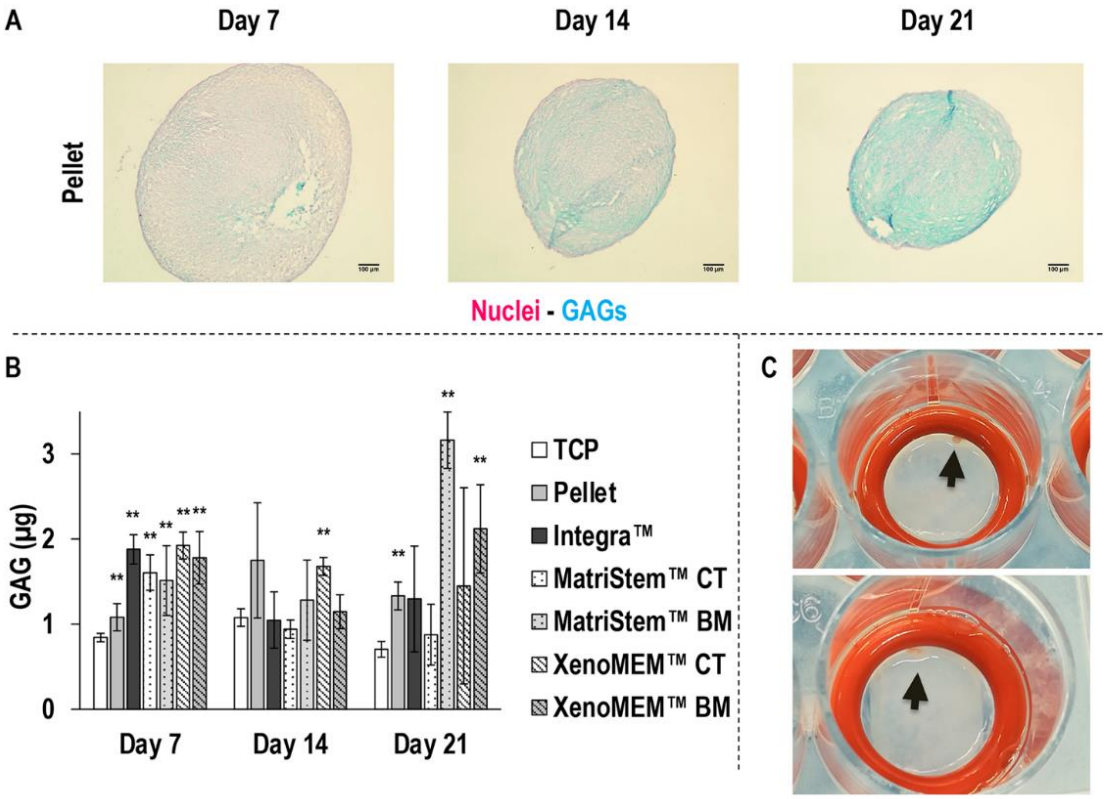

Figure 4.8. Alcian blue and fast red staining of pellets (**A**) after chondrogenic differentiation showed shrinking of the pellet and a denser deposition of GAG (blue), confirming the suitability of the differentiation protocol. GAG quantification of hADSCs under differentiation (**B**) showed a significant increase in GAG deposition on the BM sides of MatriStem™ and XenoMEM™ and a collapsed pellet hADSCs-sheet structure was observed (**C**). Scale bars 100 μm. Data presented as average ± standard deviation n=3). ** indicates a significantly ($p < 0.05$) higher value than the TCP group.

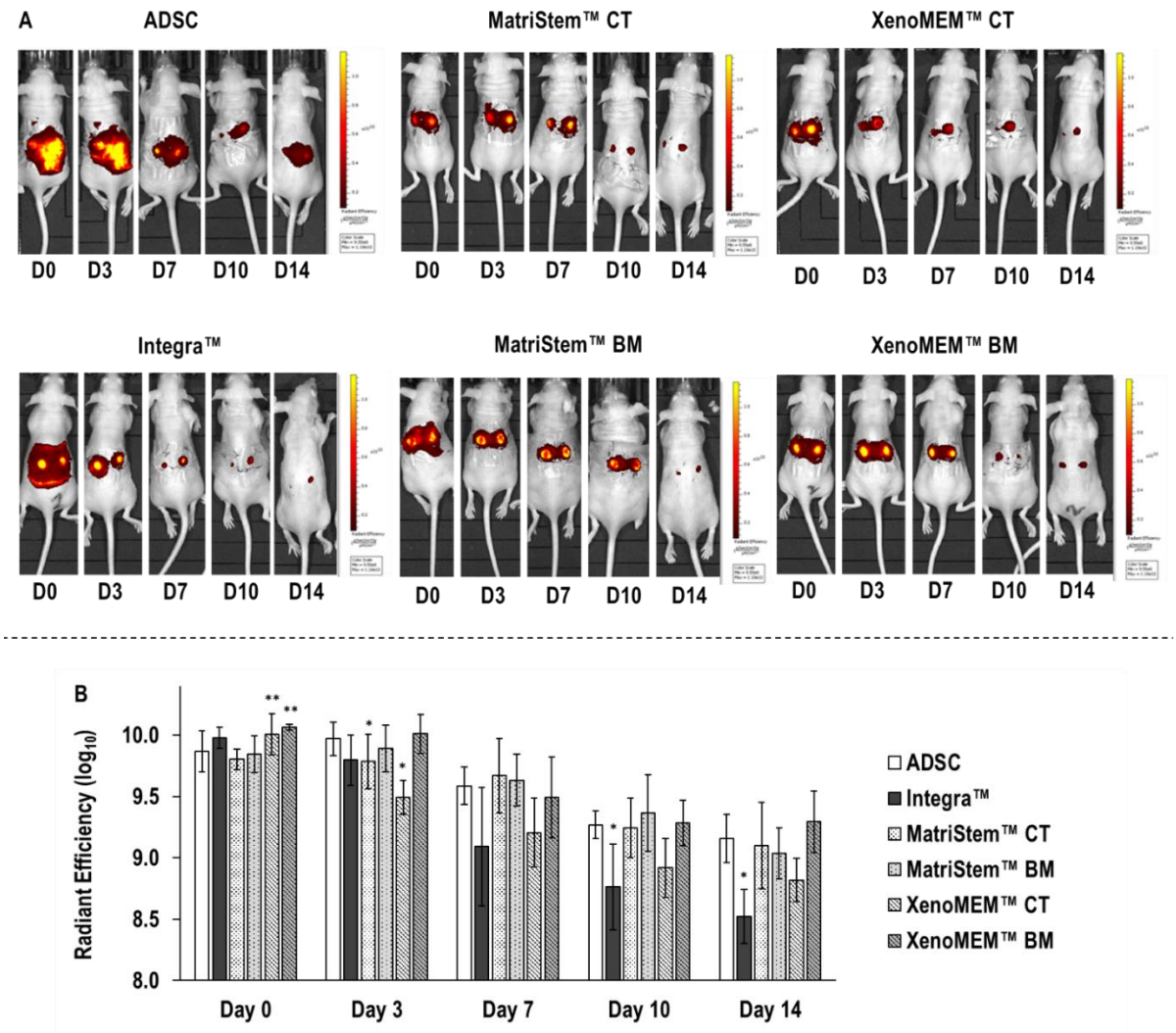

Figure 4.9. *In vivo* tracking of hADSC (**A**) revealed a disperse signal of the injected cells group and a localised signal for all materials groups, which was gradually lost in all groups. Quantification of radiant efficiency in the wound areas (**B**) made apparent a higher signal than the injected hADSC in both sides of XenoMEM™ at day 0, a lower signal in the CT sides of MatriStem™ and XenoMEM™ at day 3, and in Integra™ Matrix Wound Dressing at days 10 and 14. Data presented as average ± standard deviation (n=6). * indicates a significantly ($p < 0.05$) lower value than the injected hADSC, ** indicates a significantly ($p < 0.05$) higher value than the injected hADSC.

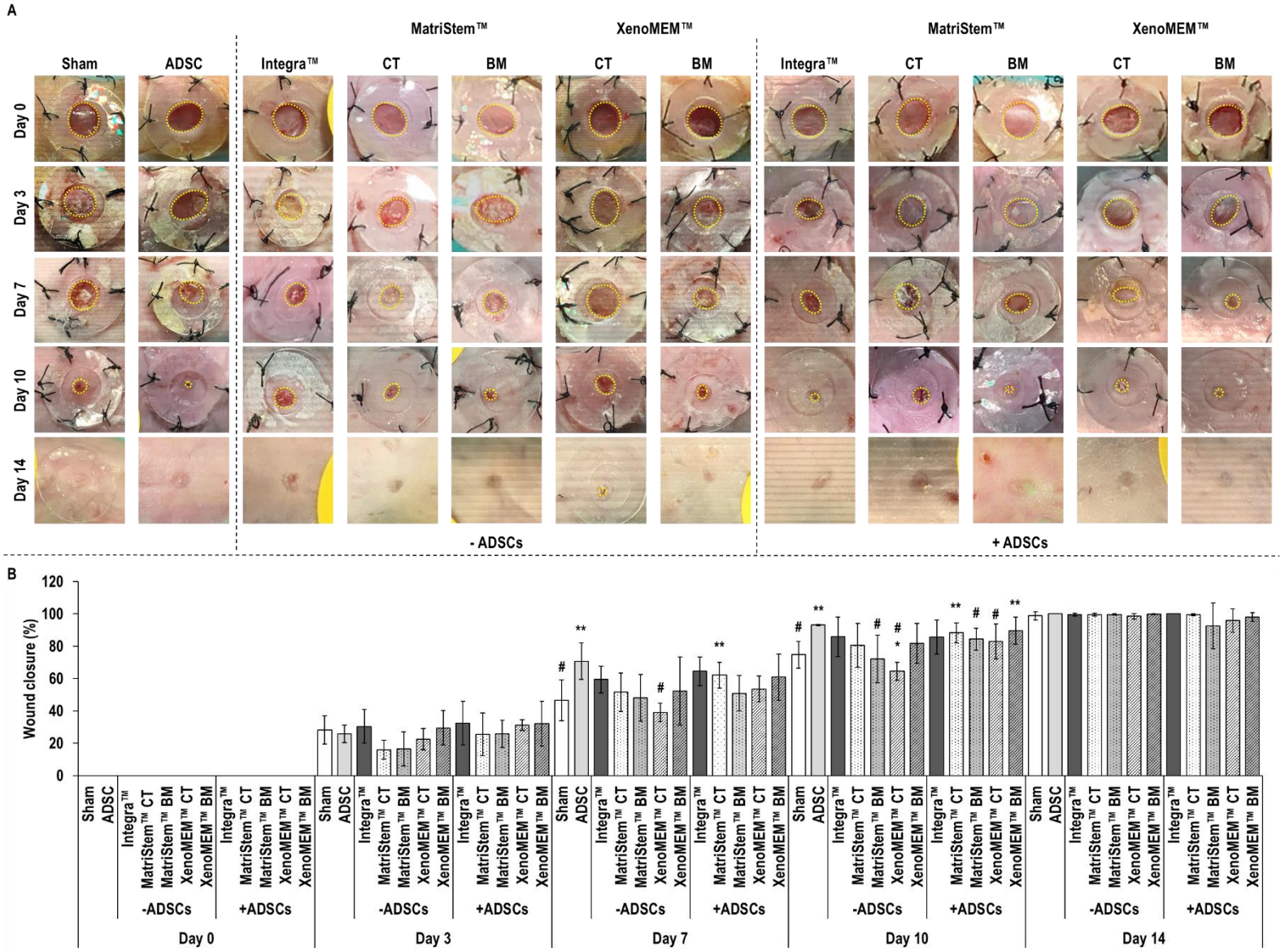
A
MatriStem™
XenoMEM™
MatriStem™
XenoMEM™
Sham
ADSC
Integra™
CT
BM
CT
BM
Integra™
CT
BM
CT
BM
Day 0
Day 3
Day 7
Day 10
Day 14
- ADSCs
+ ADSCs
B
Wound closure (%)
120
100
80
60
40
20
0
Sham
ADSC
Integra™
MatriStem™ CT
MatriStem™ BM
XenoMEM™ CT
XenoMEM™ BM
-ADSCs
+ADSCs
Day 0
Day 3
Day 7
Day 10
Day 14

Figure 4.10. Macroscopic analysis (A) of the wounds (dashed yellow line) showed no complications nor scarring tissue during healing; all conditions reached wound closure after 14 days; and hADSC accelerated the wound closure process. Quantification of wound closure (B) in the absence of hADSCs showed that the CT side of the XenoMEM™ induced significantly lower wound closure at day 7 in comparison to hADSC injection and at day 10 in comparison to sham and hADSC injection. The BM side of MatriStem™ BM also presented significantly lower wound closure than hADSC injection at day 10. Wound closure in the presence of hADSCs was significantly higher than the sham group for the hADSC injection and the CT side of MatriStem™ with hADSCs at day 7. The hADSC injection, the CT side of MatriStem™ with hADSCs and the BM side of XenoMEM™ with hADSCs showed significantly higher wound closure than sham at day 10. In comparison to hADSC injection, significantly lower wound closure was observed for the BM side of MatriStem™ and the CT side of XenoMEM™ at day 10. Data presented as average ± standard deviation (n=6). * indicates a significantly ($p < 0.05$) lower value than the sham group, ** indicates a significantly ($p < 0.05$) higher value than sham group, # indicates a significantly ($p < 0.05$) lower value than ADSC control.

4.3.4. Wound closure analysis

Macroscopic analysis of the wounds (**Figure 4.10A**) revealed no apparent complication or excessive scarring in any of the conditions at any timepoint, all conditions resulted in an almost complete wound closure after 14 days and the use of hADSCs appeared to accelerate wound closure at a given timepoint.

Wound closure quantification (**Figure 4.10B**) revealed no differences among groups at days 0, 3 and 14, whilst some differences were observed at days 7 and 10. Specifically, at day 7, the hADSC injection showed a significantly ($p < 0.05$) higher wound closure than the sham; the CT side of XenoMEM™ without hADSCs had significantly ($p < 0.05$) lower wound closure than the hADSC injection; and the CT side of MatriStem™ with hADSCs had a significantly ($p < 0.05$) higher wound closure than the sham. At day 10, the hADSC injection showed a significantly ($p < 0.05$) higher wound closure than the sham; the BM of MastriStem™ without hADSCs presented a significantly ($p < 0.05$) lower wound closure than hADSC injection; the CT side of the XenoMEM™ without hADSCs had significantly ($p < 0.05$) lower wound closure than the sham and hADSC injection; the CT side of MatriStem™ and the BM side of XenoMEM™ with hADSCs had significantly ($p < 0.05$) higher wound closure than the sham; and the BM side of

MatriStem™ and CT side of XenoMEM™ with hADSCs had significantly ($p < 0.05$) lower wound closure than hADSCs injection (**Figure 4.10B**).

4.3.5. Histological analysis

Visual assessment of haematoxylin/eosin and Masson's Trichrome stained sections of wounds at day 14 (**Figure 4.11A**) revealed that the epidermis had been fully regenerated in all conditions; most of the materials had been remodelled [although some remnants were still present (**Figure 4.12**) and the wound gap had been reduced when hADSCs had been used. Quantification of the wound gap (**Figure 4.11B**) revealed that in comparison to the sham group, in the absence of hADSCs, the CT and BM sides of the MatriStem™ showed significantly ($p < 0.05$) lower wound gap; in the presence of hADSCs, only the BM side of the MatriStem™ had similar ($p > 0.05$) wound gap to the sham group and all other groups had significantly ($p < 0.05$) lower wound gap. In comparison to the hADSC injection group, in the absence of hADSCs, only the BM side of the XenoMEM™ had a similar ($p > 0.05$) wound gap and all other groups presented a significantly ($p < 0.05$) higher wound gap; and in the presence of hADSCs, the BM side of the MatriStem™ and the CT side of the XenoMEM™ presented a significantly ($p < 0.05$) higher wound gap. When comparing each material without and with hADSCs, both sides of XenoMEM™ with hADSCs resulted in significantly ($p < 0.05$) lower wound gap than its without hADSCs counterpart. Quantification of the scar index (**Figure 4.11C**) revealed that in comparison to sham, in the absence of hADSCs, the CT and BM sides of the MatriStem™ showed significantly ($p < 0.05$) lower scar index. In the presence of hADSCs, the BM side of the MatriStem™ and the CT side of the XenoMEM™ had similar ($p > 0.05$) scar index to the sham and all other groups had significantly ($p < 0.05$) lower scar index than the sham. In comparison to the hADSC injection, in the absence of hADSCs, the Integra™ scaffold and the CT side of XenoMEM™ showed a significantly ($p < 0.05$) higher scar index and, in the presence of hADSCs, only the CT side of XenoMEM™ had a significantly ($p < 0.05$) higher scar index. All materials with hADSCs, but the CT and BM sides of the MatriStem™, resulted in significantly ($p < 0.05$) lower scar index than their counterparts without hADSCs. Epidermal thickness analysis (**Figure 4.11D**) revealed no significant ($p > 0.05$) differences between the groups and within the groups in the absence and presence of hADSCs.

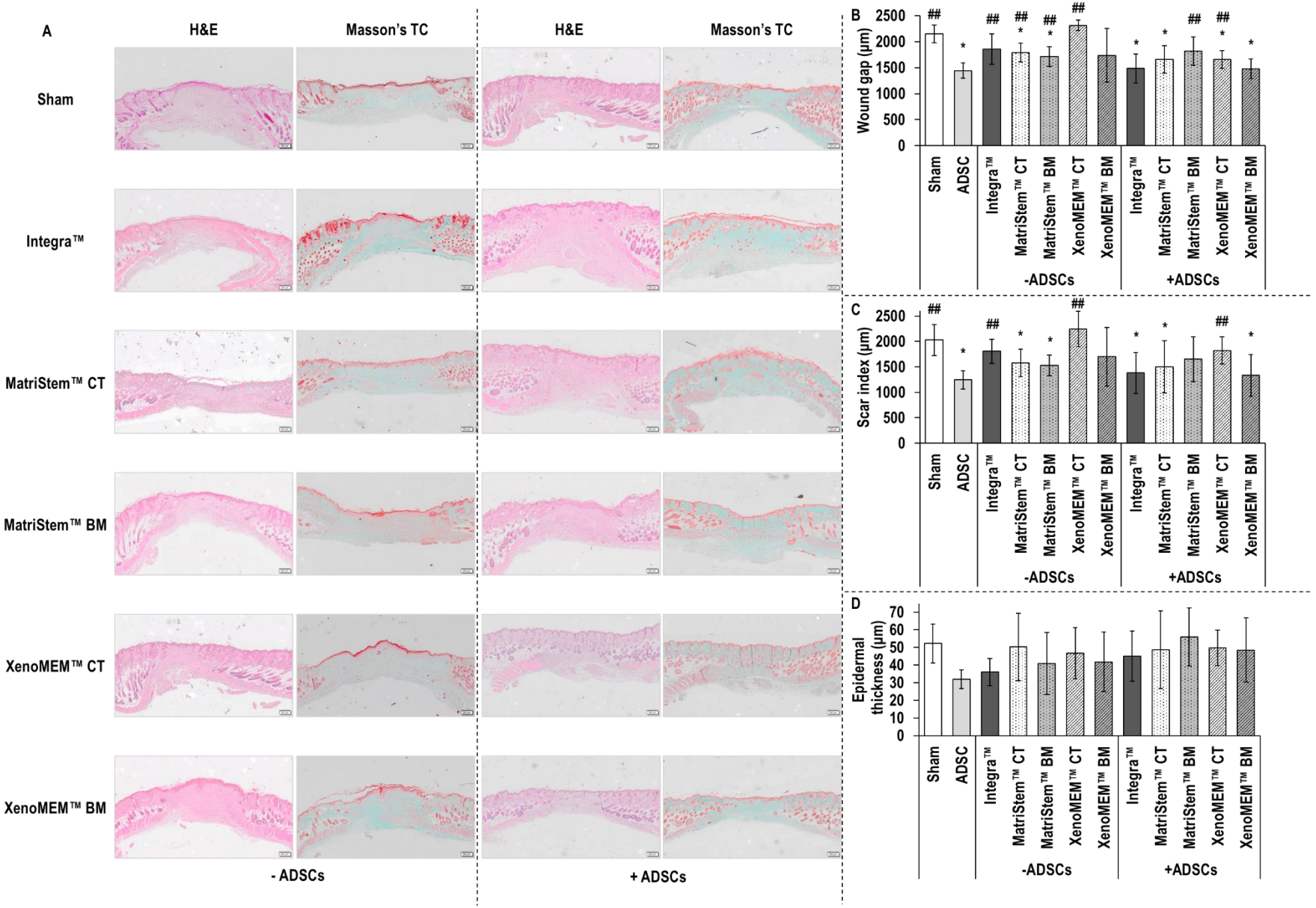
A
H&E
Masson's TC
H&E
Masson's TC
Sham
Integra™
MatriStem™ CT
MatriStem™ BM
XenoMEM™ CT
XenoMEM™ BM
- ADSCs
+ ADSCs
B
Wound gap (µm)
C
Scar index (µm)
D
Epidermal thickness (µm)
Sham
ADSC
Integra™
MatriStem™ CT
MatriStem™ BM
XenoMEM™ CT
XenoMEM™ BM
-ADSCs
+ADSCs

Figure 4.11. Haematoxylin/eosin (H&E) and Masson's Trichrome (Masson's TC) stainings (**A**) revealed the gap in the dermis and *panniculus carnosus* filled with connective tissue and cells corresponding to the wound and made apparent that the use of hADSC decreased the wound gap. Scale bars 200 μm. Quantification of wound gap (**B**) showed that in the absence of hADSCs, a significantly lower wound gap was observed in both sides of MatriStem™ in comparison to the sham and significantly higher wound gap than the hADSC injection was found in all groups, but the BM side of the XenoMEM™. In the presence of hADSCs, all groups, but the BM side of the MatriStem™, significantly decreased the wound gap in comparison to sham and the BM side of the MatriStem™ and the CT side of the XenoMEM™ showed a significantly higher wound gap than the hADSC injection. Scar index quantification (**C**) showed that in the absence of hADSCs, a significantly lower scar index was observed in both sides of MatriStem™ in comparison to sham and significantly higher scar index than the hADSC injection was observed with the Integra™ scaffold and the CT side of the XenoMEM™. In the presence of hADSCs, the hADSC injection and hADSCs with the CT side of the MatriStem™ and the BM side of XenoMEM™ showed a significantly lower scar index than the sham and only the CT side of the XenoMEM™ showed a significantly higher scar index than hADSC injection. Epidermal thickness quantification (**D**) in the absence or presence of hADSC did not show any differences between groups. Data presented as average ± standard deviation (n=6). * indicates a significantly ($p < 0.05$) lower value than the sham group, ## indicates a significantly ($p < 0.05$) higher value than ADSC group.

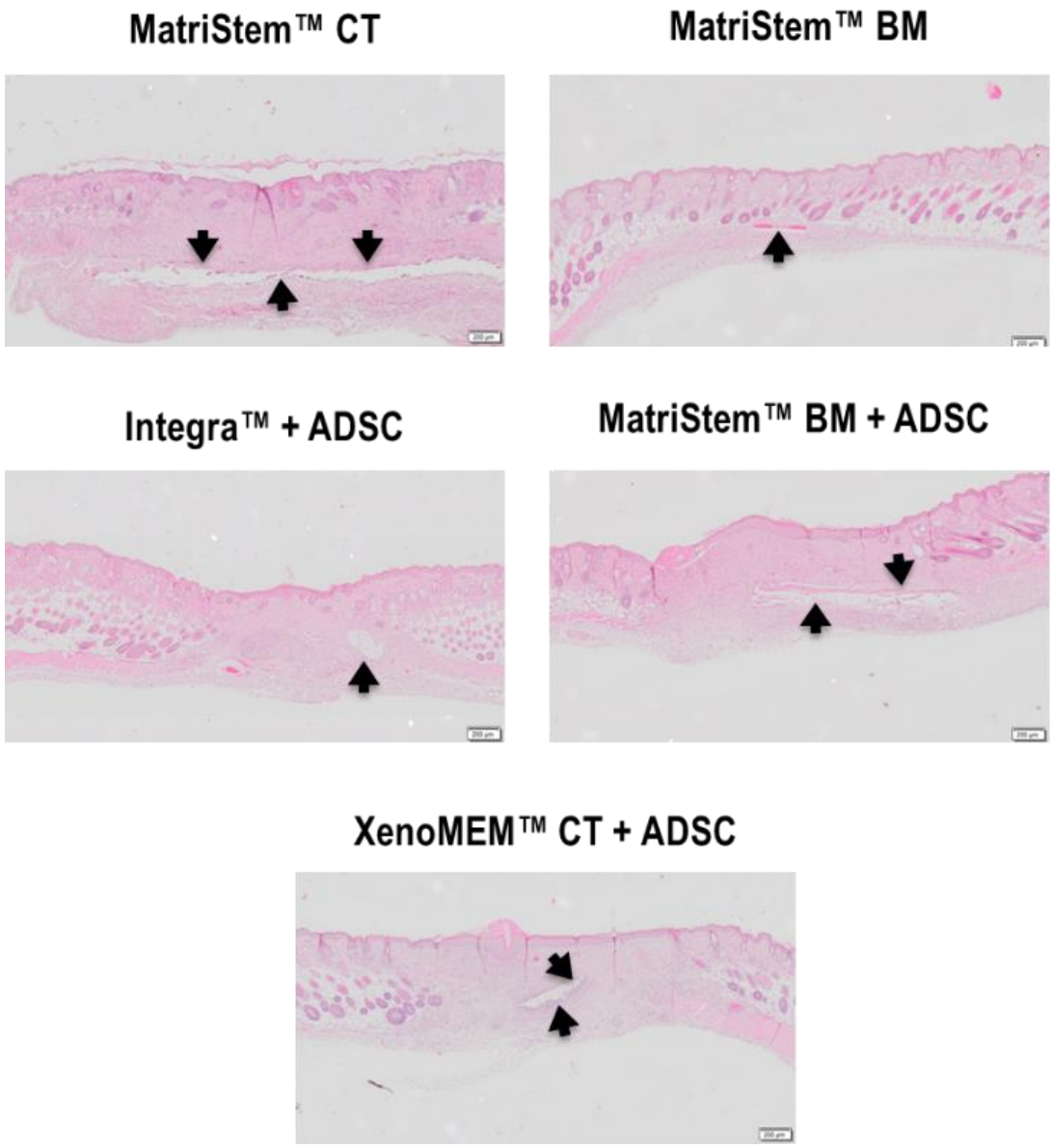

Figure 4.12. Histology analysis showed occasionally some remnants of materials that were not completely absorbed. Scale bars 200 μm.

Polarised light microscopy of picrosirius red stained sections (**Figure 4.13A**) revealed the presence of disorganised collagen fibres in the wound area in all conditions, from which only the sham and the Integra™ scaffold in the absence of hADSCs and both sides of the XenoMEM™ in the presence of hADSCs induced matured collagen fibres. Total collagen area quantification (**Figure 4.13B**) revealed that, in comparison to sham, in the absence of hADSCs, no significant ($p > 0.05$) differences were observed between the groups and, in the presence of hADSCs, the hADSC injection showed the highest ($p < 0.05$) total collagen area and the BM sides of the MatriStem™ and the XenoMEM™ showed significantly ($p < 0.05$) lower total collagen area. In comparison to the hADSC injection,

all groups except the CT side of MatriStem™ without hADSCs had a significantly ($p < 0.05$) lower total collagen area. Materials with hADSCs had similar ($p > 0.05$) total collagen area to the materials without hADSCs, except for MatriStem™, which exhibited significantly ($p < 0.05$) lower total collagen area when loaded with hADSCs. Mature collagen quantification (**Figure 4.13C**) revealed that in the absence of hADSCs, only the BM side of the XenoMEM™ had significantly ($p < 0.05$) higher mature collagen area in comparison to the sham group and all groups without hADSCs, but the BM side of the XenoMEM™, had a significantly ($p < 0.05$) lower mature collagen area compared to the hADSC injection. In the presence of hADSCs, all groups had significantly ($p < 0.01$) higher mature collagen area in comparison to the sham and presented no differences ($p > 0.05$) with the hADSC injection. Materials with hADSCs had similar ($p > 0.05$) mature collagen area to the materials without hADSCs, except of the CT side of the XenoMEM™ with hADSCs, which had significantly ($p < 0.05$) higher mature collagen area than its without hADSCs counterpart.

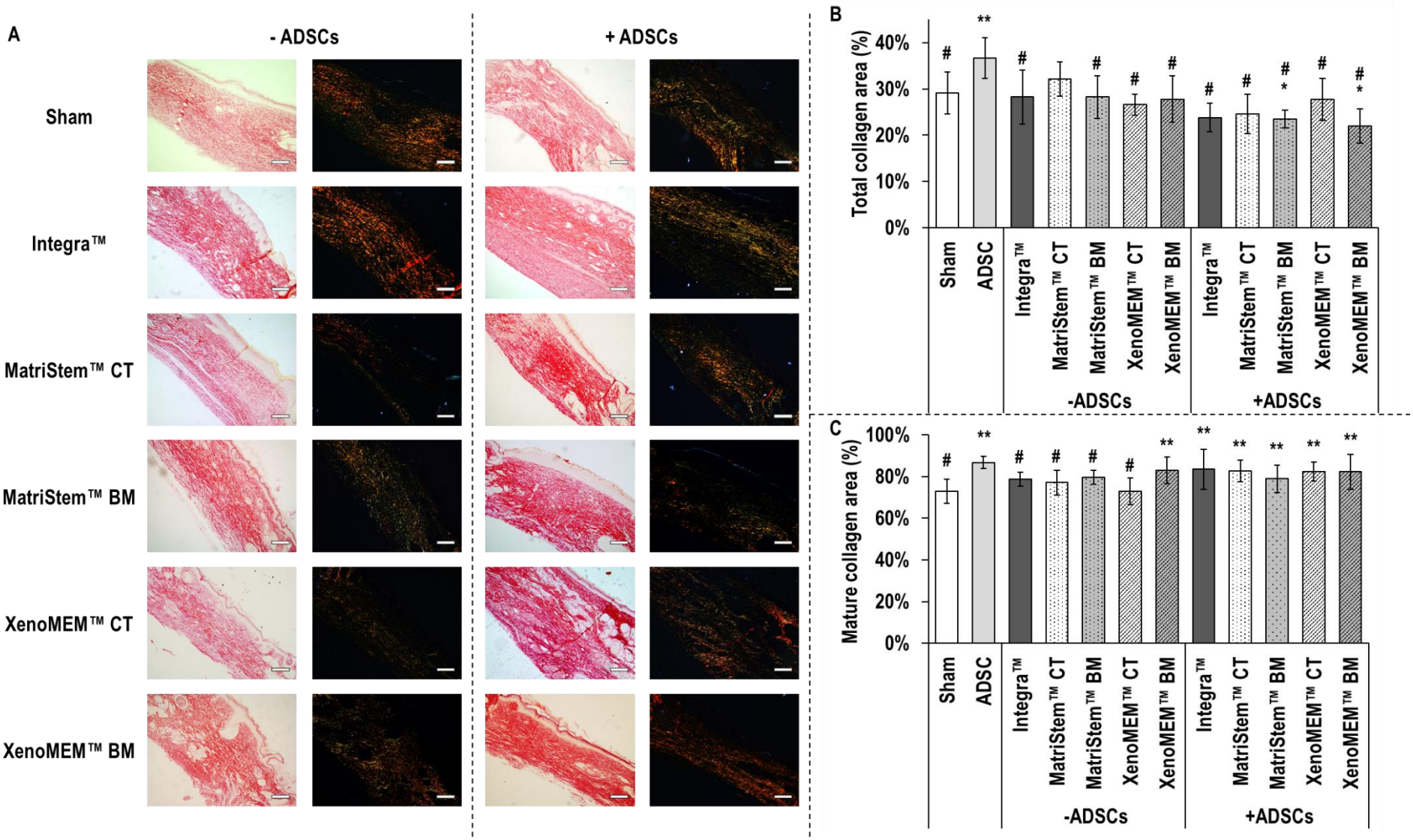
A
- ADSCs
+ ADSCs
Sham
Integra™
MatriStem™ CT
MatriStem™ BM
XenoMEM™ CT
XenoMEM™ BM
B
Total collagen area (%)
40%
30%
20%
10%
0%
Sham
ADSC
Integra™
MatriStem™ CT
MatriStem™ BM
XenoMEM™ CT
XenoMEM™ BM
-ADSCs
+ADSCs
C
Mature collagen area (%)
100%
80%
60%
40%
20%
0%

Figure 4.13. Polarised light microscopy of picrosirius red stained sections (**A**) showed the presence of disorganised mature (polarised red / yellow staining) and immature (polarised green staining) collagen in the wounds of all groups. Scale bars 50 μm. Quantification of total collagen (**B**) showed no differences among groups in the absence of hADSC and in the presence of hADSC, a significantly higher total collagen was observed in injected hADSC in comparison to the sham group and the significantly lower total collagen when cells were delivered with BM sides of the MatriStem™ and XenoMEM™ groups; in comparison to the hADSC injection, all groups, but the CT side of the MatriStem™ without hADSCs, showed a significantly lower total collagen area. Mature collagen quantification (**C**) in the absence of hADSC revealed a significantly higher amount of mature collagen in the BM side of XenoMEM™ in comparison to sham and all groups, but the BM side of the XenoMEM™ exhibited significantly lower mature collagen area than the hADSC injection. In the presence of hADSC, the injected cells and cells delivered with Integra™ Matrix Wound Dressing, the CT side of MatriStem™ and both sides of XenoMEM™ groups had significantly higher proportion of mature collagen than the sham group. Data presented as average ± standard deviation (n=6). * indicates a significantly ($p < 0.05$) lower value than the sham group, ** indicates a significantly ($p < 0.05$) higher value than sham group, # indicates a significantly ($p < 0.05$) lower value than ADSC group.

4.3.6. Immunohistochemical analysis

Immunohistochemistry analysis of CD31 (**Figure 4.14A**) revealed the formation of microvessels within the wound area in all conditions. Complementary image intensity analysis of CD31 (**Figure 4.14B**) revealed in the absence of hADSCs no apparent differences ($p > 0.05$) between the groups; in the presence of hADSCs all groups exhibited significantly ($p < 0.05$) higher CD31 expression than the sham group; and both sides of XenoMEM™ and Integra™ with hADSCs resulted in significantly ($p < 0.01$) higher CD31 expression than their without hADSCs counterparts. In comparison to the hADSC injection, only the BM side of XenoMEM™ with hADSCs showed a significantly ($p < 0.01$) higher CD31 expression. DAPI staining (**Figure 4.14A**) revealed a homogenous distribution of cells in the wound area. Subsequent cell quantification in the wound area (**Figure 4.14C**) revealed no differences ($p > 0.05$) between the groups in the absence and presence of hADSCs; and all materials with hADSCs, but the BM side of the XenoMEM™ ($p < 0.05$), resulted in similar ($p > 0.05$) cell number in the wound area than their without hADSCs counterparts.

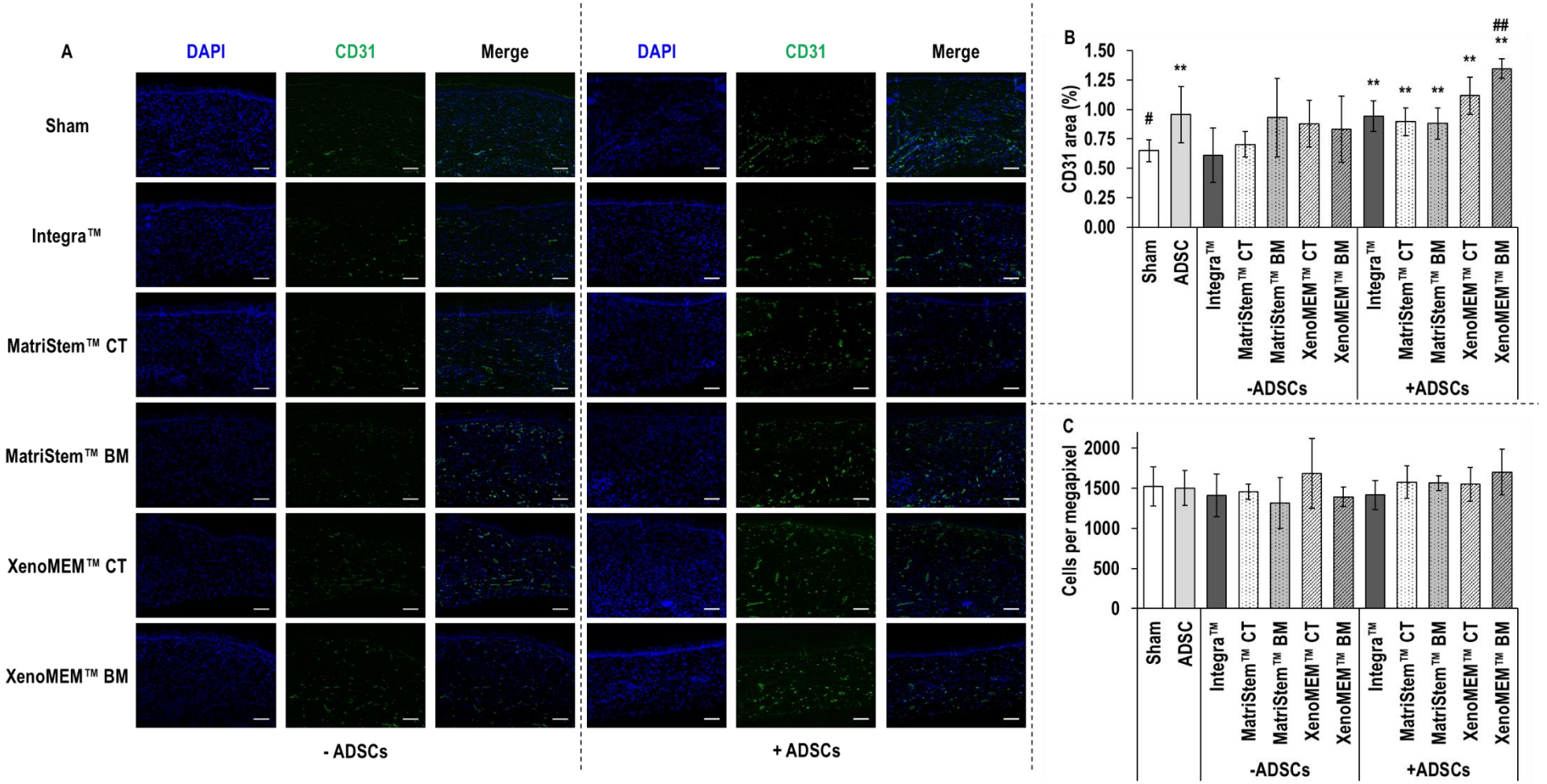
A
DAPI
CD31
Merge
DAPI
CD31
Merge
Sham
Integra™
MatriStem™ CT
MatriStem™ BM
XenoMEM™ CT
XenoMEM™ BM
- ADSCs
+ ADSCs
B
CD31 area (%)
1.50
1.25
1.00
0.75
0.50
0.25
0.00
Sham
ADSC
Integra™
MatriStem™ CT
MatriStem™ BM
XenoMEM™ CT
XenoMEM™ BM
Integra™
MatriStem™ CT
MatriStem™ BM
XenoMEM™ CT
XenoMEM™ BM
-ADSCs
+ADSCs
C
Cells per megapixel
2000
1500
1000
500
0
Sham
ADSC
Integra™
MatriStem™ CT
MatriStem™ BM
XenoMEM™ CT
XenoMEM™ BM
Integra™
MatriStem™ CT
MatriStem™ BM
XenoMEM™ CT
XenoMEM™ BM
-ADSCs
+ADSCs

Figure 4.14. Immunohistochemistry analysis of sections (**A**) for CD31 (green) showed the formation of microvessels in all groups. DAPI (blue) staining (**A**) showed a homogenous dispersion of cells in the wound area in all conditions. Scale bars 100 μm. CD31 area quantification (**B**) showed no differences between groups in the absence of hADSC and in the presence of hADSC, a significantly higher area of CD31 in comparison to sham was observed in all groups and only the BM side of the XenoMEM™ showed significantly higher CD31 expression than the hADSC injection. Cell counting from DAPI stained sections (**C**) sections did not reveal any differences in cell density in the wounds between the groups in the absence or presence of hADSC. Data presented as average ± standard deviation (n=6). ** indicates a significantly ($p < 0.05$) higher value than sham group, # indicates a significantly ($p < 0.05$) lower value than ADSC group, ## indicates a significantly ($p < 0.01$) higher value than ADSC group.

4.4. Discussion

Direct (stem) cell injections have failed to deliver consistent results in clinical practice, as the mode of administration neither protects nor localises the injected cell suspension at the side of implantation (26). ECM-based biomaterials (e.g. extracted collagen scaffolds and decellularised tissue grafts) have the potential to act as excellent cell-delivery vehicles, considering their well demonstrated cytocompatibility *in vitro* and remodelling capacity *in vivo* (27-29). Unfortunately, the ideal ECM-based biomaterial remains elusive, largely attributed to their scattered clinical outcomes (‘from unacceptable to excellent’ (30)). Although *in vitro* and *in vivo* data advocate the potential of porcine peritoneum for regenerative medicine applications (17-19) and a few products are already clinically available (e.g. Meso BioMatrix®, DSM, for breast reconstruction; XenoMEM™, Viscus Biologics, hernia repair), its potential in wound healing and, in particular, as stem cell carrier has yet to be elucidated. Herein, we assessed the potential of porcine peritoneum (XenoMEM™, Viscus Biologics) as a human adipose derived stem cell carrier in a splinted nude mouse wound healing model, taking also into consideration its layer-dependent composition (connective tissue and basement membrane layers). To ensure that the derived data will inform future clinical studies, we also used as control groups a collagen-based scaffold (Integra™ Matrix Wound Dressing, Integra Life Sciences Corporation) and another bilayer tissue graft (porcine urinary bladder, MatriStem™, Acell®), both with a well-documented clinical history in wound healing (20, 21).

Starting with *in vitro* cytocompatibility assessment on the various materials, it was found that hADSC proliferation was enhanced when seeded on the tissue grafts, which is in agreement with previous work with porcine urinary bladder (31) and is expected, due to the presence of growth factors (e.g. FGF-b, TGF-β1) in these matrices (32, 33) that are known to promote ADSC proliferation without affecting their stemness (34). Furthermore, this proliferation was enhanced on the BM side of the tissue grafts, as has been previously observed with other cell types (11, 12), since BM is rich in collagen type IV and laminins (35) that are known to elicit such effect (36, 37). When though the hADSCs were seeded on the collagen / GAG scaffold, a decreased proliferation and an increased metabolic activity were observed, indicative of cell stress, which can be probably attributed to the crosslinking method employed and is in agreement with previous publications using human bone marrow stem cells (38).

In general, none of the materials assessed affected the stemness and multilineage potential of the hADSC, as has been shown before for porcine urinary bladder (39) and collagen / GAG (40) devices. With respect to osteogenic potential, all materials induced osteogenesis after 21 days in culture, as has been shown before for urinary bladder (41) and collagen / GAG (40) devices using different stem cell populations. Although during adipogenic differentiation the lipid production was reduced at day 21 in comparison to day 14 in all tissue grafts, such reduction has been previously attributed to hADSC donors' characteristics / conditions (42) or to the detachment of mature differentiated hADSC after long culture periods (43). With respect to chondrogenic differentiation, it is worth noting that the BM sides of the tissue grafts exhibited significantly higher chondrogenic capacity even over the pellet culture that is considered the gold standard in *in vitro* setting (44). It is worth noting that protocols similar to this study induced chondrogenesis in hADSC only in combination with TGF-β3 and/or other growth factors (e.g. FGF-18, IGF-1 BMP-6) (45-48). This BM side preferential chondrogenic differentiation of the hADSCs may again be attributed to the composition of this tissue layer [e.g. laminin-1, collagen type IV and fibronectin have been shown to improve chondrogenesis in human bone marrow stem cells (37)].

Moving on to the preclinical assessment, it was evidenced that all materials retained more cells at the side of implantation than the cell injection approach, despite the fact that only half of the cells that were used in the direct injection approach were loaded on the materials. In fact, XenoMEM™ presented a higher signal at day 0, which is indicative of a higher presence of cells and therefore loading efficiency. Further, among the materials assessed, the collagen / GAG scaffold lost fluorescent signals the fastest, which we

attribute to the potential cytotoxicity of the material that was observed *in vitro* or to the absence of as many cell attachment sites as the tissue grafts offer. Similar results have been reported before in the literature with a range of tissue grafts, cell populations and preclinical models (e.g. hADSC delivered by a porcine small intestinal submucosa graft to a rat ventral model (49), hADSC delivered by a decellularised porcine nucleus pulposus device to a rabbit intervertebral disc degeneration model (50), rat bone marrow stem cells delivered by a porcine decellularised meniscus materials to a full-thickness rat meniscus defect model (51)). The gradual loss in fluorescent signal observed in all conditions could be also attributed to the loss of scar tissue after 2 weeks, as has been suggested before in the same model (52, 53).

Histology and immunohistochemistry analyses showed the absence of a fibrotic response, as indicated by a lower scar index than the sham and no increase of cellularity in the wounds. In general, cell-loaded materials, even though they were loaded with half of the cells that were delivered through the direct injection approach, exhibited low levels of total collagen, high levels of mature collagen and high angiogenesis potential, which further advocate the paracrine antifibrotic effect, regenerative / remodelling capacity and vascularisation competence of ADSCs (54-56). The injected hADSCs resulted in higher collagen deposition, which could be related to a slower activity during the remodelling phase (57, 58). Overall, the cell-loaded decellularised matrices showed higher regenerative capacity over the cell-loaded collagen/GAG scaffold, which is in agreement with previous publications with that have shown decellularised porcine small intestinal submucosa and dermis to promote ADSC production of immunomodulatory (e.g. TGF-β, COX-2) (54) and angiogenic (VEGF, FGF-2) molecules and to reduce inflammation (e.g. IL-6, iNOS) markers (23, 54). It is worth noting that angiogenesis was particularly enhanced when hADSCs were delivered through the BM side of XenoMEM™. Again, we believe that compositional differences may be responsible for this, considering that previous studies have shown improved angiogenetic capacity of scaffolds loaded with basement membrane components (59, 60).

4.5. Conclusion

In the quest of the ideal biomaterial for adipose derived stem cell delivery in a wound healing scenario, this study demonstrated the capacity of extracellular matrix-biomaterials to achieve higher cell localisation at the side of implantation than direct injections, even though they (the biomaterials) were loaded with half of the cells. Further, the combined biofunctionality of the extracellular matrix-biomaterials and the stem cells

resulted in enhanced regenerative capacity. Collectively, our data further support the use of extracellular matrix-based biomaterials, in particular decellularised porcine peritoneum, as adipose derived stem cell carriers in a wound healing scenario.

4.6. References

[1] T.R. Heathman, A.W. Nienow, M.J. McCall, K. Coopman, B. Kara, C.J. Hewitt, The translation of cell-based therapies: Clinical landscape and manufacturing challenges, Regen Med 10(1) (2015) 49-64.

[2] S. Lee, E. Choi, M.J. Cha, K.C. Hwang, Cell adhesion and long-term survival of transplanted mesenchymal stem cells: A prerequisite for cell therapy, Oxid Med Cell Longev 2015 (2015) 632902.

[3] F. Catena, L. Ansaloni, F. Gazzotti, S. Gagliardi, S. Di Saverio, L. D'Alessandro, A.D. Pinna, Use of porcine dermal collagen graft (Permacol) for hernia repair in contaminated fields, Hernia 11(1) (2007) 57-60.

[4] M.M. Abdelfatah, N. Rostambeigi, E. Podgaetz, M.G. Sarr, Long-term outcomes (>5-year follow-up) with porcine acellular dermal matrix (Permacol™) in incisional hernias at risk for infection, Hernia 19(1) (2015) 135-140.

[5] A. Adeel, B. Tyler, R. Brian, Repair of complete atrioventricular septal defects with decellularized extracellular matrix: Initial and midterm outcomes, World J Pediatr Congenit Heart Surg 8(3) (2017) 310-314.

[6] T.M. Kelley, M. Kashem, H. Wang, J. McCarthy, N.D. Carroll, G.W. Moser, T.S. Guy, Anterior leaflet augmentation with CorMatrix porcine extracellular matrix in twenty-five patients: Unexpected patch failures and histologic analysis, Ann Thorac Surg 103(1) (2017) 114-120.

[7] N.S. Hillberg, P.I. Ferdinandus, R.E.G. Dikmans, B. Winkens, J. Hommes, R.R.W.J. van der Hulst, Is single-stage implant-based breast reconstruction (SSBR) with an acellular matrix safe?: Strattice™ or Meso Biomatrix® in SSBR, Eur J Plast Surg 41(4) (2018) 429-438.

[8] C.A. Salzberg, C. Dunavant, N. Nocera, Immediate breast reconstruction using porcine acellular dermal matrix (Strattice®): Long-term outcomes and complications, J Plast Reconstr Aesthet Surg 66(3) (2013) 323-328.

[9] C.A. Witz, I.A. Montoya-Rodriguez, S. Cho, V.E. Centonze, L.F. Bonewald, R.S. Schenken, Composition of the extracellular matrix of the peritoneum, J Soc Gynecol Investig 8(5) (2001) 299-304.

[10] T. Jasna, N. D, L. Z, O. Miljana, B. G, S. Biljana, Histological characteristics of healthy animal peritoneum, Acta Vet 56(5-6) (2006) 405-412.

[11] H. Capella-Monsonis, J. Kelly, S. Kearns, D.I. Zeugolis, Decellularised porcine peritoneum as a tendon protector sheet, Biomed Mater 14(4) (2019) 044102.

[12] H. Capella-Monsonís, M.A. Tilbury, J.G. Wall, D.I. Zeugolis, Porcine mesothelium matrix as a biomaterial for wound healing applications, Mater Today Bio 7 (2020) 100057.

[13] I. Arnaoutova, J. George, H.K. Kleinman, G. Benton, Basement membrane matrix (BME) has multiple uses with stem cells, Stem Cell Rev Rep 8(1) (2012) 163-169.

[14] A. Singh, C.B. Yadav, N. Tabassum, A.K. Bajpeyee, V. Verma, Stem cell niche: Dynamic neighbor of stem cells, Eur J Cell Biol 98(2-4) (2019) 65-73.

[15] S. Werner, R. Grose, Regulation of wound healing by growth factors and cytokines, Physiol Rev 83(3) (2003) 835-870.

[16] L.E. Tracy, R.A. Minasian, E.J. Caterson, Extracellular matrix and dermal fibroblast function in the healing wound, Adv Wound Care 5(3) (2016) 119-136.

[17] D.M. Hoganson, G.E. Owens, E.M. O'Doherty, C.M. Bowley, S.M. Goldman, D.O. Harilal, C.M. Neville, R.T. Kronengold, J.P. Vacanti, Preserved extracellular matrix components and retained biological activity in decellularized porcine mesothelium, Biomaterials 31(27) (2010) 6934-6940.

[18] X. Luo, K. Kulig, E. Finkelstein, M. Nicholson, X. Liu, S. Goldman, J. Vacanti, B. Grottkau, I. Pomerantseva, C. Sundback, C. Neville, In vitro evaluation of decellularized ECM-derived surgical scaffold biomaterials, J Biomed Mater Res B Appl Biomater 105(3) (2017) 585-593.

[19] M.J. Cronce, R.A. Faulknor, I. Pomerantseva, X.H. Liu, S.M. Goldman, E.C. Ekwueme, O. Mwizerwa, C.M. Neville, C.A. Sundback, In vivo response to decellularized mesothelium scaffolds, J Biomed Mater Res B Appl Biomater 106(2) (2018) 716-725.

[20] J. Kim, A. Kaminsky, J. Summitt, W. Thayer, New innovations for deep partial-thickness burn treatment with ACell MatriStem matrix, Adv Wound Care (New Rochelle) 5(12) (2016) 546-552.

[21] D. Heimbach, G. Warden, A. Luterman, M. Jordan, N. Ozobia, C. Ryan, D. Voigt, W. Hickerson, J. Saffle, F. DeClement, R. Sheridan, A. Dimick, Multicenter postapproval clinical trial of Integra dermal regeneration template for burn treatment, J Burn Care Rehabil 24(1) (2003) 42-48.

[22] X. Wang, J. Ge, E.E. Tredget, Y. Wu, The mouse excisional wound splinting model, including applications for stem cell transplantation, Nat Protoc 8(2) (2013) 302-309.

[23] S. Liu, H. Zhang, X. Zhang, W. Lu, X. Huang, H. Xie, J. Zhou, W. Wang, Y. Zhang, Y. Liu, Z. Deng, Y. Jin, Synergistic angiogenesis promoting effects of extracellular matrix scaffolds and adipose-derived stem cells during wound repair, Tissue Eng Part A 17(5-6) (2011) 725-739.

[24] M.T. Lam, A. Nauta, N.P. Meyer, J.C. Wu, M.T. Longaker, Effective delivery of stem cells using an extracellular matrix patch results in increased cell survival and proliferation and reduced scarring in skin wound healing, Tissue Eng Part A 19(5-6) (2013) 738-747.

[25] M. Li, X. Luo, X. Lv, V. Liu, G. Zhao, X. Zhang, W. Cao, R. Wang, W. Wang, In vivo human adipose-derived mesenchymal stem cell tracking after intra-articular delivery in a rat osteoarthritis model, Stem Cell Res Ther 7(1) (2016) 160.

[26] S. Baldari, G. Di Rocco, M. Piccoli, M. Pozzobon, M. Muraca, G. Toietta, Challenges and strategies for improving the regenerative effects of mesenchymal stromal cell-based therapies, Int J Mol Sci 18(10) (2017) 2087.

[27] I. Swinehart, S. Badylak, Extracellular matrix bioscaffolds in tissue remodeling and morphogenesis, Dev Dyn 245(3) (2016) 351-360.

[28] A. Sorushanova, L. Delgado, Z. Wu, N. Shologu, A. Kshirsagar, R. Raghunath, A. Mullen, Y. Bayon, A. Pandit, M. Raghunath, D. Zeugolis, The collagen suprafamily: From biosynthesis to advanced biomaterial development, Adv Mater 31(1) (2019) e1801651.

[29] H. Xing, H. Lee, L. Luo, T. Kyriakides, Extracellular matrix-derived biomaterials in engineering cell function, Biotechnol Adv 42 (2020) 107421.

[30] M. Cramer, S. Badylak, Extracellular matrix-based biomaterials and their influence upon cell behavior, Ann Biomed Eng 48(7) (2020) 2132-2153.

[31] X. Hou, C. Shi, W. Chen, B. Chen, W. Jia, Y. Guo, C. Ma, G. Ye, J. Kang, J. Dai, Transplantation of human adipose-derived mesenchymal stem cells on a bladder acellular matrix for bladder regeneration in a canine model, Biomed Mater 11(3) (2016) 031001.

[32] S.Y. Chun, G.J. Lim, T.G. Kwon, E.K. Kwak, B.W. Kim, A. Atala, J.J. Yoo, Identification and characterization of bioactive factors in bladder submucosa matrix, Biomaterials 28(29) (2007) 4251-4256.

[33] B. Yang, Y. Zhang, L. Zhou, Z. Sun, J. Zheng, Y. Chen, Y. Dai, Development of a porcine bladder acellular matrix with well-preserved extracellular bioactive factors for tissue engineering, Tissue Eng Part C Methods 16(5) (2010) 1201-1211.

[34] M. Tobita, S. Tajima, H. Mizuno, Adipose tissue-derived mesenchymal stem cells and platelet-rich plasma: Stem cell transplantation methods that enhance stemness, Stem Cell Res Ther 6 (2015) 215.

[35] S.C. Blackburn, M.P. Stanton, Anatomy and physiology of the peritoneum, Semin Pediatr Surg 23(6) (2014) 326-330.

[36] J. Kruegel, N. Miosge, Basement membrane components are key players in specialized extracellular matrices, Cell Mol Life Sci 67(17) (2010) 2879-2895.

[37] U. Lindner, J. Kramer, J. Behrends, B. Driller, N.O. Wendler, F. Boehrnsen, J. Rohwedel, P. Schlenke, Improved proliferation and differentiation capacity of human mesenchymal stromal cells cultured with basement-membrane extracellular matrix proteins, Cytotherapy 12(8) (2010) 992-1005.

[38] G.P. Huang, S. Shanmugasundaram, P. Masih, D. Pandya, S. Amara, G. Collins, T.L. Arinzeh, An investigation of common crosslinking agents on the stability of electrospun collagen scaffolds, J Biomed Mater Res A 103(2) (2015) 762-771.

[39] L. Penolazzi, S. Mazzitelli, R. Vecchiatini, E. Torreggiani, E. Lambertini, S. Johnson, S.F. Badylak, R. Piva, C. Nastruzzi, Human mesenchymal stem cells seeded on extracellular matrix-scaffold: Viability and osteogenic potential, J Cell Physiol 227(2) (2012) 857-866.

[40] S.R. Caliari, B.A. Harley, Collagen-GAG scaffold biophysical properties bias MSC lineage choice in the presence of mixed soluble signals, Tissue Eng Part A 20(17-18) (2014) 2463-2472.

[41] J. Kim, S.Y. Jeong, Y.M. Ju, J.J. Yoo, T.L. Smith, G. Khang, S.J. Lee, A. Atala, In vitro osteogenic differentiation of human amniotic fluid-derived stem cells on a poly(lactide-co-glycolide) (PLGA)-bladder submucosa matrix (BSM) composite scaffold for bone tissue engineering, Biomed Mater 8(1) (2013) 014107.

[42] P.C. Baer, H. Geiger, Adipose-derived mesenchymal stromal/stem cells: Tissue localization, characterization, and heterogeneity, Stem Cells Int 2012 (2012) 812693.

[43] T. Fink, V. Zachar, Adipogenic differentiation of human mesenchymal stem cells, Methods Mol Biol 698 (2011) 243-251.

[44] M.S. Lach, J. Wroblewska, K. Kulcenty, M. Richter, T. Trzeciak, W.M. Suchorska, Chondrogenic differentiation of pluripotent stem cells under controllable serum-free conditions, Int J Mol Sci 20(11) (2019) 2711.

[45] H. Cho, A. Lee, K. Kim, The effect of serum types on chondrogenic differentiation of adipose-derived stem cells, Biomater Res 22 (2018) 6.

[46] B.T. Estes, B.O. Diekman, J.M. Gimble, F. Guilak, Isolation of adipose-derived stem cells and their induction to a chondrogenic phenotype, Nat Protoc 5(7) (2010) 1294-1311.

[47] F. Hildner, A. Peterbauer, S. Wolbank, S. Nurnberger, S. Marlovits, H. Redl, M. van Griensven, C. Gabriel, FGF-2 abolishes the chondrogenic effect of combined BMP-6 and TGF-beta in human adipose derived stem cells, J Biomed Mater Res A 94(3) (2010) 978-987.

[48] L. Huang, L. Yi, C. Zhang, Y. He, L. Zhou, Y. Liu, L. Qian, S. Hou, T. Weng, Synergistic effects of FGF-18 and TGF-β3 on the chondrogenesis of human adipose-derived mesenchymal stem cells in the pellet culture, Stem Cells Int 2018 (2018) 7139485-7139485.

[49] A. Klinger, M. Kawata, M. Villalobos, R.B. Jones, S. Pike, N. Wu, S. Chang, P. Zhang, P. DiMuzio, J. Vernengo, P. Benvenuto, R.D. Goldfarb, K. Hunter, Y. Liu, J.P. Carpenter, T.N. Tulenko, Living scaffolds: surgical repair using scaffolds seeded with human adipose-derived stem cells, Hernia 20(1) (2016) 161-170.

[50] X. Zhou, J. Wang, X. Huang, W. Fang, Y. Tao, T. Zhao, C. Liang, J. Hua, Q. Chen, F. Li, Injectable decellularized nucleus pulposus-based cell delivery system for differentiation of adipose-derived stem cells and nucleus pulposus regeneration, Acta Biomater 81 (2018) 115-128.

[51] G. Zhong, J. Yao, X. Huang, Y. Luo, M. Wang, J. Han, F. Chen, Y. Yu, Injectable ECM hydrogel for delivery of BMSCs enabled full-thickness meniscus repair in an orthotopic rat model, Bioact Mater 5(4) (2020) 871-879.

[52] J.E. Millan-Rivero, C.M. Martinez, P.A. Romecin, S.D. Aznar-Cervantes, M. Carpes-Ruiz, J.L. Cenis, J.M. Moraleda, N.M. Atucha, D. Garcia-Bernal, Silk fibroin scaffolds seeded with Wharton's jelly mesenchymal stem cells enhance re-epithelialization and reduce formation of scar tissue after cutaneous wound healing, Stem Cell Res Ther 10(1) (2019) 126.

[53] K.C. Rustad, V.W. Wong, M. Sorkin, J.P. Glotzbach, M.R. Major, J. Rajadas, M.T. Longaker, G.C. Gurtner, Enhancement of mesenchymal stem cell angiogenic capacity and stemness by a biomimetic hydrogel scaffold, Biomaterials 33(1) (2012) 80-90.

[54] Z. Zhu, Z.Q. Yuan, C. Huang, R. Jin, D. Sun, J. Yang, X.S. Luo, Pre-culture of adipose-derived stem cells and heterologous acellular dermal matrix: Paracrine functions promote post-implantation neovascularization and attenuate inflammatory response, Biomed Mater 14(3) (2019) 035002.

[55] M. Velier, S. Simoncini, M. Abellan, P. Francois, S. Eap, A. Lagrange, B. Bertrand, A. Daumas, B. Granel, B. Delorme, F. Dignat George, J. Magalon, F. Sabatier, Adipose-

derived stem cells from systemic sclerosis patients maintain pro-angiogenic and antifibrotic paracrine effects in vitro, J Clin Med 8(11) (2019) 1979.

[56] L. Mazini, L. Rochette, M. Amine, G. Malka, Regenerative capacity of adipose derived stem cells (ADSCs), comparison with mesenchymal stem cells (MSCs), Int J Mol Sci 20(10) (2019) 2523.

[57] J.Q. Coentro, E. Pugliese, G. Hanley, M. Raghunath, D.I. Zeugolis, Current and upcoming therapies to modulate skin scarring and fibrosis, Adv Drug Deliv Rev 146 (2019) 37-59.

[58] M. Xue, C. Jackson, Extracellular matrix reorganization during wound healing and its impact on abnormal scarring, Adv Wound Care (New Rochelle) 4(3) (2015) 119-136.

[59] G. Damodaran, W.H. Tiong, R. Collighan, M. Griffin, H. Navsaria, A. Pandit, In vivo effects of tailored laminin-332 alpha3 conjugated scaffolds enhances wound healing: A histomorphometric analysis, J Biomed Mater Res A 101(10) (2013) 2788-2795.

[60] S. Tyeb, P.A. Shiekh, V. Verma, A. Kumar, Adipose-derived stem cells (ADSCs) loaded gelatin-sericin-laminin cryogels for tissue regeneration in diabetic wounds, Biomacromolecules 21(2) (2020) 294-304.

Chapter 5

Summary, limitations, future directions and conclusions

5.1. Introduction

While biomaterials are an indispensable tool in tissue engineering and regenerative medicine, it is acknowledged that, with the current technologies, no human-developed material can match the extracellular matrix's (ECM) native structure, composition and biofunctionality. In this matter, decellularised tissue grafts offer a material source that faithfully maintains the native ECM properties and, therefore, benefits of them. Among them, tissue grafts from animal origin or xenografts pose the advantage of higher availability than autografts and allografts [1-4], making them attractive for use in clinics. In fact, appropriately processed xenografts are related to a high remodelling and low immune response *in vivo*, which boosts their regenerative potential [5-7].

Nonetheless our understanding of tissue grafts behaviour *in vivo* and interaction with the host upon implantation is still in an early stage. This is illustrated by the fact that, even though processing techniques have improved and many xenografts are commercially available for their use in clinics, scattered results with the same tissue graft have been observed in clinical studies [8-11]. In addition, although xenografts are a valuable option in clinical scenarios like hernia repair, skin replacement or reconstructive surgery, in other fields like tendon repair and bone regeneration, they seem far from obtaining solid positive clinic outcomes [12-15]. Thus, there is need for investigating new materials and their performance in fields where their potential is yet to be demonstrated.

Herein, we ventured to assess the potential of porcine peritoneum, which despite its advantageous features observed in several preclinical studies [16-18] and breast reconstruction [11], remains an under-investigated but readily available xenograft source. Therefore, we investigated the potential of decellularised porcine peritoneum in three different regenerative medicine applications: as a tendon antiadhesion barrier, as a skin wound dressing and as a stem cell carrier.

5.2. Summary

In chapter 2, the potential of decellularised porcine peritoneum as an antiadhesion barrier for tendon was assessed. To this end, its biochemical, biophysical, and biological properties were compared to a commercially available collagen/GAG scaffold used as antiadhesion barrier. Biochemical analysis showed the ECM components and structure preservation of the porcine peritoneum together with a lower crosslinking ratio than the collagen/GAG scaffold, whilst the biophysical analysis showed a differential topography between sides of the porcine peritoneum and a lower coefficient of friction in the tissue graft. Regarding the biological response, it was observed that porcine peritoneum

presented a higher cytocompatibility with tenocytes and acted as an effective isolating barrier for dermal fibroblasts and tenocytes. In addition, no immune reaction *in vitro* on macrophages was elicited by the porcine peritoneum, whilst the collagen/GAG scaffold triggered an inflammatory reaction.

In chapter 3, the aptitude of porcine peritoneum (PM-PC) as skin wound dressing was assessed by comparing its biochemical and biological properties to clinically available dressings: a collagen-oxidized regenerated cellulose (CORC-PG) scaffold, an ovine forestomach (OF-EF), a porcine urinary bladder (PUB-MS) and the only commercially available porcine peritoneum (PM-MB), which is employed in soft tissue regeneration. All tissue grafts showed a multicomponent structure, whilst maintaining the tissue structure and ECM components (ECM proteins and growth factors). As per adult dermal fibroblasts response, tissue grafts presented higher cytocompatibility and their basement membrane sides enhanced their proliferation, whilst none of the materials elicited an immune reaction *in vitro* by THP-1 cells. Angiogenesis analysis showed how porcine urinary bladder and porcine peritoneum (PM-PC) had a higher angiogenetic effect *ex vivo*, related to a higher content of growth factors.

In chapter 4, the capacity of decellularised porcine peritoneum as a stem cell carrier was assessed. To this end, its effect on human adipose derived stem cells (hADSC) phenotype *in vitro* and its efficacy at delivering these cells in a full-thickness wound murine mice model were assessed. Results were correlated to those obtained with hADSC direct injections at the wound and two materials: a collagen/GAG scaffold and a porcine urinary bladder (both with and without hADSC). Results showed that tissue grafts had a higher cytocompatibility, particularly in the basement membrane side, which enhanced cell proliferation. None of the materials affected hADSC phenotype. *In vivo* results demonstrated the capacity of the materials at delivering cells. Tissue grafts promoted a longer presence of cells in the wound site. Histology analysis confirmed the regenerative effect of hADSC delivered by the materials even using half of the cell load than the injection. In addition, when porcine peritoneum delivered the cells on its basement membrane side, an enhanced angiogenesis was observed.

5.3. Limitations and future directions

Although objectives were met and the potential of porcine peritoneum in both three scenarios was demonstrated, studies carried out present some limitations, which give an opportunity to be addressed in future studies. These aspects are discussed in this section.

5.3.1. Decellularised porcine peritoneum as a tendon barrier biomaterial

Although a complete *in vitro* analysis was carried out to demonstrate the potential of porcine peritoneum as antiadhesion barrier, the *in vitro* settings tested are not representative enough of the complex environment in the healing tendon and adhesion formation [19-21]. This, therefore, should be evaluated with an *in vivo* model, which includes analysis at molecular (inflammatory and fibrinolytic pathways), histological (material re-absorption, adhesion formation, tissue remodelling) and functional (biomechanical analysis, degree of flexion) levels. Such analysis would serve to confirm the observations found in this chapter and further confirm the potential of porcine peritoneum for this application. A pilot rabbit flexor tendon repair model study was conducted, with preliminary data demonstrating absence of foreign body / inflammatory reaction to porcine peritoneum. Therefore, a full study should be conducted that will include analysis for inflammatory markers in macrophages, presence of fibrinolytic pathway molecules and biomechanical analysis in repaired tendons.

5.3.2. Porcine peritoneum matrix as a biomaterial for wound healing applications

Similarly to the previous chapter, the *in vitro* analysis carried out to evaluate the potential of porcine peritoneum as wound healing biomaterial, although complete and accurate, is not fully representative of the skin wound healing scenario, where many correlated molecular pathways and different cell types play their own role [22, 23]. Therefore, further analysis *in vivo* employing these materials as wound healing materials would serve as corroboration of the events observed in this chapter.

5.3.3. Decellularised porcine peritoneum as a stem cell carrier

In this part of the project, we employed an established splinted full-thickness wound model in athymic mice to assess the performance of the used materials as stem cell delivery vehicles. Despite the suitability of the model for this end [24, 25], it presents limitations. Whereas this model allows the delivery of xenogeneic cells, it does not fully recapitulate the expected response to the materials with and without cells, since adaptative immunity is a crucial role-player in these scenarios [26-28]. Also, the intrinsic characteristics of the model (i.e. material exposure to air, desiccation, scar formation, skin stretching due to animal movement) may have affected hADSC viability and behaviour, although these events were equally likely in all conditions / animals. Finally, all groups presented an almost complete healing at the end of the study, which suggests that further

studies should directed to more challenging models, such as diabetic non-healing wounds or larger initial wound gaps.

5.3.4. Other future directions

Despite the extensive and accurate analysis carried out on porcine peritoneum in this study, little is known about how this decellularised tissue graft behaves upon implantation by only few preclinical studies and clinical studies [16-18]. Future studies investigating its composition and the composition of its degradation products through proteomics would add valuable information to the current findings, as recent studies show in other decellularised tissue grafts employed in clinics [27], further substantiating the mechanism of action which motivates the observed results. In addition, recent investigations have also shown that decellularised tissue grafts preserve matrix bound vesicles (MBV) [29], which have an important effect on the hosts immune response and the material's regenerative potential. Finally, the positive results observed in this project motivate the investigation of porcine peritoneum potential in other clinical fields such as hernia repair, tendon augmentation or nerve regeneration, for which of each application specific *in vitro* and *in vivo* studies would be required.

5.4. Conclusions

The present thesis has demonstrated the potential of decellularised porcine peritoneum as antiadhesion barrier, wound dressing and stem cell delivery system thanks to its preserved properties after processing (i.e. structure, composition and biological activity). These findings support further research on porcine peritoneum in the aforementioned fields in preclinical and clinical studies, whilst opens the door for its evaluation for other clinical fields.

5.5. References

[1] J.N. Parrish, S.E. Metzinger, Autogenous fat grafting and breast augmentation: a review of the literature, Aesthet. Surg. J. 30(4) (2010) 549-56.

[2] P.C. Parodi, L. Moretti, G. Saggin, F. De Biasio, V. Alecci, L. Vaienti, Soft tissue and tendon reconstruction after achilles tendon rupture: adipofascial sural turnover flap associated with cryopreserved gracilis tendon allograft for complicated soft tissue and achilles tendon losses. A case report and literature review, Ann. Ital. Chir. 77(4) (2006) 361-7.

[3] G.B. Luciani, F. Santini, A. Mazzucco, Autografts, homografts, and xenografts: overview on stentless aortic valve surgery, J. Cardiovasc. Med. 8(2) (2007) 91-96.

[4] H.V. Precheur, Bone graft materials, Dent. Clin. North Am. 51(3) (2007) 729-46, viii.

[5] T.J. Keane, R. Londono, N.J. Turner, S.F. Badylak, Consequences of ineffective decellularization of biologic scaffolds on the host response, Biomaterials 33(6) (2012) 1771-1781.

[6] S.F. Badylak, T.W. Gilbert, Immune response to biologic scaffold materials, Semin. Immunol. 20(2) (2008) 109-16.

[7] K. Sadtler, M.T. Wolf, S. Ganguly, C.A. Moad, L. Chung, S. Majumdar, F. Housseau, D.M. Pardoll, J.H. Elisseeff, Divergent immune responses to synthetic and biological scaffolds, Biomaterials 192 (2019) 405-415.

[8] M.M. Abdelfatah, N. Rostambeigi, E. Podgaetz, M.G. Sarr, Long-term outcomes (>5-year follow-up) with porcine acellular dermal matrix (Permacol) in incisional hernias at risk for infection, Hernia 19(1) (2015) 135-40.

[9] F. Catena, L. Ansaloni, F. Gazzotti, S. Gagliardi, S. Di Saverio, L. D'Alessandro, A.D. Pinna, Use of porcine dermal collagen graft (Permacol) for hernia repair in contaminated fields, Hernia 11(1) (2007) 57-60.

[10] T. Eisenberg, Implant exposure through a breast augmentation incision repaired with porcine acellular dermal matrix (Strattice): a technique to ensure graft take, Aesthetic Plast. Surg. 35(4) (2011) 681-3.

[11] N.S. Hillberg, P.I. Ferdinandus, R.E.G. Dikmans, B. Winkens, J. Hommes, R.R.W.J. van der Hulst, Is single-stage implant-based breast reconstruction (SSBR) with an acellular matrix safe?: Strattice™ or Meso Biomatrix® in SSBR, Eur. J. Plast. Surg. 41(4) (2018) 429-438.

[12] F.A. Barber, M.A. Herbert, D.A. Coons, Tendon augmentation grafts: biomechanical failure loads and failure patterns, Arthroscopy 22(5) (2006) 534-8.

[13] U.G. Longo, A. Lamberti, N. Maffulli, V. Denaro, Tendon augmentation grafts: A systematic review, Br. Med. Bull. (2010) ldp051.

[14] Y. Fillingham, J. Jacobs, Bone grafts and their substitutes, Bone Joint J 98-B(1 Suppl A) (2016) 6-9.

[15] H.J. Haugen, S.P. Lyngstadaas, F. Rossi, G. Perale, Bone grafts: which is the ideal biomaterial?, J. Clin. Periodontol. 46 Suppl 21(S21) (2019) 92-102.

[16] M.J. Cronce, R.A. Faulknor, I. Pomerantseva, X.H. Liu, S.M. Goldman, E.C. Ekwueme, O. Mwizerwa, C.M. Neville, C.A. Sundback, In vivo response to

decellularized mesothelium scaffolds, J. Biomed. Mater. Res. B Appl. Biomater. 106(2) (2018) 716-725.

[17] A. Bramos, D.P. Perrault, A.N. Fedenko, G.H. Kim, S. Bougioukli, J.R. Lieberman, J.W. Calvert, A.K. Wong, Porcine mesothelium-wrapped diced cartilage grafts for nasal reconstruction, Tissue Eng Part A 24(7-8) (2018) 672-681.

[18] D.M. Hoganson, G.E. Owens, E.M. O'Doherty, C.M. Bowley, S.M. Goldman, D.O. Harilal, C.M. Neville, R.T. Kronengold, J.P. Vacanti, Preserved extracellular matrix components and retained biological activity in decellularized porcine mesothelium, Biomaterials 31(27) (2010) 6934-6940.

[19] H. Capella-Monsonis, S. Kearns, J. Kelly, D.I. Zeugolis, Battling adhesions: from understanding to prevention, BMC Biomed Eng 1(1) (2019) 5.

[20] G.M. Saed, M.P. Diamond, Molecular characterization of postoperative adhesions: the adhesion phenotype, J. Am. Assoc. Gynecol. Laparosc. 11(3) (2004) 307-14.

[21] Z. Alpay, G.M. Saed, M.P. Diamond, Postoperative adhesions: from formation to prevention, Semin. Reprod. Med., Thieme Medical Publishers, 2008, pp. 313-321.

[22] A.J. Singer, R.A. Clark, Cutaneous wound healing, N. Engl. J. Med. 341(10) (1999) 738-46.

[23] E.R. Zielins, D.A. Atashroo, Z.N. Maan, D. Duscher, G.G. Walmsley, M. Hu, K. Senarath-Yapa, A. McArdle, R. Tevlin, T. Wearda, K.J. Paik, C. Duldulao, W.X. Hong, G.C. Gurtner, M.T. Longaker, Wound healing: an update, Regen. Med. 9(6) (2014) 817-30.

[24] S. Liu, H. Zhang, X. Zhang, W. Lu, X. Huang, H. Xie, J. Zhou, W. Wang, Y. Zhang, Y. Liu, Z. Deng, Y. Jin, Synergistic angiogenesis promoting effects of extracellular matrix scaffolds and adipose-derived stem cells during wound repair, Tissue Eng Part A 17(5-6) (2011) 725-39.

[25] M.T. Lam, A. Nauta, N.P. Meyer, J.C. Wu, M.T. Longaker, Effective delivery of stem cells using an extracellular matrix patch results in increased cell survival and proliferation and reduced scarring in skin wound healing, Tissue Eng Part A 19(5-6) (2013) 738-47.

[26] M.T. Wolf, S. Ganguly, T.L. Wang, C.W. Anderson, K. Sadtler, R. Narain, C. Cherry, A.J. Parrillo, B.V. Park, G. Wang, F. Pan, S. Sukumar, D.M. Pardoll, J.H. Elisseeff, A biologic scaffold-associated type 2 immune microenvironment inhibits tumor formation and synergizes with checkpoint immunotherapy, Sci. Transl. Med. 11(477) (2019).

[27] K. Sadtler, S.D. Sommerfeld, M.T. Wolf, X. Wang, S. Majumdar, L. Chung, D.S. Kelkar, A. Pandey, J.H. Elisseeff, Proteomic composition and immunomodulatory properties of urinary bladder matrix scaffolds in homeostasis and injury, Semin. Immunol. 29 (2017) 14-23.

[28] Y.H. Wang, D.B. Wu, B. Chen, E.Q. Chen, H. Tang, Progress in mesenchymal stem cell-based therapy for acute liver failure, Stem Cell. Res. Ther. 9(1) (2018) 227.

[29] L. Huleihel, J.G. Bartolacci, J.L. Dziki, T. Vorobyov, B. Arnold, M.E. Scarritt, C. Pineda Molina, S.T. LoPresti, B.N. Brown, J.D. Naranjo, S.F. Badylak, Matrix-bound nanovesicles recapitulate extracellular matrix effects on macrophage phenotype, Tissue Eng Part A 23(21-22) (2017) 1283-1294.

Chapter 6

Appendices

A. List of protocols

A.1. Cell culture

A.1.1. Cell thawing and passaging

1. Remove vial from liquid nitrogen container and thaw in water bath at 37 ºC.
2. Transfer contents to culture flask of appropriate size and add pre-warmed culture medium.
3. Change medium every 2-3 days and monitor cell proliferation with a phase contrast microscope.
4. When cells cover more than 80 % of the culture flask, remove culture medium, wash cell layer with Phosphate Buffer Solution (PBS) and add 5 ml of trypsin / EDTA. Incubate at 37 ºC for 5 minutes until cells start detaching. Assist the detachment by gentle tapping.
5. Add 5 ml of culture medium to neutralise the action of trypsin / EDTA and transfer flask contents into a tube and centrifuge at 1,200 rpm for 5 minutes.
6. Discard the supernatant and resuspend cells in desired amount of medium.

A.1.2. Cell freezing

1. Aspirate culture medium and wash cell layer with PBS.
2. Add trypsin / EDTA and incubate at 37 ºC for 5 minutes. Tap gently.
3. Add culture medium to neutralise the action of trypsin, collect flask contents into a tube and centrifuge at 1,200 rpm for 5 minutes.
4. Resuspend supernatant in 1 ml of medium and count cells using a Neubauer chamber.
5. Resuspend cells in necessary amount of freezing medium (90% growth medium with 10 % of DMSO) to have 1 million cells per millilitre of medium.
6. Add 1 ml of cell suspension per cryogenic vial and place in Mr. Frosty overnight at -80 ºC.
7. Move to liquid nitrogen for long term storage.

A.2. Collagen material characterisation techniques

The techniques employed throughout this thesis to analyse collagen scaffolds and collagen tissue grafts including:

1. SDS-PAGE
2. Free amine analysis through ninhydrin and TNBSA assays
3. Differential scanning calorimetry
4. Collagen quantification through hydroxyproline assay
5. Enzymatic degradation

Are accurately described and available in the protocol publication:

Capella-Monsonís H, Coentro JQ, Graceffa V, Wu Z, Zeugolis DI. *An experimental toolbox for characterization of mammalian collagen type I in biological specimens*. **Nat Protoc**. 2018 ;**13**(3):507-529

From which Héctor Capella-Monsonís is first author, where he contributed with the design of the experiments, experimental work and writing of the paper.

A.3. alamarBlue® assay

1. Prepare a 10 % alamarBlue® solution in PBS.
2. Remove culture medium from the cells and wash with PBS.
3. Add 1 ml of the diluted alamarBlue® solution to the cells and a negative control of alamarBlue® at 10 % alone
4. To obtain the background absorbance, add PBS to empty wells.
5. Incubate for 4 hours at 37 ºC, 5 % CO_2.
6. Transfer 100 µl of the alamarBlue® solution and of the negative control and background to a clear 96 well plate.
7. Measure the absorbance at 550 nm and at 595 nm.
8. Subtract the values of HBSS to the values of alamarBlue® alone from both absorbances to obtain the absorbance of alamarBlue®. For 550 nm this value is called absorbance of the oxidised form at lower wavelength (AOLW) and for 595 nm it is called absorbance of the oxidised form at higher wavelength (AOHW).
9. Calculate the correlation factor: $Ro = \frac{AOLW}{AOHW}$
10. To calculate the percentage of alamarBlue® reduced (AR) by the cells use the following: AR=ALW-(AHW*Ro) *100

A.4 Live / Dead assay

1. Prepare staining solution by diluting calcein AM to 4 µM and ethidium homodimer-1 to 2 µM in PBS.
2. To prepare a negative control, sample can be immersed in dimethyl sulfoxide (DMSO) to kill all cells before staining.
3. Remove culture medium from the cells and wash cells with PBS.
4. Add staining solution to cells (enough volume to cover completely the sample).
5. Incubate at 37 ºC, 5 % CO_2 for 30 minutes.
6. Image under inverted fluorescence microscope:

A.5. PicoGreen® assay

1. Remove the media and gently rinse the cells with PBS.

2. Add DNAse free water and carry out three freeze-thaw cycles at -80 ºC to break the cells and release the DNA. If necessary, employ digestion protocols.

3. Prepare solutions for DNA standard curve in DNAse free water using the **Table D.1**.

4. Make up the calculations for the amount of necessary diluted PicoGreen® solution (Concentrated PicoGreen® solution in TE buffer 1x), following the equation below and accounting for the number of wells necessary (add some more as a precaution) for the standard curve and the samples, at least in triplicate:

$$\text{PG 200x (µl)} = \frac{71.3\text{µl} * \text{Number of wells}}{200}$$

PG 200x - concentrated PicoGreen® solution in TE 1x buffer.

$$\text{TE 1x (µl)} = (71.3\text{µl} * \text{Number of wells}) - \text{PG200x}$$

TE 1x – Diluted TE buffer 1x

5. Make up the calculations for the amount of necessary diluted TE buffer® solution (concentrated TE buffer 20x in DNAse free water), following the equation below and accounting for the number of wells necessary for the standard curve and the samples, at least in triplicate:

$$\text{TE 20x (µl)} = \frac{(100\text{µl} * \text{Number of wells})}{20}$$

TE 20x – Concentrated TE buffer 20x

TE 1x - Diluted TE buffer 1x

Table 6.1. Detailed standard curve for DNA quantification.

Final DNA concentration (ng / ml)	Volume of DNA standard (µl)	Volume of DNAse free water (µl)
2000	20	980
1000	10	990
500	5	995
375	3.75	996.25
200	2	998
0	0	1000

6.Add 100µl of TE buffer (1x), 71.3 µl of diluted PicoGreen® solution and 28.7 µl of samples / standard to an opaque, flat-bottom 96-well plate. Protect the plate from the light (e.g. with aluminium foil).

7. Gently agitate the well plate in a shaker for 2 minutes.

8. Incubate at room temperature for 5 to 8 minutes in the dark.

9. Read the plate for fluorescence (excitation: ~480nm; emission: ~520nm).

10. Plot a graph concentration *vs.* the fluorescence values. Determine the concentration of DNA as a function of the standard curve.

A.6. Histological stainings

A.6.1. Haematoxylin – Eosin Staining

Reagents needed:

- Mayer's Haematoxylin
- Eosin (0.15 g Eosin Y in 100 ml 50% EtOH + 50 µl Acetic acid)
- 1% Acetic Acid
- Graded alcohols and Xylene for Rehydration and Dehydration

1. Take slides out from – 80 °C freezer and let them dry at room temperature for 10 minutes

2. Before starting the staining, incubate in PBS for 10 mins.

3. Proceed with the staining.

- Mayer's Haematoxylin - 5 -10 min
- Stop reaction in 1 % Acetic Acid
- Bluing: running tap water - 5-15 min (colour change: red → blue)
- Eosin- 20-30 sec
- Stop reaction in 1% Acetic Acid

Dehydration

- EtOH 70 % - <30 sec (Eosin will be washed out)
- EtOH 96 % - 30 sec - 1 min
- EtOH 100 % I - 30 sec - 1 min
- EtOH 100 % II - 30 sec - 1 min
- Xylene I - 2 min
- Xylene II - 2 min – until mounting
- Mounting with dibutylphthalate polystyrene xylene (DPX)

A.6.2. Masson Goldner Trichrome Staining

Reagents needed:

- Weigert's Iron-Haematoxylin
    - Weigert A – Haematoxylin solution (X906.1, Carl Roth)
    - Weigert B - Ferric chloride solution (X907, Carl Roth)
    - Freshly prepare a 1:1 mixture of solution A and B (solution is stable up to 8 days at RT)
- 1% Acetic Acid
- Goldner I solution (Ponceau – Acidfuchsin)
- Goldner II solution (Phosphotungstic acid - Orange G)
- Goldner III solution (Light green SF yellowish)
- Graded alcohols and Xylene for Rehydration and Dehydration

1. Take slides out from – 80 °C freezer and let them dry at room temperature for 10 minutes
2. Before starting the staining, incubate in PBS for 10 mins.
3. Proceed with the staining.

- Weigert's Iron-Haematoxylin - 3 min
- Stop reaction in 1% Acetic Acid
- 0.5% HCl-EtOH - 5 sec (dip 1-2x) → for de-staining of connective tissue
- Bluing: running tap water - 5-15 min (colour change: brown-blue → blue)
- Goldner I solution - 5-10 min
- Stop reaction in 1% Acetic Acid
- Goldner II solution - 1-3 min (until connective tissue is de-stained)
- Stop reaction in 1% Acetic Acid
- Goldner III - 2-5 min (up to 20 min)
- Stop reaction in 1% Acetic Acid

Dehydration

- EtOH 70 % - <30 sec
- EtOH 96 % - 30 sec - 1 min
- EtOH 100 % I - 30 sec - 1 min
- EtOH 100 % II - 30 sec - 1 min
- Xylene I - 2 min
- Xylene II - 2 min – until mounting

A.6.3. Picrosirius red

Reagents needed:

- Dissolve 0.1g Siriusred in 100 ml saturated aqueous solution of Picric acid (= 1.2 % in H_2O).

1. Take slides out from – 80 °C freezer and let them dry at room temperature for 10 minutes
2. Before starting the staining, incubate in PBS for 10 mins.
3. Proceed with the staining:
    - Stain section with Picrosirius red solution
    - Stop reaction in 1 % Acetic Acid

Dehydration

- EtOH 70 % - <30 sec
- EtOH 96 % - 30 sec - 1 min
- EtOH 100 % I - 30 sec - 1 min
- EtOH 100 % II - 30 sec - 1 min
- Xylene I - 2 min
- Xylene II - 2 min – until mounting

A.7. Immunocytochemistry

1. At the end of culture time points, aspirate the medium and was cell layer with PBS.
2. Fix with 4 % PFA (pre-cooled at 4 °C) for 20 minutes.
3. To make 4 % PFA (in glass bottle with magnetic stirrer): Weight 0.4 g of PFA and add 10 ml of PBS. Put on a magnetic stirrer with heater. Leave it for around 1 hour (put the cap on but loosen it). Cool it and keep it at 4 °C.
4. Drain away fixative and wash 3x with PBS, 5 minutes each.
5. Block with 3 % (w / v) BSA in 1x PBS for 30 minutes at room temperature (RT). To make 3 % BSA: weight 0.3 g of BSA and add 10 ml of PBS. Put on a magnetic stirrer and leave it for around 1 hour. Store it at 4 °C.
6. Incubate with primary antibody in 3 % BSA overnight at 4 °C.
7. Wash 3x with 1x PBS, 5 minutes each.
8. Incubate with secondary antibody in 1x PBS for 1 hour at room temperature.
9. Wash 3x with 1x PBS, 5 minutes each.
10. Incubate with DAPI in 1x PBS for 5 minutes at room temperature.

11. Wash 3x with PBS, 5 minutes each.
12. Image samples on Olympus IX-81 inverted fluorescence microscope.

A.8.Trilineage differentiation of adipose derived mesenchymal stem cells

A.8.1. Osteogenic differentiation

Osteogenic medium

- Complete Basal Medium:
  - GlutaMax™ (α-MEM)
  - 10% FBS
  - 1% P / S
- 100 nM Dexamethasone (10^{-7}M) (Stocks of dexamethasone 1mM (10,000X) in pure ethanol)
- 50 μM Ascorbic acid-2-phosphate (stock: 129.5 mM in PBS)
- 10 mM β-Glycerophosphate disodium salt hydrate (1M stocks in H_2O)

Procedure

1. Seed human adipose stem cells in multi-well plates and culture until confluent.
2. Treat cells with osteogenic differentiation medium by changing medium every 3 days for 21 days. Freshly prepare medium before use and filter sterile.

A.8.2. Adipogenic differentiation

Adipogenic Maintenance Medium (up to 21 days)

- Complete Basal Medium:
  - GlutaMax™ (α-MEM)
  - 10% FBS
  - 1% P / S
- 1 μM Dexamethasone (1 mM stocks in pure ethanol)
- 1 μM Rosiglitazone (28 mM stocks in DMSO, 10 mg / ml)
- 0.5 mM 3-Isobutyl-1-Methyl-Xanthine IBMX (500 mM stocks, 1000X, in DMSO)
- Insulin (10 μg / ml)

Adipogenic Maintenance Medium (up to 21 days)

- Complete Basal Medium:
  - GlutaMax™ (α-MEM)
  - 10 % FBS

  - 1 % P / S
- Insulin (10 µg / ml)

Procedure:

Seed human adipose stem cells in multi-well plates and culture until confluent. Treat cells with adipogenic induction medium for 7 days and subsequent adipogenic maintenance medium for up to 21 days.

A.8.3. Chondrogenic differentiation

Chondrogenic medium

- DMEM High-Glucose
  - 1 % P / S (optional)
- 100 nM Dexamethasone (10^{-7} M, 39.25 ng / ml)
  - Prepare stocks of dexamethasone 1 mM (10,000X stocks, 0.392 mg/ml) in pure ethanol
- 100X ITS+1 Liquid Media Supplement (Contains 1.0 mg / ml bovine insulin, 0.55 mg / ml human transferrin (substantially iron-free), 0.5 µg / ml sodium selenite, 50 mg / ml bovine serum albumin and 470 µg / ml linoleic acid at the 100X concentration)
- 40 µg / ml L-Proline (347.43 µM) (0.1M stocks in PBS)
- 37.5 µg / ml Ascorbic acid-2-phosphate (129.5 µM) (1000X stocks in PBS, 129.5 mM)
- 10 ng / ml recombinant human TGF-β3 or (TGF-β1). Reconstitute at 50 µg/ml in 4mM HCl (store at -20°C)

Procedure for micro-mass pellet

1. Prepare cell suspension with 2.5 x 10^5 cells / pellet and resuspend in in 200 µl chondrogenic medium:
2. Add cell suspension (containing 2.5 x 10^5 cells) to a round-shape well of 96 well-plate and place in incubator at 37°C and 5% CO2. Change medium every 3 days
3. Quality control: At first medium change the pellet should be compact and nearly spherical (should already be after 24 h). Forcefully add medium to make the pellet float and prevent zone of necrosis at the bottom of the well
4. Keep in chondrogenic medium for 21 days
5. Prepare control pellets in complete basal media

Procedure for scaffold / TCP

Seed human adipose stem cells in multi-well plates and culture until confluent. Treat cells with chondrogenic media up to 21 days

Fixation of pellets

1. Fix pellets in 4% PFA - up to 1 hour on 4 °C (shaker)
2. Wash with PBS at 4°C.
3. Cryoprotection (for cryo-embedding)
    - Incubate in 15 % Sucrose-PBS at 4°C (shaker) (1 hour – up to several days)
    - Incubate in 30 % Sucrose-PBS at 4°C (shaker) (1 hour – up to several days)
    - Optional: incubate in a 50 vol% / 50vol% mixture of 30% Sucrose-PBS and OCT (shaker) (1 hour – up to several days)
    - Optional: incubate in OCT only for 1 hour on 4°C
4. Embed the pellets in fresh OCT and snap freeze with isopentane and liquid nitrogen and store at -80 °C.
5. Cut sections between 5 and 8 µm.
6. Let slides air dry at RT for at least 1 hour. Store slides at -20 °C (avoid freeze-thaw cycles).

A.8.4. Alizarin red staining

1. Remove media, rinse with PBS
2. Fix cells with Methanol for 20 min at 4 °C
3. Wash with PBS at 4 °C.
4. Dissolve 2g of Alizarin Red S in 100 ml distilled water. Mix well and adjust pH to 4.1 ~ 4.3 (always check pH before staining and adjust pH or make fresh solution)
5. Stain cells with Alizarin Red S solution for 5- 20 mins at RT
6. Remove the dye and wash 3-5 x with deionised water to remove any unbounds stain
7. Cover with deionised water for microscopy

A.8.5. Calcium colorimetric detection (Sigma Aldrich, MAK022)

Standard curve

Dilute 10 ml of the 500 mM Calcium Standard Solution with 990 ml of water to prepare a 5 mM (0.2 mg / ml). Add 0, 2, 4, 6, 8, and 10 ml of the 5 mM standard solution into a 96 well plate, generating 0 (assay blank), 0.4, 0.8, 1.2, 1.6, and 2.0 mg / well standards. Bring the volume to a total of 50 ml with water

Sample Preparation

1. 3x Wash the cells / scaffolds with PBS

2. Add 0.2 ml of 0.5 M HCl and scratch the cells with a pipette tip. Collect and transfer to an Eppendorf.

3. Shake the tubes overnight at 4 ºC

4. Spin down the solution briefly and carry out the assay on the supernatant

Assay Reaction

1. Add 90 ml of the Chromogenic Reagent to each well containing standards, samples, or controls. Mix gently.

2. Add 60 ml of Calcium Assay Buffer to each well and mix gently.

3. Incubate the reaction for 5–10 minutes at room temperature. Protect the plate from light during incubation.

4. Measure the absorbance at 575 nm (A575) and calculate the concentration employing the standard curve

A8.6. Oil red O staining

1.Remove media, rinse with PBS

2. Fix cells with 4 % PFA for 20 min at 4 °C

3. Wash with PBS at 4 °C

4. Dissolve 0.5g of Oil red O stock in 100 ml of isopropanol using gentle heat

5. Prepare working solution diluting 30 ml of stock oil red O stain with 20 ml distilled water (3 parts + 2 parts - 3:5). Stain should be made up fresh from the stock solution each time

6. Incubate 10 min, filter the solution 2 times.

7. Stain cells with Oil Red O staining solution for 15 - 30min at RT

8. Wash 3x with PBS or deionised water

9. Cover with deionised water for microscopy

Semi-quantitative analysis of Oil Red O staining

1. After 3 washing steps, dissolve bound Oil red O in 400µL isopropanol

2. Measure absorbance at OD 540 nm

A.8.7. Alcian Blue staining

1. Take slides out from – 80 °C freezer and let them dry at room temperature for 10 minutes

2. Before starting the staining, incubate in PBS for 10 mins.

3. Proceed with the staining.

- Incubate the slides in 1 % acetic acid – 1 min (up to 5 mins)
- Stain with Alcian blue solution pH 2.5 for 30 min
- Dip slides in 1 % acetic acid
- Rinse slides briefly in distilled water
- Counterstain with nuclear fast red solution – 1 min (up to 5 mins)
- Rinse slides briefly in distilled water
- Dehydrate in 70, 90 and 100 % EtOH
- Clear in Xylene and mount

A.8.8. Blyscan™ Glycosaminoglycan Assay

1. Remove medium microwell plate and retain cell pellets.
2. Wash cells with PBS and drain. Add 250 µl of papain extraction reagent. Incubate for 3 h at 65 ºC with occasional mixing.
3. Remove digested extract from microwells and centrifuge at 10,000 g for 10 min. Retain supernatant for use with Blyscan GAG assay protocol.
4. Prepare Glycosaminoglycan standards using aliquots containing 1.0, 2.0, 3.0, 4.0 and 5.0 µg of the reference standard. Make each standard up to 100 µl using deionised water. The standards and the reagent blank (0 µg) are used to produce a calibration curve.
5. For the test samples use 100 µl of the previously digested samples.
6. To each tube add 1 ml of Blyscan dye reagent Cap tubes and mix by inverting contents and place tubes in a gentle mechanical shaker for 30 minutes During this time period a sulphated glycosaminoglycan-dye complex will form and precipitate out from the soluble unbound dye.
7. Transfer the tubes to a microcentrifuge and spin at 12,000 rpm for 10 min
8. Carefully invert and drain tubes. Any remaining droplets can be removed from the tubes by gently tapping the inverted tube on a paper tissue. Do not attempt to physically remove any fluid that is in close contact to the deposit.
9. Add dissociation reagent (0.5 ml) to tubes. Re-cap the tubes and release the bound dye into solution. When all the bound dye has been dissolved, (usually within 10 minutes), centrifuge at 12,000 rpm for 5 mins to remove foam. Keep the tubes capped until ready to measure absorbance
10. Transfer 200 µl of each sample to individual wells of a 96 micro well plate. Measure absorbance at 656 nm.

A.9. Cell transplantation into the mouse excisional wound splinting model

A.9.1. Cell fluorescent labelling

1. Suspend cells at a density of 1×10^6 / ml in any serum-free culture medium
2. Add 5 µl of the cell-labeling solution supplied per ml of cell suspension. Mix well by gentle pipetting
3. Incubate for 20 minutes at 37 °C
4. Centrifuge the labelled suspension tubes at 1,500 rpm for 5 minutes
5 Remove the supernatant and gently resuspend the cells in warm (37 °C) medium.
6 Repeat the wash procedure (4 and 5) two more times.

A.9.1. Surgery

Materials needed:

- Sterile silicon rings (2 x animals)
- Sterile disposable biopsy punches (5mm)
- 6-0 nylon sutures
- Sterile surgical tools
- Superglue
- Tegaderm® transparent dressing (3M, 2-3/8 inches x 2-3/4 inches)
- Mouse Jackets

Drugs required

- Isoflurane (Induction 5%, maintenance 1-2 %)
- Buprenorphine (analgesic – sub cutaneous injection, .05-0.1 mg / kg)
- Enrofloxacin (antibiotic – sub cutaneous injection, 5 mg / kg)

Procedure

1. Use a 12-mm-diameter circle cutter to cut discs from a 0.5-mm-thick silicone sheet, and then use a 6-mm-diameter biopsy punch to cut a small hole in the centre of each disc to form donut-like splints. Sterilise the splints the day before the surgery with an autoclave.
2. Perform preoperative clinical examination. All animals need to be observed for signs of abnormal behaviour and distress.
3. Record the accurate weigh of the animals to calculate the correct amount of medications to administer. Administer a dose of analgesic to each animal 30 minutes before the surgery.

4. Anesthetise the animals with isoflurane. Set the oxygen supply to 0.8 – 1 l / min. Put the animal in the anaesthetic chamber and set isoflurane at 5%. After the animal is fully anesthetised, reduce to ½ % for anaesthesia maintenance with an anaesthetic mask on the pre-warmed surgical table.

5. Monitor anaesthesia during the surgery by recording depth, breathing and absence of pedal reflex. The eyes need to be hydrated during the procedure.

6. Disinfect the skin surface with povidone-iodine followed by a rinse with 70% (vol / vol) ethanol.

7. Put the mouse on its side on a sterile sheet. Pull the dorsal skin of the chest from the midline with forceps, and punch through the folded skin (both layers) with a 5-mm-diameter sterile biopsy punch to create two symmetrical full-thickness excisional wounds besides the midline

8. Spread an instant-bonding adhesive (superglue) on one side of a splint and carefully place the splint around the wound (with the glue side down) so that the wound is centred within the splint

9. Secure the splint to the skin with four interrupted sutures of 6.0 nylon.

10. Apply the selected treatment (cell injection, material, PBS (sham))

11. Take photographs of individual wounds with a digital camera.

12. Completely cover the wounds and splints with Tegaderm (3M) sterile transparent dressing.

13. Adjust the tightness of the jacket so as not to restrict the breathing and movement of the mice but preventing the mice from reaching the wounds.

14. Inject analgesic and broad-spectrum antibiotic treatment prior anaesthetic recovery

15. Place the mice in individual cages in a warm environment until they are fully recovered from anaesthesia.

16. House the animals in individual cages (to avoid chewing of wounds and bandages) facility. Check the animals daily to ensure that the bandage is on.

17. At each time point, anaesthetise the animals as described. Carefully remove the jackets and the Tegaderm dressing. Take photographs of individual wounds with a digital camera. For groups including labelled cells, take fluorescent images of the animals employing the *in vivo* imaging system (IVIS® Lumina III, PerkinElmer, UK). And the Living Image® software (IVIS® Lumina, PerkinElmer, UK) for measures.

A.10. Tissue harvesting and processing

1. After 14 days, euthanise the animals using carbon dioxide (CO_2). Place all the animals in the euthanasia chamber and start pumping CO_2. This will produce rapid unconsciousness with minimal distress in the animals.
2. Upon completion of the procedure, death must be confirmed by performing cervical dislocation
3. Collect wound tissue samples using a 8-mm biopsy punch to harvest the entire wound along with the surrounding healthy skin tissue.
4. Place fresh wound tissue on a clean container and fix it in cold 4 % (wt / vol) paraformaldehyde in PBS at 4 °C for 24 hours. The sample should be submerged in the fixative.
5. On the next day, wash it with PBS on a shaker five times, for 30 min each.
6. Process the tissue with the Excelsior AS Tissue Processor (ThermoFisher) and run a routine overnight programme:
7. Cut the wound samples in half and carefully orient them in the mould. A cassette is placed on top of the mould, topped up with more wax and the whole thing is placed on a cold plate to solidify. When this is completed the block with its attached cassette can be removed from the mould and is ready for microtomy.

Table 6.2. Overnight routine protocol for tissue processing with Excelsior AS Tissue Processor (ThermoFisher).

Step	Reagent		Temp (°C)	Time (hh:mm)	Vac	Drain time (sec)
1	10% Formalin		RT	0:30	Off	30
2	10% Formalin		RT	0:30	Off	60
3	Dehydrant Group (Alcohol)	75%	30	1:00	On	30
4		90%	30	1:00	On	30
5		95%	30	1:00	On	30

6		100%	30	1:00	On	30
7		100%	30	1:00	On	30
8		100%	30	1:00	On	60
9	Clearant Group (Xylene)		30	1:00	On	30
10			30	1:00	On	30
11			30	1:00	On	120
12	Infiltration Group (Wax)		62	1:20	On	120
13			62	1:20	On	120
14			62	1:20	On	120

A.11. Immunohistochemical staining

1. Place paraffin embedded tissue section slides in dewaxing xylene I for 5 minutes, followed by dewaxing xylene II for another 5 minutes. Rehydrate for 5 min for each ethanol dilution (100 % x 2 times, 90, 70, 50 %), followed by running tap water for 5 minutes.

2. Block endogenous peroxidase activity using 1 in 10 dilution of 30% H_2O_2 in 100% methanol for 20 minutes (refresh the solution every 3-5 minutes due to evaporation). Wash in water for 5 min.

3. Antigen retrieval step. Fill the pressure cooker with 2 litres of 1X Tris EDTA buffer (from 10X solution made with 100 mM Tris base and 0.01M EDTA, adjusted to pH 9

with HCl / NaOH). Alternatively, sodium citrate buffer (10 mM Sodium citrate, 0.05% Tween 20, pH 6.0) can be utilised. Place slides inside a slide holder. Lock the lid of the pressure cooker, turn dial to setting 2 and turn heat up to the max. Once there is a strong consistent head of steam, begin a 3 minute timer.

After 3 minutes plunge pressure cooker into sink full of cold water. Wait for the red button to fall before opening lid. Lift slide holder out with forceps straight into a waiting cold water bath.

4. Block the sample with 5% normal goat serum in PBS for 30 min at room temperature (roughly 100 µl per slide).

5. Incubate primary antibody solutions in 5 % goat serum in PBS overnight at 4 ºC on the slide tray.

6. Wash 3 times in PBS (5 minutes each)

7. Dilute the Biotinylated swine anti-rabbit / rabbit anti-mouse secondary antibody 1:400 in PBS for 1 h

8. Wash 3 times in PBS (5 minutes each)

9. While the biotinylated secondary incubation is ongoing, take the Vector ABC Kit. Mix equal volumes (2 and 2 drops) of solution A and B to 5 ml of PBS. Leave for 30 min at room temperature to complex.

10. Incubate the sections for 30 min at RT with the ABC vector

11. Activate DAB (3,3′-Diaminobenzidine) with 3 µl of H_2O_2 (for each 2.5 ml of DAB) immediately before application to slide. Watch colour development (up to max 3 min) and stop reaction with tap water for 5 minutes.

12. Counterstain with Gill's Haematoxylin for 15-20 seconds

13. Wash in tap water until clear

14. Dehydration

- EtOH 70 % - <30 sec
- EtOH 96 % - 30 sec - 1 min
- EtOH 100 % I - 30 sec - 1 min
- EtOH 100 % II - 30 sec - 1 min
- Xylene I - 2 min
- Xylene II - 2 min – until mounting

B. Outputs

B.1. Journal publications

(1) Héctor Capella-Monsonís, Dimitrios I Zeugolis, *Decellularised xenografts in regenerative medicine: From processing to clinical application.* **Xenotransplantation**, Submitted.

(2) Héctor Capella-Monsonís, Andrea De Pieri, Rita Peixoto, Stefanie Korntner, Dimitrios I Zeugolis, *Extracellular matrix-based biomaterials as adipose derived stem cell delivery vehicles in wound healing: A comparative study between a collagen scaffold and two xenografts* **Stem Cell Research & Therapy** Submitted

(3) Ignacio Sallent, Héctor Capella-Monsonís, Philip Procter, Ilia Y Bozo, Roman V Deev, Dimitri Zubov, Roman Vasyliev, Giuseppe Perale, Gianni Pertici, Justin Baker, Peter Gingras, Yves Bayon, Dimitrios I Zeugolis, *The few who made it: Commercially and clinically successful innovative bone grafts* **Frontiers in Bioengineering and Biotechnology** (2020) **8 IF 2018: 3.64**

(4) Héctor Capella-Monsonís, Maura A Tilbury, J Gerard Wall, Dimitrios I Zeugolis, *Porcine mesothelium matrix as a biomaterial for wound healing applications* **Materials Today Bio** (2020) **7 IF 2018: n.a.**

(5) Héctor Capella-Monsonís, Jack Kelly, Stephen Kearns, Dimitrios I Zeugolis, *Decellularised porcine peritoneum as a tendon protector sheet* **Biomedical Materials** (2019) **14**(4) **IF 2018: 3.44**

(6) Héctor Capella-Monsonís, João Q Coentro, Valeria Graceffa, Zhuning Wu, Dimitrios I Zeugolis, *An experimental toolbox for characterization of mammalian collagen type I in biological specimens* **Nature Protocols** (2018) 13 **IF 2018: 12.42**

(7) Héctor Capella-Monsonís, Stephen Kearns, Jack Kelly, Dimitrios I Zeugolis, *Battling adhesions: from understanding to prevention* **BMC Biomedical Engineering** (2019) 1 **IF 2018: n.a.**

B.2. Book chapters

(1) Héctor Capella-Monsonís, Salomé Guillaumin, Sofia Ribeiro, Stefanie Korntner, Yves Bayon, Dimitrios I Zeugolis, *Scaffolds for tendon tissue engineering*, **Handbook of Tissue Engineering Scaffolds** (2019) Volume One

(2) João Quintas Coentro, Héctor Capella-Monsonís, Valeria Graceffa, Zhuning Wu, Anne Maria Mullen, Michael Raghunath, Dimitrios I Zeugolis, Collagen *quantification in tissue specimens* **Methods in Molecular Biology** (2017) Fibrosis

(3) Ignacio Sallent, Héctor Capella-Monsonís, Dimitrios I Zeugolis *Production and characterization of chemically cross-linked collagen scaffolds,* **Methods in Molecular Biology** (2017) Collagen

B.3. Conference podium presentations

(1) Héctor Capella-Monsonís, Dimitrios I Zeugolis, *A basement membrane-derived extracellular matrix for regenerative medicine,* **Matrix Biology Ireland Annual Meeting,** 2019 (Dublin, Ireland)

(2) Héctor Capella-Monsonís, Dimitrios I Zeugolis, *Decellularised porcine matrix as a multifunctional biomaterial for regenerative medicine,* **TERMIS EU Chapter,** 2019 (Rhodes, Greece)

(3) Héctor Capella-Monsonís, Dimitrios I Zeugolis *Decellularised porcine peritoneum as a multifunctional material for tendon tissue engineering* **European Orthopedic Research Society 26th Annual Meeting,** 2018 (Galway, Ireland)

(4) Héctor Capella-Monsonís, Dimitrios I Zeugolis, *Tissue grafts versus collagen mono-domain scaffolds: Improved mechanical properties and cytocompatibility,* **World Congress of Biomechanics** 2018 (Dublin, Ireland)

(5) Héctor Capella-Monsonís, Dimitrios I Zeugolis, *Multifunctional tissue graft for musculoskeletal applications,* **Orthopedic Research Society Annual Meeting**, 2018 (New Orleans, USA)

(6) Héctor Capella-Monsonís, Dimitrios I Zeugolis, *Multifunctional extracellular matrix for musculoskeletal tissue engineering applications,* **AMBA,** 2017 (Ghent, Belgium)

(7) Héctor Capella-Monsonís, Dimitrios I Zeugolis, *The potential of porcine peritoneum tissue as an anti-adhesion barrier for flexor tendon regeneration* **European Orthopedic Research Society 25th Annual Meeting**, 2017 (Munich, Germany)

(8) Héctor Capella-Monsonís, Dimitrios I Zeugolis, *Tissue grafts: Multifunctional implantable devices* **European Society for Biomaterials Annual Meeting** TERMIS-EU Symposium, 2017 (Athens, Greece)

B.4. Rapid fire presentations

(1) Héctor Capella-Monsonís, Dimitrios Tsiapalis, Dimitrios I Zeugolis, *Porcine-derived extracellular matrix for musculoskeletal tissue engineering* **European**

Society for Biomaterials 2018 (Maastricht, The Netherlands)

(2) Héctor Capella-Monsonís, Dimitrios I Zeugolis *The potential of a porcine extracellular matrix for tissue engineering applications owing to its preserved multifunctionality* **Matrix Biology Ireland** 2017 (Dublin, Ireland)

B.5. Poster presentations

(1) Héctor Capella-Monsonís, Dimitrios I Zeugolis *Enzymatic resistance, cytocompatibility, and angiogenesis: Porcine ECM as an advanced wound dressing material*, **Wild on Wounds** 2018 (Las Vegas, USA), **Innovations in Wound Healing** 2018 (Key West, USA), **Symposium on Advanced Wound Care** 2018 (Las Vegas, USA).

(2) Héctor Capella-Monsonís, Dimitrios I Zeugolis *Preserved properties and subsequent advantages of a gently processed dermal collagen powder,* **Wild on Wounds** 2018 (Las Vegas, USA), **Innovations in Wound Healing** 2018 (Key West, USA), **Symposium on Advanced Wound Care** 2018 (Las Vegas, USA).

(3) Héctor Capella-Monsonís, Dimitrios I Zeugolis, *A multifunctional porcine peritoneum matrix for musculoskeletal regenerative medicine,* **TERMIS World Congress** 2018 (Kyoto, Japan)

(4) Héctor Capella-Monsonís, Dimitrios I Zeugolis, *The potential of porcine peritoneum tissue as antiadhesion barrier for flexor tendon regeneration* **Matrix Biology Ireland Annual Meeting**, 2016 (Dublin, Ireland), **TERMIS-EU,** 2017 (Davos, Switzerland), **European Society for Biomaterials** 2017 (Athens, Greece)